Preclinical Investigation of Immunomodulatory Thermosensitive Liposomes

von

Bettina Sonja Heiß

Inaugural-Dissertation zur Erlangung der Doktorwürde
der Tierärztlichen Fakultät der Ludwig-Maximilians-Universität München

Preclinical Investigation of Immunomodulatory Thermosensitive Liposomes

vorgelegt von

Bettina Sonja Heiß

aus Gräfelfing

München 2023

Aus dem Zentrum für Klinische Tiermedizin der Tierärztlichen Fakultät
der Ludwig-Maximilians-Universität München

Lehrstuhl für Innere Medizin der Kleintiere

Arbeit angefertigt unter der Leitung von: Univ.-Prof. Dr. Johannes Hirschberger

Angefertigt in der Medizinischen Klinik und Poliklinik III
des Klinikums der Universität München in Großhadern
Mentor: Prof. Dr. Lars Lindner

Gedruckt mit Genehmigung der Tierärztlichen Fakultät
der Ludwig-Maximilians-Universität München

Dekan:	Univ.-Prof. Dr. Reinhard K. Straubinger, Ph.D.
Berichterstatter:	Univ.-Prof. Dr. Johannes Hirschberger
Korreferent/en:	Univ.-Prof. Dr. Marcia Ferraz
	Prof. Dr. Monika Rinder
	Univ.-Prof. Dr. Cornelia A. Deeg
	Univ.-Prof. Dr. Dr. h.c. Erwin P. Märtlbauer

Tag der Promotion: 22. Juli 2023

to the mighty rodents
that help testing countless drugs
to save lives of people

Table of Content

List of Abbreviations

ABC	Accelerated blood clearance
ACN	Acetonitrile
ADR	Adverse drug reaction
ADUI	ADU-S100 = MIW815 = ML RR-S2 CDA
AUC	Area-under the curve
BD	Biodistribution
BL6	C57BL/6 mice
BN	Brown Norway rat
BN175	BN175 soft tissue sarcoma model
B16	B16F10 melanoma model
C	Concentration
CAD	Charged-aerosol detector
CARPRA	Complement activation related pseudoallergy
CDN	Cyclic di-nucleotides
CF	Carboxyfluorescein
C_{max}	Theoretical maximum concentration in plasma immediately after injection
CO_2	Carbon dioxide
CP	Cyclophosphamide
CRO	Contract research organization
CTLA-4	CTL associated protein 4
c-di-AMP	Cyclic dimeric adenosine monophosphate
DAMPs	Damage-associated molecular pattern molecules
DC	Dendritic cell
DMEM	Dulbecco's Modified Eagle Medium
D/L	Drug to lipid ratio
DLS	Dynamic light scattering
DMSO	Dimethyl sulfoxide
DMXAA	Di-methylxanthone acetic acid
DOX	Doxorubicin
DPBS	Dulbecco’s phosphate-buffered saline
DPPC	1,2-Dipalmitoyl-sn-glycero-3-phosphocholine
$DPPG_2$	1,2-Dipalmitoyl-sn-gylcero-3-phospho-di-glycerol
DSPC	1,2-Distearoyl-sn-glycero-3-phosphocholine
EE	Encapsulation efficacy
EL	Endothelial lipase
Em	Emission
EPR	Enhanced permeability and retention
EtOH	Ethanol
Ex	Excitation
FA	Formic acid

FCS	Fetal calf serum
F/T	Freezing and thawing
G	Gauge
H	Hours
HBS	HEPES-buffered saline
HBW	HEPES-buffered water
HL	Hepatic lipase
HPLC	High-performance liquid chromatography
HT	Hyperthermia
ID	Injected dosage
IFN	Interferon
IL	Interleukin
i.t.	Intratumoral
i.v.	Intravenous
KDP	Potassium di-hydrogenphosphate
LC-MS	Liquid chromatography - mass spectrometry
LNP	Lipid-based nanoparticle
LOD	Limit of detection
LOQ	Limit of Quantification
MatBIII	MATBIII mamma adenocarcinoma model
MeOH	Methanol
Min	Minutes
MDSC	Myeloid-derived suppressor cell
MSC	Mesenchymal stem cells
N_2	Nitrogen
NaCl	Natrium chloride
NaOAc	Sodium acetate
NH_4OAc	Ammonium acetate
NP	Nanoparticle
NT	Normothermia
OD	Optical density
PAMPs	Pathogen-associated molecular pattern molecules
PC	Phosphocholine
PDI	Poly-dispersity index
PD-L1	Programmed cell death protein 1 ligand 1
PD-1	Programmed cell death protein 1
PEG	Poly-ethylene glycol
PG	Phosphatidyl-glycerols
PK	Pharmacokinetic
PLRP-2	Pancreas lipase related protein-2
PNP	Platelet-coated nanoparticle
PPE	Palmar Plantar Erythrodysthesia

PRR	Pathogen-recognition receptor
R^2	Coefficient of determination
R837	Imiquimod
R848	Resiquimod
RES	Reticuloendothelial system
RT	Room temperature
Saline	Isotonic 0.9 % NaCl solution
SD	Standard deviation
SPE	Solid-phase extraction
SRB	Sulforhodamine assay
STING	Stimulator of interferon genes
S.c.	Subcutaneous
t_α	Half-life
TAA	Tumor-associated antigen
TFA	Trifluoroacetic acid
TG	Triacylglycerol
TLR	Toll-like receptor
TME	Tumor microenvironment
T_m	Phase transition temperature
TNF	Tumor-necrosis factor
TSL	Thermosensitive liposome
WB	Water bath
ζ -Potential	Zeta-potential

List of Tables

List of Figures

List of Presentations

Oral Presentations

1. ENHANCING DRUG DELIVERY WITH AN HEAT-ACTIVATED NANOCARRIER BASED ON PHOSPHATIDYL-(OLIGO)-GLYCEROL

   S.B. Muckenthaler, K. Zimmermann, I. Brummelhuis, S. Kort, B. Wedmann, P. Schweizer, M. Hossann, L.H. Lindner

   Virtual Congress, 13. Internationale Congress of Hyperthermic Oncology (ICHO), October 2021

2. PAVING THE WAY TOWARDS CLINICAL TRANSLATION: ENHANCING DRUG DELIVERY WITH THERMOSENSITIVE LIPOSOMES IN RELEVANT PRE-CLINICAL SETTINGS

   B.S. Heiss, K. Zimmermann, R. Schmidt, F.J. van Valenberg, I. Brummelhuis, L. Sebeke, J.C. Gomez, K. Troedson, B. Wedmann, F. Kuhnle, S. Kort, J. Hirschberger, H. Gruell, M. Hossann, L.H. Lindner

   Schloss Hohenkammern, 22. Wissenschaftliches Symposium der Medizinischen Klinik und Poliklinik III, April 2022

Poster Presentations

1. TARGETED DELIVERY OF CHEMOTHERAPEUTICS VIA THERMOSENSITIVE LIPOSOMES AND MILD-HYPERTHERMIA FOR THE TREATMENT OF DRUG-RESISTANT SOLID TUMORS

   X. Zhu, **B.S. Heiss**, L. Pointner, M. Petrini, L.H. Lindner

   Schloss Hohenkammern, 22. Wissenschaftliches Symposium der Medizinischen Klinik und Poliklinik III, April 2022

2. ENHANCING DRUG EFFICACY WITH A HEAT-ACTIVATED DRUG-DELIVERY PLATFORM BASED ON PHOSPHATIDYL-(OLIGO)-GLYCEROL NANOCARRIER

   B.S. Heiss, K. Zimmermann, I.R. Schmidt, K. Troedson, S. Kort, M. Hossann, J. Hirschberger, T.L. ten Hagen, L.H. Lindner

   Virtual Summit, 13th European and Global Summit for Nanomedicine (CLINAM), May 2022

   * Poster-prize: EMPA Awards, Category Translational Nanomedicine Priorities, Rank 1

3. A HEAT-ACTIVATED DRUG-DELIVERY PLATFORM BASED ON PHOSPHATIDYL-(OLIGO)-GLYCEROL NANOCARRIER

   B.S. Heiss, K. Zimmermann, I.R. Schmidt, K. Troedson, S. Kort, M. Hossann, J. Hirschberger, T.L. ten Hagen, L.H. Lindner

   Montréal, Controlled Release Society (CRS) Annual Meeting & Expo, July 2022

   * Poster-prize: Merck KGaA GRAD Awards, Best Poster

I. Introduction

Chemotherapy, radiotherapy, and surgical excision are nowadays standardized methods to treat solid cancer [1]. While radiotherapy and surgery primarily provide local control over a tumor, only modest effects on secondary, distant tumors can be achieved. However, metastases are the main cause of death for cancer patients [2, 3]. Conventional chemotherapy is based on the systemic application of a cytotoxic agent, which can achieve an antitumor effect in both, primary and secondary locations. However, this broad therapeutic spectrum is accompanied by low tumor specificity driving high off-site toxicity. In addition, the formation of resistance may result in reduction of therapeutic response [4-6]. As early as 1979, it was stated that an ideal tumor therapy should have three characteristics: it must be potent, specific, and systemic [7]. The strength of therapeutic efficiency is often given, whereas the specificity and systemic dosage of conventional tumor therapies (surgery, radio-, and chemotherapy) have strong limitations. It is precisely these limitations that immunotherapy is designated to overcome [7]. Thereby facing two challenges: the first is to overcome the host immune tolerance present in the immediate tumor microenvironment (TME) and the second is to induce the formation of an endogenous, durable, and long-lasting immune response against cancer [5, 8]. To achieve these goals, immunmodulatory substrates are explored in novel strategies ranging from anti-cancer vaccination to cell- or nanocarrier-based approaches [9-11]. Although none of these immunomodulators have antitumor activity per se, they can stimulate specific receptors (e.g., PD-L1, TLR) or activate pathways (e.g., STING, STAT3) and thereby achieve an increase in expression of pro-inflammatory signals (e.g., cytokines, interferons, interleukins), activation of antigen-presenting cells, or maturation of active T cells [12]. Efficacy of such immuno-oncology strategies is evident as several novel immunomodulatory drugs have been approved by the US Food and Drug Administration (FDA) [13] or are part of clinical trials. Problems are arising as plasma half-life of immunomodulators is often short. Simply increasing their dosage is not recommended as systemic immune activation has been reported. Extensive activation of patient-specific immunoreaction has been reported to lead to severe adverse events with serious consequences [14, 15]. By approaches utilizing an immunoadjuvant, for example TLR or STING agonists, this was circumvented by i.t. application in clinical trials [16, 17]. Nevertheless, such molecules catch research attention due to their potential to induce antitumor response in so called immunological cold tumors [12]. Consequently, future efforts should involve prolonging plasma stability while promoting targeting of tumor tissue, thereby possibly elevating safety and therapeutic efficacy at once.

II. Review of Current Literature

A) Criteria for selecting preclinical cancer model

For the exploration of novel therapeutic approaches, it is essential that animal models mimic the complex development of represented human diseases. Particularly cancer research requires precise preclinical investigation due to its multitude of cancer phenotypes, host organ-associated factors, vascular structures as well as cell populations [18]. Thereby, differentiation of the genomic heterogeneity of malignant cells and immune contextual composition involved in the tumor microenvironment (TME) is essential [19, 20]. Several authors have discussed that by choosing the tumor model, the prognostic value of preclinical data for later clinical application has been pre-set. Hence, an adequate animal model must be carefully chosen with utmost care [18, 21-23]. Tumor formation is commonly either generated autochthonous or triggered by tumor cell injection at orthotopic (= identical to origin) or heterotopic (= different to origin, e.g., subcutaneous (s.c.)) location (figure 1). D*e novo* tumor formation in an autochthonous host can be induced by utilizing carcinogens or implementation of genetic modifications. These so-generated tumors can be exploited for subsequent creation of *in vitro* cell lines which, upon injection in syngeneic host (= identical to autochthonous host), reproduce tumor growth in an immunocompetent setting. Whenever human tumor cell lines are of interest, a xenograft transplantation in immunodeficient rodents must be conducted to suppress host immune-derived rejection [23].

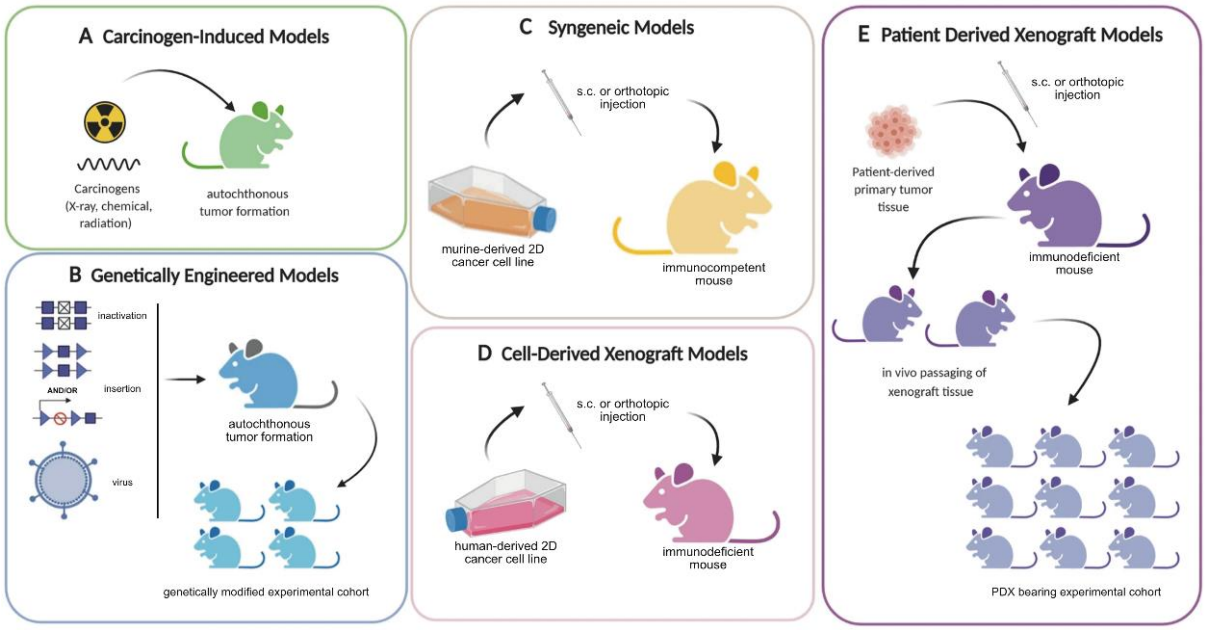

Figure 1: Generation of common preclinical murine cancer models.
(A) Carcinogens can boost *de novo* tumor formation in wildtype animals, while **(B)** genetic modifications reproduce genetic events necessary for tumor development. **(C)** Rodent cells can be cultured *in vitro* and injected (subcutaneous (s.c.) or orthotopic) in syngeneic hosts to induce reproducible tumor growth in immunocompetent environment, whereas **(D)** cultured human cells need an immunodeficient xenograft host. **(E)** Patient-derived xenografts are established by transplantation of whole patient-derived tumor tissue into immunodeficient host followed by *in vivo* passages. Modified Illustration [23].

Many animal models have drawbacks for preclinical research of immunotherapies. For example, xenografts (patient-derived or cell-derived) models show low correlation of preclinical and clinical efficacy [24]. The necessity of immunodeficient animals in such models cause difficulties in correlations to human immune response against cancer, as a low success rate of human tumor cell implantation and a rapid washout of tumor-infiltrating human lymphocytes must be expected in particular [23, 25]. Even additional 'humanization' of the xenograft host with functional peripheral blood mononuclear cells or hematopoietic progenitor cells can only temporarily mimic the human TME and often leads to an undesired substantial rejection reaction (human xenograft versus host disease) [18, 21]. One way out may be provided by genetic modification. Here, specific mutations are implemented in the host genome, promoting the autochthonous development of tumors. Timespans of up to one year need to be considered until a stable genetic modification may be generated *in vivo*, as tumor development despite high animal numbers cannot be guaranteed. Additionally, high phenotypic variances and mutation rates as well as continuous management of breeding prolong the experimental period [22, 23].

The most commonly used cancer models are still cell injected tumors in syngeneic host. Their well-known characteristics of reproducible tumor induction, rapid growth kinetics, and no rejection reactions in the immunocompetent host make them an ideal model in research [18, 25]. In comparison to clinical data of the respective human cancer, inconsistencies are an alteration in tumor immunophenotype, mutational burdens as well as rapid growth, rendering no time for metastatic behavior [23, 24]. It is guessed that during the timespan of cancer evolvement, relationship and interaction with the host immune response is shaped. Hence, the immune contextual characteristics that influence human antitumor responses cannot be recapitulated in fast growing rodent models [26]. Contrary to biological critics, it must always be considered to keep necessary number of animals as low as possible. This is achieved by high successful implantation rates of s.c. tumors. Especially in this regard, some orthotopic models show disadvantages due to the reduced implantation success and increased risks associated by reaching site of implantation [18]. Bibby *et al.* discussed the advantages and disadvantages of s.c. implantation compared to orthotopic tumor models. While the latter allegedly have benefits due to their more complex tissue- and/or organ-specific aspects, the authors argue that two questions should be answered by any chosen tumor model: Can the *in vitro* effective drug concentration be achieved *in vivo* and does the molecule interact with the desired target [27]?

B) Cancer development and immunoediting

The importance of how a tumor is induced preclinically becomes most evident when looking at the evolvement of cancer in context of host immune reactions [26]. Immunodeficient animals develop more carcinogen-induced and spontaneous cancers, and their tumors are more immunogenic in comparison to the one's of immunocompetent mice [28]. Accordingly, a crosstalk between host immunity and tumor cells defines tumorigenesis. The fact that cancer not only has different phenotypes and occurs in different organs but is rather associated with unique host factors, leading to a distinctive microenvironment is increasingly appreciated [19, 20, 29, 30]. Whereas initially, a 'cancer immunosurveillance' was debated, now a more dynamic appreciation of 'cancer immunoediting' is discussed. This concept focuses on a dual role of the immune system: on the one side a host-protection by suppressing tumor growth and on the other side a tumor-promotor by shaping tumor immunogenicity [28, 31]. The host immune system shapes tumor fate in three phases: *elimination*, *equilibrium* and *escape* (figure 2) [28, 32, 33]. The evasion of immune destruction is now an established hallmark of cancer [34].

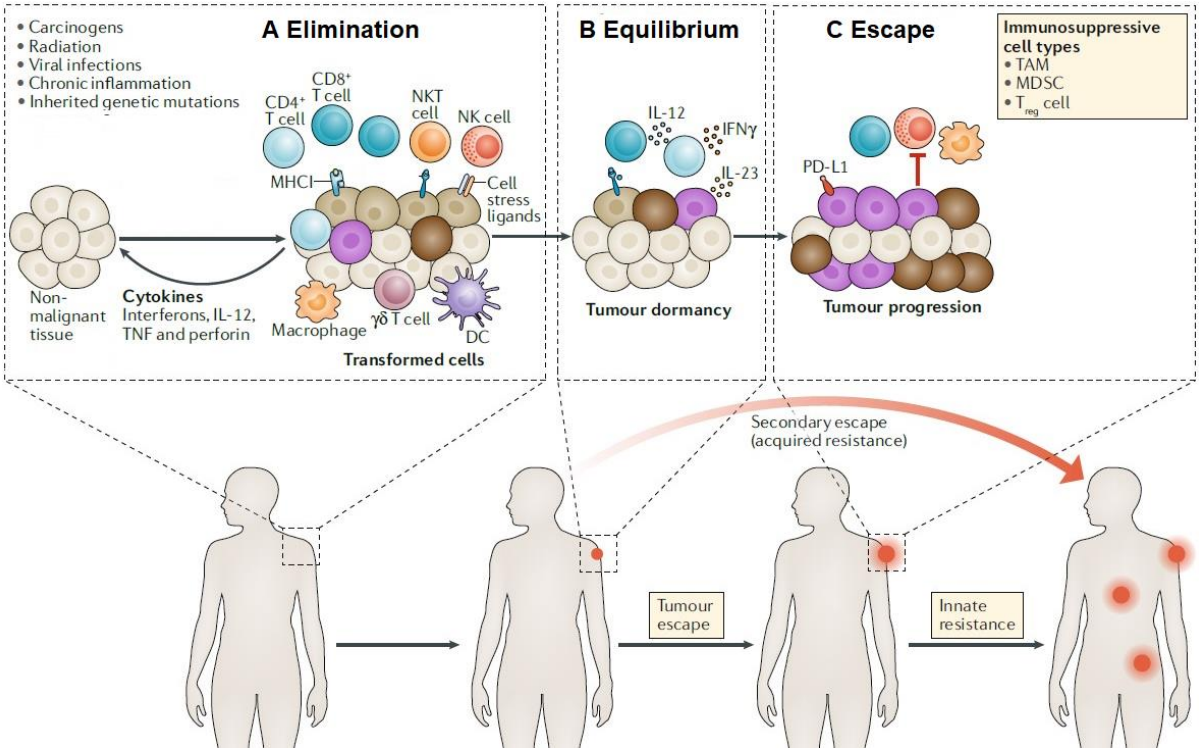

Figure 2: Cancer immunoediting is divided in three phases.
(A) During ***elimination***, the innate and adaptive immune system act together to battle the expansion of transformed cells. If initial attempts of host immune system failed eradication, the tumor progresses into **(B)** ***equilibrium*** phase. The overall tumor burden is controlled, implying a tumor 'dormancy', which is misleading as constant suppression by adaptive immune system edits tumor immunogenicity. This paves the way to **(C)** ***escape*** phase during which tumor immunosuppressive and tumor evasive tactics allow unrestrained growth leading to clinical relevant tumors. Modified Illustration [33].

During ***elimination*** (figure 2.A), the initial recognition promotes antitumor responses and the tumor cell proliferation occurs in parallel to apoptosis [33]. Danger signals such as type I interferons (IFN) α and β are expressed early during tumor development by antigen-presenting cells upon sensoring damage-associated molecular pattern molecules (DAMPs), such as cytoplasmatic DNA. Tumor associated antigens (TAA) are directly recognized and cytolyzed by natural killer (NK) or activate dendritic cells (DC) [28, 31, 35, 36]. Upon activation, the DC mature and locally produce cytokines and present TAA to naïve $CD3^+$ T cells in the draining lymph nodes or tertiary lymphoid structures (TLS) [37]. This priming induces the transformation into $CD4^+$ T-helper cells (TH_1 cells) or $CD8^+$ cytotoxic T cells (CTLs). Whereas CTL directly induce tumor cell apoptosis, TH_1 cells are associated with expression of type II IFN (IFNγ) which are necessary for mediation of antitumor effects by inhibiting tumor cell proliferation and angiogenesis [19, 28, 38]. Macrophages of the M1-subtype release pro-inflammatory TNF, Interleukin (IL)-1, IL6 as well as reactive oxygen and reactive nitrate species to further upregulate pro-inflammatory signals [19]. Consequently, the innate and the adaptive immune system battle the developing tumor within the TME and in peripheral tissues [32, 33]. At some point in time, a quiescent ***equilibrium*** phase (figure 2.B) starts, during which proliferation or expansion of tumor cells can be counteracted by balancing IL-23 and IL-10 promoting persistence with IL-12 and IFNγ furthering elimination [28]. Tumor burden is maintained by constantly suppressing tumor cells. Thereby, resistance variants are selected which critically edit cancer cell immunogenicity (e.g., loss of TAA and MHC I, defects in TAA-presentation, expression of immunosuppression ligands) [32, 33]. During this phase, NK and M1 cells are dispensable [28]. It is unclear why the progression to ***escape*** phase (figure 2.C) occurs: if the tumor cell population changes in response to the immunoediting and/or the host immune system alters its response to overwhelming cancer immunosuppression or -deterioration [31, 33]. However, the gained resistance mechanisms during dormancy reduce immune recognition as well as enhance tumor cell survival rates leading to disease progression, causing clinical relevant cancer [39]. It has been reported that T cell exhaustion plays a pivotal role in progression of several cancer subtypes such as colorectal cancer or melanoma [20]. In accordance, metastases tend to have lower $CD8^+$ T cell densities than those of their initial lesion, although the overall immune contexture of most metastases generally resembles that of the primary tumor [37]. The effect of intratumoral B cells in cancer is far from clear. Despite the known capacity to induce memory which helps control tumor evasion and metastasis development, reports on converting resting $CD4^+$ T cells into regulatory T cells (T_{reg}) would indicate a role in promoting metastasis [19, 37]. T_{reg} are a physiologically suppressive subtype and play an important role in maintaining the homeostasis of the immune response. Multiple roles include the production of immunosuppressive cytokines (e.g., IL-10 and TGF-β), the expression of negative co-

stimulatory molecules such as CTL associated protein 4 (CTLA-4), programmed cell death protein 1 (PD-1) and its ligand 1 (PD-L1) as well as the consumption of IL-2 [40, 41]. Recruitment of T_{reg} can be driven by chemokines (e.g., CCL-22) expressed by macrophages in the TME having differentiated to a M2 subtype. M2 can add to the expression of IL-10 or PD-L1, promote angiogenesis and are therefore correlated with tumor progression [19, 40, 41] and immune suppression [42]. Myeloid-derived suppressor cells (MDSC) further impair the function of T cells, NK cells, and DCs by facilitating tumor escape from immune attack; via expression of a cellular stress sensor protein and IL-6 [40, 41]. Dysfunctionality or senescence of NK cells and natural killer T cells (NKT) in TME has been reported recently. Despite different origins, both cell lines have comparable phenotypes and functions during the antitumor response [43]. Alteration in their functionality might be another factor driving escapes. Overall, upregulation of PD-L1 expression on tumor cells and tumor-infiltrating immune cells in response to the secretion of IFNγ is part of the process known as adaptive immune resistance [28, 33].

Chronic exposure to TAA, unproductive interactions from DCs combined with pressure from down-regulating cytokines and cell types (such as T_{reg}, M2 and MDSC) may create an immunosuppressive TME, which is likely linked to T cell exhaustion [41, 42]. Furthermore, variations in infiltrating immune cells are not only tumor type specific, but they are also found in different tumors of the same type and even different locations within and around a single tumor indicating a distinctive impact of surrounding stromal tumor bed [19, 30]. Taken together, the process of tumor development is drastically influenced by host immune reactions [26], which form a distinctive contexture within the TME consisting of tumor cells, all of the above-mentioned immune cells, endothelial cells, stromal cells and tertiary lymphoid structures.

C) Immune contexture gaining clinical relevance

Fridman *et al.* proclaimed in 2012 that clarifying if the immune contexture of the primary tumor can predict a later therapeutic responses is of paramount importance [19]. Rossie *et al.* went further by declaring that an effective therapeutic strategy can only be determined after analysis of involved cell populations in the TME and these criteria should, therefore, be implemented in the preclinical research [44]. This might not be essential for single target methods forcing cell death but are key for the dynamic approaches aiming at host immune activation. In addition, samples from patients receiving therapy will be essential to promote this process [45] as an immune cell specific impact of certain therapeutics being associated with the therapeutic efficacy in various cancer types has become increasingly evident [45-47]. T cells are the central mediators of the adaptive immune system and play a crucial role in tumor surveillance and eradication [20]. The observation that density and location of specific T cell subtypes within the tumor tissue could predict the survival in colorectal cancer

more accurately than the classical staging fired a powerful concept. Shortly after, the Immunoscore was executed in a clinical consensus [48]. For the first time in any type of cancer, a robust and standardized scoring system based on the quantification of $CD3^+$ and $CD8^+$ T cells at the tumor center and the invasive margin was developed [30, 49]. The implemented novel score allowed classification in three tumor subtypes with respect to infiltration ratios. A tumor without $CD3^+$ and $CD8^+$ T cells is classified as 'cold', a tumor with many is classified as 'hot', and a tumor with a low proportion or only at the tumor margin is classified as 'altere'. This classification has a high prognostic value and at the same time can be applied as a marker for the success of a therapy [30, 48-50]. Oriented on this immunoscore, better prognostic and predictive information in the clinic has already been reported for melanoma and breast cancer, with enhanced antitumor efficacy of immunomodulators exclusively in hot tumors [51-53]. While breast cancer was declared a cold tumor for many decades, up to six subtypes have now been identified: all of them immunoactive in different gradation and none of them cold. The extent to which the immunological phenotype influences the therapeutic response remains to be elucidated in ongoing clinical trials [54]. In melanoma, lymphocyte infiltrations have been considered a positive prognostic issue due to high mutational burden correlating with high immunogenicity but long-term functional exhaustion [30, 32]. Further cancer types such as hepatocellular carcinoma [55] or cervical cancer [55] have been positively correlated with the immunoscore as prognostic marker, whereas others are not as easily categorized. Although few subtypes of soft tissue sarcomas have T cell infiltrates correlating to positive outcomes, these reports may not be representative for non-immune cell infiltrated subtypes [41].

With a high count of infiltrating cells, the immune-active tumors are an obvious target of immunotherapy approaches. However, dysfunctional or exhausted T cells need to be transformed in order to unleash the pre-existing immunity from tumor suppression. Immune checkpoint inhibitors can block suppressive T cell receptors (e.g. CTLA-4 and PD-1) specifically and trigger the expansion of tumor-reactive T cells [30]. Promising clinical results in melanoma were reported especially in regard to T cell function [51, 56]. For patients with previously treated metastatic melanoma, the anti-CTLA-4 agent ipilimumab was approved in 2011, which was the first immunotherapy agent ever approved by the FDA and European Medicines Agency (EMA) [57]. Shortly after, the FDA and EMA (in 2014 and 2015, respectively) approved two anti-PD-1 antibodies, pembrolizumab and nivolumab, for patients with unresectable or metastatic melanoma [58, 59]. For all three antibodies mentioned, more significant improvements were registered in tumors with high immunological repertoire or increased tumor mutational burden [30].

D) Critical aspects for initiation of immune infiltration

It is already clear that future treatment successes might fall easier to cancer types with a profitable immune contexture. One of the major challenges is to convert an immune-altered or cold tumor [12]. Several therapeutic approaches must be considered in respect to their mechanisms triggering absence or dysfunction of T-cell infiltration (figure 3).

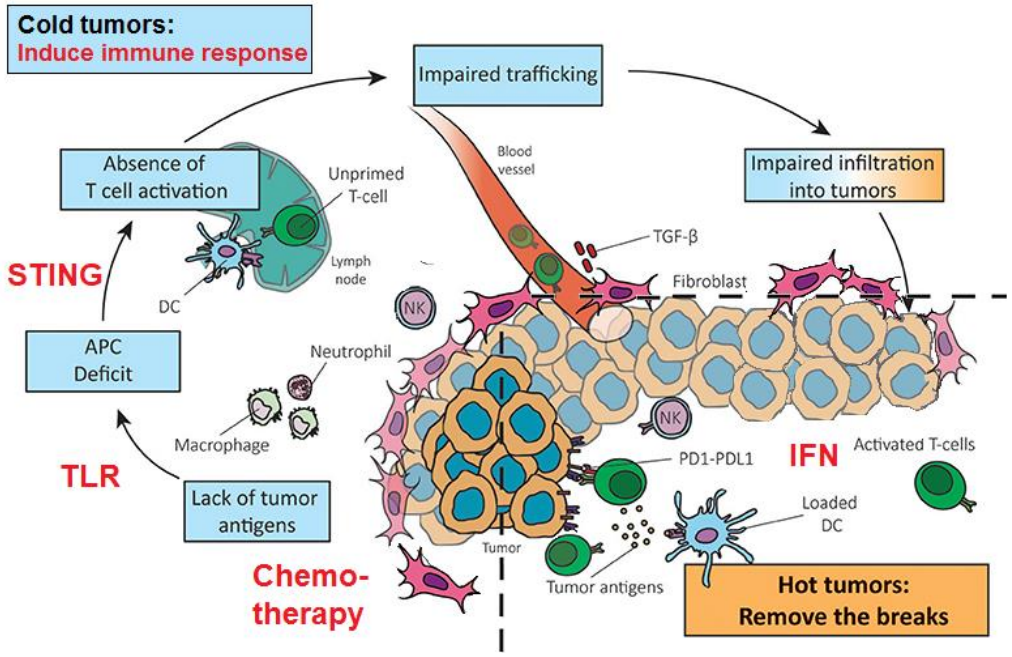

Figure 3: Altering tumor's immune contexture to initiate host immune reaction.
In case of cold tumors low immunogenicity is evident in a lack of tumor-associated antigens (TAA), deficient TAA-presentation by antigen presenting cells, absence of T cell priming, impaired trafficking of activated T cells or lack of infiltration of tumor tissue. An immune response could be induced at several steps by activating critical elements, e.g. via chemotherapy or activation of Toll-like Receptor (TLR) or Stimulator of Interferone Genes (STING). In contrast, hot tumors are immune cell infiltrated but suppressive signals are predominant. The breaks could be removed by e.g. Interferones (IFN). Modified Illustration [12].

Simply harnessing T cell trafficking and enabling access to tumor tissue could be achieved by blocking exclusion signals, such as TGF-β, or with anti-angiogenic drugs. While injection of influx mediating cytokines such as IL-2 or IL-12 seems feasible, significant systemic toxicity has been reported in clinical trials forcing an adaptation for the tumor targeting of these substrates [12, 30]. Further investigation of IL-15 and IL-21 are conducted to solidify the initial, promising reports [30]. Low amounts of TAA can be elevated by reversing epigenetic silencing or by targeting NK cells. Utilization of TAA in vaccination approaches pave the way to personalized cancer vaccine development. However, the patient specific T cell repertoire and the risk of specific loss of heterozygosity MHC I challenge this approach [12]. Engineering chimeric antigen receptors (CAR) targeting patient-specific TAA are renewing the field of adoptive cell therapy. Typically, CARs are transduced into patient derived T cells with promising clinical results in melanoma [60] but can also be attached to NK cells [12, 30]. For tumors with defective priming or activation of T cells, additional activation of systemic immune response is of interest. Intrinsic abnormalities in signaling

pathways make tumor cells a fertile environment for viral replication enabling cancer cell targeting. Exploration of oncological virus revealed a release of damage-associated and pathogen-associated molecular pattern molecules (DAMPs and PAMPs), which are associated with generation of TAA and immune activation. However, response rates were low, probably due to low lyse rates [30]. Enhancing local cell death increases DAMP-associated signaling has already been reviewed for conventional radio- or chemotherapy and is increasingly appreciated. Either approach has been reported to restart systemic immune activity and enhance the potency of immunotherapeutic agents [12, 20, 30, 61]. Perception of created DAMPs and PAMPs via pattern recognition receptors (PRR) activates subsequent pathways inducing antigen-presentation by myeloid cells residing in the TME. This receptor family consisting of five subtypes, RIG-I-like, NOD-like and C-type lectin and toll-like receptors (TLRs) as well as cytoplasmic DNA sensors [38] [12]. The latter are widely explored for immunotherapeutic approaches and will be discussed in greater detail below.

STING Agonists

In contrast to classic PRR receptors, cyclic guanosine monophosphate (cGMP)-cyclic adenosine monophosphate (cAMP) synthase (cGAS) acts as enzymatic sensor. The recognition of the cytoplasmic danger signal DNA induces a conformation change thereby catalyzing the formation of the STING ligand cGMP-AMP (cGAMP). This second messenger travels the signal to the endoplasmic reticulum, where it activates the transmembrane protein STING (stimulator of interferon genes). The induction of STING signaling cascade leads to the downstream expression of type I IFN, such as IFNβ, and inflammatory cytokines, e.g., TNFα and IL-6 [30, 62, 63].

Using a series of gene-targeted mice deficient in innate immune sensing pathways, Woo *et al.* proved the critical role of STING activation for spontaneous priming of antitumor T cells [35]. In further detail, induction of type I IFN signaling in the TME is implicated to bridge the innate and adaptive immune responses towards subsequent infiltration of tumor tissue by primed T cells [64, 65] [36]. Accordingly, a type I IFN signature predicts favorable clinical outcome in breast carcinoma following treatment with cancer vaccine and classic chemotherapy [30] [12]. Production of type I IFN in tumor tissue falls to tumor-associated DCs or STING activation upon sensing of cytoplasmic tumor-derived DNA in antigen-presenting macrophages, DCs and T cells [65]. NK cells are activated upon type I IFN, but do not express it themselves [36], correlating to no therapeutic loss of function of STING-agonist in mice depleted of NK cells [64]. Noteworthy, STING-dependent expression was reported in stromal cells, hinting at a contribution of TME to acute cytokine responses [65]. According to current literature, the expression levels of STING are however rather down- than upregulated in most human cancer types and especially in patients with advanced cancer disease [62]. In accordance, currently explored STING-activating strategies are trying to utilize the effective

initiation of *de novo* immune responses in non-T cell inflamed tumors [38, 61, 62]. Hence, a critical role can be postulated (figure 3). Natural ligands such as cytoplasmic DNA being induced by cell damage caused by radio- or chemotherapy have been reviewed to activate STING pathway. This treatment-induced senescence is a promising approach to achieve tumor cell stagnation [61]. More precise tuning can be achieved via cyclic di-nucleotides (CDN), e.g. including cGMP, cAMP, cyclic dimeric adenosine monophosphate (c-di-AMP) that mimic the endogenous STING ligand cGAMP or small molecule STING agonist such as di-aminobenzimidazole (di-ABZI) [63, 66].

An initial reported CDN agonist, di-methylxanthone acetic acid (DMXAA), failed clinical translation due to lack of efficacy despite the promising preclinical data. It was later reported that although DMXAA is a direct ligand for murine STING, polymorphisms in human STING led to the failed binding upon systemic injection [67, 68] and explained the unproven partial responses in the clinical trial of solid cancer and melanoma in 2009 [69]. Up to now, DMXAA is therefore categorized as non-CDN derivate [63]. However, driven by its pivotal T cell response in murine cancer models, the group of Corrales *et al.* synthesized a large panel of CDNs and selected most promising molecules capable of activating all know human STING alleles. Their lead-candidate ML RR-S2 CDA, later re-named MIW815 or ADU-S100 (ADU), reproduced therapeutic efficacy upon i.t. injection in various tumor models, based on STING-induced IFN-β production in antigen presenting cells [64]. Why focus was shifted to i.t. injection can only be speculated. ADU has been widely reported since then for antitumor response in mice with all studies preferring i.t. dosages below 100 µg [65, 70, 71]. In higher local dosages (500 µg), TNFα-dependent innate immune signaling led to tumor necrosis and no systemic immunity but upon dose-reduction to 100 µg, a robust long-term antitumor response was induced. These dosages were then named ablative and immunogenic, respectively [64]. In parallel, it was shown by Francica *et al.* that therapeutic response to ADU was dependent on STING-activation in TME and tumor-surrounding stroma [72]. Despite the profound immune-mediated tumor elimination in preclinical models after i.t. injection and high translational potential [64], the first clinical phase I trial of ADU was terminated due to low antitumor activity as partial response was observed in 5 % of patients [73]. Even though, safety of i.t. administration of ADU was proven as no toxicity to the hosts was reported in the assessed 40 patients with solid tumors or lymphomas [66].

STING-dependent proprietary effects on cancer immune contexture are also exploitation for enhancing the reach of immune checkpoint inhibitor strategies [38, 61, 62]. Initial clinical attempts were not promising. ADU combined with ipilimumab in a phase I study in solid cancers and lymphomas [73] and pembrolizumab in a phase II trial in head and neck cancer [74] have been terminated early due to no substantial antitumor activity. A phase Ib trial of MIW815 combined with PD-1 checkpoint inhibitor PDR001 was terminated early by

sponsor's decision [75]. The only trial completed was a phase I in solid cancers and lymphomas, where treatment with their ADU variant (MK-1454) combined with pembrolizumab showed safety but no response upon treatment [76]. A follow up phase II trial has been recently completed with head and neck cancer patients; results are pending [77]. A possible explanation for the lack of efficacy in humans was given by Richie *et al.*, whose data promoted that despite having the molecular repertoire, immune cells differ in their CDN transport mechanism. Adding to that, humans have more than one importer and currently investigated ADU might just not be efficiently imported by cell types that would promote an antitumor immune response in humans [78].

TLR Agonists

The TLR family is an evolutionarily conserved transmembrane PRR that plays a critical role in early impact of inflammatory immune response [79, 80]. Accordingly, expression of TLR is not limited to antigen-presenting cells (e.g., macrophages, DCs, mast cells, neutrophils) but spreads through epithelial cells, endothelial cells, adipocytes, and cardiomyocytes implicating [81, 82]. PAMPs, such as lipoproteins, lipopolysaccharide and flagellin are recognized by TLR 1, 2, 4, 5, and 6 on cell membranes whereas nucleic acids serving as DAMPs bind TLR 3, 7, 8, and 9 located on endosomal membranes [81-83]. As type I transmembrane glycoproteins, TLRs are characterized by an extracellular recognition domain consisting of leucine-rich repeats for ligand binding, a single transmembrane domain, and an intracellular Toll/IL-1R homology signaling domain [80, 83]. Upon ligand binding, a downstream signaling cascade is launched, subsequently inducing expression of proinflammatory cytokines (TNFα, IL-6 and IL-12), upregulation of co-stimulatory molecules, enforcing antigen presentation capacity and migration of DCs in the draining lymph nodes combining initiation of innate and adaptive immune cells [79, 81]. TLR on effector T cells contribute to their antitumor activity and survival, whereas TLR signaling in memory T cells may assist in maintaining their homeostasis [80]. Overall, a role for altering cold tumors can be postulated (figure 3).

For immune-oncology approaches, endosomal location is of pivotal interest, providing recognition of double-stranded RNA by TLR 3, single-stranded RNA by TLR 7 and 8, unmethylated cytosine-phosphate-guanine, or DNA by TLR 9. TLR agonists showed controversial results in preclinical studies by either promoting or inhibiting tumor progression depending on the TLR and the tumor type [12]. While preclinical investigation of a TLR 3 agonist showed contradictory results (tumor response but increase in suppressive T cell receptors), several approaches with TLR 9 agonists were more promising [79] leading to clinical exploration in prostate cancer, pancreatic adenocarcinoma, solid cancers and lymphoma and several other agonists in comparable tumor identities [81, 84]. Although high degrees of sequence homology and structural similarity is given among TLR subtypes,

distinctive biological responses to small molecule binding are reported driven by the expression on mainly antigen-presenting cells (TLR 7) or myeloid cells (TLR 8). In mice, the latter was reported to be biological inactive due to a lack of responsiveness towards TLR 7/8 agonist Imiquimod (R837) in TLR 7 knock-out mice [84]. R837 holds an approval for topical treatment of basal cell tumor, actinic keratosis and external genital warts [83, 84]. In a recent review discussing TLRs, R837 was reported to having shown clinical acceptable tolerability, evident immune stimulation and benefits in some patients with renal cell carcinoma, melanoma, lung cancer, hematologic malignancies, breast cancer, ovarian cancer, and cervical cancer. The TLR 7/8 agonist Resiquimod (R848) has been investigated for treating lung-associated allergies, vaccinations, several skin lesions and melanoma via inhalation or topical application [81, 83, 84]. New approaches currently investigate a R848-pro drug formulation (TransCon) given i.t. in combination with pembrolizumab in solid cancers [85] and intraoperatively administered STM-416 (R848) in recurrent bladder cancer [86].

Both trials mentioned above are good examples for how poor solubility of most TLR ligands are circumvented by i.t. or topical application. Therefore, a practical and valid delivery system for systemic application is urgently needed [16, 17, 80]. Within the next years, so-called multifunctional NP might prove feasible for this [87]. A pilot canine trial of spontaneous mast cell tumors had proven efficacy of a polymeric nanosuspension, which was made of a R848-Tocopherol prodrug conjugated to a hyaluronic acid polymer. Beforehand, the local immune stimulation had been demonstrated in rabbits, where signs of inflammation were visible at injection site. R848 injected i.v. served as control and elevated plasmatic TNFα within 120 min but did not lead to a systemic response [88]. Schmid *et al.* have reported effective T cell priming to mice models upon targeted delivery of TLR 4 agonist in an antibody-conjugated polymer [89]. Comparable T cell involvement in a respective knock-out model was documented via intravital fluorescent microscopy for R848 encapsulated in non-polar cavity of cone-shaped molecule β-cyclodextrin, after having visualized empty carrier accumulation in tumor-associated macrophages [90]. Incorporating R848 in phototherapy approaches in breast cancer had been investigated by several authors with photothermal triggered release from NP [91-93]. Nanoemulsions with R848 for antitumor vaccination approaches clearly broaden the spectrum [84, 94].

Despite great achievements in NP-platforms great potential for TLR agonists also lies in synergistically acting combinations with clinically established chemo- or radiotherapy, as recently reviewed [80]. Stereotactic body radiotherapy used in adjuvant treatment of pancreatic ductal adenocarcinoma profited from additional R848. The authors suggested that the initially immunosuppressive TME had been altered upon the combinational treatment plan [95]. In addition, promising preclinical results were documented upon combination of R848 with focal ablation in hepatocellular carcinoma [96] or with radiation in lymphoma [97].

However, the future field of application should not end with cancer and vaccination but rather explore, such as applying R848 on hydrogels to enhanced healing after surgery [71] or inhalation for asthma treatment [98] to name a few.

Considering all preclinical reports mentioned above claiming efficacy of immunoadjuvant-treatments, some patients might not benefit from these strategies. Urban-Wojciuk *et al.* reviewed the association of TLR expression in multiple cancer types to patient's outcome (e.g., immune status tumor, survival). Better clinical outcome was correlated to TLR 5, 7, 8, and 9 and poorer for TLR 4, 7, and 9 expression, which is opposite to preclinical data of the respective tumor models [82]. This highlights the needs to further characterize and optimized preclinical models. Animal models however can only benefit of refinement if data from replacement strategies is considered and selection of species is reviewed to a greater extend.

E) Lipid-based nanoparticles

NP's are widely discussed for their capacity to improve safety and deliver efficacy by modifying the spatiotemporal release profile of enveloped immunomodulatory compounds. Additionally, approaches can profit from local delivery by triggerable release or biological targeting [99]. As recently reviewed, the concepts surrounding NP platforms are manifold and range from inorganic, polymer- or lipid particles to combinations of either with organic materials. The latter compromises viral-derived structures, minicells, membrane-based vesicles that are expelled from mammalian cells, so called exosomes, or that artificially envelope biological active proteins and/or nucleic acids, so called lipid-based NP (LNP) [100, 101]. The utilization of such biomaterials has gained key interest due to the SARS-CoV2 pandemic and associated vaccine development, with three out of nine emergency use authorizations granted by the FDA being mRNA-vaccines making use of a lipid core-shell model [102]. The first use of a LNP as vaccine delivery systems was approved by Allison and Gregoriadis in 1974. A formulation based on egg lecithin, cholesterol and phosphatidic acid demonstrated a safe and effective delivery of diphtheria toxoid [103]. As recently reviewed, various LNP-based vaccination techniques of classical infectious disease, e.g. human papilloma, influenza, or hepatitis A virus as well as in the veterinary field for protection against e.g., Newcastle disease, *Salmonella enteritidis*, or pathogenic *Escherichia coli* strains have since been established. Many more are in the pipeline of clinical trials [104, 105]. With increasing impact, LNP utilized for vaccination approaches have matured to target cancerous disease [99, 100]. The lipid organization of LNP's are the base for their advantages (fast production, flexible lipid composition) as well as their disadvantages (lipids in core, encapsulated cargo affects structure). It is explained by a core-shell model, consisting of a surface layer and an amorphous isotropic core (figure 4.B). This unorganized structure is the key aspect that differentiates them from spherical vesicles such as liposomes. The latter consist of at least one bilayer of phospholipids and an aqueous core [101]. Thereby, the

incorporated lipids can add more than an enveloping value as, depending on the lipid composition and preparation method, different vesicle structures can be achieved forming either unilamellar or multilamellar bilayers (figure 4.A). Either structure can be of interest as both form a protective sphere to their cargo. Multilamellar structures have a higher order of disorganization and tend to entrap lipophilic compounds (e.g., lipopeptides, adjuvants, linker molecules) whereas unilamellar vesicles consist of a sole lipid bilayer enveloping a larger aqueous core additionally allowing the entrapment of hydrophilic (e.g., drugs, proteins, peptides, nucleic acids) and lipophilic drugs [105]. Liposomes additionally allow manipulation of size, charge and surface modification such as attaching antigens [105, 106]. Overall, liposomes represent the most promising drug carrier system known to date because of their high biocompatibility, biodegradability, lack of cytotoxicity, and capability to stability encapsulated their payload, no matter if hydro- or lipophilic [105].

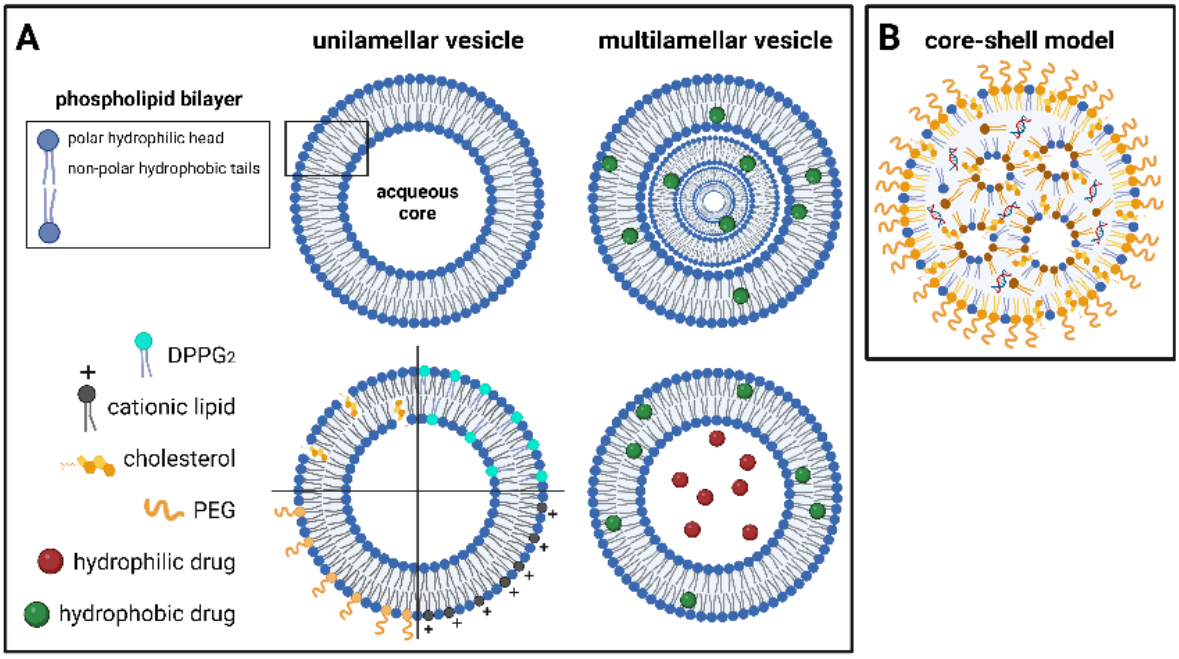

Figure 4: Structural differences of lipid nanoparticles.
(A) Liposomes are formed by phospholipid bilayers in either unilamellar or multilamellar vesicle organization. Thereby enveloping an aqueous core, in which hydrophilic drugs can be loaded. Hydrophobic drugs tend to incorporated into the lipid bilayer. Modifications are achieved by incorporating different phospholipids (e.g. $DPPG_2$ or cationic) or addition of helpers (e.g., cholesterol, PEG). **(B)** A core-shell model illustrates the formation of lipid-based nanoparticles (LNP) encapsulation mRNA.

Early in development, unilamellar liposomes were formed with natural occurring phospholipids, such as phosphocholine (PC), -glycerol (PG), -serine, or phosphatidic acid with either one adding its own value towards functionalizing liposomes [107]. With growing interest of enhancing plasma circulation of such liposomal carriers, further structure-functional properties were achieved by adding cholesterol or synthetic phospholipid derivates [106, 108]. Cholesterol reduces the permeability of membrane structures, hinders phospholipase attacks and increases stability [105, 108, 109]. Another optimization is implementation of synthetic polymers, for example polyethylene glycol (PEG) [106, 108]. The

covalent attachment of PEG on NP (PEGylation) has brought significant advancement in formulating drugs. During production, PEG helps to control particle size and prevents the aggregation during storage. Its ability to co-localized water molecules enhances the solubility of lipophilic carrier. Formation of a corona of plasmatic proteins gives steric hindrance to prevent aggregation or enzymatic attack *in vivo*. Altogether, resulting in increased plasma stability and circulation time upon i.v. injection of a PEGylated particle [100, 110-112]. Currently, there are 21 PEG-containing drugs approved by the FDA of which five having cancer indications. Among these, one is protein-based, two are enzyme-based and another two are lipid-based nanodrugs [111]. In 1995, Doxil®, a DOX-loaded PEGylated liposome was granted approval, for ovarian cancer, AIDS-related Kaposi's Sarcoma, metastatic breast cancer and multiple myeloma [110]. Twenty years later, Irinotecan encapsulated in a PEG-based liposomal formulation, named Onivyde™, was approved for metastatic adenocarcinoma of the pancreas and was extended as a combination regime for patients with gemcitabine-based resistance to chemotherapy [113].

Obstacles in clinical application of conventional lipid nanoparticle

Despite the above-mentioned advantages for liposomes, PEG-based NP have significant liabilities, as unwanted immune responses upon i.v. injection have been reported [100]. The initial contact with PEG can cause IgM-based antibody formation which upon re-presentation of the polymer to the human immune system accelerates clearance, reduces plasma stability, and thereby lowers the therapeutic effect (figure 6.A) [100, 114]. First reports on accelerated blood clearance (ABC) upon second injection of PEG-based liposomes in rats and monkey was reported by Dams *et al.*, who then postulated the presence of a circulating, heat-sensitive, opsonizing factor as probably cause [115]. Mohamed *et al.* had further strengthened this data by proving ABC phenomena in mice, rats, minipigs, and beagle dogs as well as T cell but not B cell deficient mice. All data suggested an involvement of splenic B cells in forming anti-PEG IgM antibodies as well as complement activation [114]. Authors reviewing ABC phenomenon discussed that the prolonged plasma stability of PEGylated formulations might even enforce the response as the immune system has more time to spot PEG [111]. Additionally, the reaction of IgE antibodies towards PEG can cause immediate adverse events like anaphylaxis [100]. This reaction presents complement activation related pseudoallergy (CARPA), which may occur directly upon PEG-injection without the need of pre-exposure [114]. For the already mentioned approved Doxil®, approximately 10 % of treated patients experienced acute infusion-related reactions that resulted in the termination of treatment, which were then correlated to CARPA once mechanism of actions became clear. Noteworthy, CARPA was avoided by choosing slower infusion rates [110].

In addition to adverse events driven by the chosen lipid composition, Doxil®-treated patients were also found to suffer from Palmar Plantar Erythrodysthesia (PPE) or "foot and hand

syndrome". This form of desquamating dermatitis was not induced upon conventional DOX treatment, appointing this off-side toxicity to a formulation dependent effect. Unfortunately, a dose-dependency was found as well as enhancement upon shortening treatment schedule [116]. The mechanism behind this is an immune-mediated inflammatory reaction in the skin due to the accumulation of liposomal drug in skin-resident phagocytes, so called Langerhans cells, in hands and feet. This causes redness, swelling, and pain summarized as PPE [100, 111, 116]. The main lessons learned from Doxil® confirmed paradigm of drug development for clinical translation: the addition of polymers, lipids, and other materials can create additional toxicity concerns [100]. Despite all hurdles, Doxil® enabled a DOX circulation half-life time in humans of ~90 hours (h) and DOX presence in the human circulation of >350 h [110]. If an alternative, non-PEG strategy for DOX can reach comparable efficacy in humans but proprietary safety is up for future preclinical and clinical investigations.

In addition to obstacles derived from chosen lipids, the uptake mechanism into tissue of long-lasting stable formulations is heavily discussed. In NP-derived research, passive accumulation in tumor tissue and at sites of inflammation is attributed to the enhanced permeability and retention (EPR) effect. By forming unorganized capillaries, leaky gap junctions between endothelial cells as well as pore up to a size of 200 nm are formed. The tumor is postulated to counteract the resulting lack of vascularization by promoting sole metabolite diffusion from the peripheral capillaries into the tissue, once a diameter of more than 2 cm is reached [117]. However, there is controversy regarding EPR as only 0.7 % of the administered NP dose is found to be delivered to a solid tumour [118]. For Doxil®, significant reduction of side effects, especially cardiac toxicity, and improvement of the overall patient compliance and quality of life was proclaimed to be attributed to EPR-related pharmacokinetics (PK) and biodistribution (BD) [110]. Even as evidence for enhanced accumulation in tumor tissue upon NP-delivery has been given in mice models, the feasibility of translation is questioned due to altered vesicle structures in comparison to human setting [117, 119]. A recent publication shed light on the occurrence of gaps in tumor vessels of mouse and human tumors with three techniques: transmission electron microscopy, 3D imaging and computational analysis. The authors concluded that the gaps occurred rarely and drug transport through them was not the dominant mechanism of entry [120]. Whether efficacy of penetration is also hampered by high intratumoral pressure building up during tumor growth is questionable [121]. Concern regarding EPR-mediated passive targeting of nanomaterials has led to significant criticism of these technologies for chemotherapeutic drugs and highlights the need for active triggered accumulation approaches [100].

Thermosensitive liposomes

In addition to the above-mentioned structure-functional values of lipids, another feature can be implemented upon careful selection of certain phospholipids: a temperature-triggered change in the integrity of the formed bilayer. The mechanism relies on the physical property of phospholipids to transit at a specific temperature from a solid phase state composed of conformationally ordered lipids acyl chains (gel phase) to a liquid phase with predominantly disordered lipid acyl chains [109]. This phase transition temperature (T_m) is dependent on acyl chain length of the incorporated lipids and their molar ratio within the bilayer [122]. For example, commonly used 1,2-distearoyl-sn-glycero-3-phosphocholine (DSPC) or 1,2-Dipalmitoyl-sn-glycero-3-phosphocholine (DPPC) facilitated the transition at 55 or 42 °C [123]. The increased permeability of lipid-bilayers at T_m can translate to triggered release of an encapsulated drug, so called payload. The challenge is to find a most narrow temperature range still compatible with physiological functions for *in vivo* application [123]. However, the efficacy of drug delivery always goes hand in hand with the plasma stability of the formulation. Some lipids can give stability as they suppress bilayer fluctuations by forming a so-called liquid-ordered phase. The latter is characterized by lipid acyl chains being tightly packed and ordered in a liquid-like bilayer matrix [109]. For cholesterol, presence of > 30 mol% induces this state of stability [122], which leads to the above mentioned prolonged circulation time *in vivo* [105, 108].

In 2004, Lindner *et al.* reported the characteristics of a proprietary synthetic di-palmitoyl-phosphatidyl-diglycerol ($DPPG_2$) with a molecular weight close to the natural di-palmitoyl-phosphatidyl-glycerol (DPPG) but slightly elevated T_m from 40 to 42 °C. Varying ratios of DPPC, DSPC and $DPPG_2$ were explored to form a thermosensitive liposome (TSL). Within this study, heat-triggered release of payload was assessed by loading the fluorescent marker substance, Carboxyfluorescein (CF). Most promising release efficacy at temperatures of mild hyperthermia (HT, 41-42 °C) were reported for TSL with the molar ratio 50:20:30 of DPPC:DSPC:$DPPG_2$ [124]. Robustness of this carrier has been tested by loading several drugs, every time revealing a prolonged plasma half-life (t_α) and rapid HT-triggered release of payload [125-128]. In addition, a comparison to a PEGylated TSL formulation was drawn, highlighting the pivotal characteristics given by the novel synthetic $DPPG_2$-TSL *in vitro* [129]. Clinically, temperatures ranging from 39-43 °C are considered beneficial for cancer treatment. Since the first trials in the 1970s, an increasing amount of devices are being implemented which allowed application of regional HT (40-43 °C) during cancer treatments with increasing relevance [130, 131]. In 2015, the combination of regional HT with chemo- and radiotherapy in several clinical trials has been reviewed elsewhere and the authors postulated promising developments upon optimization of HT devices and protocols [130]. In a recent clinical trial of neoadjuvant chemotherapy in soft tissue sarcoma, the combined

treatment with regional HT led to higher tumour responses, improved survival outcomes and a change in immune contexture [132]. The latter is of interest, as in depth analysis of immune infiltrates of these patients attributed a turn of their initial cold sarcoma into an immunogenic tumor to the addition of regional HT [133]. Mechanisms behind this effect are widely discussed but might be explained by the postulated six 'hallmarks of hyperthermia': blockage of cell survival, activation of cellular stress response, modulation of immune response, evasion of DNA repair, change in TME, and sensitization to radiation and chemotherapy [134]. All are adding to a systemic antitumor immune response [131, 135, 136].

Besides the biological rational for adding regional HT to cancer protocols, it can also enable targeted delivery of chemotherapeutics from TSL. Their selective delivery could help reduce the generalized toxicity encountered in many patients [130]. For the widely used cytostatic DOX, i.v. injection is associated with adverse side effects (e.g., nausea, alopecia, myelosuppression) and, most importantly, high cardio- and nephrotoxicity [137]. Taken together with its concentration-dependent cytostatic effect, DOX is a promising candidate for local delivery approaches. In preclinical settings, DOX-loaded $DPPG_2$-TSL have met these expectations. In an oncological study with feline fibrosarcoma, the combination of $DPPG_2$-TSL-DOX and regional HT has resulted in a significantly better histopathological response in comparison to free DOX. While cats treated with free DOX reached metabolic partial response in 50 %, application of $DPPG_2$-TSL-DOX + HT elevated this to 100 %. In addition, i.v. injection of $DPPG_2$-TSL-DOX was well-tolerated and a promising plasma stability revealed in cats [125]. *In vitro* data of $DPPG_2$-TSL-DOX predicted stability in rat and human plasma [138]. In rats, prolonged plasma stability was confirmed as well as the intravascular HT-triggered release of DOX from $DPPG_2$-TSL-DOX proven (figure 5) [125].

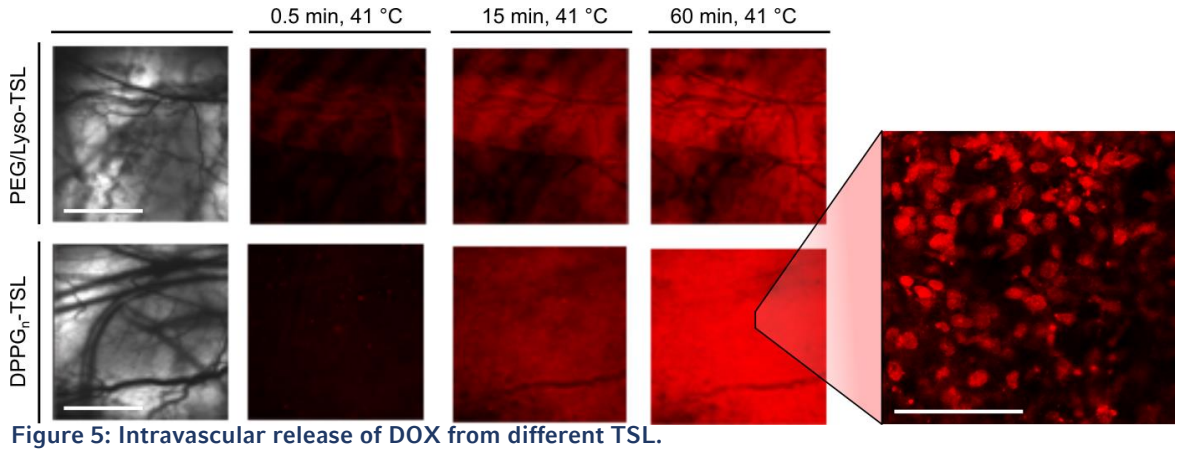

Figure 5: Intravascular release of DOX from different TSL.
In a dorsal skin fold chamber in rats, the release of auto-fluorescent DOX from PEGylated TSL and $DPPG_n$-TSL was recorded via confocal imaging. As long as within the thermosensitive liposome (TSL), DOX is self-quenched and not detectable. Increase in fluorescent intensity started at 0.5 min after injection and was more pronounced at 15 and 60 min. At 60 min, signal strength was stronger in rats injected with $DPPG_n$-TSL. Close up: nuclear uptake of DOX. Corresponding bright-field images are given as first image in each row. Bars are 2 mm [125].

In vitro data of $DPPG_2$-TSL-DOX had also predicted reduced stability in mouse [138].

A consecutive *in vivo* study confirmed this data. While the composition of plasma proteins may be discussed as a key factor for species-specific instability, the additional stress on the

carrier in mice due to accelerated metabolism rates, higher blood pressures and flow rates were assumed [139]. Investigations of human plasma proteins revealed a distinct variation in the formation of a protein corona around different TSL. A unique interaction of high apoprotein C-III and low apoprotein E binding on PEGylated TSL (5 mol% PEG) switched to the opposite for $DPPG_2$-TSL (30 mol% of $DPPG_2$). Following this data, the author studied the effect of multiple application *in vivo*. To do so, TSL were loaded with CF and after i.v. injection in rats, the CF concentration was measured in plasma and tissue. The plasma stability of $DPPG_2$-TSL was reproducible in repetitive injections (figure 6.E) while significant elimination of PEGylated TSL was documented (figure 6.C). In good accordance, repetitive $DPPG_2$-TSL injection did not impact CF accumulation in liver (figure 6.F) while concentrations in liver increased between first and second injection for PEGylated TSL (figure 6.D) [140]. Data is in accordance with initial reports on Doxil®, where elevated liver accumulation upon second injection was reported. This was driven by ABC phenomena and enhanced opsonization after complement activation [110]. Noteworthy, kidney and spleen accumulated less CF upon second injection of PEGylated TSL in above mentioned study. It was discussed that local enhanced liver-entrapment lowers plasmatic content available for organ accumulation [140]. Overall, the absence of antibody formation can be postulated for $DPPG_2$-TSL (figure 6.B).

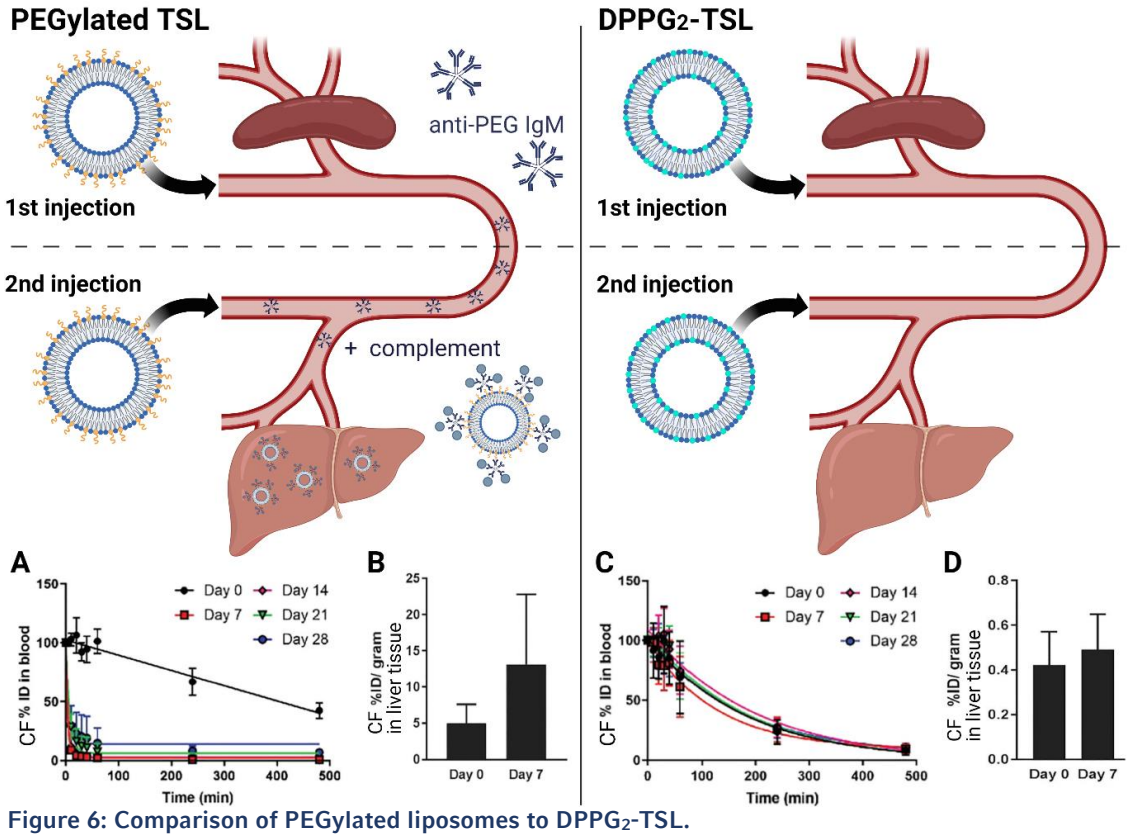

Figure 6: Comparison of PEGylated liposomes to $DPPG_2$-TSL.
First injection of PEGylated TSL induces formation of plasmatic anti-PEG antibodies which eliminate the target upon second injection. For $DPPG_2$-TSL antibody formation was not reported upon multiple injection. In a comparative study in rats, impact of multiple injection was compared between a Carboxyfluorescein (CF)-loaded PEGylated TSL (5 % PEG, 5 µmol/kg) and CF-loaded $DPPG_2$-TSL (30% $DPPG_2$, 75 µmol/kg). Upon second injection of PEGylated TSL, CF **(A)** cleared with accelerated speed from plasma and **(B)** accumulated to a greater extend in liver. Upon second injection of $DPPG_2$-TSL, CF **(C)** plasma profile was comparable and **(D)** liver accumulation did not alter. A-D: modified graphs [14].

F) An insight on used animal models

In 1985, a spontaneous **fibrosarcoma** was discovered in a Brown Norway (BN) rats, which was successfully established as a s.c. non-immunogenic tumor model in 1986 (table 1) [141]. Intensive studies of local perfusion of the hind limb with TNFα in combination with chemotherapeutic agent melphalan showed a therapeutic response of 70-75 % in s.c. BN175 tumor with concomitant hemorrhagic necrosis. The latter was induced by TNFα, which, however, failed to induce a reduction in tumor growth when applied alone [142, 143]. Manusana *et al.* also demonstrated the elicited immune response to be primarily granulocyte-dependent [144]. A study in the same model using the chemotherapeutic agent DOX showed a reduction in tumor growth in only 54 % of animals [145]. Since DOX was applied i.v. with a total dose of 400 µg, the full potential of this chemotherapeutic drug has probably not been reached. In studies with $DPPG_2$-TSL-DOX, dosages of 2 mg/kg (~ 500 µg) were i.v. injected and 10-15-fold increased drug concentration and better therapeutic outcome in the locally heated tumor compared to free agents, other TSLs, and traditional non-thermosensitive liposomes reported [125, 146].

As described above, in **breast cancer** the assessment of infiltrating T cells made clear that this tumor type is never immunological quiescent but rather exhibits highly inhomogeneous infiltration [54]. New therapeutic approaches are needed to circumvent the predominant, tumor-specific immunosuppression. Several immunotherapies are already in clinical trials, including mainly checkpoint inhibitors and CTLA-4 blockers, not least in combination with the established chemotherapeutic agent DOX [147, 148]. PEGylated liposomal DOX is investigated in combination with ipilimumab (monoclonal antibody that enhances T cell-mediated immune response by binding to CTLA-4) and nivolumab (monoclonal antibody that binds PD-1 receptor on T cells and inhibits interaction with ligands on cancer cells) in breast cancer patients [149]. Preclinically, a research group showed that Doxil® or STAT3 inhibition can induce a reduction in tumor growth after radiofrequency ablation in several studies in the R3230 orthotopic mammary adenocarcinoma, later named MatBIII, of Fisher 344 (Fisher) rats [150-152]. In the same rat line, this research group also reported that MatBIII s.c. breast carcinoma has comparable tumor characteristics and treatment responses [153]. More recently, this tumor model shown responsiveness to DOX (2 mg/kg) with a 60 % prolonged survival. The additional injection of the cardioprotective agent dantrolene had further increased the 3-week survival rate to 84 % [137]. This highlights the need for a targeted delivery of DOX to minimize cardiac side effects and realize its full antitumorale potential. Particular attention in previous studies with s.c. MatBIII tumors has been focused on imaging and visualization of liposome distribution. This showed tolerance towards liposomes in Fisher rats and the typical distribution pattern in liver, spleen and tumor [154, 155]. With high reproducibility of of s.c. growth, responsiveness to DOX and an immune contexture of an

immunological 'cold' to 'altered' tumor, this tumor model is a great candidate for combinational approaches (table 1).

The B16 **melanoma** of C57BL/6 (BL6) mouse is a well-established syngeneic tumor model which is widely used in immunological research [156]. It was first described in 1975 by Fidler *et al.* evaluating its ability to metastasize [157]. This tumor has many immunogenic properties and is recognized by the innate and acquired immune system of the host. However, the immune system is not triggered to eliminate the growing tumor. The degenerated melanoma cells possess strategies to inhibit existing immune response, collectively this is referred to as 'immune editing' of the tumor. Inhibitory signals from tumor cells are significantly involved, which ultimately lead to an immune exhaustion [158]. Due to the constant interaction between melanoma and host on an immunological level, this tumor type is an ideal and relevant model for the evaluation of a 'hot' tumor (table 1).Stimulation with an immunoadjuvant may bypass the blocking mechanisms of the tumor and potentially lead to a change in the immune contexture. Exemplary, the successful activation of immune cells by peritumoral application of IL-2 has already been shown [159]. Increasing evidence is given that the activation of the STING signaling pathway can induce an antitumor response to B16 melanoma [35, 160]. Upon i.t. application of CDN, a STING agonist, promising data were reported in B16 model [64, 65].

Table 1: Summary of specificities of used tumor models.

Tumor model	Application within this thesis	Cell line	Origin of cell line
BN175 soft tissue sarcoma	s.c. growth in syngeneic BN rats	BN175	Isolated from spontaneous fibrosarcoma occurring in female BN rats [141]. Immunological 'cold' tumor.
MatBIII mammary adenocarcinoma	s.c. growth in syngeneic Fisher rats	MatBIII	Isolated from metastatic site (ascites tumor) of R3230 solid mammary adenocarcinoma in mammary glands of female Fischer rats (ATCC-CRL-1666 13762 MAT B III). Immunological 'cold' or 'altered' tumor with low rate of metastasis formation.
B16 melanoma	s.c. growth in syngeneic BL6 mice	B16F10	B16F10 isolated from skin tissue with melanoma in BL6 mice (ATCC-CRL-6475). Immunological 'hot' tumor with high metastatic potential and infiltration into skin (orthotopic location).

G) Scope of the thesis

The main focus of the thesis was the in-depth investigation of $DPPG_2$-TSL-DOX and novel $DPPG_2$-TSL-ADU and $DPPG_2$-TSL-R848 for stimulating an antitumor response in preclinical settings. The thesis is formed by the following three main parts:

Objective of the first part was to gain a deeper understanding of *in vivo* behaviour of $DPPG_2$-TSL-DOX in two different species: rats and mice. For the first time, DOX versus $DPPG_2$ biodistribution (BD) was assessed with lamp-HT, which led to in depth analysis in rats bearing one or two tumors. Consecutively, responsiveness of BN175 soft tissue sarcoma model was tested for the first time with lamp-HT in comparison to clinical relevant controls, which led to an analysis of DOX and $DPPG_2$ in a pharmacokinetic (PK) study. A comparison of species was enabled by implementing protocols for mice, mimicking experimental rat set up as close as possible. Feasibility of protocols was tested with $DPPG_2$-TSL-DOX, thereby revealing PK profile and efficacy of water bath-based versus lamp-based HT on DOX accumulation in heated tumor tissue. A B16 melanoma model in mice was established beforehand.

In the second part, impact of osmotic condition of newly designed liposomal formulation of STING agonist ADU ($DPPG_2$-TSL-ADU) was investigated *in vivo* and the most promising formulation selected to assess the therapeutic response in BN175 soft tissue sarcoma model in comparison to preclinically-relevant controls. Analysis of *in vivo* distribution of ADU and $DPPG_2$ was conducted to investigate efficacy of HT-triggered accumulation in heated tumor tissue. A second rat model was established to enable future confirmation of therapeutic efficacy of ADU.

In the third part, liposomal formulation of R848 ($DPPG_2$-TSL-R848) was investigated *in vivo* with respect to plasma stability, HT-triggered release efficacy, HT-dependent tumor accumulation, and feasibility of therapeutic application in BN175 soft tissue sarcoma model. Within the latter, most robust parameters for evaluating antitumor response upon single and repetitive injection of $DPPG_2$-TSL-R848 in comparison to free R848 were found. With $DPPG_2$-TSL-DOX at hand, impact of tumor tissue priming with DOX was investigated in a combinational treatment approach as well as metastasis model.

III. Materials and Methodology

A) Materials

Table 2: Lipids.

Lipid	Sum Formula	Molar mass (g/mol)	Supplier
1,2-Dipalmitoyl-sn-glycero-3-phosphocholine (DPPC)	$C_{40}H_{80}NO_8P$	734.06	Corden Pharma, Liestal, Switzerland
1,2-Dipalmitoyl-sn-glycero-3-phosphodiglycerol (DPPG$_2$)	$C_{41}H_{81}O_{12}P$	819.04	Thermosome GmbH, Planegg, Germany
1,2-Distearoyl-sn-glycero-3-phosphocholin (DSPC)	$C_{44}H_{88}NO_8P$	790.17	Corden Pharma, Liestal, Switzerland

Table 3: Chemicals.

Component	Supplier
Acetic acid	Carl Roth GmbH, Karlsruhe, Germany
Acetonitrile (ACN)	J.T. Baker, New Jersey, USA
Ammonium acetate (NH_4OAc)	Merck KGaA, Darmstadt, Germany
Ammonium sulfate	PanReacAppliChem, Darmstadt, Germany
Chloroform	Carl Roth GmbH, Karlsruhe, Germany
Citrate	Carl Roth GmbH, Karlsruhe, Germany
Di-methyl sulfoxide (DMSO)	Carl-Roth, Karlsruhe, Germany
Ethanol (EtOH)	Carl Roth GmbH, Karlsruhe, Germany
Formaldehyde	Carl Roth GmbH, Karlsruhe, Germany
Formic acid (FA)	Merck KGaA, Darmstadt, Germany
HEPES	Carl Roth GmbH, Karlsruhe, Germany
Methanol (MeOH)	Carl Roth GmbH, Karlsruhe, Germany
potassium di-hydrogenphosphate (KDP)	Merck KGaA, Darmstadt, Germany
Sodium acetate (NaOAc)	Carl Roth GmbH, Karlsruhe, Germany
Sodium bicarbonate	Merck KGaA, Darmstadt, Germany
Sodium chloride (NaCl)	Carl Roth GmbH, Karlsruhe, Germany
Silver nitrate	Merck KGaA, Darmstadt, Germany
Trichloroacetic acid	Merck KGaA, Darmstadt, Germany
Trifluoroacetic acid (TFA)	Carl-Roth, Karlsruhe, Germany
Triton X-100	Carl Roth GmbH, Karlsruhe, Germany

Table 4: Laboratory prepared buffers and solutions.
All buffers and solutions were prepared with purified deionized water from an ultrapure Milli Q Advantage water system.

Component	Composition
Ammonium sulfate buffer, pH 4	300 mM ammonium sulfate adjust to pH 4.0
Citrate buffer	300 mM citrate adjust to pH 3.0 or pH 4
Cryo-buffer pH 7.4	300 mM Sucrose 40 mM HEPES 60 mM NaCl adjust to pH 7.4 with NaOH
HEPES-buffered saline (HBS) pH 6.4	80 mM HEPES 120 mM NaCl adjust to pH 6.4 with NaOH

HEPES-buffered saline (HBS) pH 7.4	20 mM HEPES 150 mM NaCl adjust to pH 7.4 with NaOH
HEPES-buffered water (HBW) pH 7.4	20 mM HEPES adjust to pH 7.4 with NaOH
SRB	0.5 % SRB 1 % acetic acid

Table 5: Commercially available buffers, solutions, culture media and biologicals.

Component	Supplier
Dulbecco's Modified Eagle's medium (DMEM), **s**odium bicarbonate, L-glutamine, high glucose	ATCC, Virginia, USA
Dulbecco's phosphate-buffered saline	PAN-Biotech, Aidenbach, Germany
Fetal calf serum (FCS)	Biochrom, Berlin, Germany
Human plasma	BioIVT, West Sussex, UK
Isopropanol 70 %	B.Braun SE, Melsungen, Germany
Isotonic 0.9 % NaCl solution (saline)	B.Braun SE, Melsungen, Germany
McCoy's 5A modified (McCoy's 5A), **s**odium bicarbonate, L-glutamine	Thermo Fisher Scientific Inc, Waltham, USA
Mouse plasma	BioIVT, West Sussex, UK Biotrend, Köln, Germany
Penicillin/Streptomycin	Biochrom, Berlin, Germany
Porcine plasma	BioIVT, West Sussex, UK
Rat plasma	BioIVT, West Sussex, UK Biotrend, Köln, Germany
RPMI 1640 medium (RPMI 1640), HEPES, L-glutamine	Thermo Fisher Scientific Inc, Waltham, USA
RPMI 1640 medium (RPMI 1640), **s**odium bicarbonate, L-glutamine	Biochrom, Berlin, Germany Merck KGaA, Darmstadt, Germany
Trypan-blue staining solution	Thermo Fisher Scientific Inc, Waltham, USA
Trypsin-EDTA	Biochrom, Berlin, Germany

Table 6: Consumables.

Consumable	Supplier
Amicon Ultracel 30K filters	Merck KGaA-Millipore, Darmstadt, Germany
Cannula (23 G, 25 G, 27 G or 30 G)	BD Mikro Lance, Becton Dickson GmbH, Franklin Lakes, USA Stefica®, B.Braun SE, Melsungen, Germany
Cell culture flask	Thermo Fisher Scientific Inc, Waltham, USA
Column filter KurdKatcher ULTRA HPLC In-line (0.5 µm)	Phenomenex Ltd., Aschaffenburg, Germany
Cryo-nunc tubes	Thermo Fisher Scientific Inc, Waltham, USA
C18 pre-column SecurityGuard Ultra Cartridges (3 mm)	Phenomenex Ltd., Aschaffenburg, Germany
C18 column Luna Omega PS® (1.6 µm, 50 × 2.1 mm)	Phenomenex Ltd., Aschaffenburg, Germany
C18 column Kinetex® (1.6 µm, 50 × 2.1 mm)	Phenomenex Ltd., Aschaffenburg, Germany
C18 column Kinetex® (2.6 µm, 50 × 2.1 mm)	Phenomenex Ltd., Aschaffenburg, Germany
C18 column Kinetex® (2.6 µm,100 Å, 100 x 3 mm)	Phenomenex Ltd., Aschaffenburg, Germany
Disposable scalpel	Feather, Kita-KU, Japan
Falcon (50 or 15 ml)	Thermo Fisher Scientific Inc, Waltham, USA
Glass beads	SiLibeads Typ M, 3 mm
Glass test tubes	Duran®, Mainz, Germany
HPLC vial	WICOM GmbH, Heppenheim, Germany

Illustra™ MicroSpin™ columns	Cytiva Europe GmbH, Freiburg im Breisgau, Germany
IN-stopper	B.Braun SE, Melsungen, Germany
Insulin syringe	Becton Dickson GmbH, Franklin Lakes, USA
Introcan safety (23 G)	B.Braun SE, Melsungen, Germany
Lancette	B.Braun SE, Melsungen, Germany
LDPE Tubing (internal diameter 0,28mm)	RCT Reichelt Chemietechnik GmbH, Heidelber, Germany
LIGNOCEL FS 14-bedding	Ssniff-Spezialdiäten GmbH, Soest, Germany
Litium-Heparin Microvette	Sarstedt, Nürmrecht, Germany
Makroloncage (Typ IV long, Typ V) including open-top	Techniplast S.p.A., Buguggiate, Italy
Makroloncage (Typ II long, Typ V) including open-top	Techniplast S.p.A., Buguggiate, Italy
Metal tungsten carbide bead (3 mm)	Qiagen, Hilden, Germany
Mice enrichment (red hut, red tunnel)	Bio-Serv, Flemington, USA
Neubauer Couting chamber	Semadeni, Ostermundingen, Switzerland
Phenyl column XBridge® BEH (3.5 µm, 5 x 2.1 mm)	Waters, Eschborn, Germany
Phenyl column XBridge® (3.5 µm, 130 Å, 5 x 2.1 mm)	Waters, Eschborn, Germany
PD-10 columns Sephadex-G25 MPD-10 column	GE Healthcare, München, Germany
Polycarbonate Whatman® membrane, diam. 19 mm (200 or 100 nm)	Merck KGaA, Darmstadt, Germany
Polycarbonate membrane, diam 25 mm (200 or 100 nm)	Merck KGaA, Darmstadt, Germany Avestin, Mannheim, Germany
Rat enrichment (Fat rat hut, red tunnel, red crawl ball)	Bio-Serv, Flemington, USA
Reaction tubes (0.5, 1 or 2 ml)	Eppendorf GmbH, Hamburg, Germany
Rodent diet	Ssniff-Spezialdiäten GmbH, Soest, Germany
Round-bottom flask	Schott AG, Mainz, Germany
Sepharose™ CL-4B	GE Healthcare, Illinois, USA
Serological pipettes	Thermo Fisher Scientific Inc, Waltham, USA
Silkam® needle and thread combination	Carl Roth GmbH, Karlsruhe, Germany
STRATA-X columns	Phenomenex Ltd, Aschaffenburg, Germany
Syringe	Becton Dickson GmbH, Franklin Lakes, USA B.Braun SE, Melsungen, Germany
Syringe filter (0.22 µm)	Sartorius AG, Göttingen, Germany
Vacutainer butterfly safety lok	Becton Dickson GmbH, Franklin Lakes, USA

Table 7: Devices.

Device	Supplier
Analytical work	
Fluorometer	Cary Eclipse, Varian Inc., Palo Alto, California, USA
Heat block Reacti-Therm	Thermo Fisher Scientific Inc, Waltham, USA
High-pressure extruder	Lipex™ Thermobarrel Extruder, Northern Lipids Inc., Burnaby, Canada
High-speed centrifuge	Avanti-J26XP, Beckman Coulter, Krefeld, Germany
Milli Q Advantage	Merck KGaA Millipore, Darmstadt, Germany
Avanti J-26XP Zentrifuge (Rotor JA.25.50)	Beckman Coulter Inc, Krefeld, Germany
Osmometer	Vapro 5600, Wescor Inc., Logan, Utah, USA
Precision scale 205 a SCS	Precisa Gravimetrics, Dietikon, Swiss

Rotary evaporator	Laborota 4001, Heidolph Instruments GmbH, Schwabach, Germany
Scientific UltiMate 3000 with charged aerosol detector (CAD Corona Veo)	Thermo Fisher Scientific Inc, Waltham, USA
Scientific UltiMate 3000 with diode array detector	Thermo Fisher Scientific Inc, Waltham, USA
Sciex ExionLC AD with Sciex X500B	AB Sciex Pte. Ltd., Framingham, Massachusetts, USA
Table centrifuge 5415 D	Eppendorf GmbH, Hamburg, Germany
Thermoshaker comfort	Eppendorf GmbH, Hamburg, Germany
TissueLyser	Qiagen, Hilden, Germany
Ultracentrifuge RC-5	Thermo Electron Corporatins, Ostercode, Germany
Vacuum chamber Supelco	Sigma Aldrich GmbH, München, Germany
Vacuum pump	Arcotronics GmbH, Landsberg, Germany
Waters HPLC system with 510 HPLC pumps, 717plus autosampler and 470 fluorescence detector	Waters GmbH, Eschborn, Germany
Zeta Sizer Nano ZS	Malvern Panalytical Ltd, Worcestershire, UK
Cell culture work	
Centrifuge labofuge 400 R	Haereus Deutschland GmbH, Hanau, Germany
Circulation thermostat	Reitz Medical GmbH, Rosenheim, Germany
Cool cell cryocontainer	Thermo Fisher Scientific Inc, Waltham, USA
Incubator chamber	Binder, Tuttlingen, Germany
Laminar flow	Thermo Fisher Scientific Inc, Waltham, USA
Microplate reader MRX	Dynatech Laboratories, Rückersdorf, Germany
Microscope Axiovert 40 CFL	Carl Zeiss Microscopy GmbH, Jena, Germany
Suction pump unit BVC 21	Vacuubrand, Olching, Germany
Water bath GFL	Memmert, Schwabach, Germany
Animal work	
Aldabsorber ventilator (mice)	Rothacher Medical GmbH, Spisi, Switzerland
Aldabsorber ventilator (rats)	Vettech Solutions Ltd, Cheshire, UK
Circulating-thermostat (rats)	Julabo Labortechnik GmbH, Seelbach, Germany
Cold-light lamp 3000 G	Exacta Optech Labcenter S.p.A., San Prospero, Italy
Electrical heating plate (mice), TCAT-2LV Controller	Physitemp, Clifton, USA
Heating pad (rats)	Vettech Solutions Ltd, Cheshire, UK
Induction box (mice)	Rothacher Medical GmbH, Spisi, Switzerland
Induction box red (rats)	Vettech Solutions Ltd, Cheshire, UK
Inhalation narcosis system (mice)	Rothacher Medical GmbH, Spisi, Switzerland
Inhalation narcosis system (rats)	Vettech Solutions Ltd, Cheshire, UK
Mice nose mask	Groppler Medizintechnik, Deggendorf, Germany
Precision scale PFB 6000-1	Kern und Sohn GmbH, Balingen, Germany
Rat nose mask	Vettech Solutions Ltd, Cheshire, UK
Shaver contura	Wella, Darmstadt, Germany
Typ K temperature probe	Voltcraft, Conrad Electronic SE, Hirschau, Germany
Water bath JB Aqua 12 (mice)	Grant instruments Ltd, Cambridgeshire, UK
Water bath JB Aqua 26 (rats)	Grant instruments Ltd, Cambridgeshire, UK
K204 temperature datalogger	Voltcraft, Conrad Electronic SE, Hirschau, Germany

Table 8: Pharmaceutical products and drug substances.

Pharmaceutical product	Supplier
ADU-S100, ammonium salt (purity 98,97%)	MedChemExpress Lcc, New Jersey, USA
Buprenorphin® sine	Elanco, Bad Homburg, Germany
Doxil®, in EU available with brand name Caelyx®	Janssen Pharmaceutical Companies, Beerse. Belgium
c-di-AMP	InvivoGen, San Diego, California, USA
Daunorubicin	Teva GmbH, Ulm, Germany
Doxorubicin Aurobindo (Doxorubicin hydrochloride)	Puren Pharma GmbH, München, Germany
$DPPG_2$-TSL	Thermosome GmbH, Planegg, Germany
$DPPG_2$-TSL-ADU	Thermosome GmbH, Planegg, Germany
$DPPG_2$-TSL-R848	Thermosome GmbH, Planegg, Germany
Imiquimod	TCI chemical, Eschborn, Germany
Isofluran CP®	CP-Pharma, Burgdorf, Germany
Metacam®	Boehringer Ingelheim Pharma GmbH, Ingelheim am Rhein, Germany
Octenisept	Schülke GmbH, Norderstedt
Release®	WDT GmbH, Garbsen, Germany
Resiquimod	MedChemExpress Lcc, New Jersey, USA
Vetaglin®	Intervet Deutschland GmbH, Unterschleißheim, Germany

Table 9: Cell lines.

Cell line	Supplier
B16F10, ATCC-CRL-6475 (B16)	ATCC, Manassas, Virginia, USA
BN175	Timo ten Hagen, Erasmus MC, Rotterdam
13762 Mat B III, ATCC-CRL-1666 (MatBIII)	ATCC, Manassas, Virginia, USA

Table 10: Experimental animals.

Animal species	Strain	Specifics	Supplier
Mouse,	C57BL/6 J (BL6)	male and female, 20 - 25 gram	Charles River Laboratories, Sulzfeld, Germany
Rat,	Brown Norway (BN)	male, 160 - 180 gram	Charles River Laboratories, Sulzfeld, Germany
Rat,	Fisher 344 (Fisher)	female, 160 - 180 gram	Charles River Laboratories, Sulzfeld, Germany

Table 11: Software.

Program	Usage
Bio Render©	Illustrations
EndNote©	Bibliotheca
Excel by Microsoft©	Transformation of raw data, calculations
Graph pad prism©	Graphs and in-graph statistics In-graph statistical analysis was conducted with t-test or TWO-WAY Anova with $P < 0.05$ (*), < 0.01 (**), < 0.001 (***) and < 0.0001 (****)
MPower Waters©	HPLC data analysis
Origin©	Statistics pharmacokinetic data
Power Point by Microsoft©	Timelines

B) Liposomal work package

Methods previously established within the working group for DOX [124, 125, 127, 138, 146] and R848 [161] were used in modified forms. Protocols conducted for ADU-S100 (ADU) were established by Thermosome GmbH (Planegg, Germany).

a. Liposome preparation

All lipid films prepared were based on a molar ratio of 50:20:30 of DPPC:DSPC:$DPPG_2$ and resulting liposomal formulation referred to as $DPPG_2$-TSL. For later *in vivo* application, solutions were pushed through a 0.22 µm syringe filter beforehand, if applicable.

DOX-/R848-loaded $DPPG_2$-TSL

Liposomes were prepared by a lipid film and extrusion method [124]. Powdery lipids were weighted, dissolved in chloroform/methanol (MeOH) solution (9:1, v:v) and mixed according to molar ratio in a round-bottom flask. Using a rotary evaporator, the organic solvent was removed under vacuum (40 °C, 375 mbar) and dried in two steps, first with 150 mbar (60 °C, > 20 min) and after discarding distillate with 30 mbar (60 °C, > 90 min) to allow formation of a homogenous dry lipid film. Hydration was conducted by adding several glass beads and appropriate buffer in relation to respective purpose (table 12) for < 15 min at 60 °C in the rotary evaporator with < 220 rpm. Obtained multilamellar vesicles were immediately extruded ten times through 200 nm polycarbonate membranes using a high-pressure extruder set at 60 °C. The resulting unilamellar vesicles were stored at 2-8 °C until active loading was performed in a thermoshaker via a gradient method already published with minor modifications [138]. When preparing for DOX-loading, acidic pH of solution was neutralized by adding 1 M sodium bicarbonate pH 8 while for R848-loading a transmembrane proton (H^+) gradient was established by buffer exchange via PD-10 column equilibrated in HEPES-buffered saline (HBS) pH 6.4. With final lipid concentration of 3 mM kept constant, dissolved drug was added to the liposomal suspension according to desired drug:lipid ratio (D:L) and placed in a thermoshaker under specific loading-conditions (table 12). For R848-loading, mixture was stirred at 37 °C for 15 min, then centrifuged at 75 000 x g for 60 min at 15 °C and liposomal pellet resuspended in cryo-buffer pH 7.4 for storage at -20 °C. For DOX-loading, encapsulation process was monitored by assessing the decrease of DOX fluorescence intensity every 10 min via fluorescence spectroscopy (Ex 470 nm /Em 555 nm) while mixture was stirred for 60 min at 37 °C. Afterwards, liposomal pellet was created by centrifuged with J-26XPcentrifuge (75600 x g, 60 min, 15 °C) and resuspended in HBS pH 7.4 for storage at -20 °C.

Table 12: Drug-dependent loading condition for high-pressure extrusion

Drug	Hydration solution	Stock solution drug	Extra-liposomal buffer	Loading	D:L (mol:mol)
R848	300 mM citrate pH 3	1 mg/ml water pH 4	HBS pH 6.4	15 min/ 37 °C	0.05
DOX	300 mM citrate pH 4	5 mg/ml water	1 M sodium bicarbonate pH 8	60 min/ 37 °C	0.05

ADU-loaded $DPPG_2$-TSL

Powdery lipids were weighted, dissolved in chloroform/MeOH solution (9:1, v:v) and mixed according to molar ratio with 50 mM lipids in a glass tube. Solvent was evaporated for 30 min at 40 °C and further 3 h at 60 °C in a heat block under steady stream of nitrogen ($N_{2\ stream}$). Drying was conducted stepwise to allow formation of a homogenous dry lipid film. Hydration was performed by adding several glass beads and ADU (8 mg/ml), solubilized in HBS pH 7.4 or HEPES-buffered water (HBW) pH 7.4, under gentle shaking in a 60 °C water bath for 30 min. Entire liposome dispersion was transferred in a fresh glass tube, immerged in liquid N_2 until fully frozen and immediately thawed in a water bath set at 60 °C. This freezing and thawing (F/T) cycle was repeated five times before obtained multilamellar vesicles were transferred in a gas tight syringe and loaded in hand-extruder mounted with 200 nm polycarbonate membrane filter. After 5 min of equilibration time, extrusion was conducted 17 times. Resulting unilamellar vesicles were stored at 2-8 °C until unencapsulated ADU was separated from liposomal fraction by size exclusion chromatography. For this, equilibrated (HBS pH 7.4) PD-10 columns were loaded with suspension and liposomes eluted with HBS pH 7.4 and stored at 2-8 °C until further characterized.

b. Liposome characterization

All $DPPG_2$-TSL formulated were characterized in a standardized order. A batch was not cleared for *in vivo* use, if significant deviation from expected size (section i), drug-content (section ii), amounts of lipids and lipid degradation products (section iii), encapsulation efficacy (section iv), or functionality in release kinetics (section v) were revealed.

i. Dynamic light scattering

By dynamic light scattering (DLS), hydrodynamic diameter (Z-average; size), Poly-Dispersity Index (PDI) and ζ-potential (ζ-POT) were estimated for produced liposomal batches. For this, samples were diluted 1:50 (v:v) in 150 mM NaCl and measured in triplicates with a Zeta Sizer.

ii. High-performance liquid chromatography

Qualitative and quantitative analysis of drug content via high-performance liquid chromatography (HPLC) was conducted with a Scientific UltiMate 3000 equipped with diode array detector. Detection of R848 was achieved with a slightly adapted method [161] whereas protocols developed by Thermosome GmbH (Planegg, Germany) were followed for ADU and DOX.

According to the type of matrix (e.g., HBS pH 5.2/pH 7.4, FCS or rat plasma), calibration samples were created by spiking drug and internal standard in in a range between 5 to 100 (R848), 0.2 to 100 (ADU), or 40 to 1000 (DOX) µg/ml. Calibration samples and drug-containing samples were prepared with acetonitrile (ACN)-method for later detection of R848 and ADU as follows: after pre-dilution to fit calibration range (R848: HBS pH 5.2, ADU: HBS pH 7.4), a mixture (v:v) with ACN (R848: 1:3, ADU: 1:9) was prepared and incubated at room temperature (RT) for 10 min under gentle shaking. For R848-detection, sample was centrifuged at 20000 x g for 6 min (RT) and 500

µl supernatant transferred in a glass tube. For ADU-detection at 14000 x g for 10 min (RT) and 950 µl supernatant transferred in a glass tube. Solvent of all glass tubes was evaporated in a heat block set a 40 °C, residual resolved in either mobile phase A (R848, table 13) or 10 % ACN (ADU) and transferred in a reaction tube. After centrifugation (20000 x g, 10 min, RT), supernatant was transferred in HPLC vials. Calibration samples and drug-containing samples were prepared with triton-method for later detection of DOX as follows: samples were mixed 1:1 (v:v) with 10 % triton-X100 and incubated for 15 min at 45 °C in a thermoshaker. Then, internal standard was added, mixture diluted in mobile phase A (table 13), vortexed, centrifuged (14000 rpm, 10 min, RT) and supernatant transferred in HPLC vials. HPLC was conducted with most critical parameters summarized in table 13.

Table 13: Parameters of Scientific UltiMate 3000 for detection of drug.

Drug	Pre-column	Column	Detection (nm)	Flow (ml/min)	Mobile phase A	Mobile phase B	Internal standard
R848	C18 (3 mm)	C18 column (2.6 µm,100 Å, 100 x 3 mm) at 30 °C	242	0.5	0.1 M NaOAc pH 4 in ACN 85:15, v:v	ACN	R837
ADU	C18 (3 mm)	C18 column (2.6 µm,100 Å, 100 x 3 mm) at 35 °C	210	0.5	20 mM NH_4OAc	ACN	-
DOX	C18 (3 mm)	C18 column (2.6 µm,100 Å, 100 x 3 mm) at 40 °C	480/560	1.0	80 mM KDP in ACN 73:27, v:v	90 % ACN	Dauno-rubicin

iii. Lipid, fatty acids and lyso-lipid determination

HPLC method for lipid-detection previously described [161] enabled qualitative and quantitative analysis of DPPC, DSPC and $DPPG_2$. Therefore, respective lipids solubilized in MeOH ranging from 116 to 497 µM were used for calibration samples. Liposomal sample was diluted 1:29 (v:v) in water to fit the range of calibration curves, vortexed and transferred in a HPLC vial. This method allows additional quantitative detection of lipid degradation products, such as fatty acids. Therefore, palmitic and stearic acid solubilized in MeOH ranging from 96 to 981 µM were used for calibration samples. Liposomal sample was diluted 1:24 (v:v) in water, vortexed and transferred in a HPLC vial. Samples were analyzed via a Scientific UltiMate 3000 equipped with charged aerosol detector (CAD Corona Veo). Most critical parameters are summarized in table 14.

Table 14: Parameters of Scientific UltiMate 3000 for detection of lipids and fatty acids.

Pre-column	Column	Flow	Mobile phase A	Mobile phase B
Phenyl column (3.5 µm, 5 x 2.1 mm)	Phenyl column (3.5 µm,130 Å, 150 x 2.1 mm) at 35 °C	0.4 ml/min	0.1 M NaOAc pH 6 in MeOH 85:15, v:v	MeOH

iv. Encapsulation efficiency

Having measured payload and lipid content via HPLC (section ii and iii), the encapsulation efficiency (EE) was calculated considering molar ratio of D:L estimated during loading (initial) and final batch (final) by using the following formula:

$$EE\ (\%) = (D{:}L)_{final} \div (D{:}L)_{initial} \times 100 \qquad \textbf{Equation 1}$$

v. Temperature-dependent drug release

In general, loaded $DPPG_2$-TSL were incubated at increasing temperatures to profile temperature-

dependent release (TDR) with a protocol previously established [138] for DOX and R848 [161] as well as a modified version developed for ADU by Thermosome GmbH (Planegg, Germany).
Sample was diluted in FCS or species-specific plasma, except for DOX-loaded TSL which were pre-diluted in HBS pH 7.4 due to high content (table 15). Each sample was incubated for 5 min at RT and 37 to 45 °C or 1 h at 37 and 45 °C. To reach sample's target temperature within few seconds when placed in thermoshaker, device was pre-heated and mildly shaking (750 rpm). Release was immediately blocked after with cold HBS pH 7.4 (table 15). Maximal content release of 100 % (I_∞) was achieved by destroying liposomal formulations via triton X-100. Therefore, samples were diluted as described previously, incubated with 10 % triton X-100 (table 15), for 15 min at 45 °C and blocked by adding cold HBS pH 7.4 (table 15). Samples were stored at 2-8 °C until measured (DOX) or further worked up (R848, ADU), as described below.

Table 15: Dilution factors depending on drug loaded in $DPPG_2$-TSL.

Drug	FCS / species-specific plasma	10 % triton X-100	Blocking cold HBS pH 7.4
DOX	1*:10 (v:v); *pre-diluted 1:3 (v:v) HBS pH 7.4	1:1 (v:v)	1*:50 (v:v); * for I∞: pre-diluted 1:4.5 (v:v) HBS pH 7.4
R848	1:10 (v:v); for I∞: 1:1 (v:v)	1:1 (v:v)	1:3 (v:v); for I∞: 1:7 (v:v)
ADU	1:10 (v:v)	2:1 (v:v)	2:1 (v:v); for I∞: 1:1.3 (v:v)

DOX release was measured by fluorescence spectroscopy (Ex 470 nm /Em 555 nm). Release was calculated with intensities (I) measured at specific temperature (T°C) or RT as follows:

$$release\ (\%) = (I_{T°C} - I_{RT}) \div (I_\infty - I_{RT}) \times 100 \qquad \textbf{Equation 2}$$

Release of R848 or ADU cannot be detected via fluorescence, hence, samples needed to be worked up by amicon filtration to separate released drug from respective liposomal fraction. Amicon filters were passivated overnight (5 % triton X-100), loaded with 300 µl of stored sample and centrifuged (14000 x g, 10 min, 2-8 °C). Flow through containing released drug was collected and stored at - 20 °C until HPLC measurement (section ii).
Driven by low recovery rates of free ADU via amicon filtration from release assays with $DPPG_2$-TSL-ADU, an alternative method was needed. Hence, extraction of liposomal bound ADU via centrifugation in spin columns was conducted. TDR was conducted as described above with samples being placed on ice instead of blocking with HBS pH 7.4. Samples were stored at 2-8 °C until self-packed spin columns were prepared. These columns were packed with 766.7 ml Sepharose™ CL-4B in two consecutive steps (900 and 250 µl) via centrifugation with 1 x g for 2 min at RT after having diluted the material 2:1 (v:v) in 150 mM NaCl beforehand. Then, packed spin columns were washed three times with 150 mM NaCl via centrifugation (1 x g, 2 min, RT) and stored less than 10 min at RT until usage. So-prepared spin columns were loaded with 125 µl of sample. After elution via centrifugation (1 x g, 2 min, RT), flow through containing liposomal fraction was collected and stored at - 20 °C until HPLC measurement (section ii).

C) *In vitro* work package

Cells were cultured in a humidified atmosphere at 37 °C and 5 % CO_2 and established protocols of BN175 cells [127] were modified for the newly introduced MatBIII and B16F10 cells. Culture medium was selected according to specifics of respective cell line (table 16) and, before being used as growth medium, was supplemented with 10 % FCS and 1 % antibiotics (penicillin/ streptomycin). Cell count of alive cells was determined with a Neubauer counting chamber after staining with Trypan-blue (1:1, v:v). Contamination with mycoplasma was monitored in cell culture supernatant via PCR and results were negative for every cell line until end of this thesis.

Table 16: Specificities of cultured cell lines.

Cell line	Culture medium	Macroscopy	Centrifugation
B16F10	DMEM, sodium bicarbonate, L-glutamine, high glucose	adherent, black, elongated cells	5 min, 377 x g
BN175	RPMI 1640, sodium bicarbonate, L-glutamine	adherent, transparent, spindle like cells	2 min, 377 x g
MatBIII	McCoy's 5A, sodium bicarbonate, L-glutamine	lightly attached, formation of clusters, transparent, rounded cells	3 min, 125 x g

a. Cell passaging

Cells were passaged once confluency of 70 - 80 % was reached. Adherent cells were gently washed twice in Dulbecco's phosphate-buffered saline (DPBS) before detachment was induced by adding 0.25 or 0.5 % Trypsin-EDTA (B16F10 or BN175 cells, respectively) for ~ 2 - 5 min at 37 °C. Process was blocked by adding respective growth medium 1:5 (v:v) and cell solution transferred in a tube for centrifugation. Afterwards, supernatant was discarded, cell pellet resuspended in respective growth medium and split 1:10 (v:v) into a fresh flask. For confluent cells, flask was rigorously tapped, entire cell suspension collected in a tube and washed twice with DPBS via centrifugation. Afterwards, cell pellet was resuspended in respective growth medium, cell content counted, and a distinct number of cells split into a fresh flask.

b. Cell thawing

The respective cell-containing cryo-nunc tube was taken from the liquid N_2 tank and immediately thawed in a water bath set at 37 °C. As soon as thawing was completed, cells were slowly added to 10 ml of respective growth medium and centrifuged. Cell pellet was resuspended in respective growth medium, transferred in a flask and placed in the incubator until first passaging (section a) was conducted when ~ 90 % confluent. Cells were passaged four times for revitalization before being used in experiments.

c. Cell freezing

For long-term storage, 1.5 x 10^6 cells/ml were frozen in individual cryo-nunc tubes. Therefore, cells were counted, centrifuged, and resuspended in the corresponding volume of cold 5 % (B16F10, MatBIII) or 10 % (BN175) di-methyl sulfoxide (DMSO) in growth medium. After distribution, cryo-nunc tubes were put in a cryocontainer for 24 h at -80 °C before being stored in liquid N_2.

d. Cell density determination via SRB assay

Cell density determination was assessed via Sulforhodamine B (SRB) assay, which relies on measurement of protein content from cultured cells [162], based on the theory that only viable cells produce proteins continuously. SRB assay was conducted at point of interest after cells were cultured for a certain amount of time (section i), treated with HT (section ii) or toxicity of ADU assessed (section iii). Cells were fixed with 1 % trichloroacetic acid and placed in the fridge for at least 60 min. Then, fixated cell monolayer was washed under gentle water flow and 50 µl of SRB solution was added to each well. Upon 20 min of incubation, unbound dye was removed from cells by carefully rinsing wells with 1 % acetic acid. Plates were dried at either 3 h at 60 °C or overnight at 37 °C. Per well, 150 µl of DPBS was added and incubated for 40 min under gentle stirring on an orbital shaker for solubilizing the protein-bound dye. Optical density (OD) was quantified by measuring absorbance at 490 nm in a microplate reader and data analyzed.

i. Cell growth protocol

Cells were seeded in 96-well plate with 16000 to 500 cells/well in 200 µl growth medium. Plates were rested for 24, 48 or 72 h in the incubator before conducting SRB assay (section d).

ii. In vitro hyperthermia treatment protocol

For assessing effects of HT, plates must be sealed airtight. Resulting accumulation of CO_2 can be counterbalance by using a medium solely buffered with HEPES. This HT-medium is prepared from RPMI 1640 HEPES-buffered medium with 10 % FCS and 1 % antibiotics.

Figure 7: Set up of *in vitro* HT treatment of plates.

Cells were seeded in a 96-well plate with a concentration of 4000 cells/well in 200 µl growth medium and let adhere for 24 h in the incubator. The next day, growth medium was carefully replaced with HT-medium and entire plate sealed airtight in plastic foil and incubated at specific temperature for 60 min. For 41 °C (HT), wrapped plate was gently submerged in a pre-heated WB and water temperature checked continuously via temperature probe in the plate's proximity (figure 7). For 37°C (sham), sealed plate was placed in the incubator. Afterwards, plastic foil was removed, HT-medium gently replaced with 200 µl growth medium per well and plate placed in the incubator until SRB assay (section d) was conducted after 24, 48 or 72 h, respectively.

iii. Drug toxicity protocol

Cells were treated according to HT-treatment (section ii), but HT-medium contained different AUD concentrations ranging from 0.195 to 100 µM. To fully remove ADU after incubation, cells were washed once with DPBS before adding growth medium. Plate was placed in the incubator until SRB assay (section d) was conducted after 24 or 48 h, respectively.

e. Preparation for *in vivo* cell injection

For subcutaneous (s.c.) tumor growth induction, BN175 were prepared with 1.5 x 10^6 cells in 50 µl DPBS, B16F10 with 1.0 x 10^6 cells in 50 µl DPBS and MatBIII with 1.0 x 10^6 in 100 µl DPBS. Respective cells were cultured in growth medium without the addition of antibiotics (figure 8). Cells were harvested according to passaging protocol (section a), but final resuspension was conducted in DPBS. Then, cells were counted, respective amount separated, washed twice in DPBS, resuspended in the final volume of DPBS and placed in a reaction tube for transport.

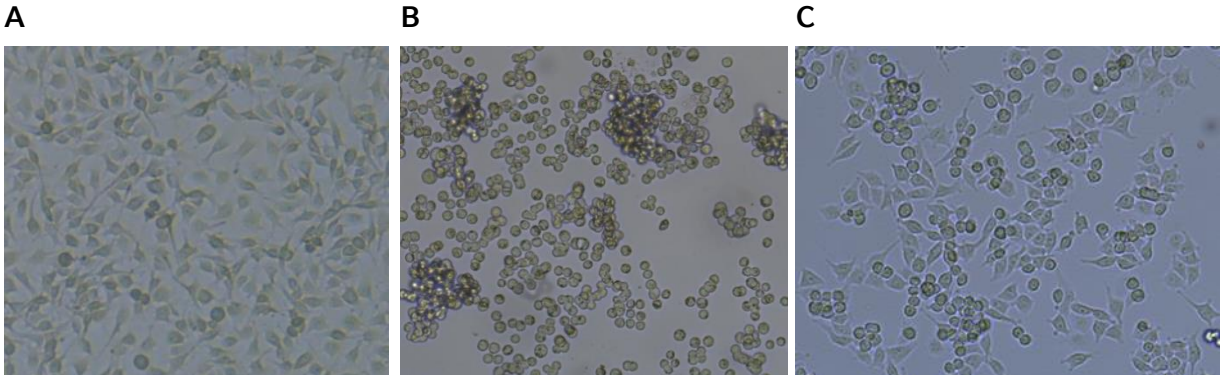

Figure 8: Representative pictures of cells used for *in vivo* tumor growth induction.
(A) B16F10, **(B)** MatBIII and **(C)** BN175 cell morphology in cell culture flask shortly being before harvested.

D) *In vivo* work package

Experiments with rats were performed in relation to previously conducted experiments [125, 139] and protocols developed further (i.t. injection, repetitive/combinational/metastasis treatment plan), whereas experimental set up and injection techniques for mice were established during this thesis. Animal experiments were performed according to protocols approved by the responsible authority (Gz. ROB.55.2-1-54-2532.0-09-2017; Az. ROB.55.2-2532.Vet_02-17-208, ROB.55.2-2532.Vet_02-18-61 and ROB.55.2-2532.Vet_02-20-3).

a. Animal housing

Experimental animals were acquired from commercial supplier and housed in equipped open-top cages at 21 °C, relative humidity of 55 ± 5 % and a 12-h day/night cycle with free access to autoclaved chow and water within the animal facility Med I, II, III, Neurology of Klinikum Großhadern, Munich, Germany. Every animal was granted an adaptation time of at least 14 days before starting experiments. To limit stress and germ load, access to animal housing was limited and only possible with mandatory single-use protectives (gown, face mask, shoe covers and gloves). Rats were housed with two to four individuals per type 4 macrolon cage, equipped with bedding, red house, red tunnel, red crawl ball and soft tissue. Mice were housed with two to five individuals per type II long macrolon cage, equipped with bedding, red house, red tunnel, and soft tissue. All cages were refreshed every 7 days with all equipment being washed and autoclaved. Health monitoring was conducted every 3 months according to FELASA recommendations [163].

b. Anesthesia and analgesia

For experiments, animals were placed under isoflurane induced inhalation anesthesia. Animals were put in an induction box with isoflurane set at 5 % until immobilized, then moved to a nose-chamber for maintenance at 1.5 - 2 % (rat) or ~ 1 % (mice) isoflurane.
Adequate pain management was conducted by s.c. injection of Meloxicam (rat: 0.5 mg/kg; mice: 2 mg/kg) and Metamizol (rat: 100 mg/kg, mice: 200 mg/kg) in accordance with GV-Solas recommendations with a 25 G needle [164]. For additional analgesia before full body perfusion, 0.05 mg/kg buprenorphine (s.c.) and 3 mg/kg pentobarbital (intracardial) were applied with a 25 G needle, respectively.

c. Tumor model

Protocols previously established for s.c. BN175 soft tissue sarcoma model in male BN rats were used and modified for newly introduced MatBIII adenocarcinoma model in female Fischer rats and B16 melanoma model in male or femaleBL6 mice (table 1).
Tumor cell injection (section i) or fragment implantation (section ii) was conducted to induce s.c. tumor growth lateral on one hind leg (figure 9.B-D). Independent of the technique, tumor growth was monitored every second day by visual inspection and caliper measurement of size (figure 9.A).

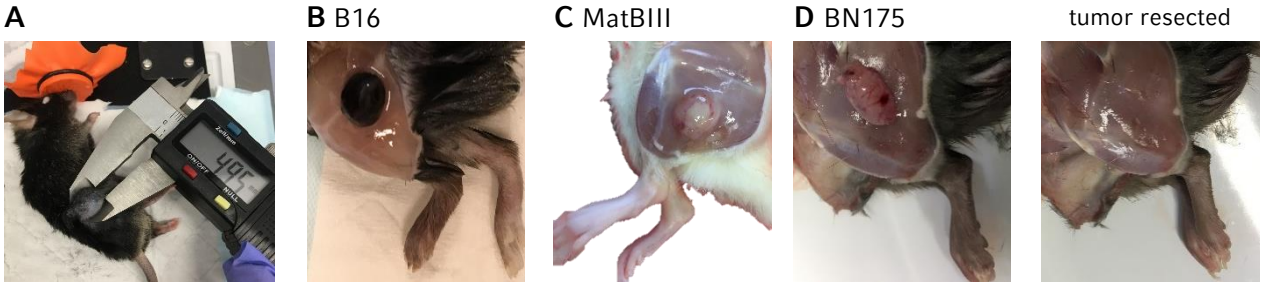

Figure 9: Representative pictures of *in vivo* tumor growth locations.
Exemplary display of **(A)** determination of tumor size via caliper measurement and tumor tissue in s.c. space after skin resection of **(B)** B16, **(C)** MatBIII and **(D)** BN175 (before and after tumor resection) model in syngeneic host.

Tumor volume was calculated with ellipsoid formula:

$$volume\ (cm^3) = height(cm) \times length(cm) \times depth\ (cm) \times \frac{\pi}{6} \qquad \text{Equation 3}$$

Relative tumor volume (%) was estimated in relation to size measured at treatment start (day 0).

i. Tumor cell injection

Tumor cells were cultured in accordance with cell specificities (chapter III.C) and harvested (chapter III.C.e) shortly before being s.c. injected with an insulin needle in anesthetized animals. The area of injection was shaved and disinfected beforehand. Tumors were allowed to grow for four days, seven days or until study-specific tumor inclusion criteria were met (section f).

ii. Tumor fragment implantation

Tumor fragments harvested from cell injected s.c. tumors in syngeneic host were frozen with two fragments per cryo-nunc in accordance to freezing protocol of respective cell line (chapter II.C.c) and stored for maximum 12 months until use. The leg of anesthetized animal was shaved and disinfected before thawing cryo-nunc in a WB set at 37 °C. Immediately after, fragments were placed in sterile DPBS to dilute the DMSO-containing growth medium. Skin was opened with scissors, a s.c. tunnel formed with atraumatic forceps and one fragment softly pushed inside. Incision was closed with 1 - 2 single stiches, which were removed after two days. Depending on the conducted study, tumors were allowed to grow to a volume of ~ 200 mm^3 (section f.ii) or 0.5 cm in one diameter (section f.iii).

d. Substance application

After skin disinfection, group-specific substance (drug or formulation) was applied i.v. or i.t. For the latter, an insulin needle was placed in tumor center under visual control and bolus injection conducted slowly. In both species, *V. coccygea lateralis* (lateral tail vein) was used for i.v. injection, with total injected volume being < 5 ml/kg in accordance with GV-Solas recommendations [164]. In rats, a 23 G catheter was placed, fixed with tape, flushed with saline, and closed with a stopper. Injection was conducted with a 25 G needle through the injection port of the stopper as bolus and flushed with 200 µl saline. After > 10 min, catheter was removed. In mice, a self-designed vein catheter, made from a 27 G needle and a 1 µm fine-tubing (figure 20), was placed immediately before bolus injection, flushed with 50 µl saline and removed. To ease this process, tail was warmed

before with a glove filled with hand warm water.

Blood volume of animal was calculated in relation to body weight [165] as follows:

$$blood\ volume\ (ml) = 0.062 \times body\ weight\ (gram) + 0.0012 \qquad \text{Equation 4}$$

With the assumption of blood consisting of 55 % plasma, theoretical maximum concentration of measured analyte in plasma immediately after injection (C_{max}) was estimated. Content measured at specific time point ($C_{time\ point}$) in relation to C_{max} presented percent injected dosage (% ID).

e. Heat-treatment of subcutaneous tumors

Clinical Hyperthermia (41 - 43 °C) was mimicked in preclinical settings by a temporary (60 min) overheating of tumor tissue to 41 °C (HT). Two techniques were available: water bath (WB) (section i) or lamp (section ii). Respective controls were conducted with water temperatures of Normothermia (NT) or sham- treatment at RT.

i. Water bath-treatment

For regional HT, WB was set to 41 °C whereas for controls at NT, 37 °C were used. Anesthetized animals (section b) were positioned on a plexiglass cover on top of a pre-heated WB set to 37 or 42 °C, for NT or HT respectively. Tumor-bearing leg was shaved, wrapped in plastic foil to prevent direct water-contact and possible oedema-formation and emerged into the water. The contralateral leg was not heated and contact to water prevented. To isolate the body under HT-condition, a styrofoam raft was placed underneath the animal to prevent systemic overheating. A temperature probe was placed in the middle of the WB for estimating intratumoral temperature as well as a rectal probe for monitoring body temperature. Both probes were attached to the same temperature data logger. A pre-heating time was granted, depending on species of 10 (mice) or 15 (rat) min, to assure homogenous warming of the submerged leg and a stable tissue temperature. Only after pre-heating, group-specific substance (drug or formulation) was injected (section d), timer set, and temperature recording started. After 60 min, animal was by placed on a warming pad and proceeded according to planned experiment. Representative pictures visualize the set up for mice and rats (figure 10).

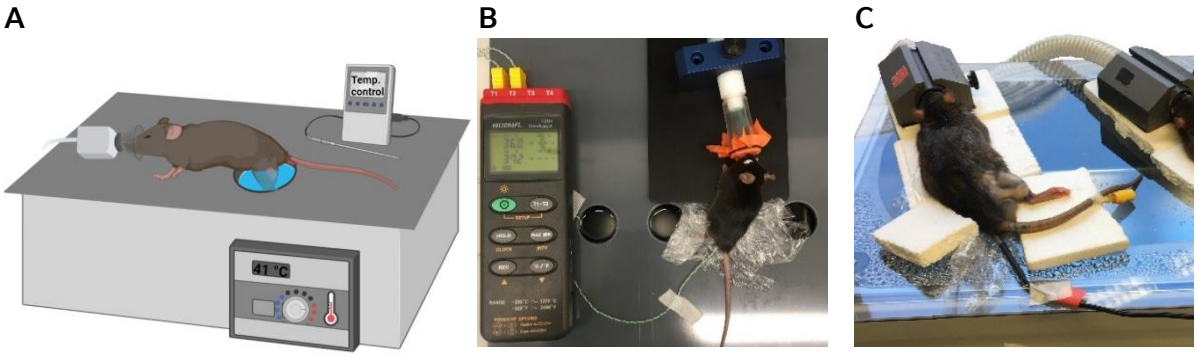

Figure 10: Translation of WB treatment of tumor-bearing leg in mice and rats.
(A) Sketch of set up and exemplary picture of treatment with **(B)** NT in mice and **(C)** HT in rats including styrofoam rafts.

ii. Lamp- and sham-treatment

Anesthetized animals (section b) were placed on a warming pad to ensure physiological body temperature. The tumor-bearing leg was tilted upwards, shaved and the skin disinfected as well as a rectal temperature probe placed. For HT-treatment, an intratumoral temperature probe was immerged in the tumor center and fixed with tape. The cold light lamp was arranged with focus on the tumor and a certain distance assured by using a space-holder. Heating of surrounding areas was prevented by covering the nearby with cellulose pads. Temperature of tumor tissue was monitored on the same device as body temperature and slowly heated to 41 °C within 20 - 30 min (pre-heating time). Only after pre-heating, group-specific substance (drug or formulation) was injected (section d), timer set, and temperature recording started. After 60 min, heat-treatment was ended by removing the probes and the lamp and proceeded according to planned experiment.
For sham-treatment, protocol was conducted accordingly but without heating of tumor tissue and intratumoral probe. Animals were placed on the heating pad. After waiting ~ 20 min, injection was conducted, body temperature recording started and monitored for 60 min. Representative pictures visualize the set up for mice and rats (figure 11).

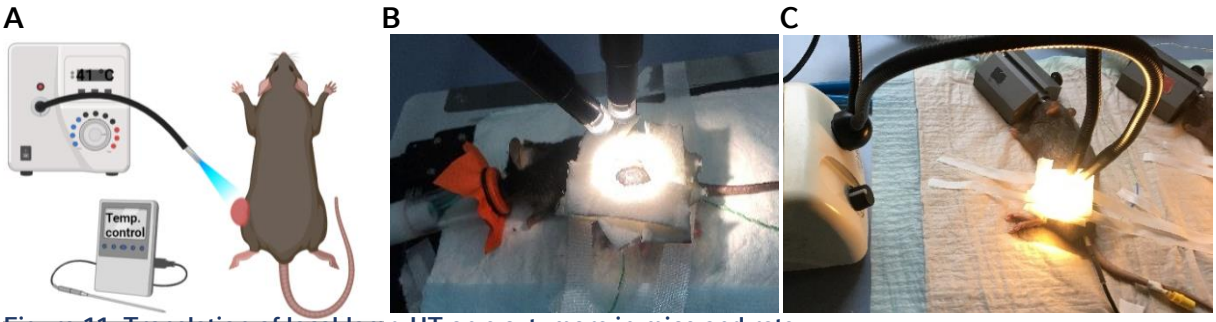

Figure 11: Translation of local lamp-HT on s.c. tumors in mice and rats.
(A) Outline of set up and exemplary pictures of treatment in **(B)** mice and **(C)** rats.

f. Study Protocols

i. Tumor growth

For monitoring tumor growth after induction via cell injection or fragment implantations (section c.i and ii), tumor growth was monitored, and animal well-being scored every second day until euthanized (section h) because of reaching an end point (section g).

ii. Pharmacokinetics

For pharmacokinetic (PK)-study, healthy animals were enrolled. Upon being anesthetized and supplied with analgesics (section b), preparations were conducted according to planned heat-treatment (section e). Group-specific substance (drug or formulation) was injected i.v. (section d) after respective pre-heating and counted as study start (0 min). Animals stayed in anesthesia during heat-treatment (0 to 60 min) and were allowed to wake up afterwards and between consecutive sampling time points. In rats, blood was sampled by inducing a bleeding on a cut in the *V. coccygea lateralis* at 15, 30, 60, 90, 120, and 240 min (figure 12). In mice, blood was sampled by puncturing

V. facialis once per side and a final blood sample at 15, 30, 60, and 120 min. Only at last sampling time point, blood was collected from the heart followed by euthanasia (section i). Blood was collected in Heparin-coated microvette and directly centrifuged (4200 g, 10 min, RT). Plasma was separated into reactions tubes and stored at -20 °C until content analysis via HPLC or LC-MS, depending on the analyte (section g), was conducted.

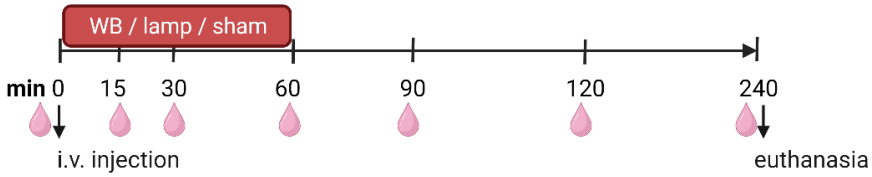

Figure 12: Schematic outline of pharmacokinetic study.
Upon i.v. injection of group-specific substance at the beginning of a 60-minutes HT- (WB or lamp) or control- (NT or sham) treatment, blood was collected at serial time points (0, 15, 30, 60, 90, 120, and 240 min).

iii. Biodistribution

Tumor-bearing animals were enrolled in the biodistribution (BD)-study (figure 13). S.c. tumor growth was induced on one/both hind legs via fragment implantation (rats) or cell injection (mice) (section c). Once tumor volume of > 200 (rats) or 50 mm^3 (mice) was reached, animals were anesthetized and supplied with analgesics (section b) before planned HT-treatment (WB or lamp) was prepared on one tumor (section e). Second tumor on contralateral leg was left untreated and served as control. After pre-heating time, group-specific substance (drug or formulation) was injected i.v. or i.t. (section d) and timer set. After 60 min, HT-treatment was ended and isoflurane increased to 5 %. When reaching deep states of anesthesia, animal was placed on the back and body opened with a scissor. With a small cut, the right auricular was opened and right ventricle punctured with a butterfly catheter for saline injection. The progress of perfusion was monitored by color changed of the liver and finalized by excision of the heart. Tissue samples of heart, lung, liver, spleen, kidney, muscle (directly under respective tumor), and tumors were harvested into reactions tubes and frozen at -20 °C until content analysis via HPLC or LC-MS, depending on the analyte (section g), was conducted.

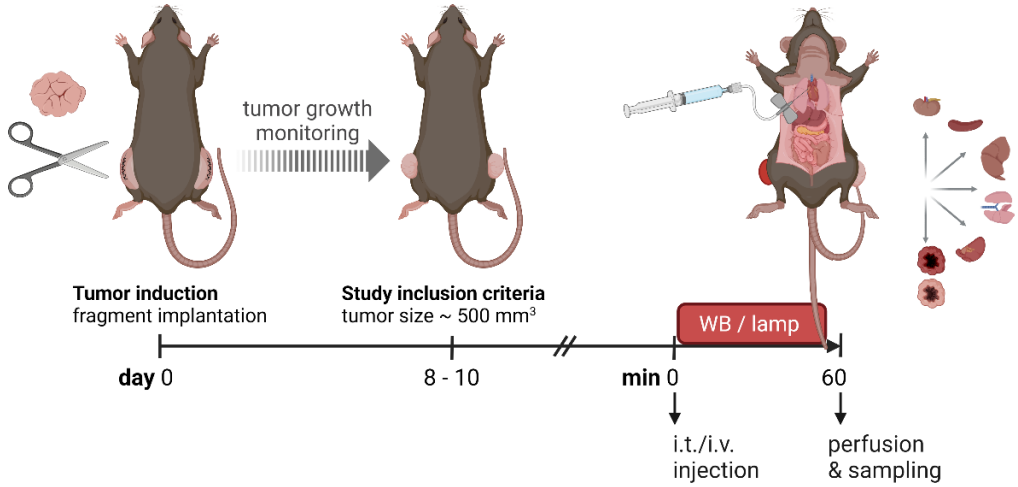

Figure 13: Schematic outline of biodistribution study.
Study was conducted once tumor size inclusion criteria were met. Treatment consisted of injection of group-specific substance at the beginning of a 60-minutes HT- (WB or lamp) treatment on one tumor, while contralateral was left untreated, and was followed by whole-body perfused and tissue sampling.

iv. Therapeutic response

Tumor-bearing animals were enrolled in the therapeutic response study. For studies with ADU or DOX in rats, fragment implanted tumors (section c.ii) needed > 5 cm in one tumor diameter to be included whereas mice studies started after reaching comparable tumor size after cell injection (section c.i). R848-studies were started after having confirmed palpable tumor growth after 4 (single, repetitive, and combinational treatment plan) or 7 days (single treatment plan) of tumor cell injection (section c.i). Once study-specific inclusion criteria was reached, standardized therapy protocol was conducted (day 0) once (single treatment plan, figure 14.A) or repeated on respective days with multiple injection of the same drug (repetitive treatment plan, figure 14.B) or different drugs (combinational treatment plan, figure 14.C). For dose-escalation studies, protocols varied with drug: free ADU i.t. was conducted with a single treatment plan, free R848 i.t. was conducted with repetitive treatment plan on day 0 and 4.

The standardized therapy protocol consisted of anesthesia and application of analgesics (section b), preparation of planned heat-treatment (section e), group-specific substance (drug or formulation) application (i.v. or i.t.) (section d) after respective pre-heating time, conducting a 60-minutes heat-treatment, stopping anesthesia immediately afterwards followed by letting animal fully awaken on a warming pad until placing it back in the housing cage. Tumor growth was monitored and animal well-being scored every second day until euthanized (section i) because of reaching an end point (section h). Overall, days of survival were counted from day 0. Injections parameters, body weight, and tumor growth development were documented and statistically analyzed (chapter III. E).

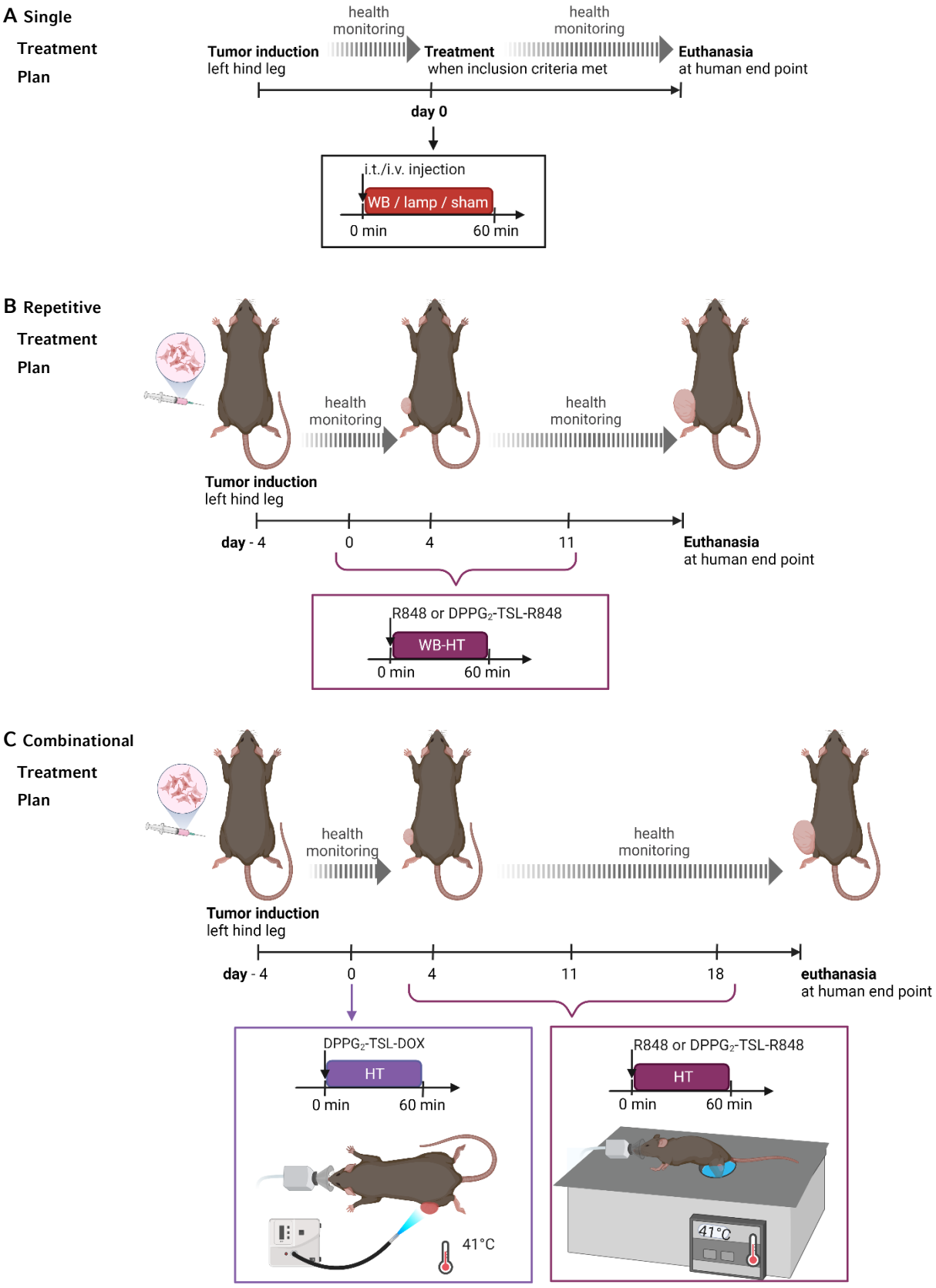

Figure 14: Schematic outline of treatment plans for evaluation of therapeutic response.
(A) Standardized therapy protocol (box) was conducted once on day 0 with injection of group-specific substance under HT- (WB or lamp) or control- (NT or sham) conditions. **(B)** Standardized therapy protocol was repeated three times in a row on day 0, 4 and 11 with application of R848 or $DPPG_2$-TSL-R848 with WB-HT on the same tumor. **(C)** Standardized therapy protocol (boxes) was conducted once with $DPPG_2$-TSL-DOX and lamp-HT on day 0 and additional three times with R848 or $DPPG_2$-TSL-R848 and WB-HT on consecutive days 4, 11 and 18 on the same tumor.

v. Metastasis model

Tumor-bearing animals were enrolled in the study. Animals bearing one tumor were enrolled 4 days after tumor cell injection if tumor growth was palpable (section c.i). Single or combinational treatment plan were conducted in the above-described manner (section iii), with the addition of a tumor cell injection in the contralateral hind leg (distant location to primary tumor) 4 days after treatment start. Tumor growth was monitored for each tumor and animal well-being scored every second day until end point was reached (section h) and euthanasia conducted (section i). Growth of second tumor was anticipated to show treatment-dependent growth speed and, hence, induction efficacy was not expected to be proven in all groups. Overall days of survival were counted from day 0. Injections parameters, body weight and tumor growth development were documented and statistically analyzed (chapter III. E).

g. Analyte recovery in animal samples

Animal plasma and tissue samples harvested in PK- and BD-studies were prepared and DOX or R848 measured via HPLC (section i or ii). Samples containing AUD or $DPPG_2$ were prepared ready-to-measure for external liquid chromatography-high resolution mass spectrometry (LC-MS) (section iii). Raw data was extracted for statistical analysis (chapter III. E).

i. HPLC for DOX-detection

For DOX detection from rat plasma, calibration samples were created by spiking DOX in a range of 2.5 to 10 µg/ml in rat plasma. Calibration samples and rat plasma samples were prepared in parallel. Respective samples were mixed 1:1 (v:v) with internal standard Daunorubicin, diluted 1:6 (v:v) in ACN, centrifuged (20000 x g, 6 min, RT) before supernatant was collected in a glass tube and dried in a heat block (40 °C, $N_{2\ stream}$). Residue was resolved in mobile phase A (120 mM KDP in ACN 74:26 (v:v), pH 5.5), transferred in a reaction tube and for final removal of undissolved particle, again centrifuged (20000 x g, 10 min, RT). Supernatant was transferred in a HPLC vial. A Waters HPLC system with 515 HPLC pumps, 717 plus autosampler and 2475 fluorescence detector equipped with C18 pre-column (3 mm) and C18 column (2.6 µm,100 Å, 100 x 3 mm) set at 30 °C and flow rate of 0.4 ml/min with mobile phase A and B (70 % ACN) was used [125].
For DOX detection from rat tissue, calibration samples were created by spiking DOX in a range of 0.5 to 10 µg/ml in calf liver tissue. Calibration samples and tissue samples were prepared in parallel. Respective tissue samples were thawed at RT and ~ 100 mg collected in a reaction tube and mixed 1:1 (v:w) with internal standard Daunorubicin, 500 µl water, 1.1 ml of MeOH and one 3 mm metal bead. Samples homogenization was conducted four times, 4 min each, with a TissueLyser at 30 Hz. Immediately after, 200 µl of 33 % silver nitrate were added, lysate cooled on ice (10 min) and centrifuged (20000 x g, 16 min, RT). For removal of proteins and lipids from sample solution, a SPE extraction protocol was conducted [161]. Therefore, STRATA-X columns were mounted in a 24-position vacuum manifold and SPE cartridge pre-conditioned with 2 ml MeOH and 2 ml water.

Then, supernatant was slowly loaded, columns washed once with water, followed by increasing MeOH solutions (10 and 30 %) and solutions fully removed under application of vacuum for 10 min. DOX was eluted (2 % FA in MeOH) in glass tubes and eluate dried in a heating block (40 °C, $N_{2\ stream}$). The residual was resuspended in mobile phase A (120 mM KDP in ACN, 74:26 (v:v), pH 5.5), vortexed, transferred in a reaction tube, centrifuged (20000 x g, 10 min, RT) and supernatant transferred to a HPLC vial for analysis with above-described Waters HPLC system.

For DOX detection from mouse plasma, calibration samples were created by spiking DOX in a range of 2.5 to 50 µg/ml in human plasma. Calibration samples and mice plasma samples were prepared in parallel and according to protocol of rat plasma samples (section i). An updated method from Thermosome GmbH (Planegg, Germany) for DOX-measurement via Scientific UltiMate 3000 (chapter III.B.b.ii) was used, with main alterations in specifics of C18 column (6 µm) and mobile phase A (0.05 % TFA: 0.05 % TFA in ACN, 1:1, (v:v)).

For DOX detection from mouse tissue, samples were prepared according to protocol of rat tissue samples (section i) but DOX calibration samples ranged from 2.5 to 50 µg/ml and updated method for Scientific UltiMate 3000 HPLC stated above was used.

ii. HPLC for R848-detection

For R848 detection from rat plasma, samples were prepared and measured via Scientific UltiMate 3000 as described for R848-containing *in vitro* samples (chapter III.B.b.ii).

For R848 detection from rat tissue, a method was developed during this thesis based on the above described SPE extraction method. In contrast to DOX-protocol, tissue sample was mixed with internal standard R837, 1200 µl HBS pH 7.4, 500 µl MeOH and one 3 mm metal bead before homogenization. Immediately after, lysate was only stored in ice (10 min) before centrifugation was conducted as stated above. In contrast to DOX, R848 was eluted from STRATAX columns stepwise with MeOH and after comparable drying step, residual was resuspended in 80 % ACN and later centrifuged. Collected supernatant was again dried in a glass tube on a heating block (40 °C, $N_{2\ stream}$) and residual resolved in mobile phase A (table 13), centrifuged (20000 x g, 10 min, RT) and supernatant collected in HPLC vials for analysis via R848-specific method of Scientific UltiMate 3000 (chapter III.B.b.ii).

iii. LC-MS for ADU and $DPPG_2$-detection

After application of ADU (free or liposomal form) *in vivo*, concentrations in recovered animal samples were expected to be too low for detection via available HPLC protocols. Hence, protocols based on chloroform extraction of ADU and $DPPG_2$ from the same sample were developed by Thermosome GmbH (Planegg, Germany) to fit more sensitive analysis via LC-MS conducted at EpiQMax (Martinsried, Germany).

For ADU/$DPPG_2$ detection from rat/mice plasma, calibration samples were created by spiking drug in a range of 0.2 to 100 (ADU), 0.5 to 500 ($DPPG_2$) µg/ml in rat/mouse plasma. Calibration samples and animal plasma samples were prepared in parallel. Respective sample was mixed 1:1 (v:v) with

internal standard (table 17) and diluted with EtOH to promote protein precipitation and rigorously shaken in a thermoshaker (1200 rpm, 10 min, RT) before centrifugation (10000 x g, 5 min, RT). Supernatant was divided in six parts for drug detection and 1 part for lipid detection. For detection of ADU, respective supernatant (6 parts) was collected in glass tubes, dried in a heat block (40 °C, $N_{2\ stream}$) and residual resuspended in mobile phase A (table 17). After centrifugation (2000 x g, 5 min, RT) supernatant was transferred in a 96-well plate. For detection of $DPPG_2$, respective supernatant (1 part) was collected in glass tubes and mixed 1:1 (v:v) with 90 % EtOH, gently vortexed, centrifuged (6000 x g, 5 min, RT) and supernatant transferred in a 96-well plate.

For ADU/$DPPG_2$ detection from rat tissue, calibration samples were created by spiking drug in a range of 0.05 to 20 (ADU), 0.5 to 200 ($DPPG_2$) µg/ml in HBS pH 7.4 on in calf liver tissue. Calibration samples and animal tissue samples were prepared in parallel. Tissue samples were thawed at RT and ~ 100 mg collected in a reaction tube, mixed 1:2 (v:w) with internal standard (table 17), 700 µl HBS pH 7.4, 850 µl ACN and one 3 mm metal bead. Sample homogenization was conducted four times, 4 min each, in a TissueLyser at 30 Hz. Lysate was cooled immediately after on ice (10 min) before being transferred into glass tubes, 1.7 ml chloroform added, vortexed and centrifuged (4200 rpm, 10 min, RT). For detection of ADU, upper fraction was collected in a glass tube and evaporated on a heat block (40 °C, $N_{2\ stream}$). Residual was resolved in 1 ml cold 80 % ACN, centrifuged (24000 x g, 10 min, RT) and supernatant transferred in a fresh glass tube. Again, solvent was evaporated in a heat block (40 °C, $N_{2\ stream}$) and residue resuspended in mobile phase A (table 17), centrifuged (14000 x g, 10 min, RT) and supernatant transferred in a 96-well plate. For detection of $DPPG_2$, lower fraction was collected in a glass tube and solvent evaporated in a heat block (40 °C, $N_{2\ stream}$). Residual was resuspended in 1 ml cold EtOH, centrifuged (24000 x g, 10 min, RT) and supernatant transferred in a fresh glass tube for drying in a heat-block (40 °C, $N_{2\ stream}$). Residue was resolved in 95 % EtOH, centrifuged (14000 x g, 10 min, RT) and supernatant transferred in a 96-well plate. All 96-well plates were transferred to EpiQMax (Martinsried, Germany) where samples were measured via a Sciex ExionLC AD device equipped with Sciex X500B. The LC was performed with HPLC methods (table 17), while MS was conducted in nitrogen at 500 °C and spray voltage -4500 V for analyte detection at 689.1 (ADU) or 328.1 Da (c-di-AMP) or nitrogen at 300 °C with spray voltage 5500 V for analyte detection at 814.6 ($DPPG_2$) or 768.6 Da (17:0 PG).

Table 17: Parameters of Sciex ExionLC AD for LC-detection of ADU and $DPPG_2$.

Analyte	In-line filter	Column	Flow	Mobile phase A	Mobile phase B	Internal standard
ADU	0.5 µm	C18 column Luna (1.6 µm, 50 × 2.1 mm) at 50 °C	0.4 ml/min	0.1 % FA	0.1 % FA	c-di-AMP
$DPPG_2$	0.5 µm	C18 column (2.6 µm, 50 × 2.1 mm) at 45 °C	0.4 ml/mín	10 mM ammonium formate in FA 100:0.2, v:v	0.1 % FA	17:0 PG

For $DPPG_2$ detection of $DPPG_2$-TSL-DOX from rat plasma, samples were transferred to Covance, North Yorkshire, UK where samples were measured with a Waters LC System equipped C8 column (1.6 µM, 50 x 2.1 mm) at 45 °C and 0.3 ml/min flow rate of mobile phase A (10 mM ammonium formate in FA, 100:0.2, v:v) and B (0.1 % FA) and a Sciex API 4000 MS with comparable settings. For $DPPG_2$ detection of $DPPG_2$-TSL-DOX from rat tissue, samples were prepared and transferred to EpiQMax (Martinsried, Germany) for LC-MS as described above.

h. End points

Throughout all studies predetermined humane end points were in accordance to approved protocol. In detail, body weight drop < 20 %, severe signs of pain on the body constitution (hair loss, redness, necrosis), or behavior (no self-grooming, itching, aggressiveness, reduction in foot or water intake, immobility) were end point criteria. For tumor-bearing animals tumor size (1.5 cm or 3 cm in one diameter for mice and rats, respectively), infiltrative growth in surrounding tissue, ex-ulceration, oedema, or redness on tumor-bearing leg were additional end points. Monitoring of health and tumor growth behavior was conducted via Score Sheets every second day. Development of body weight (%) during a therapy study was calculated in relation to body weight measured at study start (day 0).

i. Euthanasia

Under deep inhalation anesthesia (5 % isoflurane), mice were euthanized via cervical dislocation and rats by intracardial injection of 300 mg/kg Pentobarbital with 23 G needle.

E) Statistical analysis

Data was statistically evaluated with Origin© and Graph pad prism©. In-graph statistical analysis was conducted with t-test or TWO-WAY Annova with $P < 0.05$ (*), < 0.01 (**), < 0.001 (***) and < 0.0001 (****).

IV. Results

A) Deepening insight on liposomal Doxorubicin

The overall aim was to get more insight on behaviour of $DPPG_2$-TSL-DOX *in vivo* and compare data of two different species. In rats, lamp-HT was explored for the first time in respect to efficacy of triggering DOX accumulation in heated tissue (section a) and impact on therapeutic response of BN175 sarcoma model in BN rats (section b). In addition, a first report on clearance of DOX and $DPPG_2$ in the same sample of BN rats at NT was achieved (section c). In mice, newly developed protocols were conducted to clarify feasibility. $DPPG_2$-TSL-DOX was used to test PK-protocol in healthy BL6 mice (section dc.i) and evaluate BD-set up of WB- versus lamp-treatment of tumor tissue (section d.iii). Therefore, a B16 melanoma model in BL6 mice had to be implemented beforehand (section d.ii). Characteristics of used $DPPG_2$-TSL-DOX batches are summarized in table 35.

a. Exploring efficacy of lamp-hyperthermia technique

Impact on focused release on accumulation pattern

Biodistribution of $DPPG_2$ and DOX was assessed for the first time (chapter III.D.f.ii) after injecting $DPPG_2$-TSL-DOX at the beginning of a HT-treatment via lamp (chapter III.D.e.ii) in rats bearing two BN175 tumors (chapter III.D.f.iii). DOX dosage (2 mg/kg) was constant (table 39). Free DOX served as control. Harvested tissue samples were analysed via HPLC (chapter III.D.g.i).

In plasma, DOX content was < LOD_{DOX} in free DOX group while ~ 40 %ID remained in $DPPG_2$-TSL-DOX group (table 18 and figure 15.A). Liver and kidney accumulated DOX in a highly comparable manner among free and liposomal groups. Upon injection of $DPPG_2$-TSL-DOX, recovered DOX was significantly reduced ~2-fold in lung (1.8 to 0.9 %ID/g) and heart (1.2 to 0.7 %ID/g) but ~1.6-times higher in spleen (2.9 to 4.6 %ID/g) in comparison to free drug, respectively. Noteworthy, recovered content from spleen and kidney was similar after free DOX injection. Comparably to payload, $DPPG_2$ from liposomal carrier presented highest content in spleen. Nevertheless, this lipid distributed with < 1 %ID/g recovered from lung, heart, liver and kidney with lung tissue showing high SD (table 18 and figure 15. B).

Table 18: Recovered DOX and $DPPG_2$ in tissue of tumor-bearing rats.
DOX (2 mg/kg) was injected i.v. as free DOX or in $DPPG_2$-TSL-DOX, the latter resulting in 9.9 µmol/kg $DPPG_2$ being injected. After local lamp-HT for 60 min, plasma and organ tissue of BN rats was sampled and measured via HPLC (DOX) and LC-MS ($DPPG_2$), respectively. Data represent n = 6 per group.

Group	Plasma (%ID)	Lung (%ID/g)	Heart (%ID/g)	Liver (%ID/g)	Spleen (%ID/g)	Kidney (%ID/g)
free DOX, i.v.	< LOD	1.8 ± 0.4	1.2 ± 0,1	1.9 ± 0.3	2.9 ± 0.5	2.5 ± 0.5
$DPPG_2$-TSL-DOX, i.v.						
DOX	40.4 ± 9.0	0.9 ± 0.3	0.7 ± 0.2	1.8 ± 0.3	4.6 ± 0.6	2.3 ± 0.3
$DPPG_2$	Not conducted	1.0 ± 1.3	0.3 ± 0.2	0.4 ± 0.1	1.8 ± 0.3	0.7 ± 0.6

Larger tumors were selected for HT, driven by study design. Measured DOX in tumor tissue is displayed as concentration of DOX per gram or per sample (100 mg of tissue) (table 19). Graphing the latter, DOX was evenly distributed among all samples as indicated in low SD (figure 15.C).

Table 19: Effect of lamp-HT on DOX accumulation in rat tumor tissue.
BN rats were bearing two tumors, one being locally heated for 60 min via lamp HT and the contralateral left under physiological conditions (control). Injected DOX (~ 500 µg) was recovered from tissue after HT via HPLC. Data represent n = 6 per group.

Group	Tumor weight (g)		DOX per sample (µg/g)		DOX per gram (%ID/g)	
	Control	HT	Control	HT	Control	HT
free DOX, i.v.	0.6 ± 0.3	0.9 ± 0.3	1.9 ± 0.7	3.1 ± 1.8	0.4 ± 0.2	0.7 ± 0.4
$DPPG_2$-TSL-DOX, i.v.	0.6 ± 0.7	1.0 ± 0.5	2.0 ± 0.5	34.3 ± 6.4	0.4 ± 0.1	7.0 ± 1.5

Control tumors of both groups accumulated ~ 2 µg/g DOX, resembling a total recovered 0.4 %ID/g. In comparison to these, DOX content was slightly elevated after application of free drug (0.7 %ID/g) but significantly 10-fold higher after $DPPG_2$-TSL-DOX injection (7 %ID/g). Henceforth, a significant HT-dependent ~ 17-fold accumulation was proven in comparison to control tumor (table 19). Overall, a distinct HT-dependent DOX accumulation in heated tumor was proven upon injection of $DPPG_2$-TSL-DOX while their control tumors accumulated comparable amounts to free DOX group (figure 15.C).

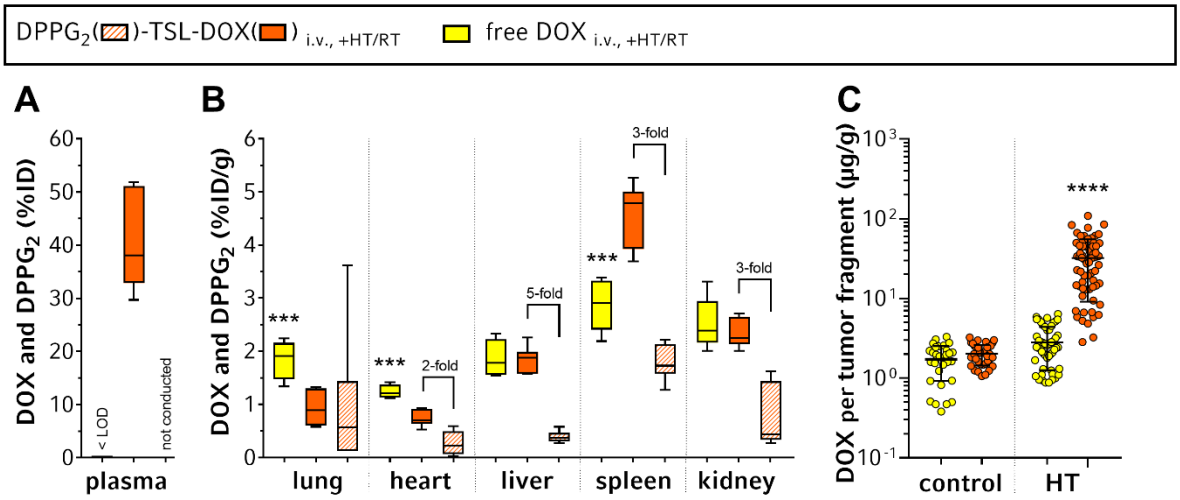

Figure 15: Biodistribution of DOX and $DPPG_2$ after lamp-HT in tumor-bearing rats.
Drug content levels were measured in **(A)** plasma, **(B)** organs and **(C)** tumor tissue (fragmented), at the end of a 60-minutes lamp-HT treatment of one tumor (tumor HT). The contralateral was left under physiological conditions (tumor control). Data represent n = 6 per group.

Robustness of biodistribution study design

After having proven significant differences in HT-dependent DOX accumulation in heated tumor tissue (section above), the question arose if released DOX had artificially elevated recovered concentrations in control tumor. This potential protocol-induced bias was assessed by conducting a BD-study with animals bearing one tumor only, either HT or sham-treated (control), and rats bearing two tumors (+HT/RT) (chapter III.D.f.iii). The latter was conducted in respect to 3R principle, as sampling of HT-treated and control tumor within the same animal allows a reduction of animal number. Among either group, $DPPG_2$-TSL-DOX was injected i.v. (table 39) at the beginning of sham- or HT-treatment via lamp (chapter III.D.e.ii). Harvested tissue samples were analysed via HPLC (chapter III.D.g.i).

A 6-fold higher DOX content in plasma was recovered from sham-treated animals (34 %ID) in comparison to both HT-groups (~ 5.6 %ID, HT and HT/RT). In contrast to this, the DOX accumulation in organs was higher in both HT- (HT or HT/RT) than in sham-treated group. In detail, DOX content in heart was elevated from 1.1 to ~1.4 %ID, in lung from 0.9 to 1.6 %ID, in liver from 2 to 2.2 %ID, in spleen from 2.9 to ~ 3.5 %ID and in kidney from 2 to ~ 3.3 %ID, respectively in sham and HT groups. Single HT-treatment elevated tumor content significantly from 3 to 4 %ID in comparison to HT tumors of HT/RT group. In accordance to organ-data, tumor of sham-treated group accumulated less DOX than control tumor of HT/RT group (~ 0.2 to 0.4 %ID/g) (figure 16).

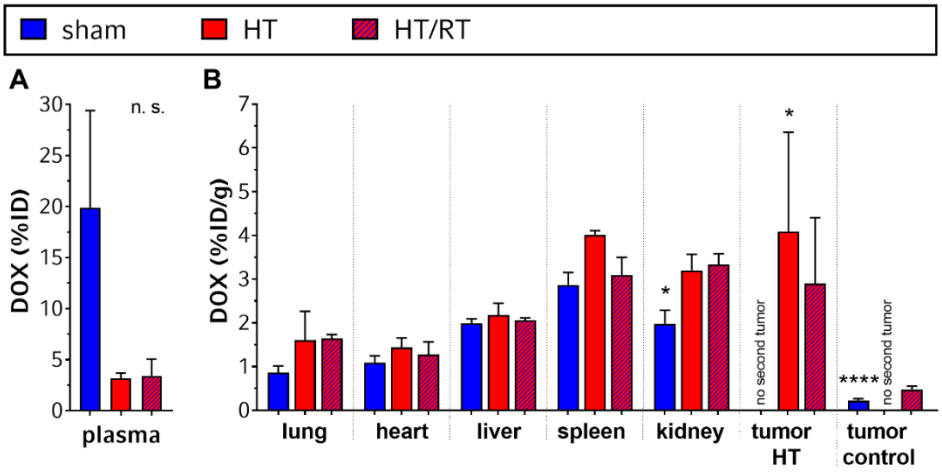

Figure 16: Comparison of DOX biodistribution in rats bearing one or two tumors.
$DPPG_2$-TSL-DOX was injected i.v. (2mg/kg) at the beginning of a 60-minutes lamp-HT or sham-treatment. Rats bearing one tumor were treated with sham-(blue) or lamp-HT (red). Both treatments were combined in rats bearing two tumors (striped red), one was treated via lamp (tumor HT) while the contralateral was left untreated (tumor control). Data represent n = 2 per group.

b. Therapeutic response of sarcoma model

With lamp-technique reproducibly elevating DOX accumulation in heated tumors (section a), the response of BN175 sarcoma model after single treatment (chapter III.D.f.iv) was evaluated. An optimized $DPPG_2$-TSL-DOX with improved shelf life [166] were injected in sham- or lamp-treated BN rats and compared to clinically relevant controls: free DOX and Doxil®.

Among all treated rats, intratumoral 41 °C was reached within ~ 30 min and remained constant for 60 min. To ensure proper placement of the probe, tumors were allowed to reach 5 mm in one diameter leading to a volume of 28 ± 13 mm^3 among all groups. Still, mild superficial skin burns occurred sporadically in each group, leading to crust formation which healed off fully. No other adverse reactions were documented during this study.

With injection of a constant dosage of 2 mg/kg DOX among all groups, a predetermined amount of lipids was injected with $DPPG_2$-TSL-DOX (55 µmol/kg) and Doxil® (25 µmol/kg) (table 39). Animals did not display signs of distress immediately after $DPPG_2$-TSL-DOX injection and any later time point. Control animals (saline + HT) reached tumor end size within ~ 6 days (figure 18.A). Injection of free DOX + HT prolonged survival by ~ 3 days (9 ± 4 days) which was comparable to $DPPG_2$-TSL-DOX injection in sham-treated animals (9 ± 2 days) (figure 18.B and C). Doxil®-treated animals survived 13 ± 4 days and $DPPG_2$-TSL-DOX prolonged survival even further to 19 ± 4 days, both in combination with HT (figure 18.F). Noteworthy, only the latter group displayed tumor growth delay (figure 18.D and E). This distinct slower tumor growth rate was HT-dependent, as effect was not visible in tumors of sham-treated animals injected with $DPPG_2$-TSL-DOX. Temperature monitoring during HT- and sham-treatment in respective groups confirmed efficacy of lamp-induced HT (figure 17).

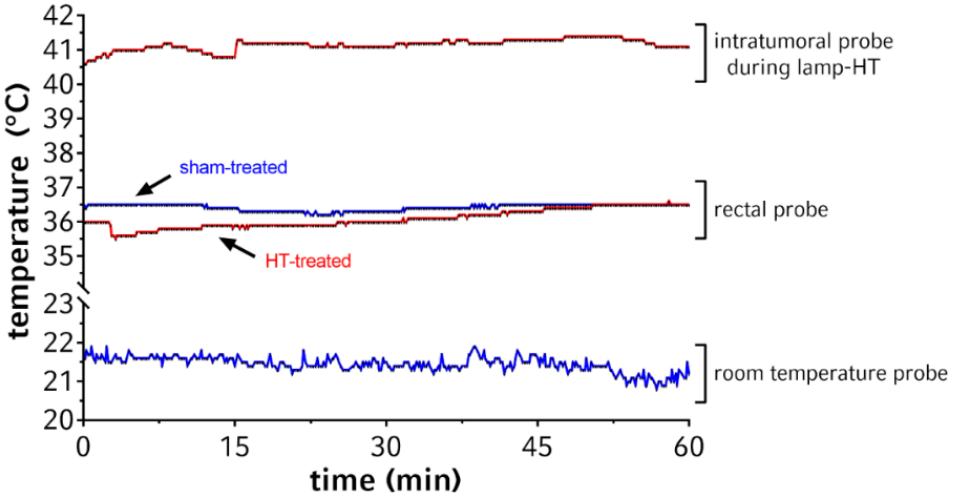

Figure 17: *In vivo* temperatures during lamp-HT and sham-treatment.
During lamp-HT (red), intratumoral and rectal temperature were monitored while in sham-treatment (blue) rectal and room temperature were documented. Injection of novel $DPPG_2$-TSL-DOX was conducted at 0 min. Representative temperatures of one animal per group are depicted.

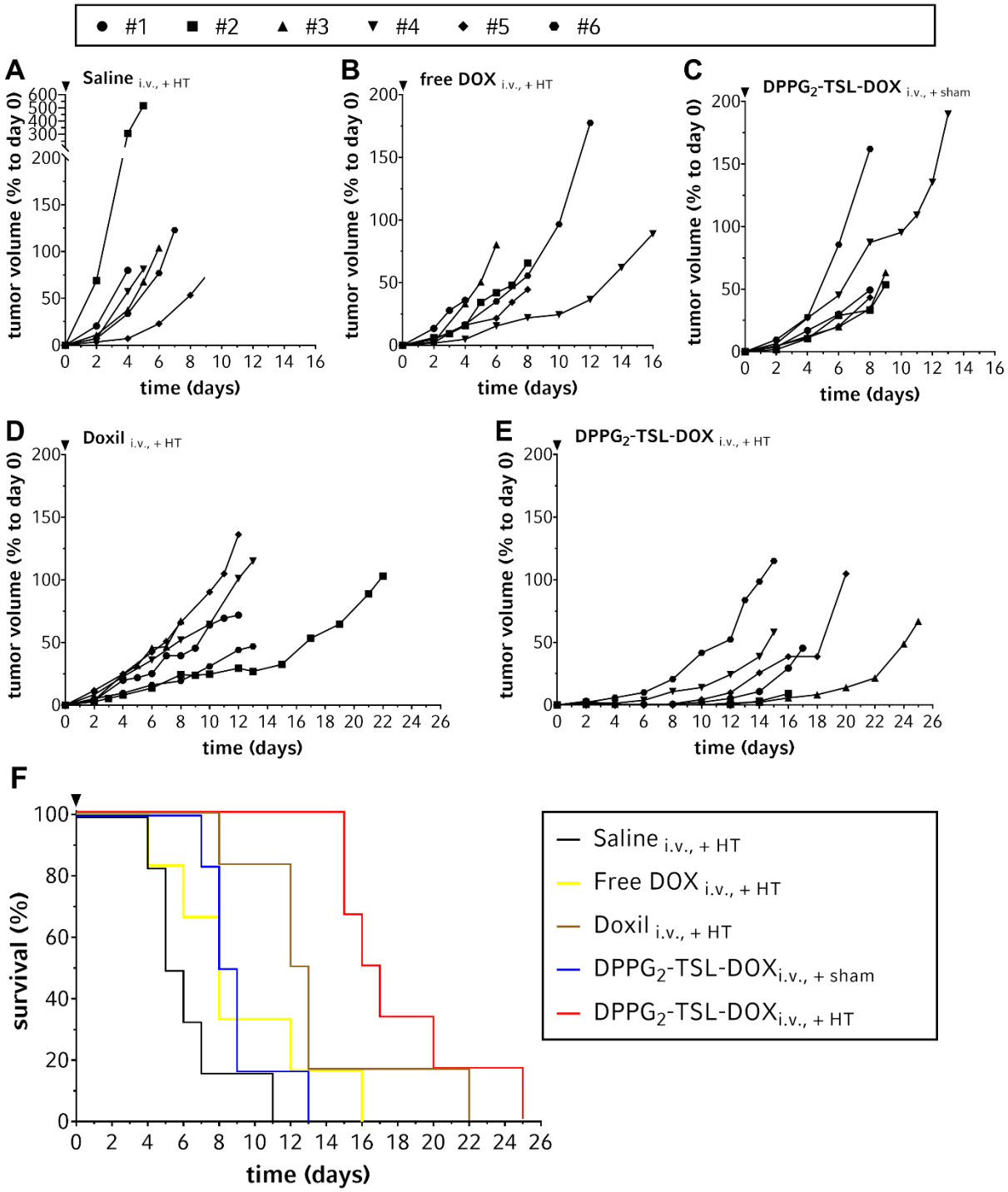

Figure 18: Exploring $DPPG_2$-TSL-DOX against clinical relevant controls in BN175 model.
Single injection of saline (black) or 2 mg/kg DOX in free form (yellow), Doxil (brown) or encapsulated in novel $DPPG_2$-TSL (orange) was conducted at the beginning of a 60-minute lamp-HT or sham-treatment (blue). **(A-E)** Tumor growth was monitored in respective group until end point was reached and **(F)** Kaplan-Meier survival plotted. Data represent n = 6 per group.

c. Plasma clearance in rats

With distinct HT-dependent therapeutic effect (section b), plasma stability of optimized $DPPG_2$-TSL-DOX [166] was to be investigated. Therefore, a PK-study in rats was performed (chapter III.D.f.ii) and harvested plasma analysed via HPLC (chapter III.D.g.i).

15 min after injection, 0.2 µg/ml DOX (~ 0.11 % ID) was recovered in free drug group. At later time points (> 15 min), DOX dropped below LOD_{DOX} (0.05 µg/ml), which is why statistical analysis was not possible. In contrast, 15 min after $DPPG_2$-TSL-DOX injection 61 %ID were recovered and 7 %ID circulating until end of experiment (240 min). This monophasic decay in plasma presented a t_α of 100 min, indicating a significantly prolonged circulation time in comparison to free DOX. Upon HT, triggered release *in vivo* was confirmed as t_α of DOX was reduced to ~ 20 min as content in plasma was overall lowered by half with 30 and 3 %ID recovered initially and at the end, respectively (figure 19.A).

With dosage of 2 mg/kg DOX being constant in all groups, a pre-determined amount of liposomal lipids were injected (9 mg), which consisted to ~ 30 % of $DPPG_2$ (3 mg) by liposomal design. Overall, a $DPPG_2$-dosage of 13.5 µmol/kg was injected in respective HT and NT groups (table 39). For the first time, $DPPG_2$ and DOX was recovered from the same sample to gain more insight on clearance patterns at NT. In detail, $DPPG_2$ was lost by 40 %within 15 min and overall 77 % until end of experiment (240 min). Resulting plasma clearance presented a monophasic decay with a t_α of 240 min (table 20).

Table 20: Pharmacokinetic parameters of DOX and $DPPG_2$ at NT in rats.
In BN rats, $DPPG_2$-TSL-DOX (DOX: 2 mg/kg; $DPPG_2$: 13.5 µmol/kg) was injected i.v. at the beginning of a 60-minutes NT-treatment via WB. Plasma was measured via HPLC. Data represent n = 6 per group.

$DPPG_2$-TSL-DOX + NT	C_{max} (µg/ml)	$C_{15\ min}$ (%ID)	$C_{240\ min}$ (%ID)	t_α (min)	$AUC_{60\ min}$ (%ID*h/ml)	$AUC_{240\ min}$ (%ID*h/ml)	R^2
DOX	58.6	60.5 ± 3.4	6.3 ± 1.7	107.9 ± 8.9	2293	5886	0.98569
$DPPG_2$	234.6	59.7 ± 4.8	23.3 ± 4.7	240.4 ± 27.1	2586	9204	0.9622

When subtracting AUC of DOX from $DPPG_2$, ΔAUC revealed the lipid to be more stable than the payload (increase from 293 to 3318 %ID*h from 60 to 240 min, respectively), hinting at DOX release from carrier (figure 19.B).

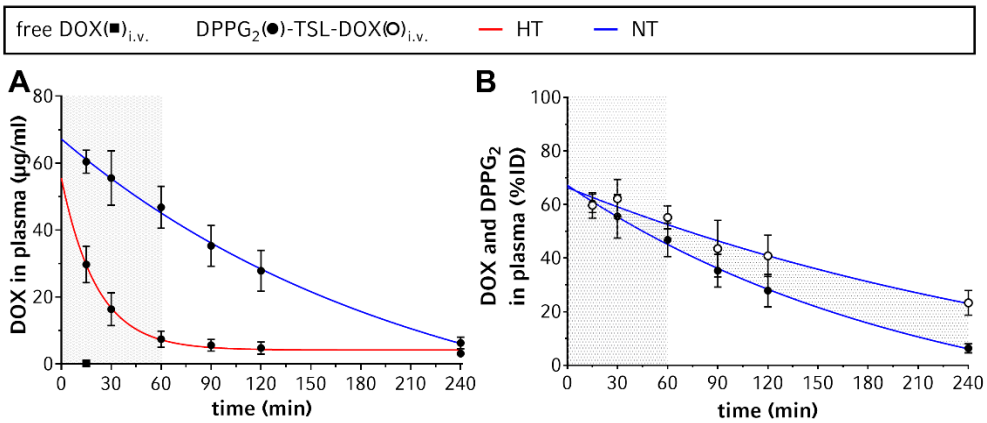

Figure 19: Plasmatic clearance of DOX and $DPPG_2$ in rats.
(A) I.v. injection of 2 mg/kg DOX in free (square) or liposomal form (circle) at the beginning of a 60-minutes WB-treatment (shaded area) with NT (blue line, fitted) or HT (red line, fitted). **(B)** Correlation between recovered DOX (filled circle) and $DPPG_2$ (empty circle) at NT with highlighted subtraction area. Data represent n = 6 per group.

Impact of lamp-HT on plasma stability could not be clarified as healthy animals without tumors are used to assess PK. Alternative local heating of muscle tissue was not seen as a sufficient control and animals spared in respect to 3R principle.

d. Exploring an additional species

Experimental set up for mice had to be established (figure 20).

Overall study protocols were met as close as possible among species, while the most critical for later comparison were enabled to be kept identical. This was in detail: isoflurane-anaesthesia (> 80 min for pre-heating and HT-treatment), style of injection (catheter) and accessibility of tumors for local WB or lamp-treatment (s.c. hind leg).

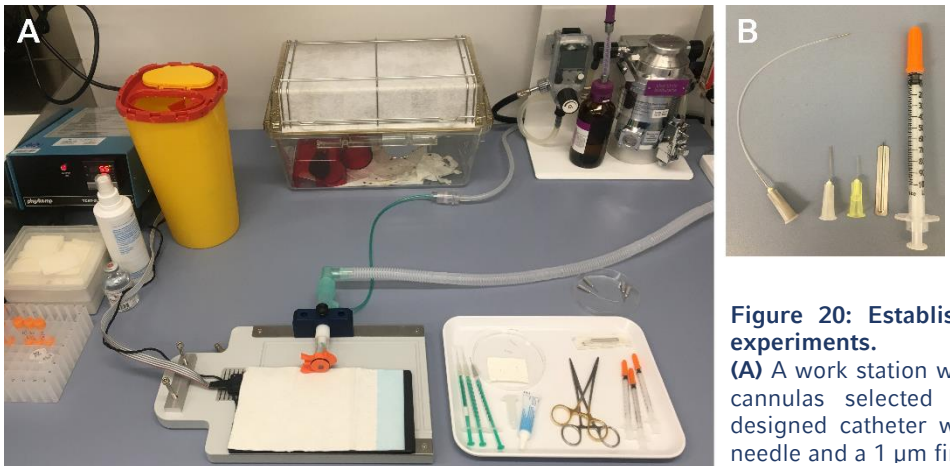

Figure 20: Established set up for mice experiments.
(A) A work station was set up as well as **(B)** cannulas selected for injection. A self-designed catheter was made from a 27 G needle and a 1 µm fine-tubing.

i. Pharmacokinetic profile in mice

Healthy BL6 mice were injected with $DPPG_2$-TSL-DOX (table 39) and plasmatic clearance determined with newly developed protocol (chapter III.D.f.ii).

At first sampling time point (15 min), DOX was recovered with ~ 4 µg/ml, which reflected an immediate loss of ~ 94 %ID from mouse plasma, independent of NT and HT. Until end of study, ADU was cleared from plasma to ~ 2 %ID in both groups in a mono-phasic decay manner leading to comparable calculated t_α and AUC of ADU (figure 21). Due to low recovery upon free DOX injection in rats, this group was spared to reduce animal numbers (3 R principle).

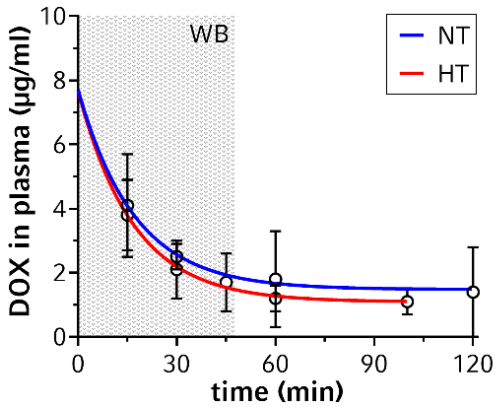

Figure 21: Impact of HT on plasma clearance of DOX in mice.
I.v. injection of $DPPG_2$-TSL-DOX in BL6 mice (2 mg/kg DOX) at the beginning of a 60-minutes (shaded area) NT-(blue line, fitted) or HT-(red line, fitted) treatment via WB. Data represent n = 2 per group.

ii. Implementation of B16 melanoma model

During this thesis, a novel B16 melanoma model was established in syngeneic BL6 mice.
At first, culture procedures from commercially available B16F10 cells were implemented (chapter III.C), followed by *in vitro* experiments on drug responsiveness (data not shown). As a second step, tumor growth induction via cell injection (chapter III.D.c.i) in syngeneic BL6 was aimed at. After having explored several concentrations (data not shown), 1.0 x 10^6 B16F10 cells had shown most robust induction of B16 tumor growth (figure 22). Within 11-12 days, tumors reached inclusion size for conducting a therapy study (chapter IV. B.b).

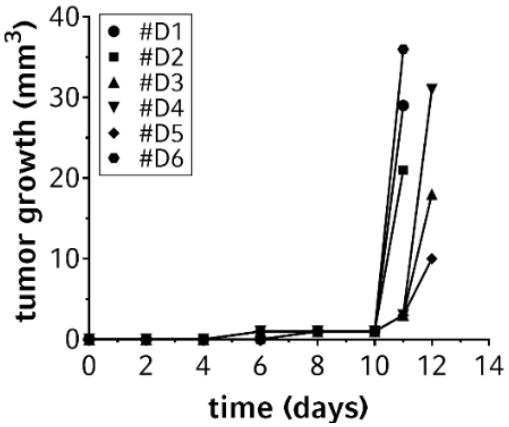

Figure 22: S.c. growth of the B16 melanoma.
Tumor growth in BL6 mice was induced via s.c. injection of B16F10 cells (1.0 x 10^6) in 50 µl DPBS. Data represent n = 6.

iii. First biodistribution study in mice

Upon successfully induction of B16 tumor growth, feasibility of tumor HT-techniques in mice were to be evaluated. Hence, developed protocols for WB and lamp (chapter III.D.e.i and ii) were explored in parallel with i.v. injection of $DPPG_2$-TSL-DOX (table 39). Harvested tissue samples were analysed via HPLC (chapter III.D.g.ii).
Feasibility of either protocol was confirmed with detectable and highly comparable DOX-distribution in plasma, lung, heart, liver, spleen, and kidney samples (figure 23.A and B). Independent of HT-technique (WB or lamp), DOX in plasma, lung, and heart samples accumulated ~1.2 ng/mg, which was < LOQ_{DOX} (0.2 ng/mg) but within LOD_{DOX} (0.1 ng/mg). Content was elevated 4-fold in spleen and kidney (~ 5 ng/mg) and 13-fold in liver (~ 15 ng/mg). Recovered DOX in muscle and tumor was again within LOD_{DOX} but < LOQ_{DOX}. Control tissue (muscle and tumor) accumulated group-dependent with 0.3 and ~ 0.7 ng/mg and elevated 1.7-fold in muscle tissue under HT, with 0.5 and 1.2 ng/mg (lamp and WB, respectively). WB-HT enhanced DOX accumulation in heated tumor 2-fold to 1.4 ng/mg in comparison to respective control tumor but not in comparison to plasma, lung, and heart samples of the same animal. In contrast, lamp-HT elevated accumulation 23-fold to ~ 7 ng/mg (0.2 %ID) in comparison to respective control tumor (figure 23.B). Temperature monitoring during HT documented stable heating of tumor tissue to 41°C while body temperature was not affected by either technique (figure 23.C).

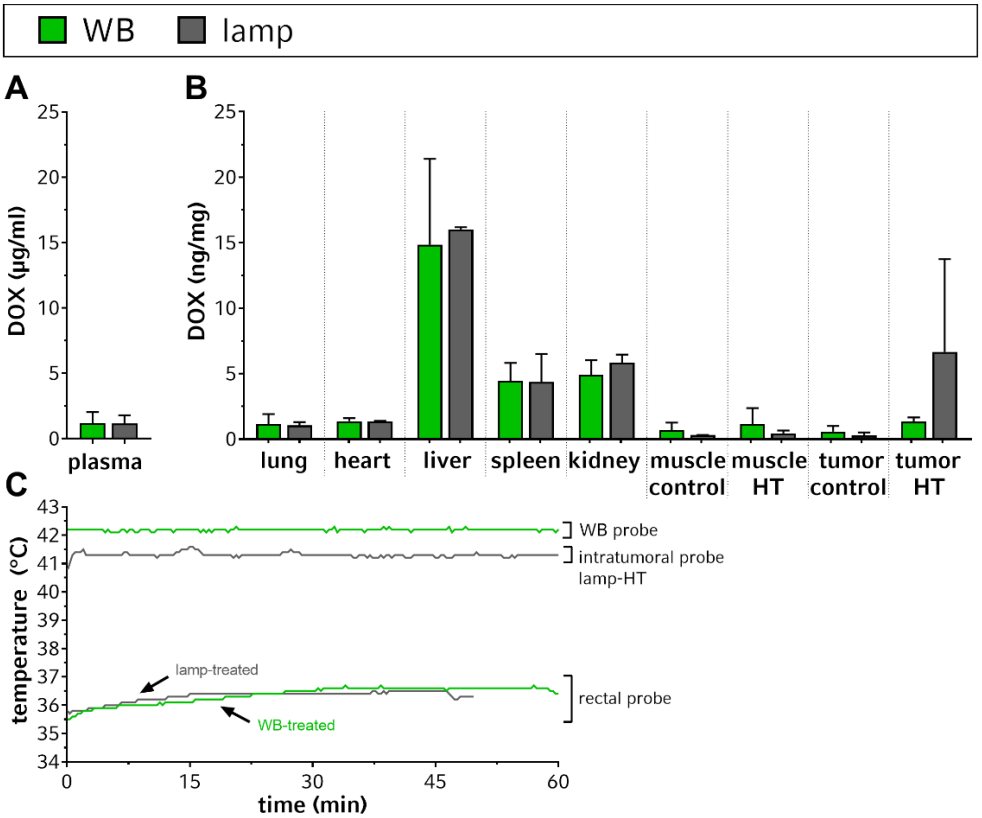

Figure 23: Impact of HT-technique on biodistribution of DOX in tumor-bearing mice.
$DPPG_2$-TSL-DOX were i.v. injection (2 mg/kg DOX) at the beginning of a 60-minutes HT-treatment of one tumor (tumor HT) via WB (green) or lamp (grey). The contralateral tumor was left under physiological conditions (tumor control). DOX was recovered from **(A)** plasma, **(B)** organ and tumor tissue of BN rats. Data represent n = 2 per group. **(C)** Representative temperatures of rectal, WB and intratumoral probe during HT of one animal per group.

B) Liposomal encapsulation of the STING agonist ADU

STING-agonist ADU has drawn attention once growing evidence of significant antitumor activity in multiple mice models was reported. However, due to low plasma stability of free ADU, these therapeutic effects were only achieved upon i.t. injection [64, 65, 72]. Driven by the lack of alternative strategies for circumventing systemic clearance in current literature, the question of whether encapsulation in $DPPG_2$-TSL could facilitate prolonged plasma stability while maintaining therapeutic efficacy was to be evaluated. Different $DPPG_2$-TSL-ADU formulations were formulated by Thermosome GmbH (Planegg, Germany) and provided for this thesis to be explored *in vivo*. Characteristics of used $DPPG_2$-TSL-ADU batches are summarized in table 37. Impact of formulation design and species on plasma stability was revealed (section a), dosage in mice explored (section b) and syngeneic BN175 sarcoma model utilized to explore antitumor ability of ADU (section c) and efficacy of tumor accumulation (section d).

a. Impact of formulation design on plasma stability

Focus of the study was to assess newly developed liposomal ADU formulations (section i) and the influence of formulation design on payload and carrier clearance from plasma of BL6 mice (section ii) and BN rats (section iii). Efficacy of heat-triggered drug release was studied by combining systemic injection with regional HT.

i. Osmotic conditions of liposomal formulations

The final protocol for producing $DPPG_2$-TSL-ADU determined lipid films composed of molar ratios 50:20:30 DPPC:DSPC:$DPPG_2$ being hydrated in HBS pH 7.4 or HBW pH 7.4, resulting in ~ 340 or 70 mOsm/kg for isosmotic or hyposmotic conditions across the lipid bilayer, respectively (chapter II.B.a). With ADU, a hydrophilic drug dissolved to 8 mg/ml was successfully encapsulated in a molar D:L ratio of 0.02 or 0.04 (iso- or hyposmotic formulation respectively), when loading was conducted for 30 min at 60 °C followed by five cycles of F/T and hand-extrusion at 200 nm (table 21).

Table 21: Parameters of liposomal design for encapsulating ADU.
$DPPG_2$-TSL designed with molar ratio of 50:20:30 DPPC:DSPC:$DPPG_2$ were loaded ADU dissolved in different hydration buffers (8 mg/ml). Values are representatives and depict formulations used in PK-studies.

Formulation	Loading condition	Hydration buffer	Extra-liposomal buffer	ADU (mM)	lipid (mM)	ADU:lipid (mol:mol)
$DPPG_2$-TSL	-	HBW pH 7.4	HBS pH 7.4	-	32.7	-
$DPPG_2$-TSL-ADU$_{isosmotic}$	60 °C / 30 min + 5x F/T	HBS pH 7.4	HBS pH 7.4	0.9	38.6	0.02
$DPPG_2$-TSL-ADU$_{hyposmotic}$	60 °C / 30 min + 5x F/T	HBW pH 7.4	HBS pH 7.4	1 ± 0.2	26.9 ± 9.3	0.04

By conducting a TDR in the matrix of mouse plasma (chapter II.B.b.v), the release efficacy of ADU from developed formulations was determined (figure 24). $DPPG_2$-TSL-ADU$_{isosmotic}$ were stable at 37 °C (60 min), while at 41 °C (60 min) 60 % of ADU were released. Increase to 42

°C elevated release to 70 %. When stepwise assessing the temperatures, release < 41 °C (5 min) was neglectable (< 10 %). Osmotically stressed formulation released ADU more pronounced upon 40 °C (~ 30 %) with release efficacy reaching 80 % at 42 °C (5 min). In accordance, 60 min release-values were elevated to 84 and 90 % at 41 and 42 °C, respectively. However, osmotic stress lowered stability by increasing leakage (11 %) at 37 °C (60 min). Utilization of spin columns allowed separation of liposomal fraction, confirming stability of up to 90 % at 37°C and payload release upon higher temperatures.

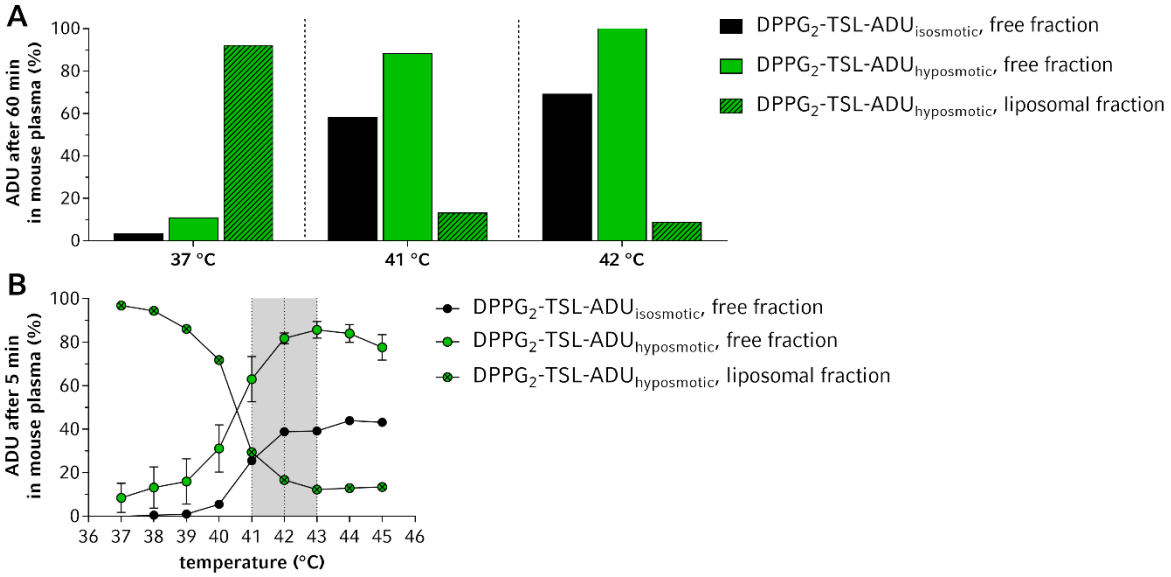

Figure 24: Influence of $DPPG_2$-TSL-ADU osmotic condition on *in vitro* release.
Isosmotic (black) and hyposmotic (green) $DPPG_2$-TSL-ADU were incubated in mouse plasma at increasing temperatures for **(A)** 60 or **(B)** 5 min. Free fraction of ADU was recovered via amicon filtration whereas retention of ADU in liposomal fraction was determined via spin columns (striped). Values are depicted from representative formulations.

Enhanced integrity of carrier in $DPPG_2$-TSL-$ADU_{isosmotic}$ was expected, as no proton gradient between intra- and extraliposomal buffer promoted release. The question was if stability could be reproduced upon i.v. injection as plasma circulation *in vivo* may induce carrier stress leading to passive ADU release (so called leakage). If so, addition of HT might enforce release *in vivo* which was only moderate efficient *in vitro* (~ 40 % at 42 °C, figure 24.B). This would give insight for further formulation designs. In $DPPG_2$-TSL-$ADU_{hyposmotic}$, osmotic stress was already present on carrier and induced release *in vitro* (> 80 %, 42 °C). If additional *in vivo* related stress is bearable for this carrier and if release only occurs upon HT was to be tested (section ii and iii).

To assess future *in vivo* feasibility, TDR of $DPPG_2$-TSL-$ADU_{hyposmotic}$ was conducted in plasma of several species (figure 25.A). A significant species-driven effect of ADU release was detected. With maximum release being achieved in mouse plasma, release efficacy dropped stepwise, for example, at 41 °C (60 min) from mouse (88 %), rat (50 %), porcine (23 %) to human plasma (16 %). In the latter, no escalation between 41 and 42 °C (~ 16 %) was detected whereas in other species an enhanced release was noted. TDR profile of free ADU fraction correlated to 60 min release data in human, porcine and mouse plasma (figure 25.B),

while reaction in rat plasma facilitated enhanced release upon 41°C. When evaluating liposomal ADU fraction, the stability of $DPPG_2$-TSL-$ADU_{hyposmotic}$ in human plasma was altered as it displayed comparable ADU retention as in plasma of other species, hinting at significant interaction with human plasma proteins (figure 25.C). It must be noted, that in all cases commercially available plasma with identical coagulant was used. Until now, no external influences on content variation had been detected. Influence of plasma origin on *in vitro* stability may be accounted to species-specific proteins and raised question of reproducibility *in vivo*, which would impact future drug development plans (section ii and iii).

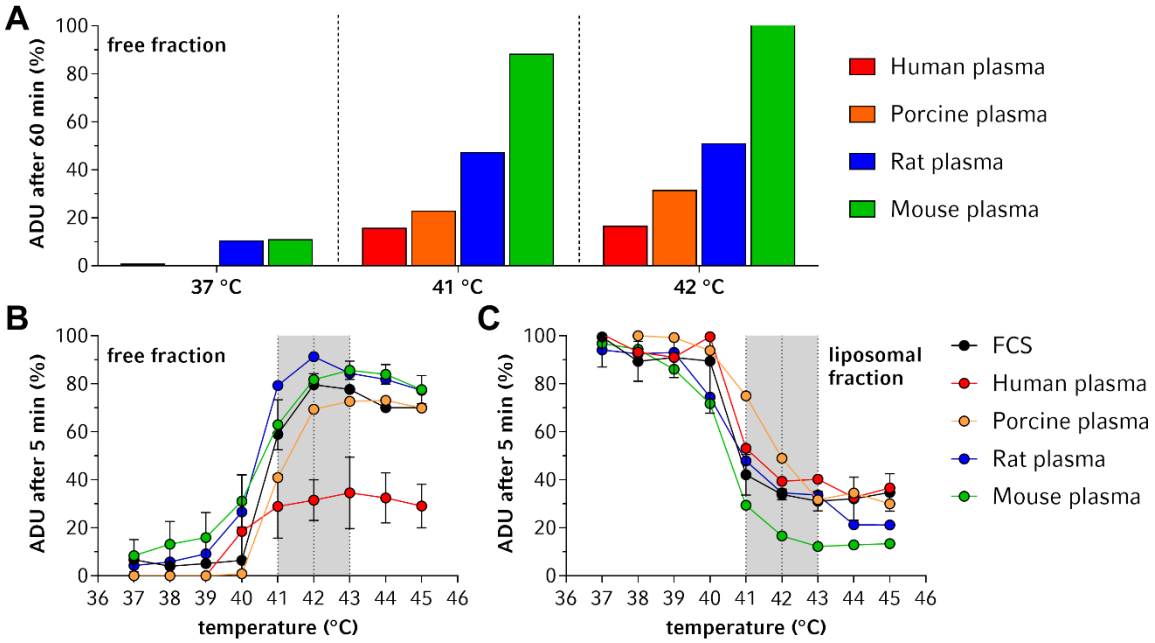

Figure 25: ADU release from hyposmotic $DPPG_2$-TSL-ADU in different plasma.
$DPPG_2$-TSL-$ADU_{hyposmotic}$ was incubated in human (red), porcine (orange), rat (blue) or mouse (green) plasma and FCS (black) at increasing temperatures (37 to 45 °C). Free fraction of ADU was recovered via amicon filtration after **(A)** 60 or **(B)** 5 min. Retention of ADU in liposomal fraction was assessed via spin columns after **(C)** 5 min. Values are depicted from representative formulations.

ii. Pharmacokinetic profile in mice

In a PK study (chapter III.D.f.ii) in BL6 mice, liposomal ADU formulations were injected i.v. (table 40) in combination with HT or NT treatment (chapter II.D.e.i). Collected plasma samples were prepared for measurement via LC-MS (chapter III.D.g.iii). Due to low volumes, only ADU was recovered from harvested plasma samples.

In NT groups, 71 %ID of ADU were lost at first sampling time point (15 min) upon injection of isosmotic formulation and 87 %ID for hyposmotic formulation. When further comparing these two groups, enhanced payload leakage upon carrier-specific osmotic stress was indicated in ~ 6-fold reduced t_α (63 to 11 min) and $AUC_{120\ min}$ (1301 to 236 %ID*h/ml). HT-triggered drug release from hyposmotic formulation further reduced $AUC_{60\ min}$ 5-fold from 231 to 47 %ID*h/ml with 98 %ID being lost within the first 15 min. ADU freed from carrier cleared in comparable t_α to NT group (table 22).

Table 22: Pharmacokinetic parameters of ADU in mice.
Iso- or hyposmotic $DPPG_2$-TSL-ADU were injected i.v. (2 mg/kg) in BL6 mice at the beginning of a 60-minutes WB-treatment with 41 (HT) or 37 °C (NT). Plasma samples were measured via LC-MS method with LOQ_{ADU} being 0.02 µg/ml. Data represent n = 2 per group.

Group	Treatment	C_{max} (µg/ml)	$C_{15\ min}$ (µg/ml)	$C_{120\ min}$ (µg/ml)	t_α (min)	$AUC_{60\ min}$ (%ID*h/ml)	$AUC_{120\ min}$ (%ID*h/ml)	R^2
$DPPG_2$-TSL-$ADU_{isosmotic}$	NT	58.6	16.8 ± 5.9	3.2 ± 2.9	62.7 ± 12.6	821	1301	0,94384
$DPPG_2$-TSL-$ADU_{hyposmotic}$	NT	58.6	12.2 ± 0.5	1.4 ± 0.7	11.3 ± 1.7	231	236	0,95079
$DPPG_2$-TSL-$ADU_{hyposmotic}$	HT	58.6	2.2 ± 1.9	0.1 ± 0.0	9.5 ± 3.6	47	38	0,77912

$DPPG_2$ suffered from systemic loss of ~ 60 %ID after 15 min for either formulation at NT. Osmotic stress reduced t_α 3-fold and $AUC_{120\ min}$ 2-fold (154 to 58 min and 3030 to 1702 %ID*h/ml) for isosmotic to hyposmotic formulation, respectively. Upon combining $DPPG_2$-TSL-$ADU_{hyposmotic}$ with HT, $DPPG_2$ was cleared initially (15 min) by 82 %ID and $AUC_{60\ min}$ decreased 3-fold (1702 to 640 %ID*h/ml) in comparison to respective NT group indicating loss of carrier within the first 15 minutes upon injection. However, still circulating $DPPG_2$ cleared in overall comparable t_α (table 23).

Table 23: Pharmacokinetic parameters of $DPPG_2$ in mice.
With a constant dosage of ADU (2 mg/kg), 39 µmol/kg or 24 µmol/kg $DPPG_2$, respectively for iso- or hyposmotic $DPPG_2$-TSL-ADU, were injected i.v. in BL6 mice at the beginning of a 60-minutes HT- or NT-treatment via WB. Plasma samples were measured via LC-MS method with LOQ_{DPPG2} being 1 µg/ml. Data represent n =2 per group.

Group	Treatment	C_{max} (µg/ml)	$C_{15\ min}$ (%ID)	$C_{120\ min}$ (%ID)	t_α (min)	$AUC_{60\ min}$ (%ID*h/ml)	$AUC_{120\ min}$ (%ID*h/ml)	R^2
$DPPG_2$-TSL-$ADU_{isosmotic}$	NT	856.4	38.1 ± 16.0	19.7 ± 10.9	153.9 ± 16.7	1553	3030	0.97141
$DPPG_2$-TSL-$ADU_{hyposmotic}$	NT	572.6	42.4 ± 3.2	6.5 ± 0.8	58.3 ± 7.8	1097	1702	0.98517
$DPPG_2$-TSL-$ADU_{hyposmotic}$	HT	572.4	18.4 ± 6.7	3.4 ± 2.3	41.2 ± 15.9	461	640	0.7847

In all groups, $DPPG_2$ and ADU cleared in a monophasic decay (figure 26.A and B). $DPPG_2$-TSL-$ADU_{isosmotic}$ presented continuous linear decline and ADU leakage with $\Delta AUC_{60\ min}$ of 732 %ID*h/ml (figure 26 C). Hyposmotic condition enforced drug leakage at NT which was by calculation only mildly increased to isosmotic condition ($\Delta AUC_{60\ min}$ of 866 %ID*h/ml) due to additional carrier instabilities (figure 26 D). Osmotic destabilization of $DPPG_2$-TSL-$ADU_{hyposmotic}$ was more pronounced upon HT-triggered drug release (figure 26 E), however, calculated $\Delta AUC_{60\ min}$ (414 %ID*h/ml) was smaller due to overall lower content recovery (ADU and $DPPG_2$).

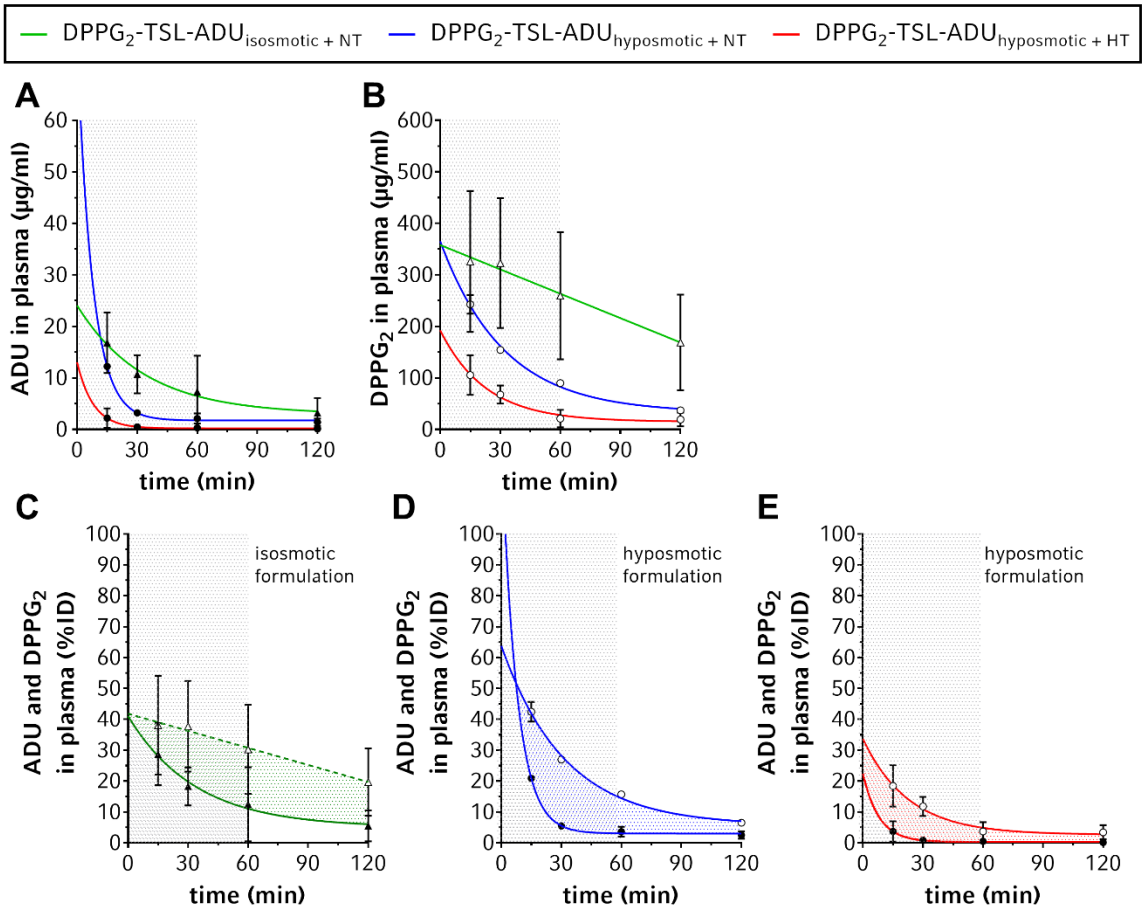

Figure 26: Plasma clearance of ADU and $DPPG_2$ in mice.
At the beginning of a 60-minutes (shaded area) WB-HT (red line, fitted) or WB-NT (blue and green line, fitted), BL6 mice were injected i.v. with 2 mg/kg ADU (C_{max} = 58.6) and 39 or 24 µmol/kg $DPPG_2$ (C_{max} = 856 and 573 µg/ml) respectively for iso- (triangle) or hyposmotic (circle) formulation. **(A)** ADU (filled symbols) and **(B)** $DPPG_2$ (empty symbols) plasma content were monitored over time and **(C-E)** placed in relation with highlighted subtraction area (△AUC). Data represent n = 2 per group.

iii. Pharmacokinetic profile in rats

It was postulated that a more pronounced exploration of the newly developed formulations might be achieved in rats. Hence, assessment of plasma stability of developed ADU formulation via PK (chapter II.D.f.ii) was conducted in BN rats and HT-treatment via WB was compared to sham-treated animals (chapter II.D.e.ii/iii). Free ADU served as control. With no payload to release, empty $DPPG_2$-TSL were injected in sham-treated animals to explore stability effect of drug-loading under hyposmotic carrier condition. Collected plasma samples were prepared for measurement via LC-MS (chapter III.D.g.iii).

$DPPG_2$ from isosmotic carrier cleared comparably with ~ 64 %ID lost after 240 min in both treatment groups (sham and HT). In sham-treated groups, plasma stability of carrier enduring osmotic stress was weakened, represented by lower content recovered after 240 min and according lower calculated $AUC_{240\ min}$ and t_a (20 to 37 %ID, 11040 to 13830 %ID*h/ml and 132 to 265 min, respectively) in contrast to isosmotic condition. The addition of HT further stressed hyposmotic carrier stability, displayed in ~1.5-fold reduction of $AUC_{240\ min}$, t_a and recovered content at 240 min (11040 to 8664 %ID*h/ml, 132 to 87 min and 20 to 16 %ID,

respectively). Noteworthy, upon injection of osmotically stressed empty carrier comparable destabilization was assessed in sham-treated animals, represented in a belly-shaped curve with lowest calculated $AUC_{240\ min}$ (8530 %ID*h/ml) and indicating a comparably behavior to drug-loaded $DPPG_2$-TSL after heat-triggered payload release (table 24).

Table 24: Pharmacokinetic parameters of $DPPG_2$ in rats.
$DPPG_2$ was injected with 72 and 21 µmol/kg for iso- or hyposmotic formulation, respectively, at the beginning of a 60-minutes WB-HT or into sham-treated BN rats, when keeping ADU-dosage constant (2 mg/kg). Plasma samples were measured via LC-MS method with LOQ_{DPPG2} being 1 µg/ml. Data represent n = 3 per group.

Group	Treatment	C_{max} (µg/ml)	$C_{15\ min}$ (%ID)	$C_{240\ min}$ (%ID)	t_α (min)	$AUC_{240\ min}$ (%ID*h/ml)	R^2
$DPPG_2$-$TSL_{hyposmotic}$	sham	521.0	90.8 ± 4.2	19.6 ± 3.8	111.0 ± 16.8	8530	0.97447
$DPPG_2$-TSL-$ADU_{isosmotic}$	sham	856.9	91.7 ± 12.3	36.7 ± 7.1	264.9 ± 18.9	13830	0.98321
$DPPG_2$-TSL-$ADU_{isosmotic}$	HT	856.9	79.7 ± 10.7	35.7 ± 5.0	290.3 ± 34.1	12270	0.94971
$DPPG_2$-TSL-$ADU_{hyposmotic}$	sham	514.7	107.2 ± 7.7	20.2 ± 9.9	131.8 ± 15.8	11040	0.97999
$DPPG_2$-TSL-$ADU_{hyposmotic}$	HT	514.7	111.0 ± 9.6	15.5 ± 11.6	86.8 ± 4.8	8664	0.98621

All investigated PK profiles presented a monophasic decay. In sham-treated groups, $DPPG_2$ of the isosmotic carrier cleared in a linear fashion, whereas osmotic stress condition accelerated clearance with even enhanced speed when payload was missing (figure 27.A). Addition of HT enforced clearance with a greater magnitude in hypo- than isosmotic formulation (figure 27.B).

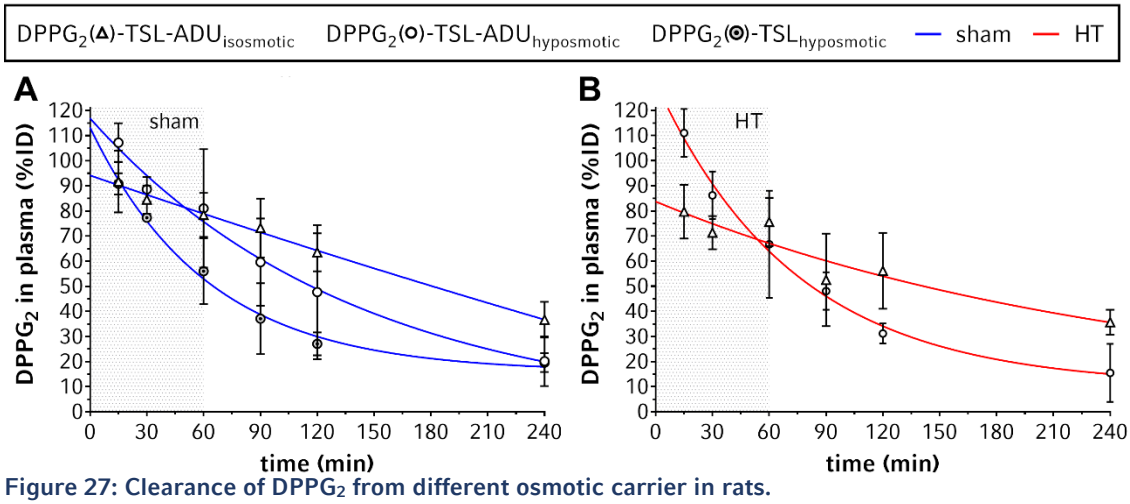

Figure 27: Clearance of $DPPG_2$ from different osmotic carrier in rats.
Liposomal formulations were designed with ~ 30 mol % of carrier lipids being $DPPG_2$ with iso-(triangle) or hyposmotic (circle) condition (C_{max} =857 or ~ 515 µg/ml, respectively). I.v. injection was conducted in BN rats at the beginning of a 60-minutes (shaded area) **(A)** sham-treatment (blue line, fitted) or **(B)** WB-HT (red line, fitted). Data represent n = 3 per group.

When comparing sham-treatment of either formulation, initial drug retention was comparable (~ 100 %ID at 15 min) but in hyposmotic formulation, ADU cleared faster shown by recovered content being 2-fold lower at 60 min (26 to 50 µg/ml) and 5-fold lower at 240 min (1 to 6 µg/ml). In accordance, $AUC_{240\ min}$ and t_α was reduced by ~2-fold (9652 to 5898 %ID/ml*h and 93 to 56 min, iso- to hyposmotic formulation). With isosmotic formulation, a 13 % drop in content 15 min after injection and $AUC_{60\ min}$ (4077 to 3520 %ID/ml*h) was recorded upon HT but accelerated clearance diminished by 90 min (figure 28.A). Hence, $AUC_{240\ min}$ stayed unchanged (9652 and 9726 µg/ml*h) and statistical prolongation of t_α (93 to 126 min) was not

representative, for sham and HT isosmotic groups, respectively (table 25). For osmotically stressed carrier, the addition of HT enhanced ADU release, as 50 %ID were cleared within 15 min and 94 %ID until end of HT, leaving a 7-fold lower plasma content (4 to 26 µg/ml) in comparison to sham-treated group at 60 min (figure 28.A). Comparing to sham-treatment, heat-triggered ADU release from hyposmotic formulation reduced t_{α} 3-fold from 56 to 19 min and $AUC_{240\ min}$ 4-fold from 5898 to 1594 %ID/ml*h. However, until end of experiment 98 %ID of ADU was cleared independent from treatment (1.2 and 1.5 µg/ml for sham and HT treated groups, respectively) (table 25).

Upon injection of free ADU, 2 % ID were recoverable at first sampling time point (15 min). At later time points (> 15 min), plasmatic content was below LOQ_{ADU} of LC-MS method (0.02 µg/ml). This is why statistical analysis was not possible (table 25 and figure 28.A). Noteworthy, ADU dosage (2 mg/kg) had been kept constant among all groups (table 40).

Table 25: Pharmacokinetic parameters of ADU in rats.
Free form or different liposomal formulations of ADU were injected i.v. (2 mg/kg) at the beginning of a 60-minutes treatment with WB at 41 °C (HT) or sham-treated (sham) BN rats. Plasma samples measured were via LC-MS with LOQ_{ADU} being 0.02 µg/ml. Data represent n = 3 per group.

Group	Treatment	C_{max} (µg/ml)	$C_{15\ min}$ (µg/ml)	$C_{240\ min}$ (µg/ml)	t_{α} (min)	$AUC_{240\ min}$ (%ID*h/ml)	R^2
free ADU	sham	58.6	0.01 ± 0.0	< LOD	*not possible*	*not possible*	*not possible*
free ADU	HT	58.6	0.02 ± 0.0	< LOD	*not possible*	*not possible*	*not possible*
$DPPG_2$-TSL-$ADU_{isosmotic}$	sham	58.6	60.2 ± 2.7	5.9 ± 0.1	92.7 ± 2.0	9652	0.99064
$DPPG_2$-TSL-$ADU_{isosmotic}$	HT	58.6	51.0 ± 4.0	8.9 ± 1.2	125.5 ± 8.3	9726	0.97998
$DPPG_2$-TSL-$ADU_{hyposmotic}$	sham	58.6	57.2 ± 7.0	1.2 ± 0.5	56.3 ± 4.2	5898	0.98028
$DPPG_2$-TSL-$ADU_{hyposmotic}$	HT	58.6	29.1 ± 9.5	1.5 ± 0.1	18.7 ± 8.2	1594	0.83177

Monophasic decay of ADU from $DPPG_2$-TSL-$ADU_{isosmotic}$ was equivalent between sham- and HT-treated groups (figure 28.A) and $\Delta AUC_{60\ min}$ comparable (297 and 247 %ID*h/ml, sham and HT group, respectively) a treatment-independent carrier elimination can be postulated (figure 28.B). Addition of osmotic stress in sham-treated animals accelerated monophasic decay of carrier and, even with lowered $DPPG_2$ contents in plasma, increase of $\Delta AUC_{60\ min}$ to 595 %ID*h/ml documented enhanced ADU leakage (figure 28.D). Within hyposmotic formulation groups, addition of HT altered monophasic clearance of ADU to biphasic decay (figure 28.A). Release being HT-triggered was evident ($\Delta AUC_{60\ min}$ = 2816 %ID*h/ml) (figure 28.C). Comparing $\Delta AUC_{240\ min}$ (hyposmotic formulation: 5142 and 7070 %ID*h/ml or isosmotic formulation: 4178 and 2544 %ID*h/ml, sham- and HT-treatment respectively) to $\Delta AUC_{60\ min}$ revealed 40 % of overall release taking place during HT in hyposmotic formulation, despite accelerated carrier clearance (figure 27.B) whereas ~ 10 % leaked in sham-treated group or isosmotic groups.

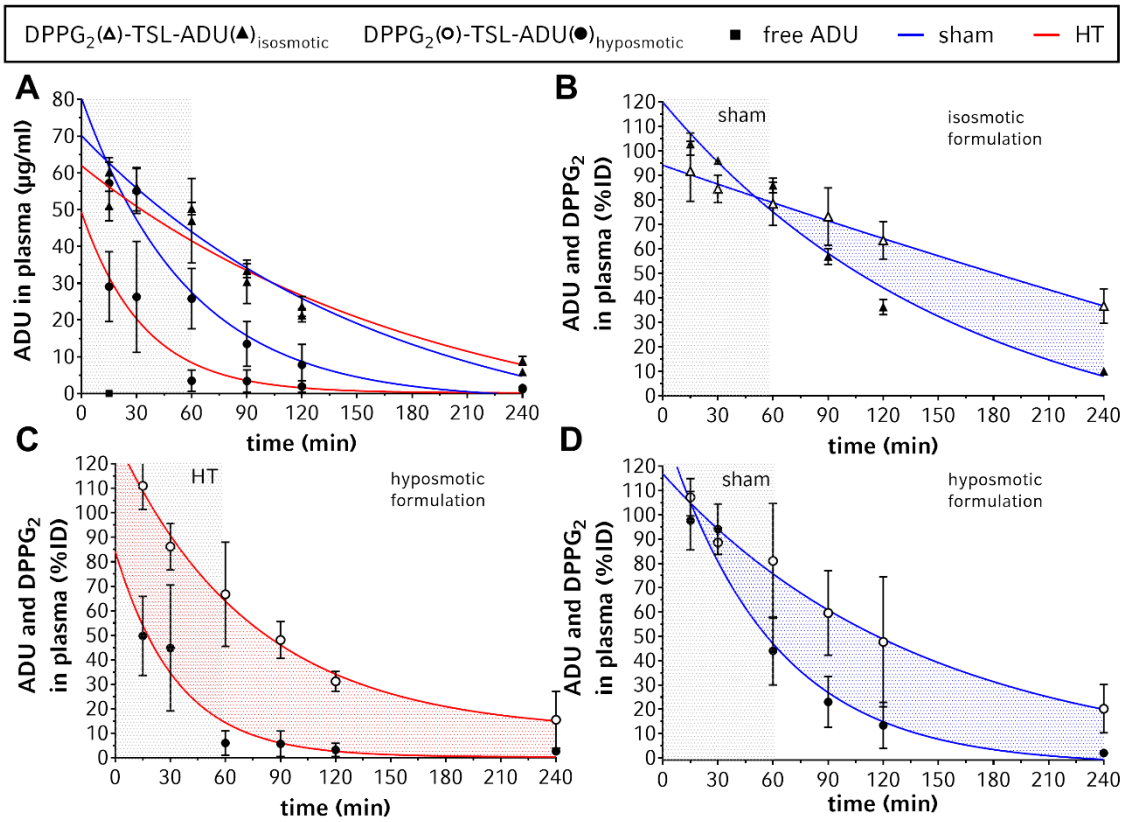

Figure 28: Influence of carrier osmotic condition on ADU release in rats.
(A) Free ADU (square) and iso-(triangle) or hyposmotic (circle) $DPPG_2$-TSL-ADU were injected i.v. (ADU: C_{max} = 58.6) at the beginning of a 60-minutes (shaded area) sham- (blue line, fitted) or HT-treatment via WB (red line, fitted). **(B-D)** Recovered ADU and $DPPG_2$ (respective filled and empty symbol) from the same sample are placed in relation with highlighted subtraction area (△AUC) for respective groups. Data represent n = 3 per group

By meeting the criteria of prolonging plasma stability of ADU and allowing triggerable drug release upon HT, hyposmotic condition was selected for consecutive *in vivo* studies.

b. Systemic response to STING-activation in mice

With current literature claiming distinct antitumor response upon i.t. injection (500 µg) free ADU in several mice tumor models [65], $DPPG_2$-TSL-$ADU_{hyposmotic}$ were injected once (chapter III.D.g.vi) with 2 mg/kg ADU (~ 500 µg per dose) and combined with WB-HT (chapter II.D.f.iii) in B16-bearing mice.

Mice, injected i.v. with 2 mg/kg ADU in hyposmotic carrier (table 40), displayed severe systemic adverse drug reaction (ADR) within 24 h, leading to animal sacrifice within 48 h (n = 2). Dose-reduction to 1 mg/ml circumvented systemic reaction and was tolerated (n = 2). As a distinct HT-triggered release had not been proven in plasma (section a.ii), additional reduction of systemic dosage was assumed to further lower ADU accumulation in heated tumor. Analysis of this was not feasible as low recovery in PK-study did not rise hope for detection in tissue with available LC-MS method (LOQ_{ADU} in tissue being 0.95 µg/ml). Hence, eexploration of liposomal formulation in B16 melanoma model was stopped at this point.

c. Proving responsiveness of sarcoma model

Driven by obtained data in mice, it was investigated whether the ADR reaction to $DPPG_2$-TSL-ADU was reproducible in rats. Therefore, a dose-escalation of free ADU (section i) before studying liposomal ADU (section ii) in a consecutive single treatment study (chapter II.D.f.iv) in syngeneic BN175 sarcoma model was conducted. Injection was combined with lamp-HT and compared to sham-treatment (chapter II.D.e.ii). In contrast to WB, lamp-technique reduces the surface area of heated tissue. Thereby, HT-triggered intravascular drug release can be limited to a more focused area and off-target accumulation reduced [125]. Addition control experiment with injection of saline + HT were conducted (section iii).

i. Testing response by dose-escalation

To assess safety and responsiveness of BN175 sarcoma model, a dose-escalation was performed. Free ADU was escalated by 2, 20, and 100 % of full i.t. dosage (500 µg) and compared to solvent (HBW pH 7.4) (table 40).

Implanted fragments grew in a standardized manner, with all groups reaching study inclusion tumor volumes within ~ 5 - 6 days. Mild, short bleeding during temperature probe implantation was documented in at least every second rat as well as drug reflux after ~ every third i.t. injection. A distinctive impact between lowest ADU dosage (10 µg) and solvent on tumor growth was not detectable. For further escalation steps, a survival was stepwise prolonged from 8 to 9 or 11 days (10 to 100 or 500 µg i.t, respectively) (figure 29).

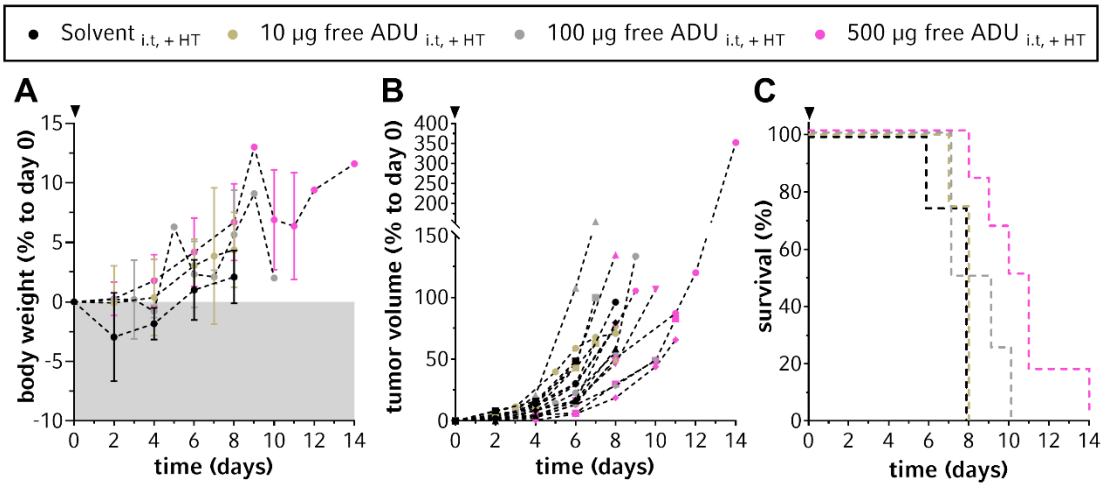

Figure 29: Dose-escalation of free ADU i.t. + HT in BN175 Model.
Free ADU was increased from 10 (brown), 100 (grey) to 500 µg (pink) and compared to solvent (black) i.t. injected at the beginning of a 60-minutes HT-treatment via lamp. **(A)** Body weight and **(B)** tumor growth development was monitored until **(C)** end point. Data represent n = 4 (solvent, 10 µg, 100 µg) or n = 6 (500 µg) per group.

However, per group 75 % of animals suffered from ulceration, unravelling a drug but not dosage driven local adverse effect. Crust formation at regions of HT (~ 1/3 of all treated animals) was not correlating to temperature probe induced bleeding or dosage and was therefore considered to be driven by lamp-heating. Signs of unwanted systemic effects (e.g., severe body weight loss, itching, and redness) were never documented.

ii. Challenging response upon systemic injection

With dosage-dependent BN175 responsiveness and safety of free ADU injection in BN rats being proven, systemic injection of ADU at a dosage of 2 mg/kg (~ 500 µg, table 40) was explored in combination with lamp-HT. Effect of HT-triggered accumulation in tumor tissue was explored in contrast to sham-treatment. Saline and free ADU served as control.

Animals from both liposomal injected groups suffered longer from temporary mild body weight loss than free ADU + HT or sham-treated control groups (figure 30.A-C), but no severe body weight loss or other signs of unwanted systemic effects were documented. Ulceration occurred in every second animal treated with free ADU i.v., every sixth animal after liposomal injection (independent of HT or ham-combination) and none in saline group (n = 6). Comparing free ADU i.v. to above described 500 µg i.t. group, local application reduced tumor growth speed to a greater extent (survival 9 and 11 days, respectively). However, liposomal delivery of ADU controlled tumor growth longer (figure 30.D) and outperformed all free drug groups (i.v. and i.t.), notably HT-independent (figure 30.E).

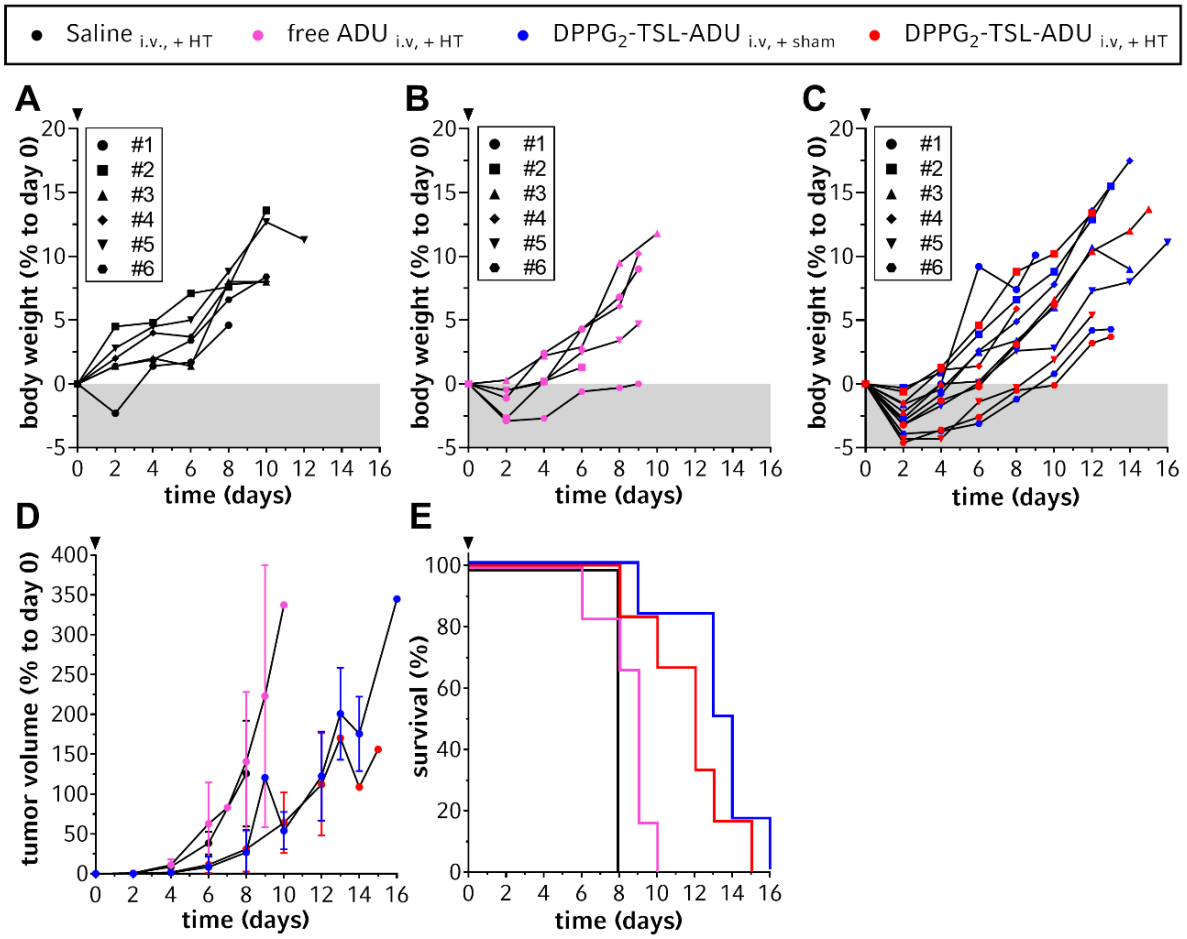

Figure 30: Therapeutic response to ADU in BN175 Model.
At the beginning of a 60-minutes HT-treatment via lamp, saline (black), free ADU (pink) and liposomal ADU (red) was injected i.v. (2 mg/kg) and compared to sham-treated animals injected with liposomal ADU (blue). **(A-C)** Tumor growth and **(D)** and body weight was monitored in respective groups until **(E)** end point was reached. Data represent n = 6 per group.

iii. Impact of Normothermia and Hyperthermia

With the prolongation of survival for animals treated with liposomal ADU in comparison to free drug (section ii), a proof of concept was given for STING encapsulation approach. However, the slightly enhanced survival rate of sham-treated animals was to be further evaluated by conducting a HT experiment with saline-treated animals.

When comparing sham to HT-treated animals injected with saline, variations in body weight were not observed. However, significant enhanced tumor growth speed was noted for HT-treated animals (figure 31.A and B).Treatment-dependent side effect were not noted, however wound closure was inefficient in one animal of HT groups, causing end point slightly earlier than tumor size end point would have been. However, data can be seen as robust as sham-treated group was conducted with n = 6 instead of n = 3 for HT-group. Upon comparison to animals treated with solvent i.t. + HT (see section ii), survival time was identical to saline i.v. injection + HT (figure 31.C).

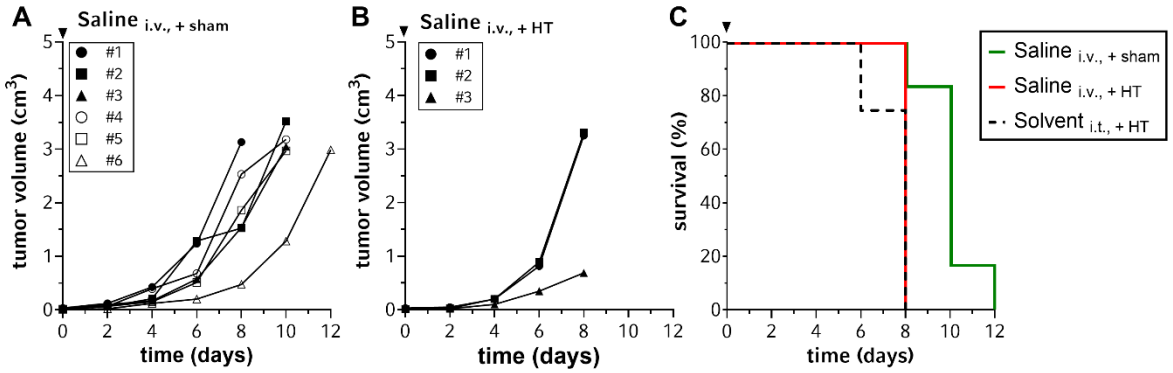

Figure 31: Comparison of HT- and sham-treated controls.
At the beginning of a 60-minutes **(A)** sham or **(B)** HT-treatment via lamp, saline was injected i.v. and tumor growth monitored. **(C)** Resulting survival is shown together with a control group for i.t. injection (solvent). Data represent n = 6 for control + sham, n = 3 for control + HT and n = 4 for solvent i.t. + HT group.

d. Efficacy of heat-triggered ADU accumulation in sarcoma model

Despite having shown HT-triggered drug release in PK (section a.iii), therapeutic response to liposomal ADU in syngeneic BN175 sarcoma model was not enhanced upon local HT. However, $DPPG_2$-TSL delivery outperformed free ADU (section c). Henceforward, accumulation capacity in heated tumor was to be assessed with a BD-study (chapter II.D.f.iii). ADU dosage was kept constant among all groups (table 40). Collected samples were prepared for measurement via LC-MS (chapter III.D.g.iii).

Elevated plasma concentration upon $DPPG_2$-TSL-ADU injection was dependent on liposomal encapsulation as ~ 60-times less (0.3 %ID/g) were recovered after i.v. application of free ADU (figure 32.A). None was detected in plasma after i.t. injection. In addition, heart, lung, liver, and spleen were cleared after free ADU application (i.v. or i.t.), leaving recoverable content only in kidney with entrapment of 0.02 %ID/g. By injecting $DPPG_2$-TSL-ADU, concentration of ADU in kidney was significantly 10-fold increased (0.2 %ID/g) (table 26 and figure 32.B).

Table 26: Recovered ADU and $DPPG_2$ in plasma and organs of tumor-bearing rats.
Free ADU or $DPPG_2$-TSL-ADU were applied i.t. (500 µg) or i.v. (2 mg/kg), with 23.9 µmol/kg $DPPG_2$ respectively for TSL. After 60-minutes local lamp-HT, injected ADU (~ 500 µg) and $DPPG_2$ (~ 5000 µg) were measured in organ tissue via LC-MS with LOQ being 0.02 and 1.0 µg/ml in plasma and 0.03 and 0.95 µg/ml in tissue, respectively. Data represent n = 6 per group.

Group	Plasma (%ID)	Lung (%ID/g)	Heart (%ID/g)	Liver (%ID/g)	Spleen (%ID/g)	Kidney (%ID/g)
free ADU, i.t.	< LOD	< LOD	< LOD	< LOD	< LOD	0.02 ± 0.0
free ADU, i.v.	0.3 ± 0.5	< LOD	< LOD	< LOD	< LOD	0.02 ± 0.0
$DPPG_2$-TSL-ADU, i.v.						
ADU	17.0 ± 7.2	0.02 ± 0.0	0.03 ± 0.0	0.5 ± 0.4	3.0 ± 0.3	0.2 ± 0.0
$DPPG_2$	4.4 ± 0.6	0.06 ± 0.0	0.03 ± 0.0	0.3 ± 0.1	4.3 ± 1.3	0.2 ± 0.1

In free drug groups, ADU was neither recovered in control nor heated tumor after i.v. injection. Local application allowed ADU recovery after 60 min, with no detectable re-distribution to contralateral control tumor (table 27). ADU accumulated homogeneously within tumors after injection of $DPPG_2$-TSL-ADU, whereas highly variating concentrations were recovered after i.t. application of free ADU with an average 9-fold enhanced accumulation in heated tissue (figure 32.C). Driven by study design, tumor volume was standardized for heated tumor but no weight dependent accumulation was visible.

Table 27: Effect of HT on ADU and $DPPG_2$ accumulation in rat tumors.
Local lamp-HT was conducted for 60 min on one tumor while the other was left under physiological conditions (control) with i.t. or i.v. application of free drug or liposomal formulation. After HT, injected ADU (~ 500 µg) and $DPPG_2$ (~ 5000 µg) were measured via LC-MS with LOQ in tissue being 0.03 and 0.95 µg/ml, respectively. Data represent n = 6 per group.

Group	Tumor weight (g)		Content per tumor (µg)		%ID per tumor tissue (%ID/g)	
	Control	HT	Control	HT	Control	HT
free ADU, i.t.	0.5 ± 0.1	0.6 ± 0.1	< LOD	1.1 ± 1.1	< LOD	0.4 ± 0.5
free ADU, i.v.	0.2 ± 0.1	0.6 ± 0.3	< LOD	< LOD	< LOD	< LOD
$DPPG_2$-TSL-ADU, i.v						
ADU	0.3 ± 0.2	0.5 ± 0.1	0.03 ± 0.0	0.1 ± 0.6	0.02 ± 0.0	0.05 ± 0.0
$DPPG_2$			0.8 ± 0.4	2.9 ± 1.6	0.08 ± 0.0	0.1 ± 0.1

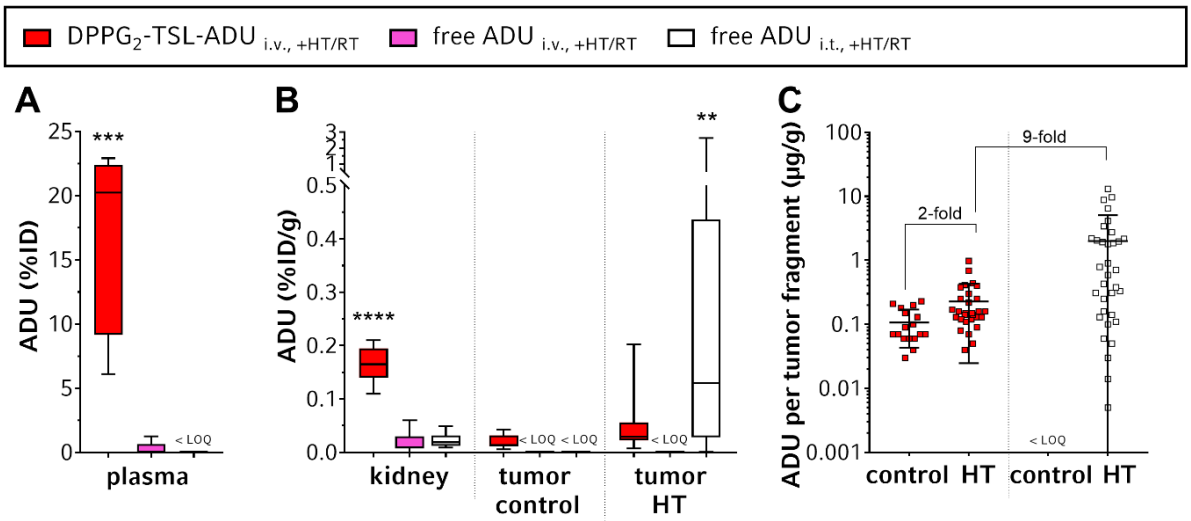

Figure 32: Recovery of ADU from tissue after local HT in tumor-bearing rats.
Injection of 500 µg free ADU i.t. (white) or 2 mg/kg in free (pink) or liposomal form (red) was combined with a 60-minutes HT via WB on one-tumor bearing leg (tumor HT), while the contralateral was not treated and its tumor left under physiological conditions (tumor control). ADU was detected in **(A)** plasma, **(B)** kidney and tumor tissue. **(C)** Display of recovered ADU per tumor fragment. Data represent n = 6 per group.

With $DPPG_2$-TSL-$ADU_{hyposmotic}$, a HT-dependent drug accumulation in heated tumor was proven with a 3.3-fold increased ADU concentration in comparison to control. A correlation 3.6-fold increase in carrier was recorded respectively (table 27). In the same group, control tumors accumulated 0.02 %ID/g ADU, whereas $DPPG_2$ entrapped ~ 2-times more in control tumor. Within organ samples of animals injected with $DPPG_2$-TSL-$ADU_{hyposmotic}$, lung and heart accumulated comparable amounts ~ 0.03 %ID/g ADU, liver entrapped significant 20-fold, and spleen significant 100-fold more (0.5 and 3 %ID/g) (table 26). Noteworthy, ADU accumulation in lung and heart was comparable to control tumor and 10-fold reduced to kidney (table 26 and 27).

For the first time, ADU and $DPPG_2$ were recovered from the same samples with the same method (LC-MS). A comparison between both was conducted in relation to %ID (figure 33). In association to ADU, $DPPG_2$ distributed comparably with recovered content being lowest in lung and heart, identical in kidney, ~ 1.5-times lower in liver and higher in spleen. $DPPG_2$ measured in spleen was equal to plasma (4 %ID/g and 4 %ID, respectively) but ADU varied by significant 6-fold among these samples (3 %ID/g and 17 %ID, respectively). Hence, plasmatic ADU was 4-times higher than $DPPG_2$ (figure 33.A).

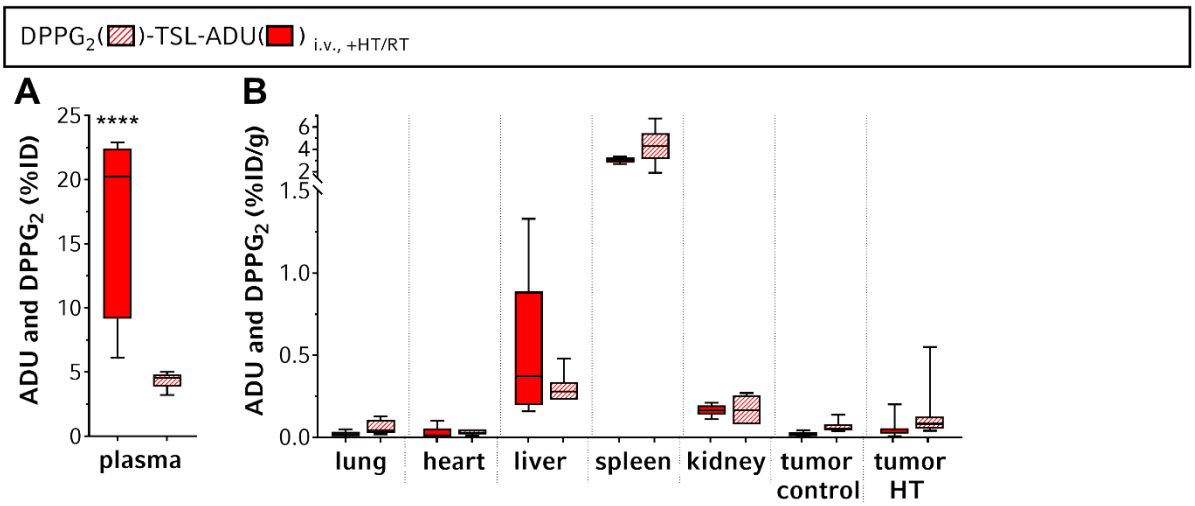

Figure 33: Biodistribution of ADU and $DPPG_2$ in tumor-bearing rats.
$DPPG_2$-TSL-$ADU_{hyposmotic}$ was injected i.v. at the beginning of a 60-minutes HT-treatment of one tumor via lamp (tumor HT), while the contralateral was left under physiological condition (tumor control). ADU and $DPPG_2$ (C_{max} = 58.6 and 573 µg/ml, respectively) were recovered within the same **(A)** plasma and **(B)** tissue sample via LC-MS. Data represent n = 6 per group.

e. Development of MatBIII breast cancer model

Driven by obtained data in the sarcoma model, the robustness of ADU-based therapy strategy was to be clarified further in a second tumor model. With promising data in current literature on predictive immunoscore in breast cancer [53] being translatable to preclinical models, selection fell on a preclinical mamma adenocarcinoma model. MatBIII cells were obtained from commercially available source and cell culture protocols successfully established (chapter III.C.). First, *in vitro* data on impact of HT in combination with free ADU (section i) was created as well as feasibility of s.c. tumor growth induction in syngeneic female Fisher

rats demonstrated (section ii) with robustness towards cell injection and tumor fragment implantation (data not shown).

i. Stressing cell viability in vitro

In order to set up future *in vitro* experimental plans with MatBIII, a feasible cell density to be seeded per well (96-welll plate) leading to a distinct growth within 48 and 72 h was determined. Therefor, increasing amounts were plated and after cell density determined via SRB assay (chapter III.C.d.i).

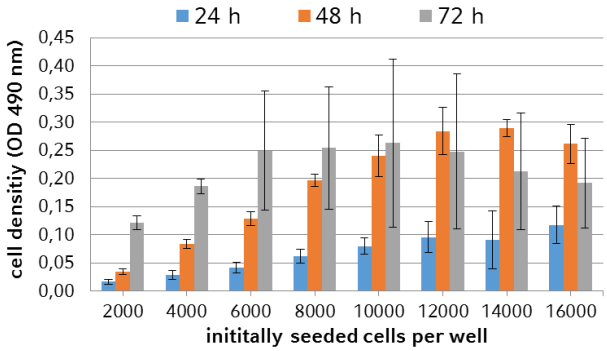

Figure 34: Density of Mat BIII cells over time.
Increasing amounts of cells were incubated for 24 (blue), 48 (orange) and 72 h (grey) before determination of density. Data represent n = 3 per group.

Cell viability after 24, 48, and 72 h was most distinct with 2000 to 4000 cells/well plated initially. When > 10000 cells/well were seeded, cell growth exceeded nutritive capacity of growth medium after 72 h, leading to cell death. Comparable drop was seen at 48 h with initial > 14000 cells/well (figure 34).

In a second step, responsiveness of MatBIII cells towards HT was to be assessed. Therefore, cells were exposed to HT (WB, 41 °C) and cell density evaluated afterwards via SRB assay (chapter III.C.d.ii). NT-(WB 37 °C) and sham-treatment (incubator) served as control. With the employed set up, MatBIII cell viability was not impacted by HT in comparison to NT and sham-treatment (figure 35). While behaviour of NT- and HT-treated cells was highly comparable, incubator treatment lowered cell density after 48 h, which was attributed to cell death due to lack of nutrition, as media-exchange on treatment day was not conducted for these samples. If it was added, effect was reversed (data not shown).

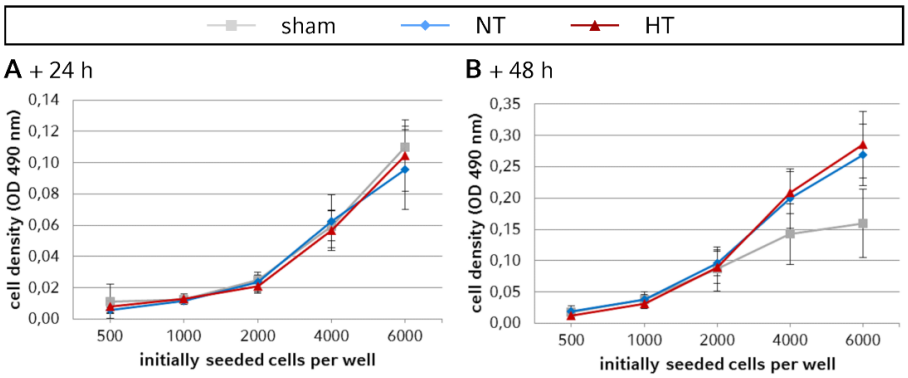

Figure 35: Effect of HT on MatBIII *in vitro*.
MatBIII cells were incubated for 60 min in a WB set at 41 °C (HT, red) or 37 °C (NT, blue) and compared to sham-treatment (grey). Cell density was assessed after **(A)** 24 and **(B)** 48 h. Data represent n = 3 per group.

In a third step, impact of free ADU on MatBIII cells cultured *in vitro* was evaluated. Increasing concentrations of ADU in growth medium were combined with HT-treatment (WB, 41 °C) and effect on cell density determined via SRB assay (chapter III.C.d. iii). Growth medium served

as control. Up until a concentration of 12.5 µM ADU in growth medium + HT, MatBIII cell density was elevated after 24 h and more pronounced after 48 h. Significance was not reached as high standard deviations were encountered. Recovered density of either treatment group (HT or NT) either was never lower than controls (figure 36) but, in general, MatBIII cells displayed reduced adherence to 96-well plate immediately after heating.

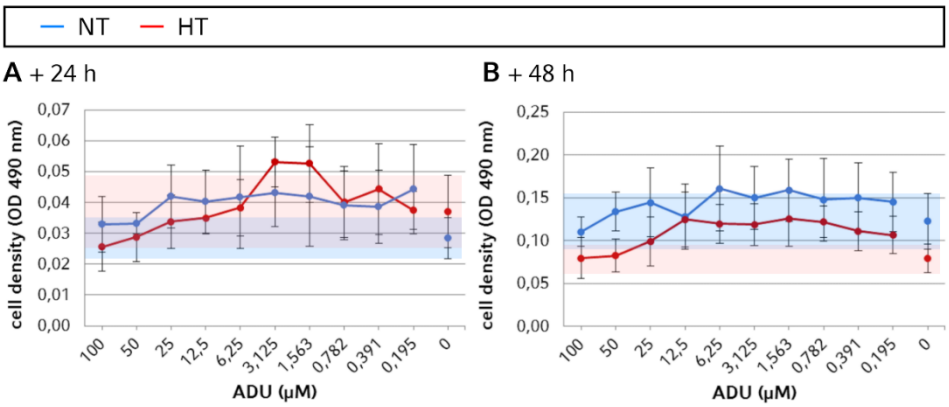

Figure 36: Impact of ADU + HT on MatBIII *in vitro*.
MatBIII cells were incubated for 60 min in a WB set at 41 °C (HT, red) or 37 °C (NT, blue) with increasing concentrations of ADU and cell density determined after **(A)** 24 and **(B)** 48 h after. Area of control samples (0 µM) is shaded in respective color of treatment. Data represent n = 3 per group.

ii. Testing reproducibility of tumor growth induction

In a final step, feasibility of MatBIII tumor growth in s.c. space at hind leg of syngeneic rats (chapter III.D.f.i) was explored for the first time. S.c. MatBIII cell injection of 1.0 x 10^6 in 100 µl DPBS led to reproducible tumor growth *in vivo*. However inducing several tumor formations in close proximity in almost every second case. Upon monitoring induction efficacy of several consecutive cell passages (#2 to 6), a tendency towards later tumor growth establishment the longer cells were cultured beforehand was noted (figure 38.A). So-established tumors were harvested, fragmented and frozen and then implanted again in syngeneic host, leading to reproducible tumor growth (figure 37.B). Hence, a protocol for fragment implantation was successfully established (chapter III.D.c.ii.).

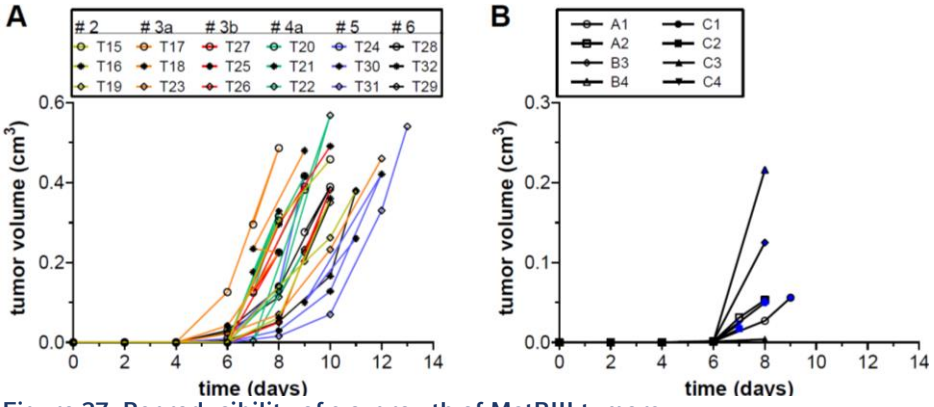

Figure 37: Reproducibility of s.c. growth of MatBIII tumors.
(A) MatBIII cells were s.c. injected (1.0 x 10^6 in 100 µl DPBS) in female Fisher rats and resulting tumor growth monitored with colors indicating consecutive cell culture passages (#) of injected cells. Data represent n = 18 per group. **(B)** Tumor growth upon MatBIII fragment implantation. Data represent n = 8 per group.

C) Liposomal encapsulation of the TLR-7/8 agonist Resiquimod

Experiments with an initial $DPPG_2$-TSL-R848 formulation showed stability *in vitro* but significant leakage upon i.v. injection in rats [161]. The author discussed loading condition, intra-liposomal pH and D:L ratio to be key factors for achieving R848 protonation potentially enhancing encapsulation stability *in vivo*. Consequently, formulation was modified by Thermosome GmbH (Planegg, Germany) (table 28) and provided for *in vivo* studies. Characteristics of used $DPPG_2$-TSL-R848 batches are summarized in table 38.

Table 28: Parameters of $DPPG_2$-TSL-R848 before and after modification.
Values are representatives and depict formulations used in PK-studies.

	Loading	Hydration buffer	Extra-liposomal buffer	Size (nm)	PDI	Z-POT (mV)	EE (%)	R848:lipid (mol:mol)
initial	8 h / 30°C	300 mM ammonium sulfate pH 6.4	HBS pH 6.4	167.9	0.05	-26.1	79	0.2
adjusted	15 min / 37°C	300 mM citrate pH 3	HBS pH 6.4	170.5	0.07	-32.1	87	0.05

During this thesis, $DPPG_2$-TSL-$R848_{adjusted}$ was thoroughly assessed after having proven superior plasma stability upon modification (section a). Efficacy of HT-triggered release (section b) and plasmatic cytokine induction (section c) were investigated followed by feasibility of heat-triggered tumor accumulation and respective biodistribution in BN175 soft tissue sarcoma model (section d). Within the same rat model, antitumor effect of R848 + HT was explored (section e) and enhanced upon combination with $DPPG_2$-TSL-DOX (section f).

a. Influence of formulation modifications on plasma stability

To allow comparison, raw data of $DPPG_2$-TSL-$R848_{initial}$ (kindly provided by Matteo Petrini) was recalculated to fit PK-data (chapter III.D.f.ii) collected for $DPPG_2$-TSL-$R848_{adjusted}$. PK-protocol of either study in BN rats was comparable, with liposomal injection at the beginning of a NT-treatment (chapter II.D.e.i). The same number of plasma samples were harvested but at 0, 2, 10, 30, 60, 90 and 120 min in previous PK-study. Comparable HPLC method (chapter III.D.g.i) were used. Safety was ensured in accordance to estimated elevated plasma contents after formulation optimization by adapting R848 dosage from 3 to 2 mg/kg (table 41).

Table 29: Pharmacokinetic parameters of R848 in initial and adjusted formulation in rats.
Liposomal formulation was injected i.v. at the beginning of a 60-minutes WB-NT. Data represent n = 3 per group.

Group	Dosage (mg/kg)	R848 C_{max} (µg/ml)	$C_{15\ min}$ (%ID)	$C_{120\ min}$ (%ID)	t_α (min)	$AUC_{60\ min}$ (%ID*h/ml)	$AUC_{120\ min}$ (%ID *h/ml)	R^2
$DPPG_2$-TSL-$R848_{initial}$	3	88.0	31.8	5.0 ± 1.5	13.2 ± 2.7	789	1236	0.99958
$DPPG_2$-TSL-$R848_{adjusted}$	2	58.6	38.7 ± 6.6	9.1 ± 2.4	88.9 ± 5.7	1231	2146	0.96801

By lowering D:L ratio during optimization, amount of injected lipids was elevated from 62 to 140 µmol/kg (table 28 and 40). Despite dose-reduction, overall higher R848 plasma levels were detected with, for example, ~ 2-fold increase at 60 and 120 min (11 to 22 %ID and 5 to 9 %ID, respectively) rendering corresponding increase in AUC. Strongest influence was detected on calculated t_α (table 29), driven by altered decay from biphasic (initial data) to monophasic (adjusted formulation) (figure 38).

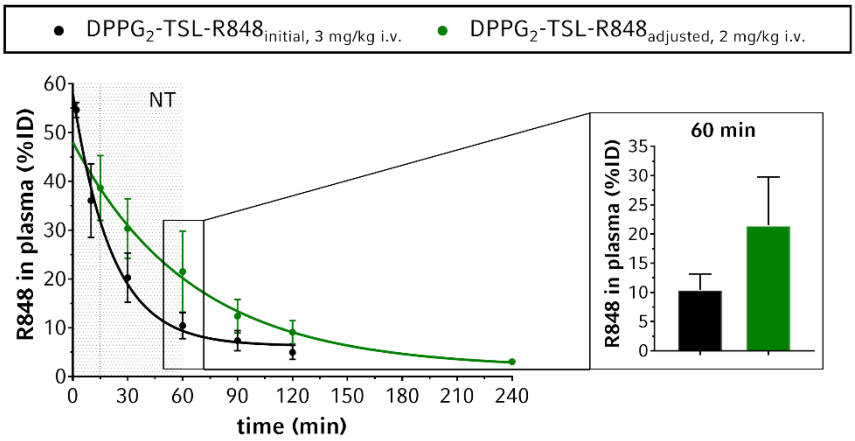

Figure 38: Influence of formulation modification on R848 plasma clearance at NT in rats.
(A) In BN rats, i.v. injection of $DPPG_2$-TSL-R848 was conducted at the beginning of a 60-minute (shaded area) NT-treatment via WB. Initial formulation (black) was applied with 3 mg/kg and an injection volume of 750 µl and adjusted formulation (green) with 2 mg/kg and 1000 µl, respectively. Dotted line resembles 15 min. **(B)** Plasma drug content at 60 min. Data represent n = 3 per group.

b. Hyperthermia-triggered release in plasma

To further explore $DPPG_2$-TSL-$R848_{adjusted}$ WB temperature was increased to 41 °C, mimicking regional HT and facilitating heat-triggered release evaluated in comparison to respective NT group stated in section a. Free R848 served as control.

Upon free R848 injection (table 41), 96 %ID were cleared treatment-independently within 15 min (2.4 and 2.6 µg/ml, NT and HT respectively). In contrast, at NT liposomal encapsulation elevated recovered content (2.4 to 22.7 µg/ml) and $AUC_{240\ min}$ (149 to 1282 µg*h/ml) 9-fold and prolonged t_α 3-times (30 to 90 min). The addition of HT in liposomal injected groups, reduced R848 at 60 min from 13 to 8 µg/ml, whereas comparable content at 15 and 240 min (40 and 3 %ID) were recovered (table 30). This gradually accelerated clearance upon HT was indicated by reduction in AUC from 1.1 to 1.3-fold between 60 to 240 min and a shift from mono- to biphasic R848 decay (figure 39.A) with respective 3-fold lower t_α (90 to 33 min) in comparison to NT-treated group. Upon liposomal release, R848 cleared with comparable speed documented for free R848 + HT (t_α 44 min, biphasic decay) (table 30).

Table 30: Pharmacokinetic parameters of R848 in rats.
Free R848 or $DPPG_2$-TSL-R848 were injected i.v. (R848: C_{max} = 58.6 µg/ml) as at the beginning of a 60-minutes NT- or HT-treatment via WB. Plasma samples were measured via HPLC. Data represent n = 3 per group.

Group	Water bath	$C_{15\ min}$ (µg/ml)	$C_{240\ min}$ (µg/ml)	tα (min)	$AUC_{60\ min}$ (µg*h/ml)	$AUC_{240\ min}$ (µg*h/ml)	R^2
free R848, i.v.	NT	2.4 ± 0.5	0.3 ± 0.05	30.4 ± 4.3	70	147	0.99351
free R848, i.v.	HT	2.6 ± 0.4	0.4 ± 0.04	44.3 ± 4.4	87	186	0.98070
$DPPG_2$-TSL-$R848_{adjusted}$, i.v.	HT	22.5 ± 2.0	1.8 ± 0.1	32.7 ± 7.9	641	1282	0.99650

Despite constant dosage of 967 µmol/kg, $DPPG_2$ recovered in HT group was ~ 60-70 µg/ml decreased throughout the study when compared to NT group, which reduced AUC and t_α accordingly (table 31). With experiments being conducted in parallel with the same batch stored at -20 °C, possible decomposition of lipids before injection was ruled out.

Table 31: Pharmacokinetic parameters of $DPPG_2$ in rats.
$DPPG_2$-TSL-R848 (R848: 2 mg/kg; $DPPG_2$: 40.3 µmol/kg) was injected i.v in BN rats at the beginning of a 60-minutes HT- or NT-treatment via WB. Plasma samples were measured via LC-MS. Data represent n = 3 per group.

Treatment group	C_{max} (µg/ml)	$C_{15\ min}$ (µg/ml)	$C_{240\ min}$ (µg/ml)	t_{α} (min)	$AUC_{240\ min}$ (µg*h/ml)	R^2
$DPPG_2$-TSL-R848$_{opmized}$, i.v. + NT	967.0	772.5 ± 111.6	310.0 ± 38.7	245.3 ± 22.4	109800	0.96730
$DPPG_2$-TSL-R848$_{opmized}$, i.v. + HT	967.0	712.0 ± 65.4	246.0 ± 14.8	218.8 ± 9.5	95780	0.98780

Overall, monophasic decay of carrier lipid $DPPG_2$ was shifted by 8 %ID throughout the study between NT and HT groups (figure 39.B). In contrast, HT-triggered R848 release and accelerated clearance. Comparing recovered payload to $DPPG_2$, $\Delta AUC_{60\ min}$ was 1943 and 1776 %ID*h for NT and HT groups (figure 39.C and D, the 9 %-difference indicating a mildly efficient heat-triggered drug release in direct comparison).

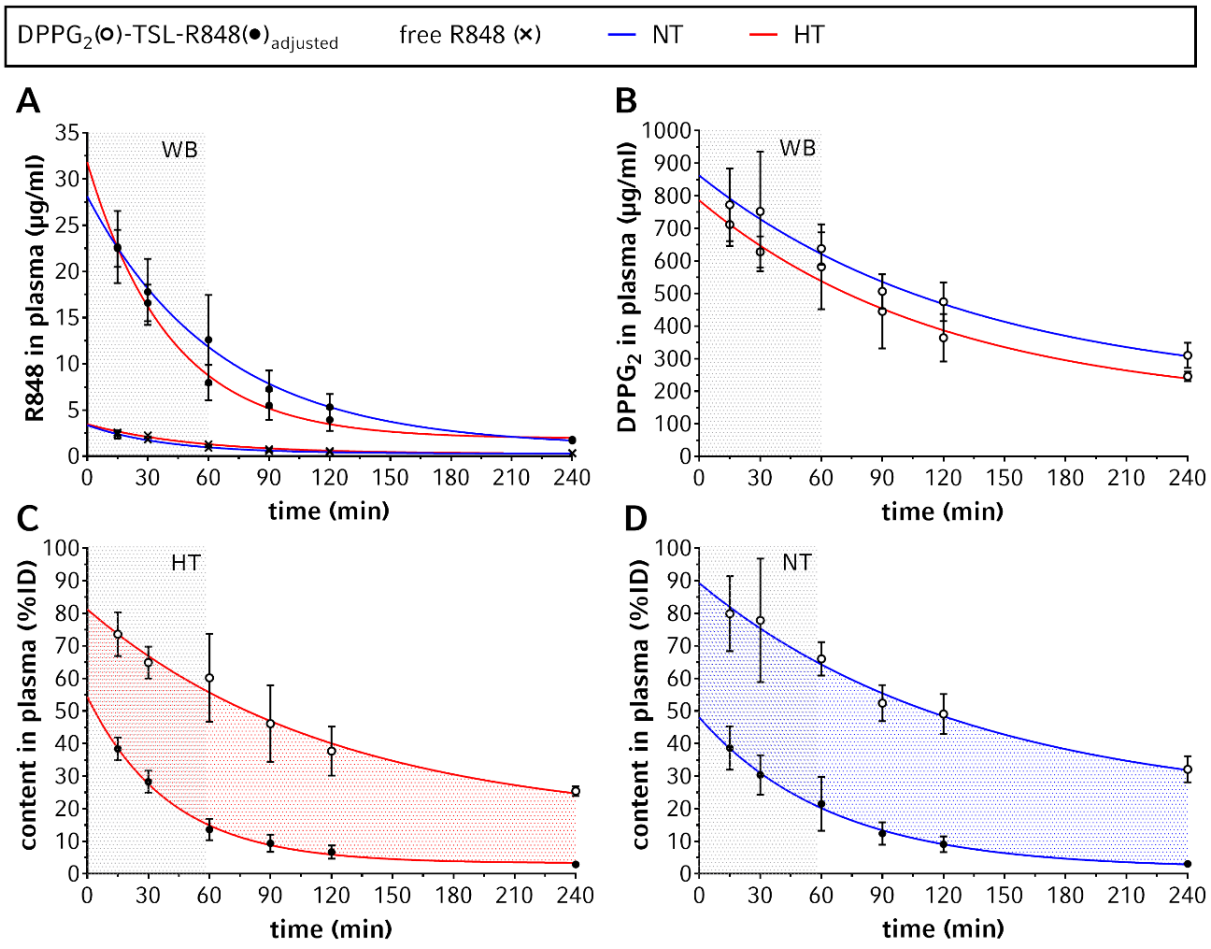

Figure 39: Influence of HT on R848 plasma stability in rats.
I.v. injection of 2 mg/kg R848 in free (cross) or adjusted liposomal form (circle) at the beginning of a 60-minutes (shaded area) WB-treatment with HT (red line, fitted) or NT (blue line, fitted) conditions in BN rats. Plasma decay of **(A)** R848 (filled circle) and **(B)** $DPPG_2$ (empty circle) in relation to treatment condition. **(C, D)** Correlation between recovered R848 and $DPPG_2$ of the same samples with highlighted subtraction area (△AUC), at HT and NT. Data represent n = 3 per group.

Due to data acquired proving successful optimization of encapsulation stability at NT conditions, $DPPG_2$-TSL-R848$_{adjusted}$ was used for all subsequent studies.

c. Organdistribution and heat-dependent tumor accumulation

To clarify if R848 encapsulation in $DPPG_2$-TSL does not only enable intravascular HT-triggered drug release but also facilitates local accumulation in heated tumor tissue, a BD-study in rats bearing two BN175 tumors was conducted (chapter II.D.f.ii).

Beforehand, a method for R848 recovery from tissue was developed. During this process, impact of sample solvent (MeOH versus ACN) in several dilution factors (10, 30, 50, 70, 90 versus 100 %) and loaded volume (500 µl versus 1600 µl) on STRATAX columns were assessed and 30 % MeOH and high volume selected. Upon loading, R848 was found to be stable on STRATAX columns in < 30 % ACN and < 50 % MeOH. Hence, 10 and 30 % MeOH were selected for washing. Addition of vacuum was confirmed to not impact stability of ADU during column washing step. Elution with MeOH was more efficient and reproducible than ACN. LOD_{R848} was confirmed to be 0.01 µg/g. Final method was used for preparing harvested tissue samples for HPLC analysis (chapter III.D.g.i).

Injected R848 content was kept constant with 500 µg i.t. or 2 mg/kg i.v., leading to 525 and 526 µg R848 for free and liposomal injected groups, respectively (table 41). As 0.7 µg/g R848 was detected in muscle control of all groups, passive tissue accumulation of ~ 0.1 %ID/g was proven. Comparable amounts were measured in muscle under HT and heart tissue for i.v. injected groups. In contrast, i.t. injection elevated these R848 levels significant 2-fold. Considering high standard deviation (SD) measured in lung tissue among all groups, no tendency towards increased accumulation was visible in this tissue (table 32). In comparison to free drug i.t. and i.v., liposomal delivery increased liver accumulation by ~ 1.2 -fold (0.6 and 0.5 to 0.7 %ID/g), spleen content by significant 2-fold (0.8 and 0.6 to 1.3 %ID/g) and in plasma further significant 6-fold (1.3 and 1.1 to 6.5 %ID/g) (figure 40.A). Noteworthy, the excreting organs liver and kidney presented elevated drug contents among all groups due to passive accumulation (figure 40.B).

Table 32: R848 recovery in plasma and organs after HT in tumor-bearing rats.
Free R848 or $DPPG_2$-TSL-R848 was injected i.t. (500 µg, C_{max} = 57.2 ± 3 µg/ml) or i.v. (2 mg/kg, C_{max} = 58.6 µg/ml). After 60 min of HT via WB, tissue samples were harvested and R848 measured with the newly developed HPLC method. Data represent n = 6 per group.

Group	Plasma (%ID)	Muscle under HT (%ID/g)	Muscle control (%ID/g)	Lung (%ID/g)	Heart (%ID/g)	Liver (%ID/g)	Spleen (%ID/g)	Kidney (%ID/g)
free R848, i.t.	1.3 ± 0.1	0.2 ± 0.0	0.2 ± 0.0	0.3 ± 0.2	0.2 ± 0.0	0.6 ± 0.1	0.8 ± 0.1	0.9 ± 0.1
free R848, i.v.	1.1 ± 0.1	0.1 ± 0.0	0.1 ± 0.0	0.2 ± 0.1	0.1 ± 0.0	0.5 ± 0.1	0.6 ± 0.1	0.9 ± 0.2
$DPPG_2$-TSL-R848, i.v.	6.5 ± 1.9	0.1 ± 0.0	0.1 ± 0.0	0.4 ± 0.3	0.1 ± 0.0	0.7 ± 0.1	1.3 ± 0.2	0.9 ± 0.1

Control tumors of i.v. groups presented R848 contents in the range of ~ 0.2 %ID/g but significant elevated contents for i.t group (table 33). Driven by study design, larger tumors were selected for HT but no weight dependent R848 accumulation was visible (data not shown).

Table 33: Effect of HT on R848 accumulation in rat tumors.
Free R848 or $DPPG_2$-TSL-R848 was applied i.t. or i.v. (~ 500 µg per rat) before HT via WB was conducted for 60 min on one tumor-bearing leg while the other was not treated, leaving its tumor under physiological conditions (control). R848 was recovered in tissue after HT via developed HPLC method. Data represent n = 6 per group.

Group	Tumor weight (g)		Total recovered R848 per tumor (µg)		R848 per gram (%ID/g)	
	Control	HT	Control	HT	Control	HT
free R848, i.t.	0.2 ± 0.2	0.8 ± 0.4	0.3 ± 0.3	19.9 ± 20.2	0.3 ± 0.1	6.3 ± 6.7
free R848, i.v.	0.3 ± 0.2	0.5 ± 0.2	0.4 ± 0.2	0.5 ± 0.2	0.2 ± 0.1	0.2 ± 0.0
$DPPG_2$-TSL-R848, i.v	0.4 ± 0.1	0.8 ± 0.3	0.5 ± 0.2	2.1 ± 0.7	0.2 ± 0.0	0.5 ± 0.2

Direct application i.t. significantly elevated content 32-times to respective control and ~ 13-fold to heated tumor of liposomal group (0.5 %ID/g). However, the increase was driven by single peak concentrations as indicated by variating concentrations of 6.3 ± 6.7 %ID/g leading to inhomogeneous distribution within tumor tissue (figure 40.D). In contrast, upon i.v. injection R848 accumulated evenly. Strongest significance was reached upon $DPPG_2$-TSL-R848 injection, with 4-fold increased HT-dependent accumulation from 0.5 to 2.1 µg, in comparison to respective control (figure 40.C).

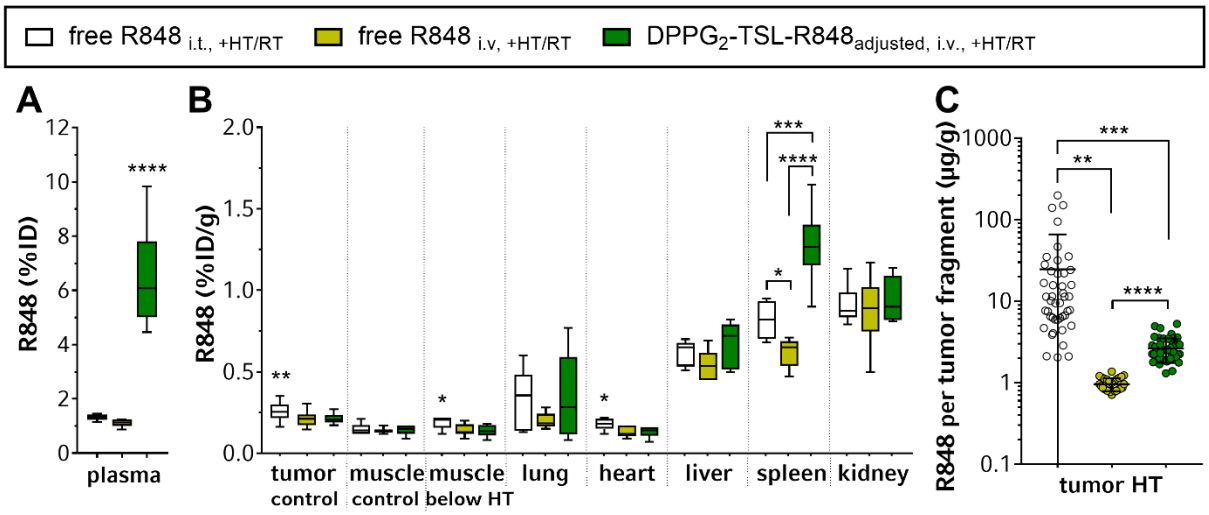

Figure 40: Biodistribution of R848 after HT in tumor-bearing rats.
Injection of 500 µg free R848 i.t. (white) or 2 mg/kg R848 (~ 500 µg per rat) in free (light green) or DPP_2-TSL-R848 (green) was combined with a 60-minutes HT via WB on one-tumor bearing leg (tumor HT), while the contralateral was not treated and its tumor left under physiological conditions (tumor control). Drug content was measured in **(A)** plasma, **(B)** organs, control and **(C)** heated tumor tissue. For the latter all measured fragments are displayed singularly. Data represent n = 6 per group.

d. Exploring application strategies in sarcoma model

Driven by promising data obtained with $DPPG_2$-TSL-$R848_{adjusted}$ as described above, consecutive studies for exploration of therapeutic response in BN175 sarcoma model were conducted. After optimizing experimental set ups and dosages (section i), efficacy of repetitive application of free R848 or liposomal formulation were studied (section ii).

i. Feasibility-assessment of therapeutic application

Optimal conditions for R848 therapy had to be unravelled. As a first step, therapeutic responsiveness was determined for the first time and influence of starting point after cell

injection explored. In a second step, the encountered survival was correlated to the R848 accumulation in heated tumor tissue (section d) and the applied R848 dosages questioned. A dose-reduction for free R848 injected i.t. and $DPPG_2$-TSL-DOX injected i.v. was conducted as well as i.t. application of $DPPG_2$-TSL-R848 explored for the first time.

Influence of tumor size at treatment start

Tumor growth was induced 4 or 7 days (Δ 3 days) before treatment was conducted once + HT (chapter III.D.f.iv). When treated earlier, saline group suffered no and R848 injected rats less drop in body weight (figure 41.A.). Tumor sizes variated from 16 ± 2 to 70 ± 50 mm^3 among all groups (day 4 to day 7, respectively) with the earlier time-point showing less deviating volumes leading to more homogeneous tumor growth patterns (figure 41.B.). Further, earlier treatment prolonged survival by 4 days after saline or TSL-injection and 6 days after free drug application. Overall, in both settings i.v. application of free R848 induced strongest, transient tumor control resulting in prolonged survival in comparison to $DPPG_2$-TSL-R848 and control (table 41.C).

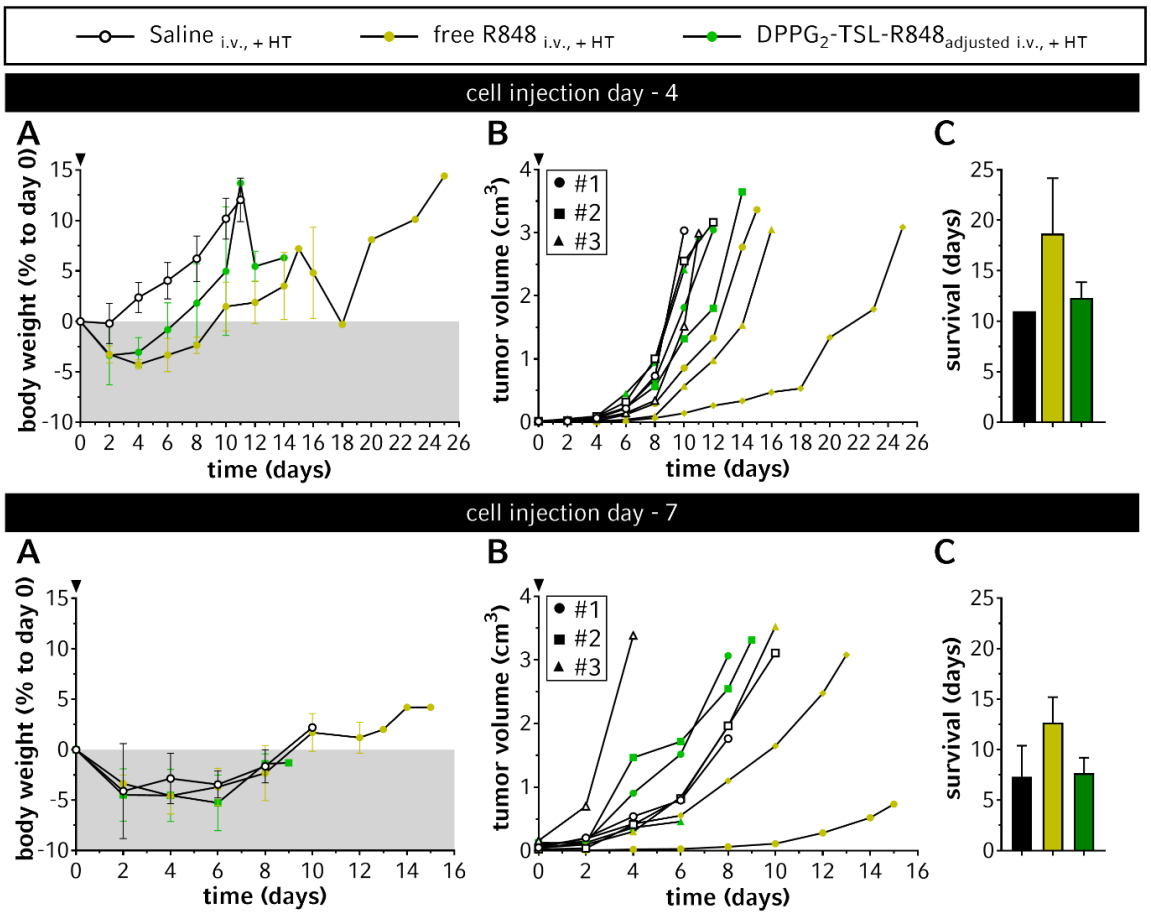

Figure 41: Impact of BN175 tumor growth time prior to treatment.
Tumors were induced via cell injection 4 or 7 days prior to treatment. All groups were i.v. injected with 2 mg/kg R848 in free (light green) and liposomal form (green) or saline (empty) at the beginning of a 60-minutes HT via WB. **(A)** Body weight and **(B)** tumor growth development were monitored until reaching end point, presented as **(C)** survival time. Data represent n = 3 per group.

Downscaling systemic dosage of liposomal formulation

As $DPPG_2$-TSL-R848 did not prolong survival in comparison to free R848, the dosage was further evaluated. In all previous studies of this thesis 2 mg/kg R848 were applied. BD-data (section d) showed a 2.8-fold higher recovered drug content from heated tumor after i.v. injection of liposomal R848 in comparison to free R848. As the latter was sufficient to prolong survival, it was addressed if $DPPG_2$-TSL-R848 had been overdosed and 2.8-fold less would enforce tumor control effect. Treatment was conducted once + HT (chapter III.D.f.iv).

By lowering drug dosage from 2 to 0.71 mg/kg R848, dosage of injected lipids was reduced from 174 to 97 µmol/kg, respectively (table 41). Body weight and tumor growth curve of lower dosed $DPPG_2$-TSL-R848 group were highly comparable to control (figure 42.A and B). In accordance, survival was in line with sham-treated animals (11 and 11 ± 1 days, respectively. Data not shown). Upon injecting a higher dose, survival was 12 ± 2 days, hinting at a moderately enhanced tumor control. However, temporary body weight loss visible in that group was accounted as signs of mild severity. Consequently, no additional dose escalation was conducted to ensure safety and 2 mg/kg chosen for $DPPG_2$-TSL-R848 i.v. injections for further studies.

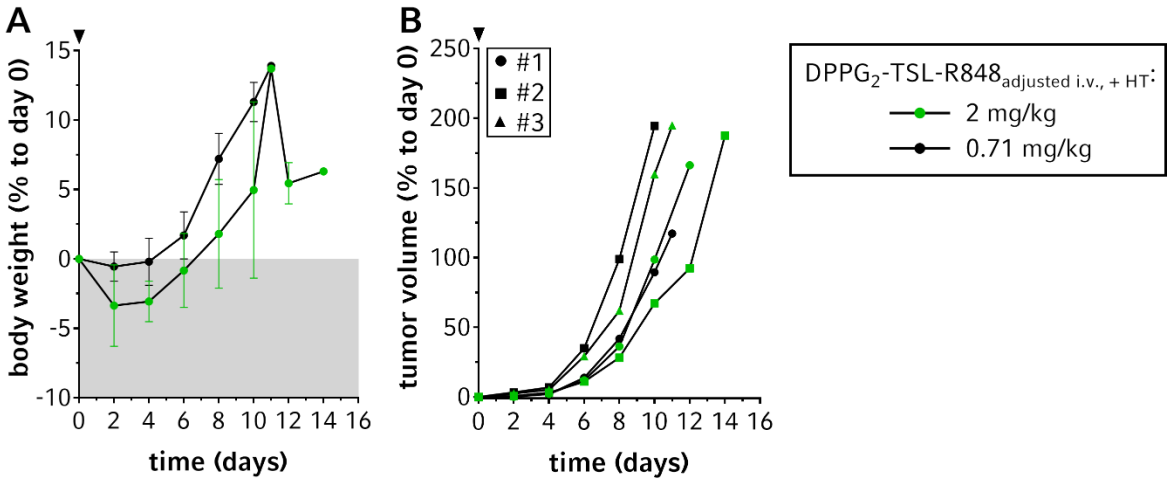

Figure 42: Exploration of $DPPG_2$-TSL-R848 i.v. dosage + HT in BN175 model.
(A) Body weight and **(B)** tumor growth development was monitored in groups injected with 0.71 mg/kg (black, n = 2) and 2 mg/kg (green, n = 3) R848 in liposomal form. Each injection was conducted once at the beginning of a 60-minutes HT via WB and tumor growth induction via cell injection 4 days prior to start.

Alternative route of application – intratumoral injection

As peak concentrations of R848 in i.t. injected tumors R848 accumulation levels of i.v. injected rats (section d), therapeutic response to i.t. + HT was to be assessed (chapter III.D.f.iv). R848 dosage from BD-study (500 µg) was downscaled to 20, 10 and 2 % (table 41) in order to span the range of accumulation levels in heated tumor after i.v. injection of liposomal and free R848 (10 and 2 % lower than after i.t. application, respectively). To ensure feasibility, safety of free R848 was challenged with a second i.t. injection + HT after 4 days.

Speed of tumor volume increase was homogeneous among groups (figure 43.B) and

resembled in equivalent survival times of 9 ± 2, 9 ± 2, 7 ± 1, and 9 ± 1 days after 500, 100, 50 and 10 µg free drug i.t., respectively (data not shown). With control animals, treated in identical study settings, having survived 7 ± 3 days (saline, figure 41), a moderate drug-related but dose-independent local tumor control after two i.t. injection of free R848 was documented. Noteworthy, even with re-challenge after 4 days, no local adverse effect was induced (e.g., itching, redness, severe bleeding or skin necrosis at injection side) and animals were euthanized due to reaching tumor size end point. However, mild temporary bleeding at application side occurred in approx. ~ 25 % of treatments (data not shown). Additionally, if higher drug content was applied, animals suffered longer from temporary body weight loss (figure 43.A). No animal exceeding a body weight drop of 4 % but, until end of the study, only rats from the lowest dose group recovered body weight fully. Consequently, 10 µg was selected as i.t. dosage for further studies to ensure safety.

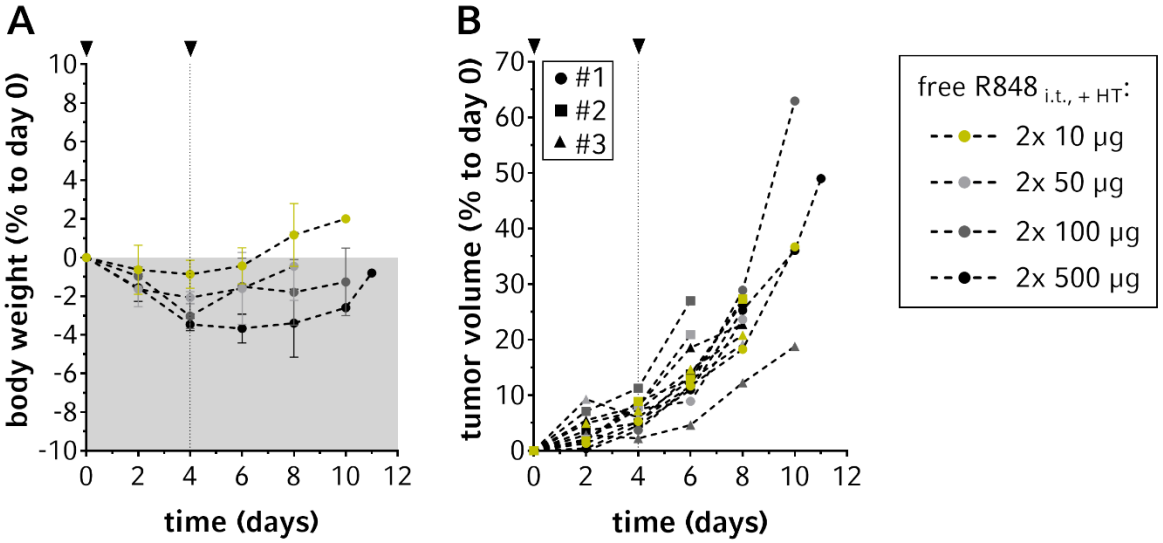

Figure 43: Dose-escalation of free R848 i.t. + HT in BN175 model.
(A) Body weight and **(B)** tumor growth development was monitored in groups i.t. injected twice (day 0 and 4) with 10 (light green), 50 (brown), 100 (grey), or 500 µg (black) free R848 at the beginning of a 60-minutes HT via WB and tumor growth induction via cell injection 7 days prior to start. Data represent n = 3 per group.

Safety assessment of intratumoral liposomal formulation

As direct R848 application did not cause severe local adverse effect, the approach of much more complex $DPPG_2$-TSL-R848 injected i.t. was tested in a next step. With free R848 showing a dose-independent tumor control and $DPPG_2$-TSL-R848 degradation rate being expected to be lower, only 10 and 100 µg were tested. Treatment was conducted once + HT (chapter III.D.f.iv).

In accordance with previous dose-escalation study, animals suffered longer from body weight loss if higher R848 amounts were applied (figure 44.A and table 41). Tumors presented comparable growth (figure 44.B) leading to a survival of 12 ± 2 and 11 ± 1 days for 10 and 100 µg liposomal drug i.t., respectively. After this study, direct application of $DPPG_2$-TSL-R848 i.t. was proclaimed to be safe as neither local nor systemic adverse drug reaction were

caused, and all animals reached end of study due to tumor size. Accounting to efficacy and safety, 10 µg were chosen for $DPPG_2$-TSL-R848 i.t. injections for further studies. In direct comparison to the previous study, 10 µg liposomal R848 showed a tendency towards prolonging survival in comparison to free form (survival 10 ± 1 days, figure 43.B).

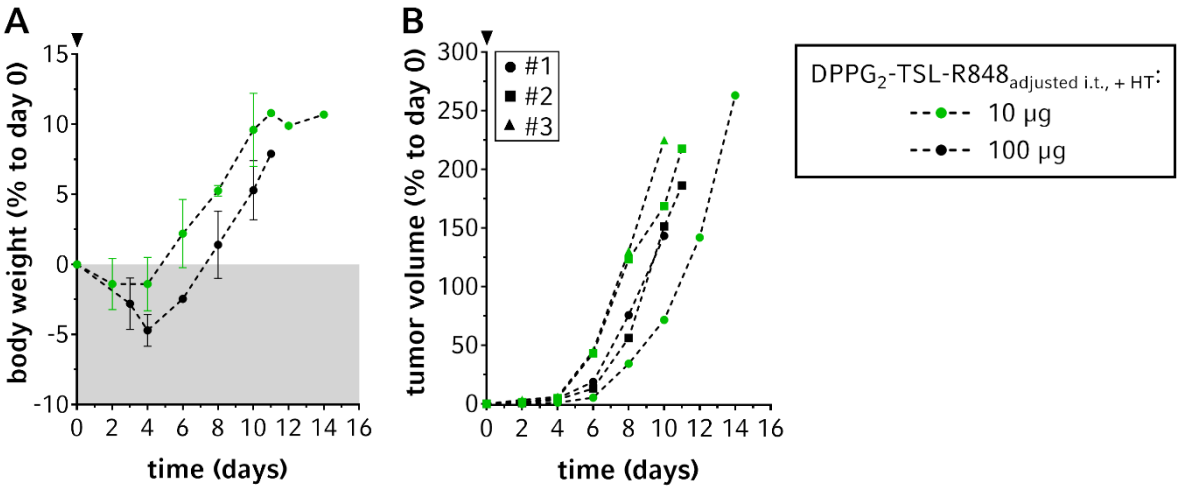

Figure 44: Exploration of $DPPG_2$-TSL-R848 i.t. dosage + HT in BN175 model.
(A) Body weight and **(B)** tumor growth development was monitored after single i.t. application of 10 (green) or 100 µg (black) liposomal R848 at the beginning of a 60-minutes HT via WB and tumor growth induction via cell injection 4 days prior. Data represent n = 2 (100 µg) and 3 (10 µg) per group.

ii. Challenging therapy response by repetitive application

With the exploration of i.t. injections, a dose-independet but drug dependent prolongation of survival was discovered and safety of repetative local high R848 contents with HT proven. As reported above, free R848 i.v. prolonged survival the most with lowest drug levels recovered in HT-treated tumor tissue (section d). This paved the way to exploring the importance of timing rather than peak concentrations via a repetative treatment plan (chapter III.D.f.iv). Driven by more homogenious tumor sizes on day 0 reported above, tumor growth was to be induced via cell injection 4 days prior to treatment.

Within this study, systemic injection of either free or liposomal R848 caused more severe temporary body weight losses than local application of loaded TSL (figure 45.A and table 41). Upon second inectino (day 4), development of tumor volumes changed among groups, with repetitive i.v. injeciton of $DPPG_2$-TSL-R848 reducing growth speed the most (figure 45.B). However, survival of this groups was comparable to 3x i.t. application of TSL (13 ± 3 and 12 ± 2 days, respectively). Repetitive i.v. injection of free drug prolonged survival to 15 days and facilitated a comparable efficacy to liposomal drug (figure 45.C)The latter stand in contrast to previous single treatment study, during which single i.v. injection of free R848 had outperformed all other groups (figure 41).

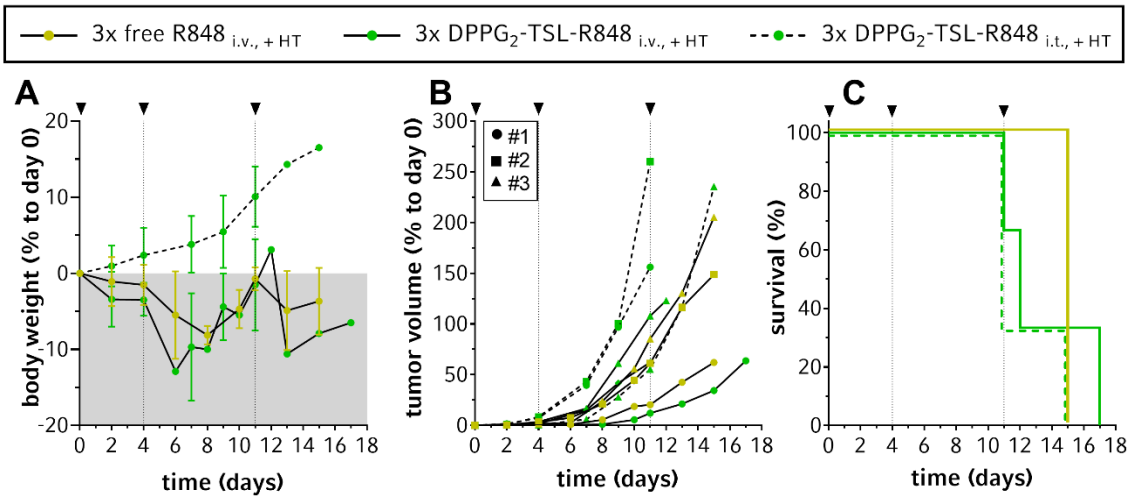

Figure 45: Repetitive R848 injection + HT in BN175 model.
R848 was administered i.t. (10 µg) in free form (green, dotted line) or i.v. (2 mg/kg) in free (light green) or liposomal form (green). Injection was repeated three times (day 0, 4, and 11), each at the beginning of a 60-minutes HT via WB and tumor growth induction via cell injection 4 days prior. **(A)** Body weight and **(B)** tumor growth development was monitored until **(C)** end points were reached. Data represent n = 3 per group.

e. Additional priming approach in sarcoma model

In accordance with current literature, multimodal treatment approaches can be key to treating cold tumors. Hence, evolving the single drug approaches further was the next step in exploring R848 in preclinical settings. If priming BN175 tumors by applying $DPPG_2$-TSL-DOX with local HT could potentiate treatment effect of R848 was to be determined in a combinational plan (chapter III.D.f.iv).

PK, BD and therapeutic response for $DPPG_2$-TSL-DOX in BN175 sarcoma model had been explored beforehand (chapter IV.A). However, feasibility of treatment protocol plan was to be assessed (section i) before combinational approach was conducted (section ii) and long-term memory effects analysed via a metastasis model (section iii).

i. Feasibility of DOX in respect to experimental set up

For repetitive treatment of same tumor, cell injected tumors were chosen over fragment implanted ones due to a more standardized size distribution at treatment start (section e.i) as well as lack of skin closure wound. Furthermore, WB was selected to be more feasible in repetitive heating of tumors as no temperature probe is placed and puncturing tumor tissue several times was seen as risk for enforcing local adverse effects as single HT had already caused crust formation in previous study (chapter IV.B.c). For $DPPG_2$-TSL-DOX treatment, these parameters had never been combined and, hence, antitumor efficacy needed to be assessed with single treatment first.

With a dosage of 2 mg/kg DOX, a predetermined 30 and 9 µmol/kg total lipid and $DPPG_2$ were applied (table 35). These were in the range of lipid contents injected in the previous study (chapter IV.A.e and table 39). Rats showed no signs of distress after bolus injection and any later time point. Application of HT via WB did not lead to behaviour changes during treatment

but within 12 days, 2 out of 3 animals developed severe redness on the food of the tumor-bearing leg. These animals were sacrificed due to reaching humane end point before tumor end point size was reached. Hence, survival of 11 ± 1 days for liposomal DOX + WB-induced HT did not correlate to DOX tumor growth reduction potential described in the previous study (table 34). Severe local toxicity was circumvented when $DPPG_2$-TSL-DOX was again combined with lamp-HT, independent if tumor growth had been induced by cell injection or fragment implanted. Prolonged survival of ~ 28 days for cell injected tumors, in comparison to ~ 19 days with fragment implanted tumors, may be driven by smaller tumor volume at treatment start (table 34). Comparable controls with lamp-HT survived 11 and 6 ± 2 days, when tumors were instilled via cell injection on day -4 or fragment implantation, respectively.

Table 34: Studies with $DPPG_2$-TSL-DOX and different HT-techniques in BN175 model.

HT-technique	Water bath	Lamp	Lamp
Tumor induction (day)	Cell injection (-7)	Cell injection (-4)	Fragment implantation (-7 ± 1)
Tumor size day 0 (mm^3)	38 ± 32	19 ± 3	37 ± 13
Tumor growth	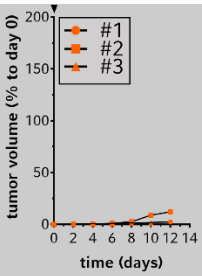	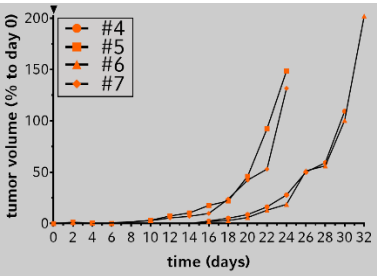	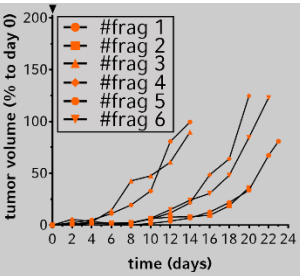
Survival (days)	11 ± 1	28 ± 4	19 ± 4
Skin color of foot	in 2 from 3 animals: redness on foot of tumor-bearing leg 	physiological 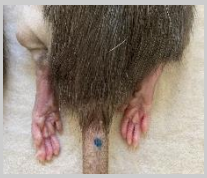	physiological 

Overall, 2 mg/kg $DPPG_2$-TSL-DOX were determined not safe for combination with WB-based HT and, hence, lamp-induced HT should always be chosen with this dosage in further studies. Dose-reduction was not explored as toxicity was assumed to be method- rather than dosage-driven.

ii. Therapeutic efficacy of combinational approach

After having shown the need for lamp-HT in combination with $DPPG_2$-TSL-DOX, the initial aim of exploring effect of BN175 priming with chemotherapy for R848 treatment was followed and the combinational treatment plan (chapter III.D.f.iv) conducted. After single treatment with $DPPG_2$-TSL-DOX + lamp-HT (1x), free or liposomal R848 was injected three times in a row (3x) with either i.v. (2 mg/kg) or i.v. (10 µg) + WB-HT (table 39 and 41). Development of body weight during treatment was comparable to respective groups of

repetitive treatment study (section d). Independent of free or liposomal R848, animals suffered longer from temporary weight loss if injected i.v. than i.t. (figure 46.A and B). Yet, no other signs of severity were recorded, and end point was reached due to tumor volume in all groups. Tumor growth was significantly reduced until day 20 in all groups Later increase was treatment dependent (figure 46.C). In combinations with $DPPG_2$-TSL-DOX + free R848, differences in survival time were moderate between i.v. and i.t. injected groups (34 ± 1 and 31± 2 days, respectively). Schedules with $DPPG_2$-TSL-DOX + $DPPG_2$-TSL-R848 prolonged survival to 40 ± 5 and 39 ± 5 days for i.v. and i.t. groups, respectively (figure 46.D). Overall, either combination of R848 enforced tumor control in comparison to single $DPPG_2$-TSL-DOX treatment (28 ± 4) conducted in comparable setting (table 34). Therapeutic effect was even more pronounced compared to single or repetitive R848-treatment studies stated above (section d).

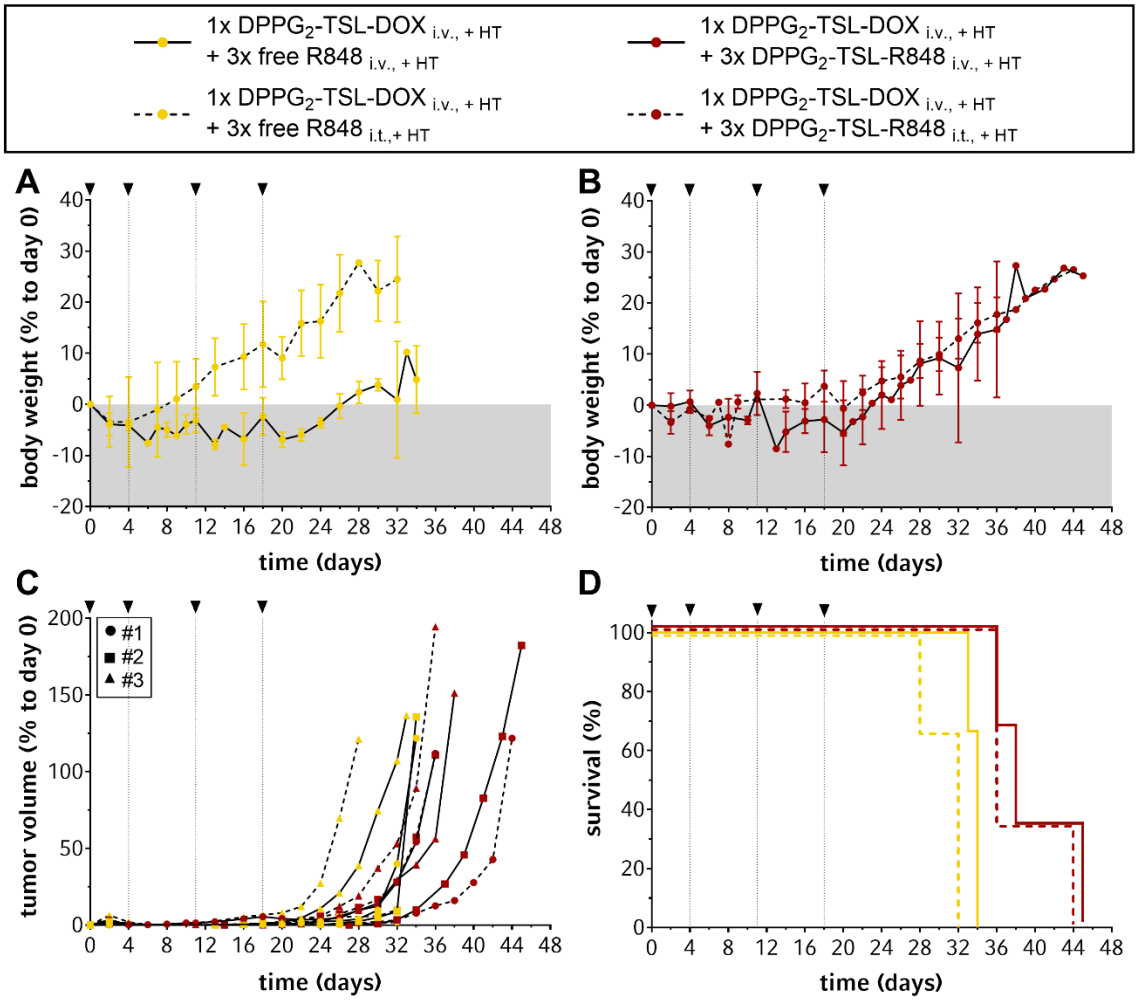

Figure 46: Exploring combinational approach in BN175 model.
(A, B) Body weight development, **(C)** tumor growth and **(D)** survival were monitored in groups treated with combinational approach. After one (1x) treatment with 2 mg/kg $DPPG_2$-TSL-DOX + HT (lamp) on day 0, a repetitive (3x) treatment with either free R848 (yellow) or $DPPG_2$-TSL-R848 (red), each with 10 µg i.t. (dashed line) or 2 mg/kg i.v. (full line), was injected + HT (WB) on days 4, 11 and 18. Tumor growth was induced via cell injection 4 days prior to start. Data represent n = 3 per group.

iii. Exploration of systemic effects in metastasis model

After having shown efficacy of multimodal approach in BN175 sarcoma model, the question arose whether a systemic antitumor response capable of controlling a second, distant tumor was possible. Consequently, a metastasis study with rats bearing two tumors, the second being injected after treatment start (day 4) in the contralateral leg, was conducted together with single or combinational treatment schedule (chapter III.D.f.v). Every injection was conducted i.v. with 2 mg/kg (table 39 and 41).

Animals did not show signs of suffering upon injection of a second tumor in the contralateral leg. Body weight development in groups of metastasis study were comparable to respective groups conducted before with one tumor only.

Table 35: Comparison of groups from single treatment study to metastasis study.
Drug injections were conducted in the same manner among respective groups. While free R848 and $DPPG_2$-TSL-R848 i.v. injections were combined with WD-HT, the i.v. injection of $DPPG_2$-TSL-DOX was conducted with lamp-HT. BN rats were bearing one BN175 tumor if treated once (single treatment) or were injected with a second BN175-tumor on contralateral leg on day 4 (metastasis model). Data represent n = 3 per group.

Group	Mean survival		Reason of end point		Distant tumor growth
	One tumor	Two tumors	One tumor	Two tumors	Compared to respective group of animals bearing one tumor
free R848, i.v.	~ 19 days	~ 13 days	primary tumor	Primary tumor	Comparable
$DPPG_2$-TSL-R848, i.v.	~ 13 days	~ 13 days	Primary tumor	Primary tumor	Slower
$DPPG_2$-TSL-DOX, i.v.	~ 28 days	~ 23 days	Primary tumor	Primary tumor	Slower

In metastasis model, survival time of $DPPG_2$-TSL-R848 group was comparable to single treatment study (section d), while end point was reached ~ 6 days earlier upon treatment with free R848 or $DPPG_2$-TSL-DOX (table 35). Distant tumors of rats treated with $DPPG_2$-TSL-DOX+ HT displayed smallest volumes of 0.12 ± 0.16 mm^3 at end point (day 23). Comparable volumes in studies with rats bearing one tumor were reached on day 11 ($DPPG_2$-TSL-DOX + HT treatment). Comparable results were seen in groups injected with $DPPG_2$-TSL-R848 + HT, were distant tumors displayed volumes of 70 ± 111 mm^3 at end point (day 13). Comparable volumes in studies with rats bearing one tumor were reached on day 4 ($DPPG_2$-TSL-R848 + HT) or day 7 (free R848 + HT). Taken together, a systemic antitumor response was induced in groups treated once with liposomal DOX or liposomal R848, as distant tumors grew slower than HT-treated tumors of respective groups (section d). Looking at free R848, distant tumors showed volumes of 332 ± 414 mm^3 at end point (day 13). Comparable volumes in studies with animals bearing one tumor were reached on day 9 ± 5 (free R848 + HT) hinting at a comparable growth speed and no induction of systemic response (table 35).

When combining both liposomal formulations (1x $DPPG_2$-TSL-DOX + 3x $DPPG_2$-TSL-R848) the above described effects were altered. Distant tumors of this groups grew faster than in either single treated group. End points were reached at ~ 25 days after treatment start. As distant tumors had been injected 4 days after treatment start, these tumors grew with comparable speed to HT-treated tumors of 3x $DPPG_2$-TSL-R848 group (survival ~ 19 days).

V. Discussion

A) Effect of osmotic condition and species on $DPPG_2$-TSL-ADU

Magnitude of ADU-release from liposomal carrier is dependent on osmotic condition of $DPPG_2$-TSL. As predicted by *in vitro* TDR data (chapter IV.B.a.i), isosmotic conditions were feasible for aiming at longer plasma circulation time and passive accumulation strategies whereas hyposmotic formulation suffered from carrier instabilities and respective ADU-leakage *in vivo* (chapter IV.B.a.ii and iii). The latter being tolerated as only destabilized carrier released encapsulated ADU upon HT. Noteworthy, hyposmotic formulation after HT-triggered ADU release displayed comparable PK profile to empty $DPPG_2$-$TSL_{hyposmotic}$ in BN rats, indicating that ADU-depletion of liposomes was indeed achieved (chapter IV.B.a.iii). For triggered release of ADU from $DPPG_2$-TSL, a balance between moderate leakages from osmotically stressed carrier at physiological conditions enabling drug release at HT needed to be found. It can be stated that a feasible candidate was developed based on described PK-data of $DPPG_2$-TSL-$ADU_{hyposmotic}$ in rats, but not in mice.

An **impact of species on ADU**-recovery rate can be postulated, as initial leakage from either liposomal formulation at control conditions was limited to < 2 %ID in rats but exceeded 70 %ID in mice. Species-effect was further indicated by stable encapsulation in rats but severe ADU leakage from isosmotic carrier at physiological treatment conditions in mice (sham (rat) and NT (mice)-treated groups). Addition of osmotic stress to carrier reduced PK parameters of ADU only 2-fold of rats but 6-fold in mice, highlighting an mice-specific escalation of carrier stress leading to significantly increased leakage upon i.v. injection. With clearance to less than 1 %ID after 30 min of HT in mice, no detailed insight on heat-dependent release slope from hyposmotic formulation was gained (figure 26). For the same group in rats, ADU was still present with 3 %ID after 240 min granting a documentation of mild HT-triggered release (figure 28). Overall, liposomal encapsulation enhanced ADU plasma stability in rats to a greater extent than in mice (chapter IV.B.a). **Ultra-fast systemic ADU clearance in mice** plasma was already documented for a STING agonist cGAMP, reaching t_α of 60 min but was drastically enhanced upon formulating in a lipid-based vesicle. The same group proved antitumor efficacy in a mouse colon carcinoma of their cGAMP-NP applied i.v. [167]. Feasibility of comparable cGAMP-loaded NP was obtained before in triple negative breast cancer [92]. To optimize cGAMP cytoplasmic transfer, Shae *et al.* designed STING-activating NP utilizing a PEG-based vehicle. Based on the latter, systemic injection was possible and compared to i.t. application. Either application form enhanced cGAMP biological activity, strengthened STING signal transduction in the TME, and enhanced tumor immunogenicity [160]. These reports rendered hope for enhancing plasma stability by liposomal encapsulation which was successfully shown for $DPPG_2$-TSL-ADU in rats. When **focusing on**

carrier lipid $DPPG_2$, overall initial loss (15 min) of $DPPG_2$ was generally significantly lower in rats (rats: ~ 100 %ID, mice: < 30 %ID), but osmotic stress on carrier enhanced ADU leakage at control condition to the same extent as in mice. In detail, hyposmotic condition elevated $DPPG_2$ loss by ~ 15 %ID at 120 min thereby reducing t_α and $AUC_{120\ min}$ accordingly (rats: 3-fold, mice: 2-fold) in both species (sham (rat) and NT (mice)-treated groups) in comparison to isosmotic formulation. Upon addition of HT to $DPPG_2$-TSL-$ADU_{hyposmotic}$, calculated $AUC_{60\ min}$ was not affected in rats (3794 to 3906 %ID*h/ml) but 2-fold decreased in mice (1097 to 461 %ID*h/ml), which was mainly attributed to species-dependent enhanced initial loss of formulation (chapter IV.B.a). Taken together, mice specifically cleared carrier faster from plasma and effect could be accelerated upon addition of HT. This significant destabilization upon injection leads to significant payload leakage, possibly explaining suboptimal plasma stability of $DPPG_2$-TSL-ADU discovered specifically in mice. Why liposomal formulations are experiencing additional stress in mice can only be suspected to be dependent on factors pressuring liposomal integrity such as plasmatic proteins, enzymatic activities, and metabolism rates (discussed further in section c). Nevertheless, driven by proprietary rat PK-data, **$DPPG_2$-TSL-$ADU_{hyposmotic}$** was further investigated in BN175 sarcoma model and, for the first time, responsiveness to liposomal-delivered ADU was proven. Antitumor response to i.v. delivery was pronounced in comparison to free ADU groups (i.v. and i.t) (chapter IV.B.c). However, HT-triggered release in rat plasma (chapter IV.B.a.iii) did not translate in enhanced therapeutic effect (chapter IV.B.c.ii). Revealing a co-delivery of payload and liposomal carrier lipid $DPPG_2$ (chapter IV.B.d), may indicate accumulation of loaded formulation rather than released ADU and would explain the documented trigger-independent therapeutic effect of hyposmotic formulation. However, why HT-treated animals presented a slightly lowered survival raised questions (chapter IV.B.c.ii). In a control experiment, the accelerated growth upon local heating was documented (chapter IV.B.c.iii) answering the above raised question.

For our approach, the lack of HT-dependency in therapy study emphasized the need of another round of optimization. For **improving the designed ADU-formulation**, focus of trouble shooting was re-evaluation of data obtained during design and production phase. Of the batches used for *in vivo*, a shift in TDR was noted from maximum-release at 42°C for PK and BD batch but 43 °C for therapy batch (figure 47). Additionally, comparing to initial batches prepared during design phase, the proclaimed release efficacy of > 80 % at 41 °C in FCS (figure 24.B) was not reproducible over time. As *in vivo* experiments cannot and should not be conducted in parallel to design work package, the importance of reproducibility of formulation characteristics cannot be stressed enough. Reason for this shift due to deviations from manufacturing protocol, variations in HPLC detection, storage-dependent lipid hydrolysis, or ADU degradation in stock solutions have not yet been entangled. Total number

of lipid films being prepared in parallel and deviations in intervals between production steps must be critically documented in future productions to gain insight on effects driven by in-lab production scale.

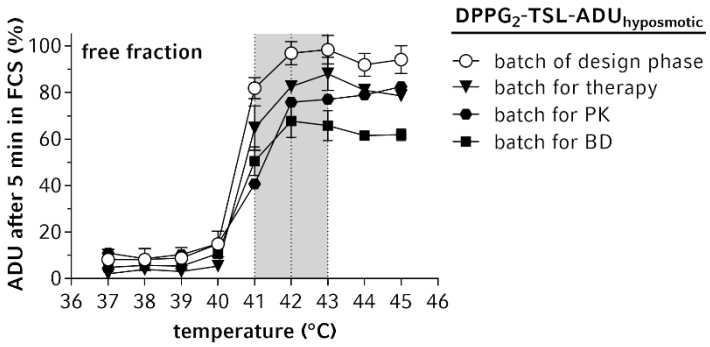

Figure 47: TDR of $DPPG_2$-TSL-$ADU_{hyposmotic}$ used *in vivo*.
During design phase a TDR profile of model formulation (empty circle) was proclaimed by Thermosome GmbH (Planegg, Germany). For later *in vivo* application, batch production was conducted shortly before start of experiment to ensure minimal storage effects on prepared formulation. Hence, different batches were used for PK-(circle), BD-(square) and therapy (triangle) study.

Despite optimizing manufacturing protocol, further **adjustments on liposomal ADU-formulation** would need to aim at intravascular release. Osmotic stress revealed significant destabilization of carrier *in vivo* (chapter IV.B.a), which could be tolerated if encapsulation efficacy was higher. In order to achieve this, increasing drug concentration in hydration solution of lipid film seems obvious. Solubility of ADU had been investigated during design phase in HBS pH 7.4 and water, revealing maximal solubility being reached at 10 mg/ml. However, precipitation during storage at 2-8 °C was noted for 10 mg/ml which is why 8 mg/ml was used for loading $DPPG_2$-TSL [168]. Other solvents may be explored, e.g., 7.5 % of sodium bicarbonate [64], to enhance concentration and thereby potentially elevating EE. During development, stress test examining impact of pH was conducting, revealing superior ADU stability at pH 4 and 7 in contrast to degradation at pH 9 [168]. Lowering pH from 7.4 to 4 for hydration could enforce release. In a next step, passive encapsulation process should be thoroughly investigated, explicitly aiming at amount of F/T cycles, elevating loading temperature or reducing volumes [169]. Alternative active loading may be explored but were overruled during formulation development due to ADU lipophilicity and reported low stability properties [64]. Other strategies to enhance payload release would include varying molar ratio of lipids to influence T_m e.g., DPPC [107]. During development of ADU-formulations a 60:10:30 DPPC:DSPC:$DPPG_2$ (mol:mol) approach resulted in leakage at RT and release starting from 39 °C [168]. However, this instability could have positive effects on release efficacy *in vivo* and should be tested in a PK-study. In addition, impact of species-specific protein interactions in the bloodstream should not be underestimated and can, unfortunately, not fully be predicted *in vitro*. Enhanced *in vitro* release efficacy of ADU from $DPPG_2$-$TSL_{hyposmotic}$ in mouse plasma at 41°C (figure 24) could not be proven *in vivo*, probably because blood sampling was conducted too late. Respective data generated in rat plasma was

contradictory, as distinct release efficacy at 41°C *in vitro* (figure 25) did not translate in significant HT-triggered release in plasma upon HT (chapter IV.B.a). Despite having picked identical anti-coagulant for plasma generation, the used commercially available plasma for *in vitro* experiments may not have been 100 % identical to samples generated during *in vivo* studies. Hence, variations depending on plasma composition (e.g., protein content, time of storage) but also number of thawing processes leading to protein degradation as well as health and stress condition of donor animal need to be mentioned. Several TSL formulation had been investigate in respect to serum interaction and responsiveness was not predictable [129]. Increasing D:L ratio is correlated with lower plasma stability and thus no option [140]. Alternating composition should be considered only after **clarifying treatment strategy** as other commercially available, commonly used lipids (e.g., Cholesterol, PEG) are known to increase stability but not HT-triggered release efficacy [109, 123]. By formulating an isosmotic formulation, data have already proven that heat-triggered release is circumvented. If therapeutic approach strategy was shifted to an alternative targeting strategy, addition of cationic or ionisable lipids such as DOTMA, DOTAP would allow carrier-driven tissue targeting [84, 170]. For the delivery of negatively charged mRNA for example, positively charged LNP have proven most effective delivery [171]. For cationic lipids DOTMA and DOTAP, systemic injection in mouse was explored and specific organ-targeting detected [170]. Hence, a cationic approach seems promising for exploring organ-targeted delivery of stable encapsulated target in osmotically balanced carrier [172]. With the current anionic $DPPG_2$-TSL-ADU formulation, specific organ targeting was neither aimed at nor achieved as only kidney accumulated ADU, probably due to active excretion of elevated plasmatic concentrations from the body (chapter IV.B.d).

B) Obstacles of ADU treatment approaches

When correlating survival upon ADU treatment in BN175 sarcoma model (chapter IV.B.c) to magnitude of drug accumulation discovered in BD-study (chapter IV.B.d), no dose-dependent effect could be correlated. Noteworthy, despite significant increase of recovered ADU from i.t. injected tumor tissue, such application approaches resulted in shortest survival. This fuels the conclusion that, instead of local peak concentration, prolonged carrier-driven availability of ADU drives STING activation in rats. This effect could be attributed to low penetration depth of ADU, off-site STING-activation (systemic or organ-specific) or low activation of rat STING feeding the need of further exploration in another rat cancer model.

Penetrations depths of ADU have not been reported in current literature until now, however with ADU being negatively charged, a repulsion from cells may hamper access to cell surface. Additionally, the import mechanisms may vary among cell types and host species. Ritchie *et al.* reported the finding of a cGAMP and ADU selective importer for the first time. The human importer SLC19A1 was proven to efficiently imported ADU in haematological cell lines and

monocytes of human donors but not in epithelial cell lines. It was shown that expression levels of SLC19A1 correlated to uptake efficacy of the investigated cell lines. It was further postulated that import mechanism on immune cells varying on molecular levels among species (e.g. human and mouse) lower impact of preclinical data for clinical translation [78]. A potential benefit could be achieved by radiolabelling ADU. Thereby, *in vivo* tracking and in-depth analysis of accumulation kinetics among different cell types would be possible. Until now, uptake was not estimated in %ID but rather correlated to efficacy of STING-activation [64, 65]. However, this approach has shown to be a pitfall for the initially designed ADU-derivate DMXAA, as preclinical data failed to unravel reported claims to be dependent on mouse STING activation [67, 68]. A lession learned from this is paying attention to species effect on molecular levels. For Corrales *et al.* this meant conducting a screen based on interaction of human and mouse STING to enlarge predictability of mice models, which resulted in the development of ADU [64]. The research surrounding ADU has achieved ADU tissue penetration leading to strong therapeutic responses by focusing on i.t. application in mice. In BN175 sarcoma model, i.t. injection did not reach comparable levels of antitumor efficacy. Systemic injection of ADU was performing better but strongest response was documented upon liposomal encapsulation (chapter IV.B.c). **Systemic distribution** could accelerate STING activation at off-target sites and activate $CD8^+$ T cells in tumor-draining lymph nodes effectively. Early reports of systemic approaches can be found for ADU-precursor DMXAA. An investigation of an acute myeloid leukaemia model in BL6 mice have proven the IFN type I dependent antitumor response upon i.v. injection. Further, the authors claim comparable results being obtained with ADU, however DMXAA prolonged survival to a greater extent [173]. Unfortunately, the higher clinical impact of ADU as mouse and human STING agonist may lead current focus of research and limit future studies with DMXAA.

A pitfall of systemic injection is potential **off-target immune activation**. Local accumulation patterns in the excreting organ kidney were significantly altered by $DPPG_2$-TSL-ADU (figure 33), rendering risk by necrosis formation. Shae et al reported cGAMP accumulation in liver, spleen, kidney and lung and declared the first two as dose-limiting organs as preclinical data histologically proved necrosis formation [160]. In contrast, positive effects could come from accumulation in immune supportive organs, such as lymph nodes. A report with cGAMP loaded NP described accumulation in tumor-draining and contralateral lymph node upon i.v. injection in mice, later being correlated local T cell activation inducing systemic immunity [167]. In case of $DPPG_2$-TSL-ADU, systemic injection of 2 mg/kg with HT induced immediate over-activation of STING, leading to severe ADR in B16-bearing mice (chapter IV.B.b), rendering this species to be rather sensitive to ADU stimulation. This might explain why most preclinical research, which mainly consists of mice cancer models, are conducting i.t. application [65, 72]. The above-mentioned study exploring systemic DMXAA in BL6 did not

mention body weight development or other indicators for toxicity [173]. The only report documenting comparable signs of acute but transient decrease in body weight was a study exploring treatment of B16 Melanoma by i.t. injection of cGAMP, postulating high sensitivity of BL6 mice towards this STING agonist [160]. Further studies need to clarify fine-tuning of dosage played a role in conducted study as dose-reduction to 1 mg/kg already circumvented ADR development (chapter IV.B.b). In addition, it can be postulated that local heating via WB may have induced ADU release in larger surface area than lamp-HT would have. As BD-data of $DPPG_2$-TSL-DOX suggest such HT-technique dependent pattern of accumulation within the same tumor model (chapter IV.A.c.iii). Resulting over-saturation might have driven toxicity in mice. This hypothesis is supported as i.t. injection of 500 µg was tolerated well in B16-bearing mice (data not shown). Potential impact of carrier itself seems unlikely, as systemic injection of other $DPPG_2$-TSL formulations in mice did not report any signs of stress [174]. In total, negative reports of lowered tolerance to systemic ADU counterbalances negative aspects of i.t. injections (e.g., local puncture of tumor). Anyhow, ADU-dependent effects in mice may still mostly be credited to mouse STING binding.

Investigations of **rat STING** have not been conducted and are not reported in current literature up to now. In rats, a transient body weight stagnation upon i.v. injection of $DPPG_2$-TSL-$ADU_{hyposmotic}$ was noted in therapy study of BN175 sarcoma model (chapter IV.B.c), which had not been reported for other $DPPG_2$-TSL formulations investigating the same sarcoma model [125, 127, 146]. Hence, nanocarrier-derived toxicity seems unlikely. Having proven profound prolongation of plasma stability in rats, timespan of ADU availability *in vivo* was extended. Chronic stimulation of STING may promote inflammatory processes resulting in inflammation-driven tumorigenesis. An optimal STING agonist, thus, must ensure to contribute to the induction of a strong antitumor immune response while not activating inflammation-induced carcinogenesis [61]. With the data of this thesis, the following can be hypothesized for rat STING: At first, low response rates of i.t. injected free ADU in BN175 sarcoma model (chapter IV.B.d.i) may be attributed to weak activation of rat STING, with temporary high intratumoral peak concentrations not being enough. Secondly, i.v. injection enhanced availability time frame of ADU thereby expanding the phase of weak rat STING binding thus mildly boosting antitumor response in BN175 to the pitfall of systemic side effect. In line with these two hypotheses, temporary signs of stress upon i.v. injection in rats (chapter IV.B.d.ii) proves enhanced rat STING activation with $DPPG_2$-TSL-ADU in comparison to free ADU.

In addition to the above-mentioned thoughts, an evaluation of ADU in a second rat model would give greater impact of harvested data and theories concerning rat STING. The established MatBIII model (chapter IV.B.e) could be a promising candidate as this tumor represent clinically relevant breast cancer, a hot topic for immunotherapeutic approaches

[53, 147, 148]. While establishing this model, deviations in speed of tumor growth as well as tumor shape after MatBIII cell injection was encountered and may be attributed to cells not attaching easily *in vivo*. Already *in vitro*, MatBIII displayed a fluid growth characteristic with low tendency towards attachment, in accordance to reports from commercial supplier. In s.c. space, some may accumulate in clusters inducing several tumor formations in close proximity, while some might 'wander' off-site, thereby not adding to any tumor development. It may be discussed if providing a matrix for cells (e.g., Matrigel) could help harmonizing. The question if cell injected MatBIII tumors may lead to re-growth upon fragmentation was positively answered.

First cell culture experiments revealed no cytotoxic effect of free ADU to MatBIII. However, addition of free ADU did alter attachment efficacy in a not directly dose-dependent manner (chapter IV.B.e.i). It was proven that a source of error was created by multiple washing with medium-removal being conducted via suction, due to weak attachment of MatBIII to cell culture plates. Loss of cells was reduced when plates were simply flipped for removal of medium and circumvented when no washing was performed (figure 48). Further investigations with coated plates (e.g., collagen or poly-l-lysin) allowing stronger attachment of MatBIII, could be of help to distinguish a possible ADU-effect more clearly.

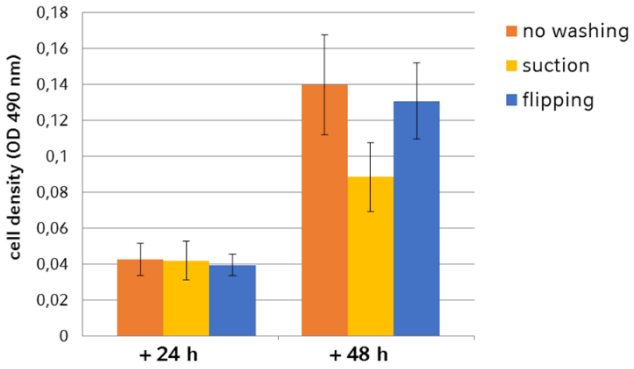

Figure 48: Influence of washing on read-out of *in vitro* experiments with MatBIII.
After plating 4000 cells/well, NT treatment (37°C) was performed without washing (organ) or washing by removing medium via suction (yellow) or flipping (blue) 24 and 48 h before determination of cell density. Data represent n = 3.

C) Species-specific carrier instability and organ targeting

Gaining insight on species-effect on $DPPG_2$-TSL-DOX behaviour *in vivo* is key for future clinical application. Therefore, implemented mouse set up was meant to mimic rat protocols as close as possible to enable an evaluation of **species-driven effects on $DPPG_2$-TSL**. In contrast to a well-defined HT-delivery documented in rats (figure 19), no treatment dependent difference in plasma clearance was documented in mice (figure 21). In direct comparison, DOX levels after $DPPG_2$-TSL-DOX + NT treatment were significantly impacted by species (figure 49.A). When directly comparing BD-data after $DPPG_2$-TSL-DOX + lamp-HT from rats (figure 15) to respective data in mice (figure 23), significant differences can be reported and are summarized in figure 49. Plasma content (60 min after injection) was significantly lower in mice (figure 49.B.a), which correlated to discovered PK profiles of either species. Within organ samples (lung, heart, liver, spleen and kidney), a comparable pattern of distribution was noted in either species. However, every mouse organ accumulated

significantly more DOX content than respective tissue in rats (figure 49.B.b), despite injection of constant DOX dosage (table 39). Noteworthy, peak concentration being reached in mouse liver (~ 25 %ID) was more than half of plasmatic content in rats (~ 40 %ID). If liposomal carrier $DPPG_2$ accumulation was altered in mice cannot be reported, as LC-MS device necessary for detection was not available at time point of study. However, backed up by data obtained in rats (chapter IV.A.b), DOX can be assumed to accumulate mostly independent from liposomal carrier *in vivo*. Therefore, low plasmatic but elevated tissue contents may indicate a significant amount of unspecific leakage in mice enabling freed DOX being drawn into tissue and entrapped in cells. For heated tumor tissue, efficacy of HT-triggered accumulation with lamp-technique was proven in either species (figure 49.B.c), despite lack of evidence to HT-triggered DOX release in mouse plasma. It can be discussed, that kinetics of release are enhanced due to above described impact of species on carrier and HT-triggered release had taken place before first sample was measured (15 min after injection). Hence, future experiments in mice should highlight earlier blood sampling time points.

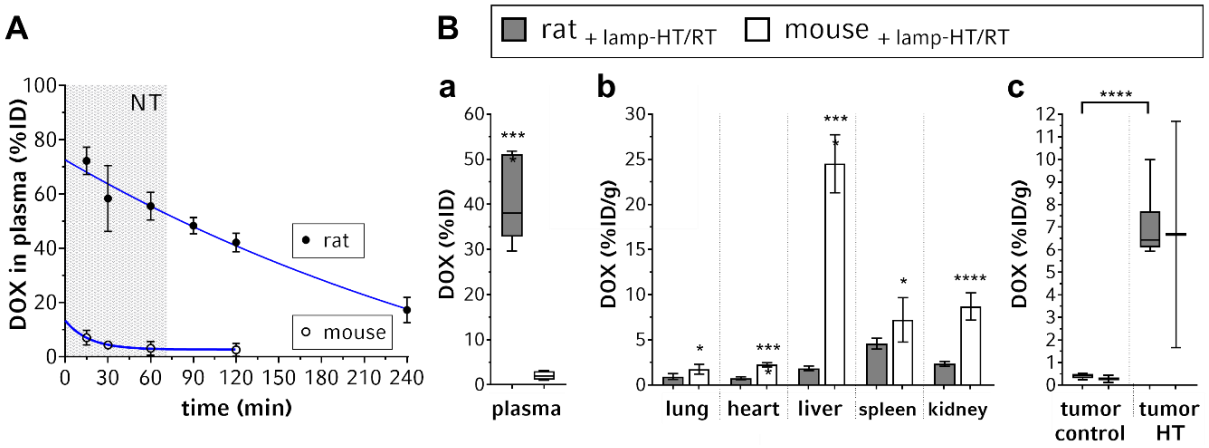

Figure 49: Effect of species on PK and BD profile of $DPPG_2$-TSL-DOX.
Data was obtained in individual experiment with rats (grey symbol) or mice (empty symbol) but identical dosage (2 mg/kg) of DOX in comparable liposomal formulations. **(A)** DOX plasma clearance in healthy recipients. **(B)** DOX biodistribution in **(I)** plasma, **(II)** organs and **(III)** tumor tissue at the end of HT conducted via lamp in B16-bearing mice and BN175-bearing rats. Data represent n = 2 (mouse) and 6 (rat) per group.

Another factor impacting carrier stabilities and clearance could be species-dependent variations in **kinetics of lipid degradation**. Early reports in 1995 have shown, that lysolipid formation increases disruption of the lipid bilayer surface, making phospholipid molecules more accessible to enzymes activity of Phospholipase A2 (PLA_2) [175]. Shortly after, enhanced hydrolysis at lipid bilayer's characteristic gel-to-fluid phase transition temperatures T_m was reported, hinting at an amplified accessibility of the membrane to the enzymatic active site of PLA_2. Furthermore, coexistence of dynamic gel and liquid domains at T_m was associated with poor packing properties. The shorter the acyl chain, the wider the temperature range of T_m, the more pronounced the dynamic heterogeneity of the membrane and the more accessible spots for enzymatic hydrolysis are formed. Hence, the impact of lipid-bilayer physical properties on heterogeneity at T_m playing an important role for the

phospholipase activity was postulated. Additionally, negatively charged vesicles promote additional PLA_2 binding [122]. The authors also discussed the impact of membrane-soluble compounds such as anesthetics or alcohols to enhance dynamic heterogeneity, again rendering accessibility to PLA_2 but also accumulating in boundary regions thereby sterically hindering the enzyme [122]. It can be hypothesized, that species-driven variations of enzymes with PLA activity on molecular levels may have impacted the documented difference between mice and rats. For examples, mutations in active cleavage site could augment the interaction with liposomes in either way. Reports on thorough assessment of rodent phospholipases are, though, missing in current literature. The addition of a lipopolymer PEG has shown enhanced accessibility of PLA_2 [109]. Hence assessing plasma stability of PEGylated NP in mice and rats could give more leverage to this hypothesis. Noteworthy, this needs to be differentiated from the enhanced plasma clearance resulting from anti-PEG antibody formation and complement activation (see report in II.E). In respect to species, PEGylated liposomes have demonstrated rapid clearance in rat, guinea pig, minipig and beagle dog models after each consecutive dose following their second administration. Anti-PEG IgM levels varied, however, depending on the immunological sensitivity of different models, thus eliciting differential impacts on ABC [176].

In contrast to these systemic lipase-dependent effects, a specific organ-targeting would need **organ-specific lipase activities,** which are rare to find. Triacylglycerol (TG) affinity is reported for pancreatic or hepatic lipase (HL) as well as for lipoprotein lipase, which is though expressed in multiple sites such as muscle, adipose, heart, mammary gland or brain tissue [177]. Endothelial lipase (EL) was first discovered in 1999, with organ specific expression and substantial phospholipid affinity in contrast to TG lipase activity claiming an impact on HDL metabolism [178]. Specific phospholipase A1 activity is reported for both, HL and EL, but only the latter prefers PC over TG. Until now, only pancreas lipase related protein-2 (PLRP-2) is also known for PC activity, together with preferences towards TG, phosphatidylethanolamines and PG's [179]. EL may be key to enable accumulation of PC containing LNP upon organ specific expression pattern in lung, liver, kidney, thyroid, testis, and ovaries [177, 178]. With LNP-like structures gaining scientific interest, organ targeting is wanted and explored [84, 100, 171] in contrast to the reported $DPPG_2$-TSL formulations. Discovered enhanced accumulation in lung, liver, spleen, and kidney (chapter IV.A.b and IV.C.d) could be hypothesised to be driven by EL dependent DPPC and DSPC hydrolysis (70 % of TSL lipids). An evaluation of thyroid, testis, or ovaries in future BD-studies could enforce this claim. It should be discussed if higher metabolism rates in mice also includes enhancing enzymatic activity of lipases, which could explain documented enhanced carrier instability (chapter IV.A.c.i) and clearance (chapter IV.B.a) as well as elevated payload release efficacy. The latter might have led to species-specific elevated DOX-entrapment rates in mouse organs

(chapter IV.A.c).

EL-targeted lipid accumulation in tumor may play a role in discovered $DPPG_2$-TSL-ADU accumulation in BN175 sarcoma model (chapter IV.B.d) and should be evaluated further. With lipase expression and secretion having been proven in several human tumor cells, e.g. sarcomas or breast cancer, an active uptake of fatty acids from the bloodstream, in addition to synthesis, to fuel growth was indicated [180]. Therefore, further insight could be granted by utilizing the newly implemented MatBIII breast cancer model. In addition, Yang *et al.* discovered an EL-specific inhibitor, cyranoside, which effectively supressed enzyme activity in triple negative breast cancer cells *in vitro* and showed antitumor activity in a respective xenograft model [181]. Lipase activity is also currently correlated to pathogenic states. For example, EL is postulated to act as pro-artherogenic molecule by enhancing monocyte adhesion to vascular endothelium in early development of atherosclerosis [177, 182]. Expression levels of PLRP-2 are related to pancreatitis [183] and are induced via IL-4 in cytotoxic T cells [184]. Whether i.v. injection of PLRP-2 substrate PG (e.g. in form of $DPPG_2$) could induce temporary upregulation in pancreas and might induce lipid-dependent T cell mediated cytotoxicity can only be hypothesized. Controversially discussed to this may be data indicating decomposition via PLA_2 stated above.

Increased **accumulation levels of anionic $DPPG_2$-TSL in liver** and spleen may be explained by hydrolysis via organ-specific lipases but significant amount of carrier degradation can be accounted to the reticuloendothelial system (RES) system. In an early report on liposomes based on DPPC and DSPC, the biodistribution pattern has been documented over 4 h in healthy rats. Specific enhanced accumulation of up to 40 %ID in liver and spleen was documented, as well as very low clearance through kidney (max 4 %ID) in a time-lagged manner. This immediate entrapment in liver and spleen was appointed to RES and increased correlating to higher mol% of DSPC within the formulation [185]. Recent exploration of organ-specific targeting in LNP-like structures from Liu *et al.* have demonstrated spleen entrapment with 13 to 16 alkyl chain length at phosphate groups of PC whereas shorter chains (9 to 12) accumulated predominantly in liver [171]. Enhanced accumulation in liver upon a second dose of Doxil® was reported to be driven by ABC phenomena, enhanced opsonisation and complement activation [110]. However, for $DPPG_2$-TSL antibody formation was not discovered [140].

Another lession learn from PEGylation was its capacity to increases the hydrodynamic diameter and molecular weight of its moiety, thereby limiting **renal clearance** and increasing circulation time. In accordance, glomerular filtration of particles larger than 8 nm were reported to suffer less from renal elimination [111]. In addition, a report on glomerular filtration in rat tissue displayed that anionic polymers and polyanions (e.g., albumin) are less likely to pass through the glomerular membrane due to stearic hindrance than uncharged or

cationic compounds [186]. In respect to reported accumulation of R848 or ADU in kidney tissue (chapter IV.B.d and C.d), the conclusion can be drawn that liposomal carrier most likely did not impact accumulation in this tissue as discussed above. In studies with DOX-loaded formulation, kidney did not suffer from enhanced drug accumulation (chapter IV.A.b and c). However, DOX accumulation in kidney and heart, must be viewed critical as elevated contents are responsible for toxicity leading to formation of fibrosis. This is so robust, that respective fields of research utilized 10 mg/kg injected i.v. for modelling respective disease in rats [187] and mice [188-190].

D) Systemic immune activation by R848

Initial reports on encapsulation of R848 in cholesterol-rich liposomes achieved EE of 40 % with passive loading but suffered from 25 % leakage at 37° [191]. This data was reproduced for the $DPPG_2$-TSL matrix, paving the way towards assessing active loading which effectively enhanced encapsulation stability [161]. Consequently, **initial design phase** was structured for maximizing EE and storage stability to the cost of suboptimal PK profile *in vivo*. Obtained data also suggested a high affinity of unprotonated R848 to the lipophilic bilayer phase, lowering release efficacy. Hence, trying to counteract this by encapsulating higher R848 content was achieved by enlarging D:L ratio from 0.1 to 0.2. EE, stability of encapsulation or release kinetics were not influence *in vitro*. In addition, the relatively low amounts of lipids injected i.v. (~ 62 µmol/kg) which might have had negative effects on PK-profile as higher amounts of total injected lipids have been reported to prolong PG_2-TSL circulation time in plasma [140]. When approaching optimization in general, a thorough assessment of type and pH strength of medium, loading condition (time, temperature, and gradient) and D:L ratio should be conducted [192, 193]. However, for *in vivo* application approaches of $DPPG_2$-TSL an additional balance between stable encapsulation and heat-triggerable release must be met [194]. Hence, **$DPPG_2$-TSL-R848 optimization** included lowering D:L ratio and enforcing loading by higher temperature and lower pH. Noteworthy, lipids are stable at neutral pH but reduction towards acidic conditions or increase to basic conditions renders lipid hydrolysis [127, 195]. In this case, this was tolerated as at pH 3 maximal protonation of R848 is achieved enabling active entrapment of drug within the $DPPG_2$-TSL and, theoretically, enforcing release *in vivo*. All of these points were achieved as, even with dose-reduction, overall lipid content injected was doubled (~140 µmol/kg), plasma stability in BN rats enhanced (chapter IV.C.a) and HT-triggered release at least mildly facilitated (chapter IV.C.b). In a recent study, 25 µg R848 covalently bound to PEG hydrogel microsphere (TransCon) was s.c. injected in rats and a plasmatic R848 concentration of ~ 0.3 ng/ml after 240 min documented [196]. Setting this data in comparison to PK-data from $DPPG_2$-TSL-R848 (chapter IV.C.a): the 20-fold reduced dosage resulted in a 6000-fold lower concentration at 240 min. Correlating to other groups aiming at long lasting formulations highlights pivotal plasma stability of $DPPG_2$-

TSL-R848 *in vivo*. However, some batches became less viscous during storage. Until now, a trigger has not yet been unravelled when assessing multiple thawing, cryo-buffer, and time of storage. Hydrolysis of lipids induced by low pH may be a key factor. Therefore, protocol will be re-assessed looking closely at production time and volumes. In another $DPPG_2$-TSL-based formulation encapsulating Gemcitabine, lipid hydrolysis was also encountered during manufacturing process due to acidic pH of hydration solution [127] and was circumvented by using a more neutral hydration solution [197].

HT-triggered release in translated in 3-fold enhanced accumulation in heated tumor in comparison to control. While highest tumor content was recovered from i.t. injected tumor (32-fold elevated in comparison to respective control), also muscle tissue under these tumors accumulated significantly more than in other groups (chapter IV.C.c), proving R848 infiltration of surrounding tissue, rendering risk of off-target reactions. To test a localization effect, Lu *et al.* had conducted an ear inflammation test with free R848 in healthy rabbits, which revealed no signs of local inflammation but plasmatic TNFα secretion within 2 h [88]. A comparable approach could be conducted in rats to estimate effect of off-target accumulation of R848 in tumor-surrounding stroma.

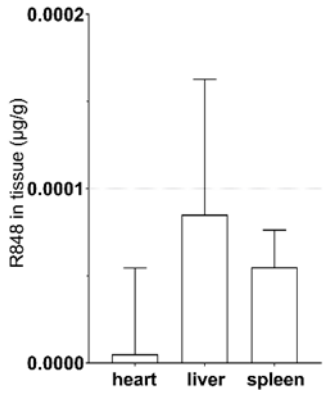

Figure 50: R848-like signal strength in naive tissue.
Heart, liver and spleen tissue from healthy, untreated BN rats was analyzed via R848 HPLC method. Data represent n = 2 per group.

Accumulation of R848 in organs (despite spleen) was not altered between free and liposomal group, indicating a R848-specific distribution. The discovered baseline accumulation in heart, muscle and tumor control tissue questioned sensitivity of established HPLC detection method. For method development and standard samples, calf liver was used to mimic tissue samples (chapter IV.C.c). To clarify potential false positive results, a control experiment was conducted (figure 50). The recovered background noise in rat tissue was significantly below LOD_{R848} of 0.01 µg/g, thereby re-confirming the integrity of the method. A passive binding of unprotonated R848 to membranes leading to background accumulation in off-target organs can be postulated. Already during design phase of initial liposomal formulation, R848 had shown this tendency [161]. Elevated signal in spleen can most likely be attributed carrier-dependent degradation via RES system (see section c). A R848-driven effect can be augmented against, as liposomal entrapment in spleen has been documented beforehand for several comparable formulations loaded with different drugs [125, 140, 185].

For the first time, **antitumor response of R848 in BN175 rat model** is reported here. Thorough exploration of experimental set up (treatment start day, dosages, safety assessment) revealed a therapeutic effect of R848 in comparison to saline + HT (chapter

IV.C.d). However, effect was not linearly related to dosage as documented 32-fold elevated concentration in tumor tissue upon i.t. application (500 µg; chapter IV.C.c) did not translate in strongest tumor control. In detail, single i.v. injection of free R848 controlled tumor growth most, whereas multiple application reduced free R848 effect but enhanced response towards $DPPG_2$-TSL-R848. However, comparable acute but transient body weight loss after i.v. injection of free or liposomal R848 indicated systemic ADR, which was more pronounced after multiple than single injection but counteracted by i.t. injection (chapter IV.C.d). Considering the discovered organ-specific distribution pattern (chapter IV.C.c) allows the assumption, that a 50-fold dosage reduction among studies (BD: 500 µg; therapy: 10 µg) correlated to overall lower R848 accumulation. Hence, noted acute drop in body weight may be attributed to **systemic response to R848 in rats**. Fever and sickness behaviour has been reported after intraperitoneal (i.p.) injection of R837 in healthy rats [198], whereas upon s.c. injection in tumor-bearing rats no ADR were documented [199]. Michaelis *et al.* investigated mechanism of R848 in mice, after having reported severe reduction in food intake and body weight upon i.p. injection of 10 µg in a pancreatic cancer model [200]. Dose-escalation of up to 100 µg i.p. in healthy mice revealed a dosage-dependent systemic toxicity [201]. Other groups injecting low contents systemically did not show dose-response curves or body weight development after i.p [95, 202, 203] or i.v. injection [97, 204]. Notable, safety of 15 µg R848 repetitively applied i.t. has been shown in a mouse colon carcinoma [205]. Toxicity in human has been reported in a phase 2 trial exploring oral application in Hepatic C virus infection [206]. The reported ADR were not correlated to $DPPG_2$-TSL as multiple application enhanced therapeutic response to R848 (chapter IV.C.d), ruling out potential systemic immune response leading to antibody formation. This correlated to previous data published by Wouter *et al.* (figure 6) where antibody formation was not observed for $DPPG_2$-TSL [140]. Furthermore, no sign of local toxicity were noted after i.t. application of $DPPG_2$-TSL-R848 or free R848. Overall, safety of multiple i.t. injection of $DPPG_2$-TSL-R848 can be reported for the first time in respect to local and systemic signs of toxicity in BN175-bearing rats. However, impact of carrier therapeutic efficacy in this approach has not been evaluated but should be conducted in the future. An example why gives Bahmani *et al.* When exploring a platelet-coated nanoparticle (PNP) encapsulating R848, significant antitumor response in two mice models (colon carcinoma and breast cancer) was reported in comparison to free R848. However, tumor growth delay upon empty PNP injection did limit expectations [205].

Justification of **selected treatment days** in repetitive plans are rarely reported in literature but should be critically reviewed as a potential impact on R848 tolerance seem likely. Reports of TLR tolerance upon serial injection of free R848 within 7 days [207] or 5 days [208] question if safety can be proclaimed without assessing a different schedule. A shortened protocol of repetitive four day intervals had been tested with BN175 model (data not shown).

Shortened schedule did enhance signs of severity in tumor-bearing rats in comparison standard metastasis protocol. Overall survival was comparable but antitumor effect was revoked as primary tumor presented accelerated growth comparable to distant tumor in two of three animals. It seems obvious that stress induced overpowered immune control of HT-treated tumor. If systemic enhanced ADR or stress due to shortened schedule was the reason, cannot be defined within this thesis. The primary tumor of the other animal from this groups went into full remission until distant tumor reached end point, indicating enhanced immune response. In this case, it may be hypothesised if timing of distant tumor injection + R848-treatment acted 'vaccine'-like and effect was only enhanced upon shortened schedule. However, distant tumor growth was unaffected, reducing the leverage of this hypothesis. Theoretically, R848 is capable to achieve **antitumoral vaccination** [80, 84, 94] or with topical application in currently ongoing clinic trials in melanoma [209] and brain tumors [210]. Efficacy has been proven in various clinical settings with melanoma [211-213] or advanced tumors refractory to conventional treatment [214] among many other TLR agonists [81].

E) Sensitivity of BN175 sarcoma model towards DOX

With BD-data of BL6 mice indicating an effect of HT-technique on accumulation levels in tumor tissue upon injection of $DPPG_2$-TSL-DOX (chapter IV.A.c), the question if overall set up with animals bearing two tumors was robust enough to detect differences in accumulation pattern. With sham-treatment lacking a heat-induced DOX-release from carrier, significantly higher plasma contents were expected. However, organs or tumors entrapped comparable or even less amounts, which indicated a stable encapsulation and low rate of leakage. Upon HT-treatment, organ and tumor distribution was independent of animal bearing one or two tumors, despite in heated tumor tissue. Overall, HT-triggered release increased circulating free DOX levels, thereby potentially enhancing accumulation in kidney and tumor tissue (chapter IV.A.d). Accordingly, reduction of animal numbers can be achieved with two-tumors per animal while still maintaining robustness of the study. Of interest is the detected significant elevation of DOX-accumulation in heated tumor tissue, which must be driven by accumulation of released DOX as none accumulated in sham-treated animals.

Pivotal data of $DPPG_2$-TSL-DOX plasmatic stability and efficacy of HT-triggered release *in vivo* upon lamp-HT pathed the way towards exploring therapeutic response in BN175 sarcoma model (chapter IV.A.e). In comparison to clinical relevant controls, $DPPG_2$-TSL-DOX did not only significantly prolong survival but was also the only drug inducing a tumor growth delay. Comparable promising data have been reported in combination with WB-HT [125] or comparable chemotherapeutic-drugs encapsulated in $DPPG_2$-TSL, such as Gemcitabine or Irinotecan [127, 197].

The addition of DNA-damaging drugs, such as DOX, could elevate later innate immune recognition and contribute to immunotherapeutic approaches [133]. With BN175-

responsiveness towards $DPPG_2$-TSL-DOX being high (chapter IV.A), an ideal candidate for tumor priming available. While the question whether this pre-treatment would enhance R848-responsiveness was positively answered (chapter IV.C.d.ii), treatment protocol had to be adapted from WB to lamp-induced HT for $DPPG_2$-TSL-DOX injection (chapter IV.C.d.i). Local signs of toxicity upon WB-induced HT had been reported after 5 mg/kg i.v. injection beforehand [125] and were confirmed also for the 2.5-fold lower dose (2 mg/kg) used during this thesis. Further dose-reduction was not performed as alternating to more focused lamp-HT prevent local toxicity (chapter IV.C.d.i). As discussed by Willerding *et al.*, total heated surface area with WB techniques exceeds lamp-heating focused on tumor excessively rendering greater DOX release followed by off-target accumulation [146]. Nevertheless, the lamp method has several inevitable downsides such as the need of an intratumoral temperature probe, a longer pre-heating phase and high risk of surface skin burns. In addition, efficacy of heating tissue was not only dependent on thickness of tumor tissue but also on orientation and distance of lamp towards tumor surface as well as cooling through air conductivity. All of these weaken robustness of technique and result in inhomogeneous 41 °C within one tumor. Nevertheless, more focused HT can be applied with an overall reduced volume of total heated surface in comparison to WB. The impact of this became most evident in $DPPG_2$-TSL-DOX therapy study. Looking at safety, more targeted DOX accumulation may circumvent toxicity. Toxicity of DOX is widely reported in the clinic as conventional cytotoxic drugs come along with low tumor specificity and high toxicity [5]. Straight forward approaches focus on co-medication of cardioprotective drugs. In a study with MatBIII tumor model, free DOX (2 mg/kg) prolonged survival by 60 % but additional administration of the cardioprotective dantrolene increased 3-week survival rate to 84 % [137]. Newer approaches aim at minimizing side effects by NP-based encapsulations. However, off-site toxicity can occur if specific organ-targeting or triggered release mechanism are lacking. An ideal example for this is, unfortunately, the approved Doxil® and the formation of PPE (discussed in II.E). Recent reports on a new version of PEGylated DOX have shown pivotal data upon co-medication with pyridoxine, as approaches proved to prevent PPE effectively in clinical settings [215]. Other side effects include severe myelosuppression, nausea, vomiting or skin derived effect resulting in alopecia and severe local tissue damage. Taking these into account, Doxil® showed a distinct superiority over "standard of care" DOX in most evaluated side effects [110]. Despite the lessions learned from this PEGylated formulation, newly reported beneficial clinical data have to be appreciated and should lead to escalating the potential given by NP-platforms. For BN175 sarcoma model, it is now evident that this rat model enables sensitive detection of clinical relevant signs of toxicity. Further effort should be taken to implement methods for monitoring cardio- and nephrotoxicity in preclinical settings, which in the end would also impact safety assessment of future formulations.

F) Lessons learned from combinational approach

Impact of priming BN175-tumors with DOX was distinctive and treatment approach benefitted significantly from liposomal encapsulation of R848. In comparison to single DOX-treatment + HT (lamp), survival was prolonged especially in combinations with $DPPG_2$-TSL-R848 + HT, independent of style of injection (i.t. or i.v.). Noteworthy, either addition of i.t. injected R848 (free or liposomal form) circumvented signs of systemic ADR (body weight) also in combinational settings (chapter IV.C.d). This highlighted the need to fine-tune resulting systemic antitumor immune response. Insight on the strength of alterations within the TME may be gained by evaluating immune-cell composition of tumor tissue, tumor-draining lymph node and spleen after treatment. In depth analysis of infiltrating immune cells via FACS is planned thereby hoping to define the most optimal time point for R848 application for future treatment schedule planning. The importance of timing within a combinational treatment was shown in study evaluating free R848 with cyclophosphamide (CP). After having proven responsiveness in a rat glioma model for either compound, addition of CP showed comparable tumor remission however failed to evoke immunological memory against re-challenge in contrast to mono-treatment with free R848. Likely, activated cytotoxic T cells were killed upon application of highly cytotoxic CP [199]. In contrast to reports with DOX, the authors discussed local enhancement of antigen presentation at a site of concentrated tumor-specific antigens induced by DOX-driven tumor cell death. This was reported to be beneficial for long-lasting immunity in a study focusing on T cell lymphoma model in mice and injection of GD5, a TLR 7 agonist [216]. The same exploration had been conducted with TLR 7 agonist SZU-101 in identical settings [217]. In contrary, antitumor effect of R848-PNP in a mouse colon carcinoma was not more pronounced when co-administered with DOX. Noteworthy, DOX was pre-mixed with R848-PNP before i.t. injected, rendering questionable state of NP integrity [205]. In a preclinical study with breast cancer, repetitive R848 application was enhanced upon combination with anti-angiogenic agent sunitinib hinting at a synergistic antitumor effect [203]. In the metastasis approach, an induction of systemic antitumor response was proven but effect was mainly driven on $DPPG_2$-TSL-DOX (chapter IV.C.d). Despite this cytotoxic effect, DOX also modulates immune contexture through induction of immunogenic cell death, generation of TAA, and expression of cytokines [218, 219]. This could explain the observations of this thesis. Overall, multiple studies claim promising results upon combinations of R848 and cytotoxic drug and data of this thesis adds to this hypothesis. Timing of combinations and/or multiple injection might be essential but with insight on decision points not being published, further exploration in BN175 model must be conducted.

VI. Summary

In order to gain a deeper understanding of the well-established $DPPG_2$-TSL-DOX formulation, the corresponding *in vivo* behaviour was investigated in two different species. A BD-study in rats demonstrated the independent distribution of DOX and $DPPG_2$ *in vivo*. Here, HT-induced DOX accumulation in HT-treated tumor tissue was reproducible in rats bearing one or two tumors. For the first time, the therapeutic effect in the BN175 sarcoma model was investigated with optimized $DPPG_2$-TSL-DOX, showing a clear HT-dependent slowed tumor growth compared to clinically relevant controls. Experiments in mice were used to gain further insight into the stability and biodistribution of $DPPG_2$-TSL-DOX. For this, a B16 melanoma model was implemented. A comparison of the distribution patterns between both species showed a significantly increased DOX accumulation in mouse organs.

Also for the first time, the STING agonist ADU was loaded in $DPPG_2$-TSL under two different osmotic conditions: hypo- and isosmotic. In rats, liposomal encapsulation of ADU significantly increased plasma stability in comparison to free ADU. Additional HT-treatment did not alter the pharmacokinetic profile of $DPPG_2$-TSL-$ADU_{isosmotic}$ but accelerated the clearance of $DPPG_2$-TSL-$ADU_{hyposmotic}$ as the carrier is more unstable *in vivo*. This resulted in a HT-triggered release of ADU and accelerated clearance of $DPPG_2$. In mice, impact of osmotic condition was less pronounced because plasma concentrations were overall very low. Despite this, $DPPG_2$-TSL-$ADU_{hyposmotic}$ + HT resulted in a systemic response in B16-bearing mice while rats tolerated the treatment well. The therapeutic effect in the BN175 sarcoma model proved to be HT-independent. A possible cause is the identical biodistribution of $DPPG_2$ and ADU shown in the subsequent BD-study. Although HT-dependent accumulation of ADU in tumor tissue could not be proven, treatment with $DPPG_2$-TSL-ADU prolonged survival in this model compared to free ADU (i.v. or i.t.). To further investigate its therapeutic potential, a MatBIII mamma adenocarcinoma rat model was established and verified.

After *in vivo* confirmation of the successful formulation modification, the adapted $DPPG_2$-TSL-R848 formulation was studied in more detail in rats. After i.v. injection, an increased stability in comparison to free R848 as well as efficient HT-triggered release in plasma were demonstrated. An associated increased accumulation in HT-treated tumor tissue was proven in a consecutive biodistribution study. Compared to i.t. injection of free R848, the total concentration within the tumor was lower upon treatment with $DPPG_2$-TSL-R848 + HT. However, the therapeutic effect in the BN175 sarcoma model on repetitive injection of $DPPG_2$-TSL-R848 + HT outperformed treatment with free R848 (i.v. or i.t.) + HT. This pronounced therapeutic response could be further enhanced by adding a pre-treatment for tumor priming which consisted of a $DPPG_2$-TSL-DOX injection in combination with lamp-HT. The response of the BN175 sarcoma model to R848 had been demonstrated in dose-escalation studies beforehand.

VII. Zusammenfassung

Um ein besseres Verständnis des *in vivo* Verhaltens zu erlangen, wurde die bewährte $DPPG_2$-TSL-DOX Formulierung in zwei verschiedenen Tierarten untersucht. Biodistributionsstudie in Ratten zeigte die unabhängige Verteilung von DOX und $DPPG_2$. Die HT-induzierte DOX-Akkumulation im erwärmten Tumorgewebe war dabei reproduzierbar bei Ratten mit einem oder zwei Tumoren. Erstmals wurde der Therapieeffekt in dem BN175 Sarkom-Modells mit optimierten $DPPG_2$-TSL-DOX untersucht, wobei sich ein HT-abhängiges verlangsamtes Tumorwachstum im Vergleich zu klinisch relevanten Kontrollen zeigte. Mit Experimenten an Mäusen wurden weitere Erkenntnisse über die Stabilität und Biodistribution von $DPPG_2$-TSL-DOX gewonnen. Hierfür wurde ein B16 Melanom-Modell implementiert. Ein Vergleich der Verteilungsmuster zwischen beiden Spezies zeigte eine deutlich erhöhte DOX-Akkumulation in den Organen der Maus.

Ebenfalls erstmalig wurde der STING-Agonist ADU unter zwei verschiedenen osmotischen Bedingungen in $DPPG_2$-TSL enkapsuliert: hypo- und isosmotisch. Bei Ratten erhöhte der liposomale Einschluss von ADU die Plasmastabilität im Vergleich zu freiem ADU erheblich. Eine zusätzliche HT-Behandlung veränderte das pharmakokinetische Profil von $DPPG_2$-TSL-$ADU_{isosmotisch}$ nicht, beschleunigte aber die Clearance von $DPPG_2$-TSL-$ADU_{hyposmotisch}$ da dieser Carrier *in vivo* instabiler ist. Dies hat zu einer HT-getriggerten Freisetzung von ADU und einer beschleunigten Clearance von $DPPG_2$ geführt. Bei Mäusen war die Auswirkung der Osmolalität weniger ausgeprägt, da die Plasmakonzentrationen insgesamt sehr gering waren. Trotzdem führte $DPPG_2$-TSL-$ADU_{hyposmotisch}$ + HT zu einer systemischen Reaktion bei Mäuse mit B16 Tumoren, während Ratten die Behandlung gut vertragen haben. Der Therapieeffekt im BN175 Sarkom-Modell erwies sich als HT-unabhängig. Eine mögliche Ursache ist die in der darauffolgenden Biodistributionsstudie gezeigten identische Gewebeverteilung von $DPPG_2$ und ADU. Auch wenn eine HT-abhängige Anreicherung von ADU im Tumorgewebe demnach nicht bewiesen werden konnte, verlängerte die Behandlung mit $DPPG_2$-TSL-ADU das Überleben in diesem Modell im Vergleich zu freiem ADU (i.v. oder i.t.). Um dieses therapeutische Potenzial weiter zu untersuchen, wurde ein MatBIII-Mammakarzinom-Modell in Ratten etabliert und verifiziert.

Nach *in vivo* Bestätigung der erfolgreichen Formulierungsmodifikation wurde die angepasste $DPPG_2$-TSL-R848 Formulierung in Ratten genauer untersucht. Nach i.v. Injektion wurde eine erhöhte Stabilität im Vergleich zu freiem R848, sowie eine effiziente HT-getriggerte Freisetzung im Plasma gezeigt. Eine damit einhergehende erhöhte Akkumulation im HT-behandelten Tumorgewebe wurde in der anschließenden Biodistributionsstudie nachgewiesen. Im Vergleich zur i.t. Injektion von freien R848 war die Gesamtkonzentration im Tumor bei Behandlung mit $DPPG_2$-TSL-R848 + HT niedriger. Der Therapieeffekt im BN175 Sarkom-Modell durch die mehrfache Injektion von $DPPG_2$-TSL-R848 + HT übertraf

dagegen die Behandlung mit freiem R848 (i.v. oder i.t.) + HT. Diese ausgeprägte therapeutische Wirkung konnte durch ein vorhergegangenes Tumorpriming mit $DPPG_2$-TSL-DOX in Kombination mit Lampen-HT weiter verstärkt werden. Das Ansprechen des BN175 Sarkom-Modells auf R848 war zuvor in Dosis-Eskalationsstudien nachgewiesen worden.

VIII. Outlook

The principle that any exploration of novel therapeutic strategies should goal to ensure function in various animal species before clinical trials are conducted has been followed for decades [7]. With immunotherapy approaches in the pipeline, this is even more important than when stated in 1976. Species-dependent effects should be exploited to a greater extent, as is forms the predictability of preclinical research for clinical translation. Approaches focusing solely on immune-derived antitumor response must be progressively refined to characterize human constitution of target which, always, includes profiling human immune cells [18, 119, 220]. The need for advancing refinement to grant easily accessible and robust humanized xenograft models is immense [29, 39]. For the first time, a fully immunosuppressed rat line allowing humanization was introduced to the marked in 2022 [221]. This does not only highlight the pressing need for models but also features a comeback of rats as experimental animals. In respect to STING activation, insight on responses in such a model may impact further agonist screens to identify high-impact candidates. Further, encapsulation in LNP may enable specific organ-targeting and hamper unspecific leakage leading to unwanted systemic activity. For R848, future may lie in combinational with cationic liposomes and application in models or species with distinct TLR 7/8 expression profile. Clinical evaluation of expression levels of markers, receptors, inhibiting signals as well as tumor-infiltrating immune cell repertoire will guide the optimization of personalized immunotherapeutic interventions, based on conclusions drawn preclinical. Either immunomodulatory drug being one of potential candidates to achieve antitumor efficacy. However, due diligence of tolerability and efficacy *in vivo* should not be exclusive but rather include thorough *in vitro* assessment. Within the recent years, an increasing amount of replacement strategies (3R principle) have been established and gain increasing appreciation within the scientific community. Organ-on-a-disc, 3D bioprinting, Organoids, or synthetic embryoid models, only to name a few, can give hints at drug efficacy and should be implement routinely together with artificial intelligence search programs for research databases before conducting or even planning animal experiments.

IX. References

[1.] Arruebo M, Vilaboa N, Saez-Gutierrez B, Lambea J, Tres A, Valladares M, et al. Assessment of the evolution of cancer treatment therapies. Cancers. 2011;3(3):3279-330.

[2.] Rove K, Crawford E. Metastatic Cancer in Solid Tumors and Clinical Outcome: Skeletal-Related Events. Oncology Journal. 2009;23:21-7.

[3.] Urruticoechea A, Alemany R, Balart J, Villanueva A, Viñals F, Capellá G. Recent Advances in Cancer Therapy: An Overview. Current Pharmaceutical Design. 2010;16:3-10.

[4.] Mansoori B, Mohammadi A, Davudian S, Shirjang S, Baradaran B. The Different Mechanisms of Cancer Drug Resistance: A Brief Review. Advanced Pharmaceutical Bulletin. 2017;7(3):339-48.

[5.] Schirrmacher V. From chemotherapy to biological therapy: A review of novel concepts to reduce the side effects of systemic cancer treatment (Review). International Journal of Oncology. 2019;54(2):407-19.

[6.] Wang LC, Thomsen L, Sutherland R, Reddy CB, Tijono SM, Chen CJ, et al. Neutrophil influx and chemokine production during the early phases of the antitumor response to the vascular disrupting agent DMXAA (ASA404). Neoplasia. 2009;11(8):793-803.

[7.] Bartlett GL, Kreider JW, Purnell DM. Immunotherapy of Cancer in Animals: Models or Muddles? Journal of the National Cancer Institute. 1979;56(2):207-10.

[8.] Makkouk A, Weiner G. Cancer immunotherapy and breaking immune tolerance: new approaches to an old challenge. Cancer Research. 2015;75(1):5-10.

[9.] Khalil D, Smith E, Brentjens R, Wolchok J. The future of cancer treatment: immunomodulation, CARs and combination immunotherapy. Nature Reviews Clinical Oncology. 2016;13(5):273-90.

[10.] Darvin P, Toor S, Sasidharan Nair V, Elkord E. Immune checkpoint inhibitors: recent progress and potential biomarkers. Experimental & Molecular Medicine. 2018;50(12).

[11.] Hirayama A, Gauthier J, Hay K, Voutsinas J, Wu Q, Pender B, et al. High rate of durable complete remission in follicular lymphoma after CD19 CAR-T cell immunotherapy. Blood. 2019;134(7):14.

[12.] Bonaventura P, Shekarian T, Alcazer V, Valladeau-Guilemond J, Valsesia-Wittmann S, Amigorena S, et al. Cold Tumors: A Therapeutic Challenge for Immunotherapy. Frontiers in Immunology. 2019;10.

[13.] https://www.cancerresearch.org/fda-approval-timeline-of-active-immunotherapies.

[14.] Petrelli F, Grizzi G, Ghidini M, Ghidini A, Ratti M, Panni S, et al. Immune-related Adverse Events and Survival in Solid Tumors Treated With Immune Checkpoint Inhibitors: A Systematic Review and Meta-Analysis. Journal of Immunotherapy. 2020;43(1):1-7.

[15.] Jamal S, Hudson M, Fifi-Mah A, Ye C. Immune-related Adverse Events Associated with Cancer Immunotherapy: A Review for the Practicing Rheumatologist. Journal of Rheumatology. 2020;47(2):166-75.

[16.] Marabelle A, Andtbacka R, Harrington K, Melero I, Leidner R, de Baere T, et al. Starting the fight in the tumor: expert recommendations for the development of human intratumoral immunotherapy (HIT-IT). Annals of Oncology. 2018;29:2163-74.

[17.] Agrawal S, Kandimalla ER. Intratumoural immunotherapy: activation of nucleic acid sensing pattern recognition receptors. Immuno-Oncology Technology. 2019;3:15-23.

[18.] Olson B, Li Y, Lin Y, Liu ET, Patnaik A. Mouse Models for Cancer Immunotherapy Research. Cancer Discovery. 2018;8(11):1358-65.

[19.] Fridman WH, Pages F, Sautes-Fridman C, Galon J. The immune contexture in human tumours: impact on clinical outcome. Nature Reviews Cancer. 2012;12(4):298-306.

[20.] Porciello N, Franzese O, D'Ambrosio L, Palermo B, Nistico P. T-cell repertoire diversity: friend or foe for protective antitumor response? Journal of experimental and clinical cancer research. 2022;41(1):356.

[21.] Sanmamed MF, Chester C, Melero I, Kohrt H. Defining the optimal murine models to investigate immune checkpoint blockers and their combination with other

immunotherapies. Annals of Oncology. 2016;27(7):1190-8.
[22.] Budhu S, Wolchok J, Merghoub T. The importance of animal models in tumor immunity and immunotherapy. Current Opinion in Genetics and Development. 2014;46-51.
[23.] Bareham B, Georgakopoulos N, Matas-Cespedes A, Curran M, Saeb-Parsy K. Modeling human tumor-immune environments in vivo for the preclinical assessment of immunotherapies. Cancer Immunology, Immunotherapy. 2021;70(10):2737-50.
[24.] Talmadge JE, Singh RK, Fidler IJ, Raz A. Murine models to evaluate novel and conventional therapeutic strategies for cancer. The American Journal of Pathology. 2007;170(3):793-804.
[25.] Gengenbacher N, Singhal M, Augustin HG. Preclinical mouse solid tumour models: status quo, challenges and perspectives. Nature Reviews Cancer. 2017;17(12):751-65.
[26.] Hegde PS, Chen DS. Top 10 Challenges in Cancer Immunotherapy. Immunity. 2020;52(1):17-35.
[27.] Bibby MC. Orthotopic models of cancer for preclinical drug evaluation: advantages and disadvantages. Eurpean Journal of Cancer. 2004;40(6):852-7.
[28.] Mittal D, Gubin MM, Schreiber RD, Smyth MJ. New insights into cancer immunoediting and its three component phases--elimination, equilibrium and escape. Current Opinion in Immunology. 2014;27:16-25.
[29.] Zitvogel L, Pitt JM, Daillere R, Smyth MJ, Kroemer G. Mouse models in oncoimmunology. Nature Reviews Cancer. 2016;16(12):759-73.
[30.] Galon J, Bruni D. Approaches to treat immune hot, altered and cold tumours with combination immunotherapies. Nature reviews Drug Discovery. 2019;18(3):197-218.
[31.] Schreiber RD, Old LJ, Smyth MJ. Cancer immunoediting: integrating immunity's roles in cancer suppression and promotion. Science. 2011;331(6024):1565-70.
[32.] Passarelli A, Mannavola F, Stucci LF, Tucci M, Silvestris F. Immune system and melanoma biology: a balance between immunosurveillance and immune escape. Oncotarget. 2017;8(62).
[33.] O'Donnell JS, Teng MWL, Smyth MJ. Cancer immunoediting and resistance to T cell-based immunotherapy. Nature Reviews Clinical Oncology. 2019;16(3):151-67.
[34.] Hanahan D, Weinberg RA. Hallmarks of cancer: the next generation. Cell. 2011;144(5):646-74.
[35.] Woo SR, Fuertes MB, Corrales L, Spranger S, Furdyna MJ, Leung MY, et al. STING-dependent cytosolic DNA sensing mediates innate immune recognition of immunogenic tumors. Immunity. 2014;41(5):830-42.
[36.] Marcus A, Gowen BG, Thompson TW, Iannello A, Ardolino M, Deng W, et al. Recognition of tumors by the innate immune system and natural killer cells. Advanced Immunology. 2014;122:91-128.
[37.] Fridman WH, Zitvogel L, Sautes-Fridman C, Kroemer G. The immune contexture in cancer prognosis and treatment. Nature Reviews Clinical Oncology. 2017;14(12):717-34.
[38.] Amouzegar A, Chelvanambi M, Filderman JN, Storkus WJ, Luke JJ. STING Agonists as Cancer Therapeutics. Cancers. 2021;13(11).
[39.] Miller IS, Shiels LP, Conroy E, Connor K, Dicker P, Gallagher WM, et al. Durability of cell line xenograft resection models to interrogate tumor micro-environment targeting agents. Scientific Reports. 2019;9(1):10.
[40.] Liu Y, Cao X. Immunosuppressive cells in tumor immune escape and metastasis. Journal of Molecular Medicine. 2016;94(5):509-22.
[41.] Sousa LM, Almeida JS, Fortes-Andrade T, Santos-Rosa M, Freitas-Tavares P, Casanova JM, et al. Tumor and Peripheral Immune Status in Soft Tissue Sarcoma: Implications for Immunotherapy. Cancers. 2021;13(15).
[42.] Binnewies M, Roberts EW, Kersten K, Chan V, Fearon DF, Merad M, et al. Understanding the tumor immune microenvironment (TIME) for effective therapy. Nature Medicine. 2018;24(5):541-50.
[43.] Liu X, Li L, Si F, Huang L, Zhao Y, Zhang C, et al. NK and NKT cells have distinct properties and functions in cancer. Oncogene. 2021;40(27):4521-37.

[44.] Rossi JF, Ceballos P, Lu ZY. Immune precision medicine for cancer: a novel insight based on the efficiency of immune effector cells. Cancer Communications. 2019;39(1):34.
[45.] Labrie M, Brugge JS, Mills GB, Zervantonakis IK. Therapy resistance: opportunities created by adaptive responses to targeted therapies in cancer. Nature Reviews Cancer. 2022;22(6):323-39.
[46.] Boland GM, Flaherty KT. Tracking early response to immunotherapy. Nature Cancer. 2020;1(2):160-2.
[47.] Becht E, Giraldo NA, Lacroix L, Buttard B, Elarouci N, Petitprez F, et al. Estimating the population abundance of tissue-infiltrating immune and stromal cell populations using gene expression. Genome Biology. 2016;17(1):218.
[48.] Pagès F, Mlecnik B, Marliot F, Bindea G, Ou F-S, Bifulco C, et al. International validation of the consensus Immunoscore for the classification of colon cancer: a prognostic and accuracy study. The Lancet. 2018;391(10135):2128-39.
[49.] Blair HA. Immunoscore((R)): A Diagnostic Assay for Clinical Management of Colon Cancer. Molecular Diagnosis & Therapy. 2020;24(3):365-70.
[50.] Angell HK, Bruni D, Barrett JC, Herbst R, Galon J. The Immunoscore: Colon Cancer and Beyond. Clinical Cancer Research. 2020;26(2):332-9.
[51.] Tumeh PC, Harview CL, Yearley JH, Shintaku IP, Taylor EJ, Robert L, et al. PD-1 blockade induces responses by inhibiting adaptive immune resistance. Nature. 2014;515(7528):568-71.
[52.] Riaz N, Havel JJ, Makarov V, Desrichard A, Urba WJ, Sims JS, et al. Tumor and Microenvironment Evolution during Immunotherapy with Nivolumab. Cell. 2017;171:934-49.
[53.] Voorwerk L, Slagter M, Horlings HM, Sikorska K, van de Vijver KK, de Maaker M, et al. Immune induction strategies in metastatic triple-negative breast cancer to enhance the sensitivity to PD-1 blockade: the TONIC trial. Nature Medicine. 2019;25(6):920-8.
[54.] Gatti-Mays ME, Balko JM, Gameiro SR, Bear HD, Prabhakaran S, Fukui J, et al. If we build it they will come: targeting the immune response to breast cancer. Nature Partner Journals Breast Cancer. 2019;5:37.
[55.] Chen QF, Li W, Wu PH, Shen LJ, Huang ZL. Significance of tumor-infiltrating immunocytes for predicting prognosis of hepatitis B virus-related hepatocellular carcinoma. World Journal of Gastroenterology. 2019;25(35):5266-82.
[56.] Nie R, Yuan S, Wang Y, Chen Y, Cai Y, Chen S, et al. Robust immunoscore model to predict the response to anti-PD1 therapy in melanoma. Aging. 2019;11(23):11576-90.
[57.] Hodi FS, O'Day SJ, McDermott DF, Weber RW, Sosman JA, Haanen JB, et al. Improved survival with ipilimumab in patients with metastatic melanoma. The New England Journal of Medicine. 2010;363(8):711-23.
[58.] Robert C, Ribas A, Wolchok JD, Hodi FS, Hamid O, Kefford R, et al. Anti-programmed-death-receptor-1 treatment with pembrolizumab in ipilimumab-refractory advanced melanoma: a randomised dose-comparison cohort of a phase 1 trial. Lancet. 2014;384(9948):1109-17.
[59.] Weber JS, D'Angelo SP, Minor D, Hodi FS, Gutzmer R, Neyns B, et al. Nivolumab versus chemotherapy in patients with advanced melanoma who progressed after anti-CTLA-4 treatment (CheckMate 037): a randomised, controlled, open-label, phase 3 trial. Lancet Oncol. 2015;16(4):375-84.
[60.] Lauss M, Donia M, Harbst K, Andersen R, Mitra S, Rosengren F, et al. Mutational and putative neoantigen load predict clinical benefit of adoptive T cell therapy in melanoma. Nature Communications. 2017;8(1):1738.
[61.] Du H, Xu T, Cui M. cGAS-STING signaling in cancer immunity and immunotherapy. Biomedicine & Pharmacotherapy. 2021;133:110972.
[62.] Luo K, Li N, Ye W, Gao H, Luo X, Cheng B. Activation of Stimulation of Interferon Genes (STING) Signal and Cancer Immunotherapy. Molecules. 2022;27(14).
[63.] Feng X, Liu D, Li Z, Bian J. Bioactive modulators targeting STING adaptor in cGAS-STING pathway. Drug Discovery Today. 2020;25(1):230-7.
[64.] Corrales L, Glickman L, McWhirter S, Kanne D, Sivick K, Katibah G, et al. Direct

Activation of STING in the Tumor Microenvironment Leads to Potent and Systemic Tumor Regression and Immunity. Cell Reports. 2015;11(7):1018-30.
[65.] Sivick K, Desbien A, Glickman L, Reiner G, Corrales L, Surh N, et al. Magnitude of Therapeutic STING Activation Determines CD8(+) T Cell-Mediated Anti-tumor Immunity. Cell Reports. 2018;25(11):3074-85.
[66.] Gogoi H, Mansouri S, Jin L. The Age of Cyclic Dinucleotide Vaccine Adjuvants. Vaccines. 2020;8(3).
[67.] Gao D, Wu J, Wu Y-T, Du F, Aroh C, Yan N, et al. Cyclic GMP-AMP Synthase Is an Innate Immune Sensor of HIV and Other Retroviruses. 2013.
[68.] Kim S, Li L, Maliga Z, Yin Q, Wu H, Mitchison TJ. Anticancer flavonoids are mouse-selective STING agonists. ACS Chemical Biology. 2013;8(7):1396-401.
[69.] NCT00863733 C.
[70.] Nicolai CJ, Wolf N, Chang IC, Kirn G, Marcus A, Ndubaku CO, et al. NK cells mediate clearance of CD8(+) T cell-resistant tumors in response to STING agonists. Science Immunology. 2020;5(45).
[71.] Park CG, Hartl CA, Schmid D, Carmona EM, Kim H, Goldberg MS. Extended release of perioperative immunotherapy prevents tumor recurrence and eliminates metastases. Science Translational Medicine. 2018;10.
[72.] Francica BJ, Ghasemzadeh A, Desbien AL, Theodros D, Sivick KE, Reiner GL, et al. TNFalpha and Radioresistant Stromal Cells Are Essential for Therapeutic Efficacy of Cyclic Dinucleotide STING Agonists in Nonimmunogenic Tumors. Cancer Immunology Research. 2018;6(4):422-33.
[73.] NCT02675439 C.
[74.] NCT03937141 C.
[75.] NCT03172936 C.
[76.] NCT03010176 C.
[77.] NCT04220866 C.
[78.] Ritchie C, Cordova AF, Hess GT, Bassik MC, Li L. SLC19A1 Is an Importer of the Immunotransmitter cGAMP. Molecular Cell. 2019;75(2):372-81 e5.
[79.] Engel AL, Holt GE, Lu H. The pharmacokinetics of Toll-like receptor agonists and the impact on the immune system. Expert Review of Clinical Pharmacology. 2011;4(2):275-89.
[80.] Huang L, Ge X, Liu Y, Li H, Zhang Z. The Role of Toll-like Receptor Agonists and Their Nanomedicines for Tumor Immunotherapy. Pharmaceutics. 2022;14(6).
[81.] Yang Y, Li H, Fotopoulou C, Cunnea P, Zhao X. Toll-like receptor-targeted anti-tumor therapies: Advances and challenges. Frontiers in Immunology. 2022;13:1049340.
[82.] Urban-Wojciuk Z, Khan MM, Oyler BL, Fahraeus R, Marek-Trzonkowska N, Nita-Lazar A, et al. The Role of TLRs in Anti-cancer Immunity and Tumor Rejection. Frontiers in Immunology. 2019;10:2388.
[83.] Zheng R, Ma J. Immunotherapeutic Implications of Toll-like Receptors Activation in Tumor Microenvironment. Pharmaceutics. 2022;14(11).
[84.] Sun H, Li Y, Zhang P, Xing H, Zhao S, Song Y, et al. Targeting toll-like receptor 7/8 for immunotherapy: recent advances and prospectives. Biomarker Research. 2022;10(1):89.
[85.] NCT04799054 C.
[86.] NCT05710848 C.
[87.] Gao Y, Wang K, Zhang J, Duan X, Sun Q, Men K. Multifunctional nanoparticle for cancer therapy. MedComm. 2023;4(1):e187.
[88.] Lu R, Groer C, Kleindl PA, Moulder KR, Huang A, Hunt JR, et al. Formulation and preclinical evaluation of a toll-like receptor 7/8 agonist as an anti-tumoral immunomodulator. Journal of Controlled Release. 2019;306:165-76.
[89.] Schmid D, Park CG, Hartl CA, Subedi N, Cartwright AN, Puerto RB, et al. T cell-targeting nanoparticles focus delivery of immunotherapy to improve antitumor immunity. Nature Communications. 2017;8(1):1747.
[90.] Rodell CB, Arlauckas SP, Cuccarese MF, Garris CS, Li R, Ahmed MS, et al. TLR7/8-agonist-loaded nanoparticles promote the polarization of tumour-associated

macrophages to enhance cancer immunotherapy. Nature Biomedical Engineering. 2018;2(8):578-88.
[91.] Lu Q, Qi S, Li P, Yang L, Yang S, Wang Y, et al. Photothermally activatable PDA immune nanomedicine combined with PD-L1 checkpoint blockade for antimetastatic cancer photoimmunotherapy. Journal of Materials Chemistry B. 2019;7(15):2499-511.
[92.] Cheng Y, Chen Q, Guo Z, Li M, Yang X, Wan G, et al. An Intelligent Biomimetic Nanoplatform for Holistic Treatment of Metastatic Triple-Negative Breast Cancer via Photothermal Ablation and Immune Remodeling. ACS Nano. 2020;14(11):15161-81.
[93.] Li J, Yu X, Jiang Y, He S, Zhang Y, Luo Y, et al. Second Near-Infrared Photothermal Semiconducting Polymer Nanoadjuvant for Enhanced Cancer Immunotherapy. Advanced Materials. 2021;33(4):e2003458.
[94.] Kim H, Niu L, Larson P, Kucaba TA, Murphy KA, James BR, et al. Polymeric nanoparticles encapsulating novel TLR7/8 agonists as immunostimulatory adjuvants for enhanced cancer immunotherapy. Biomaterials. 2018;164:38-53.
[95.] Ye J, Mills BN, Qin SS, Garrett-Larsen J, Murphy JD, Uccello TP, et al. Toll-like receptor 7/8 agonist R848 alters the immune tumor microenvironment and enhances SBRT-induced antitumor efficacy in murine models of pancreatic cancer. The Journal for ImmunoTherapy of Cancer. 2022;10(7).
[96.] Tian Z, Hong B, Chen J, Tang Z. Combination of Radiofrequency Ablation With Resiquimod to Treat Hepatocellular Carcinoma Via Inflammation of Tumor Immune Microenvironment and Suppression of Angiogenesis. Front Oncol. 2022;12:891724.
[97.] Dovedi S, Melis M, Wilkinson R, Adlard A, Stratford I, Honeychurch J, et al. Systemic delivery of a TLR7 agonist in combination with radiation primes durable antitumor immune responses in mouse models of lymphoma. Blood. 2013;121(2):251-9.
[98.] L. PV, Bardel E, Gregoire S, Vanoirbeek J, Schneider E, Dy M, et al. Treatment with the TLR7 agonist R848 induces regulatory T-cell-mediated suppression of established asthma symptoms. European Journal of Immunology. 2011;41(7):1992-9.
[99.] Goldberg MS. Improving cancer immunotherapy through nanotechnology. Nature Reviews Cancer. 2019;19(10):587-602.
[100.] Stiepel RT, Duggan E, Batty CJ, Ainslie KM. Micro and nanotechnologies: The little formulations that could. Bioeng Translational Medicine. 2023;8(2):e10421.
[101.] Schoenmaker L, Witzigmann D, Kulkarni JA, Verbeke R, Kersten G, Jiskoot W, et al. mRNA-lipid nanoparticle COVID-19 vaccines: Structure and stability. International Journal of Pharmaceutics. 2021;601:120586.
[102.] as of 31 December 2022; https://www.fda.gov.ph/list-of-fda-issued-emergency-use-authorization/.
[103.] Allison AC, Gregoriadis G. Liposomes as immunological adjuvants. Nature. 1974;252.
[104.] Bolhassani A. Lipid-Based Delivery Systems in Development of Genetic and Subunit Vaccines. Molecular Biotechnology. 2022:1-30.
[105.] Nisini R, Poerio N, Mariotti S, De Santis F, Fraziano M. The Multirole of Liposomes in Therapy and Prevention of Infectious Diseases. Frontiers in Immunology. 2018;9:155.
[106.] Schwendener RA. Liposomes as vaccine delivery systems: a review of the recent advances. Therapeutic Advances in Vaccines and Immunotherapy. 2014;2(6):159-82.
[107.] Drummond D, Meyer O, Hong K, Kirpotin D, Papahadjopoulos D. Optimizing Liposomes for Delivery of Chemotherapeutic Agents to Solid Tumors. Pharmacological Reviews. 1999;51(4):691-743.
[108.] Patel D, Patel K. Liposomal drug delivery system as an effective treatment approach for lung cancer. Journal of Drug Delivery and Therapeutics. 2020;10(3-s):367-70.
[109.] Mouritsen OG, Jørgensen K. A new look at lipid-membrane structure in relation to drug research. Pharmaceutical Research. 1998;15(10).
[110.] Barenholz Y. Doxil-the first FDA-approved nano-drug: lessons learned. Journal of Controlled Release. 2012;160(2):117-34.
[111.] Freire Haddad H, Burke JA, Scott EA, Ameer GA. Clinical Relevance of Pre-Existing and Treatment-Induced Anti-Poly(Ethylene Glycol) Antibodies. Regenerative Engineering and Translational Medicine. 2022;8(1):32-42.
[112.] Hadjidemetriou M, Al-Ahmady Z, Kostarelos K. Time-evolution of in vivo protein

corona onto blood-circulating PEGylated liposomal doxorubicin (DOXIL) nanoparticles. Nanoscale. 2016;8(13):6948-57.
[113.] Zhang H. Onivyde for the therapy of multiple solid tumors. Onco Targets and Therapy. 2016;9:3001-7.
[114.] Mohamed M, Abu Lila AS, Shimizu T, Alaaeldin E, Hussein A, Sarhan HA, et al. PEGylated liposomes: immunological responses. Science and Technology of Advanced Materials. 2019;20(1):710-24.
[115.] Dams E, Laverman P, Oyen W, Storm G, Scherphof G, Van Der Meer J, et al. Accelerated Blood Clearance and Altered Biodistribution of Repeated Injections of Sterically Stabilized Liposomes. The Journal of Pharmacology and Experimental Therapeutics. 2000;292(3):1071-9.
[116.] Lorusso D, Di Stefano A, Carone V, Fagotti A, Pisconti S, Scambia G. Pegylated liposomal doxorubicin-related palmar-plantar erythrodysesthesia ('hand-foot' syndrome). Annals of Oncology. 2007;18(7):1159-64.
[117.] Seynhaeve ALB, Amin M, Haemmerich D, van Rhoon GC, Ten Hagen TLM. Hyperthermia and smart drug delivery systems for solid tumor therapy. Advanced Drug Delivery Reviews. 2020.
[118.] Challenging paradigms in tumour drug delivery. 2020 May. Report No.: 1476-4660 (Electronic) 1476-1122 (Linking) Contract No.: 5.
[119.] Pautu V, Mellinger A, Resnier P, Lepeltier E, Martin L, Boussemart L, et al. Melanoma tumour vasculature heterogeneity: from mice models to human. Journal of Cancer Research and Clinical Oncology. 2019;145(3):589-97.
[120.] Sindhwani S, Syed AM, Ngai J, Kingston BR, Maiorino L, Rothschild J, et al. The entry of nanoparticles into solid tumours. Nature Materials. 2020;19(5):566-75.
[121.] Dewhirst MW, Secomb TW. Transport of drugs from blood vessels to tumour tissue. Nature Reviews Cancer. 2017;17(12):738-50.
[122.] Hønger T, Jørgensen K, Stokes D, Biltonen RL, Mouritsen OG. Phospholipase A2 activity and physical properties of lipid-bilayer substrates. Methods in Enzymology. 1997;286:168-90.
[123.] Drummond D, Meyer O, Hong B, Kirpotin DB, Papadopoulou D. Optimizing Liposomes for Delivery of Chemotherapeutic Agents to Solid Tumors. Pharmacological Reviews. 1999;51.
[124.] Lindner L, Eibl H, Eichhorn M, Teichert N, Schmitt-Sody M, Issels R, et al. Novel Temperature-Sensitive Liposomes with Prolonged Circulation Time. 2004;10:2168-78.
[125.] Hossann M, Hirschberger J, Schmidt R, Baumgartner C, Zimmermann K, Baer S, et al. A Heat-Activated Drug-Delivery Platform Based on Phosphatidyl-(oligo)-glycerol Nanocarrier for Effective Cancer Treatment. Advanced NanoBiomed Research. 2021.
[126.] Zimmermann K, Hossann M, Hirschberger J, Troedson K, Peller M, Schneider M, et al. A pilot trial of doxorubicin containing phosphatidyldiglycerol based thermosensitive liposomes in spontaneous feline soft tissue sarcoma. International Journal of Hyperthermia. 2016;33(2):178-90.
[127.] Limmer S, Hahn J, Schmidt R, Wachholz K, Zengerle A, Lechner K, et al. Gemcitabine Treatment of Rat Soft Tissue Sarcoma with Phosphatidyldiglycerol-Based Thermosensitive Liposomes. Pharmaceutical Research. 2014;31(9):2276-86.
[128.] Kneidl B, Peller M, Winter G, Lindner L, Hossann M. Thermosensitive liposomal drug delivery systems: state of the art review. International Journal of Nanomedicine. 2014:12.
[129.] Hossann M, Syunyaeva Z, Schmidt R, Zengerle A, Eibl H, Issels R, et al. Proteins and cholesterol lipid vesicles are mediators of drug release from thermosensitive liposomes. Journal of Controlled Release. 2012;162(2):400-6.
[130.] Datta NR, Ordonez SG, Gaipl US, Paulides MM, Crezee H, Gellermann J, et al. Local hyperthermia combined with radiotherapy and-/or chemotherapy: recent advances and promises for the future. Cancer Treatment Reviews. 2015;41(9):742-53.
[131.] Pereira Gomes I, Aparecida Duarte J, Chaves Maia AL, Rubello D, Townsend DM, Branco de Barros AL, et al. Thermosensitive Nanosystems Associated with

Hyperthermia for Cancer Treatment. Pharmaceuticals. 2019;12(4).
[132.] Issels R, Lindner L, Verweij J, Wessalowski R, Reichardt P, Wust P, et al. Effect of Neoadjuvant Chemotherapy Plus Regional Hyperthermia on Long-term Outcomes Among Patients With Localized High-Risk Soft Tissue Sarcoma. JAMA Oncology. 2018;4(4).
[133.] Issels RD, Noessner E, Lindner LH, Schmidt M, Albertsmeier M, Blay JY, et al. Immune infiltrates in patients with localised high-risk soft tissue sarcoma treated with neoadjuvant chemotherapy without or with regional hyperthermia: A translational research program of the EORTC 62961-ESHO 95 randomised clinical trial. European Journal of Cancer. 2021;158:123-32.
[134.] Issels R, Kampmann E, Kanaar R, Lindner LH. Hallmarks of hyperthermia in driving the future of clinical hyperthermia as targeted therapy: translation into clinical application. International Journal of Hyperthermia. 2016;32(1):89-95.
[135.] Koning GA, Eggermont AMM, Lindner LH, ten Hagen TLM. Hyperthermia and Thermosensitive Liposomes for Improved Delivery of Chemotherapeutic Drugs to Solid Tumors. Pharmaceutical Research. 2010;27(8):1750-4.
[136.] Chen Q, Tong S, Dewhirst M, Yuan F. Targeting tumor microvessels using doxorubicin encapsulated in a novel thermosensitive liposome. Molecular Cancer Therapeutics. 2004;3:1311-7.
[137.] Todorova VK, Siegel ER, Kaufmann Y, Kumarapeli A, Owen A, Wei JY, et al. Dantrolene Attenuates Cardiotoxicity of Doxorubicin Without Reducing its Antitumor Efficacy in a Breast Cancer Model. Translational Oncology. 2020;13(2):471-80.
[138.] Hossann M, Wiggenhorn M, Schwerdt A, Wachholz K, Teichert N, Eibl H, et al. In vitro stability and content release properties of phosphatidylglyceroglycerol containing thermosensitive liposomes. Biochimica et Biophysica Acta. 2007;1768(10):2491-9.
[139.] Schmidt R. Neuartige thermosensitive Liposomen zur zielgerichteten Therapie solider Tumoren - Charakterisierung in vitro und in vivo - 2011.
[140.] Lokerse WJM, Lazarian A, Kleinhempel A, Petrini M, Schwarz P, Hossann M, et al. Mechanistic investigation of thermosensitive liposome immunogenicity and understanding the drivers for circulation half-life: A polyethylene glycol versus 1,2-dipalmitoyl-sn-glycero-3-phosphodiglycerol study. Journal of Controlled Release. 2021;333:1-15.
[141.] Kort WJ, Hulsman LOM, Schalkwljk WPv, Weijma IM, Zondervar PE, Westbroek DL. Reductive Effect of Aspirin Treatment on Primary Tumor Growth and Metastasis of Implanted Fibrosarcoma in Rats. Journal of the National Cancer Institute. 1986;76(4):711-20.
[142.] Manusama ER, Nooijen PTGA, Stavast J, Durante NMC, Marquet RL, Eggermont AMM. Synergistic antitumour effect of recombinant human tumour necrosis factor a with melphalan in isolated limb perfusion in the rat. British Journal of Surgery. 1996;83:551-5.
[143.] Eggermonta AMM, Liénardb D, Schraffordt Koops H, Rosenkaimer d F, Lejeuneb FJ. Treatment of Irresectable Soft Tissue Sarcomas of the Limbs by Isolation Perfusion with High Dose TNFα in Combination with Interferon-y and Melphalan. Tumor Necrosis Factor: Molecular and Cellular Biology and Clinical Relevance Basel, Karger Verlag. 1993.
[144.] Manusama ER, Nooijen PTGA, Stavast J, de Wilt JHW, Marquet RL, Eggermont AMM. Assessment of the Role of Neutrophils on the Antitumor Effect of TNFa in an in Vivo Isolated Limb Perfusion Model in Sarcoma-Bearing Brown Norway Rats. Journal of Surgical Research. 1997;78.
[145.] van der Veen A, de Wilt J, Eggermont A, van Tiel S, Seynhaeve A, ten Hagen T. TNF-a augments intratumoral concentrations of doxorubicin in TNF-a-based isolated limb perfusion in rat sarcoma models and anhances anti-tumour effects. British Journal of Cancer. 2000;82(4).
[146.] Willerding L, Limmer S, Hossann M, Zengerle A, Wachholz K, ten Hagen T, et al. Method of hyperthermia and tumor size influence effectiveness of doxorubicin release

from thermosensitive liposomes in experimental tumors. Journal of Controlled Release. 2016;222:47-55.
[147.] Ayoub NM, Al-Shami KM, Yaghan RJ. Immunotherapy for HER2-positive breast cancer: recent advances and combination therapeutic approaches. Breast Cancer - Targets and Therapy. 2019;11:53-69.
[148.] Vonderheide RH, Domchek SM, Clark AS. Immunotherapy for Breast Cancer: What Are We Missing? Clincal Cancer Research. 2017;23(11):2640-6.
[149.] NCT03409198 C.
[150.] Yang W, Ahmed M, Elian M, Hady SA, Levchenko TS, Sawant RR, et al. Do Liposomal Apoptotic Enhancers IncreaseTumor Coagulation and End-Point Survival in Percutaneous Radiofrequency Ablation of Tumors in a Rat Tumor Model? . Radiology. 2010;257.
[151.] Yang W, Ahmed M, Tasawwar B, Levchenko T, Sawant RR, Torchilin V, et al. Combination radiofrequency (RF) ablation and IV liposomal heat shock protein suppression: Reduced tumor growth and increased animal endpoint survival in a small animal tumor model. Journal of Controlled Release. 2012;160(2):239–44.
[152.] Kumar G, Goldberg S, Gourevitch S, Levchenko T, Torchilin V, Galun E, et al. Targeting STAT3 to Suppress Systemic Pro-Oncogenic Effects from Hepatic Radiofrequency Ablation. Radiology. 2018;286(2):524-36.
[153.] Ahmed M, Kumar G, Moussa M, Wang Y, Rozenblum N, Galun E, et al. hepatic radiofrequency ablation–induced stimulation of Distant Tumor growth is suppressed by c-Met inhibition. Radiology. 2016;279:103-17.
[154.] Karathanasis E, Suryanarayanan S, Balusu S, McNeeley K, Sechopoulos I, Karellas A, et al. Imaging Nanoprobe for Prediction of Outcome of Nanoparticle Chemotherapy by Using Mammography. Radiology. 2008;250.
[155.] Ngoune R, Peters A, von Elverfeldt D, Winkler K, Putz G. Accumulating nanoparticles by EPR: A route of no return. Journal of Controlled Release. 2016;238:58-70.
[156.] Kuzu OF, Nguyen FD, Noory MA, Sharma A. Current State of Animal (Mouse) Modeling in Melanoma Research. Cancer Growth Metastasis. 2015;8(Suppl 1):81-94.
[157.] Fidler IJ. Biological Behavior of Malignant Melanoma Cells Correlated to Their Survival in vivo. Cancer Research. 1975;35:218-24.
[158.] Passarelli A, Mannavola F, Stucci LS, Tucci M, Silvestris F. Immune system and melanoma biology: a balance between immunosurveillance and immune escape. Oncotarget. 2017;8(62).
[159.] Cai L, Wang X, Wang W, Qiu N, Wen J, Duan X, et al. Peptide ligand and PEG-mediated long-circulating liposome targeted to FGFR overexpressing tumor in vivo. International Journal of Nanomedicine. 2012;7:4499-510.
[160.] Shae D, Becker KW, Christov P, Yun DS, Lytton-Jean AKR, Sevimli S, et al. Endosomolytic polymersomes increase the activity of cyclic dinucleotide STING agonists to enhance cancer immunotherapy. Nature Nanotechnology. 2019;14(3):269-78.
[161.] Petrini M. Cationic and anionic phosphatidyldiglycerol-based thermosensitive liposomes for the targeted delivery of chemotherapeutics and immunoadjuvants 2019.
[162.] Vichai V, Kirtikara K. Sulforhodamine B colorimetric assay for cytotoxicity screening. Nature Protocols. 2006;1(3):1112-6.
[163.] Mähler M, Berard M, Feinstein R, Gallagher A, Illgen-Wilcke B, Pritchett-Corning K, et al. FELASA recommendations for the health monitoring of mouse, rat, hamster, guinea pig and rabbit colonies in breeding and experimental units. 2014.
[164.] Dülsner A, Hack R, Krüger C, Pils M, Scherer K, Schmelting B, et al. Fachinformation aus dem Ausschuss für Tierschutzbeauftragte und dem Arbeitskreis 4 in der TVT; Empfehlung zur Substanzapplikation bei Versuchstieren. 2017.
[165.] Lee H, Blaufox D. Blood Volume in the Rat. The Journal of Nuclear Medicine. 1985;26.
[166.] Thermosome GmbH. Patent number WO2022008471.
[167.] Dane EL, Belessiotis-Richards A, Backlund C, Wang J, Hidaka K, Milling LE, et al. STING agonist delivery by tumour-penetrating PEG-lipid nanodiscs primes robust anticancer immunity. Nature Materials. 2022;21(6):710-20.

[168.] Thermosome GmbH P, Germany.
[169.] Chountoulesi M, Naziris N, Pippa N, Demetzos C. The significance of drug-to-lipid ratio to the development of optimized liposomal formulation. Journal of Liposome Research. 2018.
[170.] Ren T, Song YK, Zhang G, Liu D. Structural basis of DOTMA for its high intravenous transfection activity in mouse. Gene Therapy. 2000;7.
[171.] Liu S, Cheng Q, Wei T, Yu X, Johnson LT, Farbiak L, et al. Membrane-destabilizing ionizable phospholipids for organ-selective mRNA delivery and CRISPR-Cas gene editing. Nature Materials. 2021;20(5):701-10.
[172.] Petrini M, Lokerse WJM, Mach A, Hossann M, Merkel OM, Lindner LH. Effects of Surface Charge, PEGylation and Functionalization with Dipalmitoylphosphatidyldiglycerol on Liposome-Cell Interactions and Local Drug Delivery to Solid Tumors via Thermosensitive Liposomes. International Journal of Nanomedicine. 2021;16:4045-61.
[173.] Curran E, Chen X, Corrales L, Kline DE, Dubensky TW, Jr., Duttagupta P, et al. STING Pathway Activation Stimulates Potent Immunity against Acute Myeloid Leukemia. Cell Reports. 2016;15(11):2357-66.
[174.] Schmidt R. Neuartige thermosensitive Liposomen zur zielgerichteten Therapie solider Tumoren - Charakterisierung in vitro und in vivo. 2011.
[175.] Sheffield MJ, Baker BL, Li D, Owen NL, Baker ML, Bell JD. Enhancement of Agkistrodon piscivorus piscivorus venom phospholipase A2 activity toward phosphatidylcholine vesicles by lysolecithin and palmitic acid: studies with fluorescent probes of membrane structure. Biochemistry. 1995;34(24):7796-806.
[176.] Hoang TT, Pilkington EH, Nguyen DH, Lee JS, Park KD, Truong NP. The Importance of Poly(ethylene glycol) Alternatives for Overcoming PEG Immunogenicity in Drug Delivery and Bioconjugation. Polymers. 2020;12(2).
[177.] Choi SY, Hirata K, Ishida T, Quertermous T, Cooper AD. Endothelial lipase: a new lipase on the block. Journal of Lipid Research. 2002;43(11):1763-9.
[178.] Jaye M, Lynch KJ, Krawiec J, Marchadier D, Maugeais C, Doan K, et al. A novel endothelial-derived lipase that modulates HDL metabolism. Nature Genetics. 1999;21(4).
[179.] Inoue A, Aoki J. Phospholipase A1: structure, distribution and function. Future Lipidology. 2017;1(6):687-700.
[180.] Kuemmerle NB, Rysman E, Lombardo PS, Flanagan AJ, Lipe BC, Wells WA, et al. Lipoprotein lipase links dietary fat to solid tumor cell proliferation. Molecular Cancer Therapeutics. 2011;10(3):427-36.
[181.] Yang R, Han S, Clayton J, Haghighatian M, Tsai CC, Yao Y, et al. A Proof-of-Concept Inhibitor of Endothelial Lipase Suppresses Triple-Negative Breast Cancer Cells by Hijacking the Mitochondrial Function. Cancers. 2022;14(15).
[182.] Kojma Y, Hirata K, Ishida T, Shimokawa Y, Inoue N, Kawashima S, et al. Endothelial lipase modulates monocyte adhesion to the vessel wall. A potential role in inflammation. Journal of Biological Chemistry. 2004;279(52):54032-8.
[183.] Zhu G, Fang Q, Zhu F, Huang D, Yang C. Structure and Function of Pancreatic Lipase-Related Protein 2 and Its Relationship With Pathological States. Frontiers in Genetics. 2021;12:693538.
[184.] Alves BN, Marshall K, Tamang DL, Leong J, Redelman D, Elliott V, et al. Lipid-dependent cytotoxicity by the lipase PLRP2 and by PLRP2-positive cytotoxic T lymphocytes (CTLs). Cell Biochemistry and Function. 2009;27(5):296-308.
[185.] Iga K, Ogawa Y, Toguchi H. Rates of systemic degradation and reticuloendothelial system (RES) uptake of thermosensitive liposome encapsulating cisplatin in rats. Pharmaceutical Research. 1993;10(9):1332-7.
[186.] Deen W, Lazzara M, Myers B. Structural determinants of glomerular permeability. American Journal of Physiology-Renal Physiology. 2001;281.
[187.] Jacevic V, Djordjevic A, Srdjenovic B, Milic-Tores V, Segrt Z, Dragojevic-Simic V, et al. Fullerenol nanoparticles prevents doxorubicin-induced acute hepatotoxicity in rats. Experimental and Molecular Pathology. 2017;102(2):360-9.

[188.] Hazem RM AS, Nafea YK, Al-Karmalawy AA, Saleh MA, El-Azab MF. . Pirfenidone and vitamin D mitigate renal fibrosis induced by doxorubicin in mice with Ehrlich solid tumor. 288. 2022.
[189.] Xiang C, Yan Y, Zhang D. Alleviation of the doxorubicin-induced nephrotoxicity by fasudil in vivo and in vitro. Journal of Pharmacological Sciences. 2021;145(1):6-15.
[190.] Lee VW, Harris DC. Adriamycin nephropathy: a model of focal segmental glomerulosclerosis. Nephrology. 2011;16(1):30-8.
[191.] Duong AD, Collier MA, Bachelder EM, Wyslouzil BE, Ainslie KM. One Step Encapsulation of Small Molecule Drugs in Liposomes via Electrospray-Remote Loading. Molecular Pharmaceutics. 2016;13(1):92-9.
[192.] Zucker D, Marcus D, Barenholz Y, Goldblum A. Liposome drugs' loading efficiency: a working model based on loading conditions and drug's physicochemical properties. Journal of Controlled Release. 2009;139(1):73-80.
[193.] Eloy JO, Claro de Souza M, Petrilli R, Barcellos JP, Lee RJ, Marchetti JM. Liposomes as carriers of hydrophilic small molecule drugs: strategies to enhance encapsulation and delivery. Colloids and Surfaces B: Biointerfaces. 2014;123:345-63.
[194.] Lindner LH, Hossann M. Factors affecting drug release from liposomes. Current Opinion in Drug Discovery and Development. 2010;13.
[195.] Grit M, Crommelin D. Chemical stability of liposomes: implications for their physical stability. Chemistry and Physics of Lipids. 1993;64.
[196.] Zuniga LA, Lessmann T, Uppal K, Bisek N, Hong E, Rasmussen CE, et al. Intratumoral delivery of TransCon() TLR7/8 Agonist promotes sustained anti-tumor activity and local immune cell activation while minimizing systemic cytokine induction. Cancer Cell International. 2022;22(1):286.
[197.] Kneidl B. Formulation studies, lyophilization and in vivo investigation of 1,2-dipalmitoyl-sn-glycero-3-phosphodiglycerol-based thermosensitive liposomes for the delivery of gemcitabine, irinotecan and SN-38 2017.
[198.] Damm J, Wiegand F, Harden LM, Gerstberger R, Rummel C, Roth J. Fever, sickness behavior, and expression of inflammatory genes in the hypothalamus after systemic and localized subcutaneous stimulation of rats with the Toll-like receptor 7 agonist imiquimod. Neuroscience. 2012;201:166-83.
[199.] Stathopoulos A, Pretto C, Devillers L, Pierre D, Hofman FM, Kruse C, et al. Development of immune memory to glial brain tumors after tumor regression induced by immunotherapeutic Toll-like receptor 7/8 activation. Oncoimmunology. 2012;1(3):298-305.
[200.] Michaelis KA, Norgard MA, Zhu X, Levasseur PR, Sivagnanam S, Liudahl SM, et al. The TLR7/8 agonist R848 remodels tumor and host responses to promote survival in pancreatic cancer. Nature Communications. 2019;10(1):4682.
[201.] Michaelis KA, Norgard MA, Levasseur PR, Olson B, Burfeind KG, Buenafe AC, et al. Persistent Toll-like receptor 7 stimulation induces behavioral and molecular innate immune tolerance. Brain, Behavior, and Immunity. 2019;82:338-53.
[202.] Zhou J, Xu Y, Wang G, Mei T, Yang H, Liu Y. The TLR7/8 agonist R848 optimizes host and tumor immunity to improve therapeutic efficacy in murine lung cancer. International Journal of Oncology. 2022;61(1).
[203.] Yin T, He S, Wang Y. Toll-like receptor 7/8 agonist, R848, exhibits antitumoral effects in a breast cancer model. Molecular Medicine Reports. 2015;12(3):3515-20.
[204.] Cheadle E, Lipowska-Bhalla G, Dovedi S, Fagnano E, Klein C, Honeychurch J, et al. A TLR7 agonist enhances the antitumor efficacy of obinutuzumab in murine lymphoma models via NK cells and CD4 T cells. Leukemia. 2017;31(7):1611-21.
[205.] Bahmani B, Gong H, Luk BT, Haushalter KJ, DeTeresa E, Previti M, et al. Intratumoral immunotherapy using platelet-cloaked nanoparticles enhances antitumor immunity in solid tumors. Nature Communications. 2021;12(1):1999.
[206.] Pockros PJ, Guyader D, Patton H, Tong MJ, Wright T, McHutchison JG, et al. Oral resiquimod in chronic HCV infection: safety and efficacy in 2 placebo-controlled, double-blind phase IIa studies. J Hepatol. 2007;47(2):174-82.
[207.] Bourquin C, Hotz C, Noerenberg D, Voelkl A, Heidegger S, Roetzer LC, et al. Systemic

cancer therapy with a small molecule agonist of toll-like receptor 7 can be improved by circumventing TLR tolerance. Cancer Research. 2011;71(15):5123-33.
[208.] Koga-Yamakawa E, Murata M, Dovedi SJ, Wilkinson RW, Ota Y, Umehara H, et al. TLR7 tolerance is independent of the type I IFN pathway and leads to loss of anti-tumor efficacy in mice. Cancer Immunology, Immunotherapy. 2015;64(10):1229-39.
[209.] NCT02126579 C.
[210.] NCT01204684 C.
[211.] NCT00821652 C.
[212.] NCT00960752 C.
[213.] NCT01748747 C.
[214.] NCT00948961) C.
[215.] Xiaozhe L, Meilan C, Beihui H, Junru L, Jingli G, Lifen K, et al. Pyridoxine Is Effective for Preventing Hand-Foot Syndrome Induced by Pegylated Liposomal Doxorubicin for Multiple Myeloma: The Results of a Randomized Study. Integrative Cancer Therapies. 2022;21:15347354221140402.
[216.] Gao D, Li W, Wang W, Cai Y, Wang Y, Luo X, et al. Synergy of purine-scaffold TLR7 agonist with doxorubicin on systemic inhibition of lymphoma in mouse model. Journal of Cancer. 2017;8(16):3183-9.
[217.] Zhu J, He S, Du J, Wang Z, Li W, Chen X, et al. Local administration of a novel Toll-like receptor 7 agonist in combination with doxorubicin induces durable tumouricidal effects in a murine model of T cell lymphoma. Journal of Hematology & Oncology. 2015;8:21.
[218.] Amini MA, Abbasi AZ, Cai P, Lip H, Gordijo CR, Li J, et al. Combining Tumor Microenvironment Modulating Nanoparticles with Doxorubicin to Enhance Chemotherapeutic Efficacy and Boost Antitumor Immunity. Journal of the National Cancer Institute. 2019;111(4):399-408.
[219.] Ujhazy P, Zaleskis G, Mihich E, Ehrke MJ, Berleth ES. Doxorubicin induces specific immune functions and cytokine expression in peritoneal cells. Cancer Immunology and Immunotherapy. 2003;52(7):463-72.
[220.] Zitvogel L, Apetoh L, Ghiringhelli F, Kroemer G. Immunological aspects of cancer chemotherapy. Nature Reviews Immunology. 2008;8(1):59-73.
[221.] https://www.criver.com/.

X. Appendix

Table 36: Characteristics of used batches of $DPPG_2$-TSL-DOX.

	Study	Tumor induction	Injection	Size (nm)	PDI	Z-POT (mV)	DOX (mM)	Lipid (mM)	$DPPG_2$ (mM)	DOX:lipid (mol:mol)
Mouse	PK BD	- cell injection	i.v.	182.1	0.10	-29.4	5.4	54.2	15.5	0.1
Rat	PK BD	- fragment	i.v.	167.0	0.09	-32.7	5.3	54.9	15.2	0.1
Rat	Single therapy	fragment	i.v.	112,3	0.10	-25.8	2.8	44.6	13.0	0.2
Rat	Single therapy Combi therapy Metastasis	cells day -4	i.v.	159.1	0.10	-26.1	6.0	60.1	18.6	0.1
Rat	Single therapy	cells day -4	i.v.	118.5	0.07	-27.7	4.8	42.1	12.9	0.1

Table 37: Characteristics of used batches of $DPPG_2$-TSL-ADU.

	Study	Tumor induction	Injection	Size (nm)	PDI	Z-POT (mV)	ADU (mM)	Lipid (mM)	$DPPG_2$ (mM)	ADU:lipid (mol:mol)
Mouse	PK	-	i.v.	134.2	0.15	-26.9	0.9 (isosmotic)	38.6	11.4	0.02
Mouse	PK	-	i.v.	138.3	0.12	-29.9	1.1 (hyposmotic)	33.5	9.9	0.03
Mouse	Single therapy	cell injection	i.v.	70.8	0.09	-22.3	1.0 (hyposmotic)	43.9	13.3	0.02
Rat	PK	-	i.v.	140.7	0.11	-30.3	-	32.7	9.8	-
Rat	PK	-	i.v.	134.2	0.15	-26.9	0.9 (isosmotic)	38.6	11.4	0.02
Rat	PK	-	i.v.	126.6	0.11	-24.7	0.8 (hyposmotic)	20.3	6.0	0.04
Rat	BD	fragment	i.v.	138.3	0.12	-29.9	1.1 (hyposmotic)	33.5	9.9	0.03
Rat	Single therapy	fragment	i.v.	70.8	0.09	-22.3	1.0 (hyposmotic)	43.9	13.3	0.02

Table 38: Characteristics of used batches of $DPPG_2$-TSL-$R848_{adjusted}$.

	Study	Tumor induction	Injection	Size (nm)	PDI	Z-POT (mV)	R848 (mM)	Lipid (mM)	$DPPG_2$ (mM)	R848:lipid (mol:mol)
Rat	PK	-	2 mg/kg, i.v.	170.5	0.07	-32.1	2.4	53.0	15.3	0.05
Rat	BD	fragment	2 mg/kg, i.v.	158.0	0.05	-25.3	1.8	28.4	8.3	0.10
Rat	Single therapy	cells day -7	2 mg/kg, i.v.	159.5	0.03	-25.0	1.7	72.4	20.7	0.02
Rat	Single therapy	cells day -4	2 mg/kg, i.v.	162.0 157.9 153.8	0.04 0.05 0.05	-26.1 -27.5 -21.3	2.1 1.8 2.1	74.3 32.6 87.5	24.0 10.0 25.6	0.03 0.05 0.02
Rat	Single therapy	cells day -4	0.71 mg/kg, i.v.	159.5	0.03	-25.0	1.7	72.4	20.7	0.02
Rat	Single therapy Repetitive therapy	cells day -4 cells day -4	10, 50, 100, 500 µg i.t. 10 µg i.t.	161.9	0.05	-29.7	19.0	76.6	22.4	0.25
Rat	Repetitive therapy	cells day -4	2 mg/kg, i.v.	157.7 159.4 162.0	0.02 0.07 0.04	-25.2 -26.6 -26.1	2.7 2.2 2.1	90.7 89.1 74.3	29.0 28.3 24.0	0.03 0.02 0.03
Rat	Combi therapy	cells day -4	2 mg/kg, i.v.	157.7 158.9 157.6 160.4	0.02 0.07 0.05 0.02	-25.2 -29.0 -27.2 -23.7	2.7 2.7 2.0 2.5	90.7 37.6 85.3 97.6	29.0 11.9 28.5 28.5	0.03 0.06 0.02 0.03
Rat	Combi therapy	cells day -4	10 µg i.t.	156.3	0.07	-21.6	16.0	72.6	29.1	0.22
Rat	Metastasis	cells day -4	2 mg/kg, i.v.	158.9 157.9 157.6 158.0 160.2 158.5 159.3 160.4	0.07 0.05 0.05 0.06 0.05 0.03 0.06 0.02	-29.0 -27.5 -27.2 -26.7 -26.0 -26.9 -24.3 -23.7	2.1 1.8 2.0 2.0 2.7 2.0 2.5 2.5	37.6 32.6 85.3 86.1 81.3 78.7 94.5 97.6	11.9 10.0 28.5 28.7 28.8 22.9 28.0 28.5	0.06 0.05 0.02 0.02 0.03 0.03 0.03 0.03

Table 39: Parameters of groups from studies exploring DOX.

	Study	Tumor induction	Group	Treatment	Treatment condition	Group size (n)	Body weight (mg)	Injected DOX (mg)	Injected lipid (mg)	Injected $DPPG_2$ (mg)
Mouse	PK	-	$DPPG_2$-TSL-DOX	2 mg/kg, i.v.	NT (WB)	2	27.2 ± 4.0	0.1	0.7 ± 0.1	0.0 ± 0.0
Mouse	PK	-	$DPPG_2$-TSL-DOX	2 mg/kg, i.v.	HT (WB)	2	22.8 ± 1.8	0.1	0.6 ± 0.1	0.0 ± 0.0
Mouse	BD	cell injection	$DPPG_2$-TSL-DOX	2 mg/kg, i.v.	HT(WB)/RT	2	31.0 ± 0.9	0.1 ± 0.0	0.8 ± 0.2	0.3 ± 0.1
Mouse	BD	cell injection	$DPPG_2$-TSL-DOX	2 mg/kg, i.v.	HT(lamp)/RT	2	31.6 ± 0.4	0.1 ± 0.0	0.8 ± 0.1	0.3 ± 0.0
Rat	PK	-	free DOX	2 mg/kg, i.v.	NT (WB)	6	264.5 ± 10.7	0.5 ± 0.0	-	-
Rat	PK	-	$DPPG_2$-TSL-DOX	2 mg/kg, i.v.	NT (WB)	6	276 ± 13.7	0.6 ± 0.0	7.6 ± 0.4	2.2 ± 0.1
Rat	BD	fragment	free DOX	2 mg/kg, i.v.	HT(lamp)/RT	6	246.8 ± 9.7	0.5 ± 0.0	-	-
Rat	BD	fragment	$DPPG_2$-TSL-DOX	2 mg/kg, i.v.	HT(lamp)/RT	6	231.2 ± 8.6	0.5 ± 0.0	6.4 ± 0.2	1.9 ± 0.1
Rat	Single therapy	fragment	Saline	i.v.	HT (lamp)	6	221.4 ± 11.8	-	-	-
Rat	Single therapy	fragment	free DOX	2 mg/kg, i.v.	HT (lamp)	6	232.7 ± 14.2	0.5 ± 0.0	-	-
Rat	Single therapy	fragment	Doxil	2 mg/kg, i.v.	HT (lamp)	6	211.2 ± 11.2	0.4 ± 0.0	3.4 ± 0.2	-
Rat	Single therapy	fragment	optimized $DPPG_2$-TSL-DOX	2 mg/kg, i.v.	HT (lamp)	6	255.5 ± 9.1	0.5 ± 0.0	10.9 ± 0.4	3.4 ± 0.1
Rat	Single therapy	fragment	optimized $DPPG_2$-TSL-DOX	2 mg/kg, i.v.	sham	6	267.7 ± 10.6	0.5 ± 0.0	11.4 ± 0.5	3.5 ± 0.1
Rat	Single therapy	cells day -4	$DPPG_2$-TSL-DOX	2 mg/kg, i.v.	HT (lamp)	4	241.2 ± 7.1	0.5 ± 0.0	6.4 ± 0.2	2.1 ± 0.1
Rat	Single therapy	cells day -7	$DPPG_2$-TSL-DOX	2 mg/kg, i.v.	HT (WB)	3	281.6 ± 4.9	0.6 ± 0.0	6.5 ± 0.1	2.1 ± 0.04
Rat	Combi therapy	cells day -4	1x $DPPG_2$-TSL-DOX / 3x free R848, i.t 1. Injection	2 mg/kg, i.v.	HT (lamp)	3	204.9 ± 9.2	0.4 ± 0.0	5.4 ± 0.2	1.8 ± 0.1
Rat	Combi therapy	cells day -4	1x $DPPG_2$-TSL-DOX / 3x free R848, i.v. 1. Injection	2 mg/kg, i.v.	HT (lamp)	3	232.2 ± 23.7	0.5 ± 0.1	6.1 ± 0.6	2.0 ± 0.2
Rat	Combi therapy	cells day -4	1x $DPPG_2$-TSL-DOX / 3x $DPPG_2$-TSL- $R848_{adjusted}$, i.v. 1. Injection	2 mg/kg, i.v.	HT (lamp)	3	234.7 ± 6.5	0.5 ± 0.0	6.2 ± 0.2	2.0 ± 0.1
Rat	Combi therapy	cells day -4	1x $DPPG_2$-TSL-DOX / 3x $DPPG_2$-TSL- $R848_{adjusted}$, i.t. 1. Injection	2 mg/kg, i.v.	HT (lamp)	3	254.4 ± 2.5	0.5 ± 0.0	6.7 ± 0.1	2.2 ± 0.02
Rat	Metastasis	cells day -4	$DPPG_2$-TSL-DOX	2 mg/kg, i.v.	HT (lamp)	3	276.0 ± 11.2	0.6 ± 0.0	7.3 ± 0.3	2.4 ± 0.1
Rat	Metastasis	cells day -4	1x $DPPG_2$-TSL-DOX / 3x $DPPG_2$-TSL- $R848_{adjusted}$, i.v. 1. injection	2 mg/kg, i.v.	HT (lamp)	3	238.1 ± 5.1	0.5 ± 0.0	6.3 ± 0.1	2.1 ± 0.04

Table 40: Parameters of groups from studies exploring ADU.

	Study	Tumor induction	Group	Treatment	Treatment condition	Group size (n)	Body weight (mg)	Injected ADU (mg)	Injected lipid (mg)	Injected $DPPG_2$ (mg)
Mouse	PK	-	$DPPG_2$-TSL-$ADU_{isosmotic}$	2 mg/kg, i.v.	sham	2	26.9 ± 12	0.1	2.5 ± 0.1	0.8 ± 0.04
Mouse	PK	-	$DPPG_2$-TSL-$ADU_{hyposmotic}$	2 mg/kg, i.v.	NT (WB)	2	28.8 ± 1.5	0.1	1.8 ± 0.1	0.6 ± 0.03
Mouse	PK	-	$DPPG_2$-TSL-$ADU_{hyposmotic}$	2 mg/kg, i.v.	HT (WB)	2	20.1 ± 1.5	0.0	1.2 ± 0.1	0.4 ± 0.03
Mouse	Single therapy	cell injection	$DPPG_2$-TSL-$ADU_{hyposmotic}$	2 mg/kg, i.v.	HT (WB)	2	43.6 ± 3.2	0.1 ± 0.0	4.3 ± 0.3	3.2 ± 0.2
Mouse	Single therapy	cell injection	$DPPG_2$-TSL-$ADU_{hyposmotic}$	1 mg/kg, i.v.	HT (WB)	1	33.4	0.0	1.7	1.2
Rat	PK	-	$DPPG_2$-$TSL_{hyposmotic}$	55.8 mg/kg, i.v.	sham	3	229.2 ± 15.5	-	12.8 ± 0.9	4.1 ± 0.3
Rat	PK	-	$DPPG_2$-TSL-$ADU_{isosmotic}$	2 mg/kg, i.v.	sham	3	234.1 ± 14.9	0.5 ± 0.0	21.8 ± 1.4	6.8 ± 0.4
Rat	PK	-	$DPPG_2$-TSL-$ADU_{isosmotic}$	2 mg/kg, i.v.	HT (WB)	3	241.5 ± 7.2	0.5 ± 0.0	22.5 ± 0.7	7.1 ± 0.2
Rat	PK	-	free ADU	2 mg/kg, i.v.	sham	3	282.1 ± 11.4	0.6 ± 0.0	-	-
Rat	PK	-	free ADU	2 mg/kg, i.v.	HT (WB)	3	284.6 ± 8.8	0.6 ± 0.0	-	-
Rat	PK	-	$DPPG_2$-TSL-$ADU_{hyposmotic}$	2 mg/kg, i.v.	sham	3	289.9 ± 10.2	0.6 ± 0.0	16.2 ± 0.6	5.1 ± 0.2
Rat	PK	-	$DPPG_2$-TSL-$ADU_{hyposmotic}$	2 mg/kg, i.v.	HT (WB)	3	283.2 ± 3.5	0.6 ± 0.0	15.8 ± 0.2	5.0 ± 0.1
Rat	BD	fragment	free ADU	2 mg/kg, i.v.	HT (lamp) / RT	6	252.3 ± 13.0	0.5 ± 0.0	-	-
Rat	BD	fragment	free ADU	500 µg, i.t.	HT (lamp) / RT	6	250.7 ± 13.0	0.50	-	-
Rat	BD	fragment	$DPPG_2$-TSL-$ADU_{hyposmotic}$	2 mg/kg, i.v.	HT (lamp) / RT	6	254.5 ± 10.8	0.5 ± 0.0	15.8 ± 0.7	5.0 ± 0.2
Rat	Dose-escalation	fragment	Solvent	i.t.	HT (lamp)	4	265.7 ± 12.0	-	-	-
Rat	Dose-escalation	fragment	free ADU	10 µg, i.t.	HT (lamp)	4	251.3 ± 33.4	0.01	-	-
Rat	Dose-escalation	fragment	free ADU	100 µg, i.t.	HT (lamp)	4	239.4 ± 35.6	0.1	-	-
Rat	Dose-escalation	fragment	free ADU	500 µg, i.t.	HT (lamp)	6	228.9 ± 27.8	0.5	-	-
Rat	Single therapy	fragment	free ADU	2 mg/kg, i.v.	HT (lamp)	6	226.7 ± 11.9	0.5 ± 0.0	-	-
Rat	Single therapy	fragment	Saline	i.v.	HT (lamp)	3	229.6 ± 21.7	-	-	-
Rat	Single therapy	fragment	Saline	i.v.	sham	6	231.5 ± 14.9	-	-	-
Rat	Single therapy	fragment	$DPPG_2$-TSL-$ADU_{hyposmotic}$	2 mg/kg, i.v.	HT (lamp)	6	226.1 ± 19.1	0.5 ± 0.0	21.9 ± 1.9	7.1 ± 0.6
Rat	Single therapy	fragment	$DPPG_2$-TSL-$ADU_{hyposmotic}$	2 mg/kg, i.v.	sham	6	221.6 ± 20.2	0.4 ± 0.0	21.5 ± 2.0	6.9 ± 0.6

Table 41: Parameters of groups from studies exploring R848.

	Study	Tumor induction	Group	Treatment	Treatment condition	Group size (n)	Body weight (mg)	Injected R848 (mg)	Injected Lipid (mg)	Injected $DPPG_2$ (mg)
Rat	PK	-	free R848	2 mg/kg, i.v.	NT (WB)	3	285.2 ± 12.0	0.6 ± 0.0	-	-
Rat	PK	-	free R848	2 mg/kg, i.v.	HT (WB)	3	290.6 ± 5.6	0.5 ± 0.0	-	-
Rat	PK	-	$DPPG_2$-TSL-R848$_{adjusted}$	2 mg/kg, i.v.	NT (WB)	3	272.0 ± 9.0	0.6 ± 0.0	29.2 ± 1.0	9.0 ± 0.3
Rat	PK	-	$DPPG_2$-TSL-R848$_{adjusted}$	2 mg/kg, i.v.	HT (WB)	3	278.7 ± 6.4	0.6 ± 0.0	30.0 ± 0.7	9.2 ± 0.2
Rat	BD	fragment	free R848	2 mg/kg, i.v.	HT(WB)/RT	6	262.7 ± 17.8	0.5 ± 0.0	-	-
Rat	BD	fragment	free R848	500 µg, i.t.	HT(WB)/RT	6	256.8 ± 13.5	0.5	-	-
Rat	BD	fragment	$DPPG_2$-TSL-R848$_{adjusted}$	2 mg/kg, i.v.	HT(WB)/RT	6	262.8 ± 9.4	0.5 ± 0.0	21.1 ± 0.8	6.5 ± 0.2
Rat	Single therapy	cells day -4	Saline	i.v.	HT (WB)	3	229.1 ± 9.3	-	-	-
Rat	Single therapy	cells day -4	free R848	2 mg/kg, i.v.	HT (WB)	3	232.8 ± 5.7	0.5 ± 0.0	-	-
Rat	Single therapy	cells day -4	$DPPG_2$-TSL-R848$_{adjusted}$	2 mg/kg, i.v.	HT (WB)	3	214 ± 29.5	0.4 ± 0.0	28.6 ± 9.7	9.4 ± 3.6
Rat	Single therapy	cells day -4	$DPPG_2$-TSL-R848$_{adjusted}$	0.71 mg/kg, i.v.	HT (WB)	2	192.7 ± 10.5	0.1 ± 0.0	14.4 ± 0.8	4.4 ± 0.2
Rat	Single therapy	cells day -4	free R848	10 µg, i.t.	HT (WB)	3	203.9 ± 5.9	0.01	-	-
Rat	Single therapy	cells day -4	$DPPG_2$-TSL-R848$_{adjusted}$	10 µg, i.t.	HT (WB)	3	209.2 ± 17.5	0.01	0.1	0.03
Rat	Single therapy	cells day -4	$DPPG_2$-TSL-R848$_{adjusted}$	100 µg, i.t.	HT (WB)	2	203.4 ± 9.5	0.1	1	0.03
Rat	Single therapy	cells day -7	Saline	i.v.	HT (WB)	3	268.6 ± 10.8	-	-	
Rat	Single therapy	cells day -7	free R848	2 mg/kg, i.v.	HT (WB)	3	268.6 ± 4.7	0.5 ± 0.0	-	-
Rat	Single therapy	cells day -7	$DPPG_2$-TSL-R848$_{adjusted}$	2 mg/kg, i.v.	HT (WB)	3	262.6 ± 8.5	0.5 ± 0.0	55.3 ± 1.8	16.8 ± 0.5
Rat	Repetitive therapy	cells day -7	free R848 1. injection 2. injection	10 µg, i.t.	HT (WB)	3	286.5 ± 11.4 284.0 ± 13.2	0.01 0.01	-	-
Rat	Repetitive therapy	cells day -7	free R848 1. injection 2. injection	50 µg, i.t.	HT (WB)	3	219.1 ± 104.3 284.0 ± 24.1	0.05 0.05	-	-
Rat	Repetitive therapy	cells day -7	free R848 1. injection 2. injection	100 µg, i.t.	HT (WB)	3	283.9 ± 4.5 275.1 ± 3.9	0.1 0.1	-	-
Rat	Repetitive therapy	cells day -7	free R848 1. injection	500 µg, i.t.	HT (WB)	3	287.0 ± 10.0	0.5	-	-

			2. injection				277.0 ± 9.1	0.5		
Rat	Repetitive therapy	cells day -4	3x free R848 1. injection 2. injection 3. injection	2 mg/kg, i.v.	HT (WB)	3	218.2 ± 109.2 159.6 ± 106.5 161.8 ± 107.9	0.4 ± 0.2 0.3 ± 0.2 0.3 ± 0.2	-	-
Rat	Repetitive therapy	cells day -4	3x $DPPG_2$-TSL-$R848_{adjusted}$ 1. injection 2. injection 3. injection	2 mg/kg, i.v.	HT (WB)	3	213.6 ± 15.3 206.1 ± 12.2 212.0 ± 9.3	0.4 ± 0.0 0.4 ± 0.0 0.4 ± 0.0	38.1 ± 6.8 36.8 ± 6.3 39.4 ± 6.3	13.0 ± 2.2 12.5 ± 2.1 13.4 ± 2.0
Rat	Repetitive therapy	cells day -4	3x $DPPG_2$-TSL-$R848_{adjusted}$ 1. injection 2. injection 3. injection	10 µg, i.t.	HT (WB)	3	210.7 ± 8.7 210.2 ± 8.5 215.2	0.01 0.01 0.01	0.098 0.098 0.098	0.03 0.03 0.03
Rat	Combi therapy	cells day -4	1x $DPPG_2$-TSL-DOX / 3x free R848 2. injection 3. injection 4. injection	10 µg, i.t.	HT (WB)	3	195.7 ± 9.5 210.3 ± 0.7 227.0 ± 5.8	0.01 0.01 0.01	-	-
Rat	Combi therapy	cells day -4	1x $DPPG_2$-TSL-DOX / 3x free R848 2. injection 3. injection 4. injection	2 mg/kg, i.v.	HT (WB)	3	222.9 ± 24.2 225.1 ± 24.2 226.9 ± 27.3	0.4 ± 0.1 0.4 ± 0.1 0.4 ± 0.1	-	-
Rat	Combi therapy	cells day -4	1x $DPPG_2$-TSL-DOX / 3x $DPPG_2$-TSL-$R848_{adjusted}$ 2. injection 3. injection 4. injection	2 mg/kg, i.v.	HT (WB)	3	232.8 ± 4.2 236.6 ± 7.9 224.5 ± 18.2	0.5 ± 0.0 0.5 ± 0.0 0.5 ± 0.0	35.5 ± 14.3 35.7 ± 14.3 33.4 ± 14.4	12.3 ± 5.2 12.4 ± 5.2 10.9 ± 4.5
Rat	Combi therapy	cells day -4	1x $DPPG_2$-TSL-DOX / 3x $DPPG_2$-TSL-$R848_{adjusted}$ 2. injection 3. injection 4. injection	10 µg, i.t.	HT (WB)	3	253.0 ± 1.6 256.7 ± 1.9 261.2 ± 11.5	0.01 0.01 0.01	0.75 0.75 0.75	0.32 0.32 0.32
Rat	Metastasis	cells day -4	free R848	2 mg/kg, i.v.	HT (WB)	3	253.5 ± 9.0	0.5 ± 0.0	-	-
Rat	Metastasis	cells day -4	$DPPG_2$-TSL-$R848_{adjusted}$	2 mg/kg, i.v.	HT (WB)	3	248.6 ± 4.4	0.5 ± 0.0	46.2 ± 8.5	16.7 ± 2.5
Rat	Metastasis	cells day -4	1x $DPPG_2$-TSL-DOX / 3x $DPPG_2$-TSL- $R848_{adjusted}$, i.v. 2. injection 3. injection 4. injection	2 mg/kg, i.v.	HT (WB)	3	231.0 ± 2.5 226.7 ± 8.6 227.7 ± 6.5	0.5 ± 0.0 0.5 ± 0.0 0.5 ± 0.0	28.9 ± 14.1 43.2 ± 1.2 43.4 ± 0.4	9.2 ± 4.1 13.5 ± 0.4 13.5 ± 0.3

Acknowledgments

A large number of people and rodents have contributed to the success of my doctoral thesis and I would like to take this opportunity to thank them sincerely.

First of all, I would like to express my sincere thanks to Prof. Dr. Lars Lindner who has always supported and advised me as a mentor and has given me this unique opportunity to work in the fascinating field of thermosensitive liposomes and for letting me join his research group. I want to express my gratitude for supporting me in all aspects of my personal development as a vet in preclinical research. I want to thank him for the scientific advice, and, especially, for inspiring me throughout these years. I also want to express my gratitude to Prof. Dr. med. vet. Johannes Hirschberger, for accepting me as doctoral student and for giving me the possibility to prepare my thesis under his supervision.

My gratitude goes to the whole AG Liposomen for all these nice years of working together. Specifically, I want to thank Dr. Matteo Petrini, for all the scientific (not exclusively) discussions throughout these years and for introducing me to the animal work. I also want to thank Angela Knauerhase, and Lisa Pointner for the scientific advices, day-by-day support, and for making our laboratory a great work place. A special thanks goes to Sebastian Teschner, Sinan Güler, and Xi Zhu who I was allowed to introduce to the field of animal work.

I want to thank Dr. Martin Hossann for all the scientific advises, the constant input, the great discussions, and especially for sharing his great experiences which helped me constantly throughout the thesis and when finalizing this work. I want to express my appreciation and gratitude to all members of Thermosome GmbH for providing a constant support.

I would like to express my gratitude also to all the people who contributed greatly to this work, such as Matteo Petrini, Lisa Pointer and Vladyslav Nikitchenko for their experimental contributions. A special thanks goes to Dr. Martin Hossann for his critical review of this work. I want to thank the team of the animal facility MedI / II / III / Neurology for being so supportive and flexible, allowing me to finish this thesis in time. Furthermore, the Bundesministeriums für Bildung und Forschung (BMBF) is acknowledged for having funded this project IO-TSL.

My deepest gratitude goes to my wonderful family who stood by my side, backed me up and always believed in me. Lastly, I want to thank my husband Florian for being such an important person in my life on whom I can undoubtedly rely. Thank you for your bright love and for giving me all the strength I need to proceed further, I dedicate this work to you.